EXPANDED INSIGHT INTO PROCESSING AND ISOFORM DEPENDENT PROPERTIES OF APELIN

by

Kyungsoo Shin

Submitted in partial fulfilment of the requirements
for the degree of Doctor of Philosophy

at

Dalhousie University
Halifax, Nova Scotia
August 2017

DEDICATION PAGE

For my family

For Ash

For my supervisors

For my mentors

For my mentees

For my friends

TABLE OF CONTENTS

LIST OF TABLES

LIST OF FIGURES

ABSTRACT

Apelin is one of two peptide ligands for a class A G-protein-coupled receptor (the apelin receptor; AR/APJ). Apelin-AR signalling regulates many body systems, including the cardiovascular system, central nervous system, and adipoinsular axis. Notably, apelin can exist as various isoforms and demonstrates isoform-dependent variation in its potency and efficacy, with potency inversely correlated to isoform size. Thus, apelin processing may have an important regulatory role. The existing processing theory suggested that upon N-terminal signal peptide removal, the resulting 55-residue peptide would be an inactive proprotein (apelin-55), requiring an N-terminal truncation to a 36-residue isoform (apelin-36) for activation. Apelin-36 could then be further processed into 17- or 13-residue isoforms to increase potency. However, apelin-55 detection extracellularly did not fit this theory. Thus, I focused on better elucidating our understanding of apelin processing and the potential involvement of biological membranes in regulating the apelinergic system. I begin by demonstrating, through development of an *in vitro* assay using high performance liquid chromatography and mass spectrometry, that proprotein convertase subtilisin kexin subtype 3 (PCSK3) processes apelin-55 into apelin-13 specifically and preferentially, while PCSK1 and 7 could not process it. This showed that apelin-55 need not be initially processed to apelin-36. Secondly, I demonstrate that apelin processing can occur extracellularly. Specifically, the introduction of apelin-55 into the culture media of various cell lines resulted in observable changes in the level of apelin-55 with distinct processing patterns observable for different cell lines. Next, I examine apelin-55 biophysics. Through solution-state NMR spectroscopy, I provided clear demonstration that apelin-55 shows behaviour fully consistent with it being the longest bioactive isoform, rather than an inactive proprotein, correlating directly to our functional assays. I also examined interactions of both apelin-55 and -36 with zwitterionic and anionic micelles. Strikingly, both apelin isoforms preferentially interacted with anionic micelles and adopted a similar micelle-bound conformation independent of micelle headgroup. In combination, my studies have expanded the current understanding of the apelin processing pathway, increased the number of bioactive apelin isoforms, and demonstrated highly similar behaviour for all apelin isoforms. These factors have likely relevance to the apelinergic system function and regulation.

LIST OF ABBREVIATIONS AND SYMBOLS USED

γ	Gyromagnetic ratio
δ	Chemical shift or a pulsed field gradient duration
$\Delta\delta$	Secondary chemical shift
Δ	Diffusion time
λ	Wavelength
APJ	Apelin Receptor
AR	Apelin Receptor
ARMRC	Atlantic Region Magnetic Resonance Centre
B_0	External magnetic field
BSA	Bovine serum albumin
CD	Circular dichroism
CSD	Chemical shift displacement
CSI	Chemical shift index
D	Translational diffusion coefficient
D_b	D for a micelle-bound peptide
dH_2O	Distilled water
D_2O	Deuterated water
DANGLE	Dihedral ANgles from Global Likelihood Estimates
D_{ob}	Observed D for a mixture of peptide and micelle in buffer
D_m	D for a free micelle
DMEM	Dulbecco's modified Eagle's medium

DOSY	Diffusion ordered spectroscopy
D_p	*D* for a free peptide
DPC	Dodecylphosphocholine
DSS	4,4-dimethyl-4-silapentane-1-sulfonic acid
E	Energy
ERK	Extracellular regulated kinase
f_b	Fraction bound
FBS	Fetal bovine Serum
G	Pulsed field gradient power of a DOSY experiment
G-protein	Guanine-nucleotide binding regulatory protein
GPCR	G-protein-coupled receptor
ħ	Reduced Planck constant
H_20	Water
HPLC	High performance liquid chromatography
HSQC	Heteronuclear single quantum coherence
IPTG	Isopropyl β-D-1-thiogalactopyranoside
PCR	Polymerase chain reaction
LPPG	1-palmitoyl-2-hydroxy-sn-glycero-3-[phospho-*rac*-(1-glycerol)]
m_I	Secondary nuclear spin quantum number
NOE	Nuclear Overhauser effect
NMR	Nuclear magnetic resonance
NMR-3	Nuclear Magnetic Resonance Research Resource
NRC-IMB	National Research Council Institute for Marine Biosciences

PBS	Phosphate buffered saline
PCSK#	Proprotein convertase subtilisin kexin subtype #
PVDF	Polyvinylidene fluoride
POI	Protein of interest
Pyr	Pyroglutamate
RP	Reverse-phase
R_1	Longitudinal relaxation rate constant
R_2	Transverse relaxation rate constant
SDS	Sodium dodecyl sulphate
σ	Degree of shielding
TBS	Tris buffered saline
TBST	Tris buffered saline with 0.1% Tween-20
TFA	Trifluoroacetic acid
TOCSY	Total correlation spectroscopy
ω	Larmor frequency

ACKNOWLEDGEMENTS

First of all, I would like to thank my supervisors Dr. Jan Rainey and Dr. Younes Anini, who have always been supportive, welcoming, and available for input during not only my graduate studies but also my undergraduate degree. Without their guidance and patience, it is unquestionable that I would not have been able to learn the true joys of working in a laboratory and find my passion in research.

During my studies, I had the chance to learn from many people including Mr. Nigel Chapman, Dr. Jeffrey Gagnon, Dr. David Langelaan, Mr. Nathan Martin-Weatherbee, Dr. Aditya Pandey, Dr. Muzaddid Sarker, Mr. Andy Song, Mr. Bruce Stewart, Dr. Marie Tremblay, and Dr. Lingling Xu. I thank these people who have taught me the proper techniques and skills to succeed, provided me with valuable feedback, and been supportive during my undergraduate and graduate studies.

I also want to acknowledge many of the students who I had a chance to teach, supervise, and mentor. I am sure I probably was not the easiest person to work with, but I hope that they learned as much from me as I learned from them. In the Rainey lab, I want to show special appreciation to Ms. Shuya Huang and Mr. Calem Kenward, who have been incredibly helpful in my work by going beyond what they were asked. For the Anini lab, I want to thank Mrs. Stephanie Pelletier, Mr. Michael Landsman, and Dr. Bader Alamri, who were remarkable colleagues to work with.

I also want to thank Dr. Michael Lumsden, and Mr. Ian Burton for their expertise in NMR spectroscopy. I thank my committee members, Dr. David Byers, Dr. Valerie Chappe, and Dr. Catherine Too, who have given me thoughtful and useful suggestions throughout my graduate studies. I thank Dr. Melanie Dobson, Dr. Lois Murray, and Ms.

Joyce Chew for their helpful advice and Dr. David Waisman for allowing me access to the CD spectropolarimeter. Finally, I thank the Natural Sciences and Engineering Research Council of Canada for providing me with the funding to complete my studies.

CHAPTER 1 INTRODUCTION

In the course of the work described in this thesis, my main scientific goals were to: i) characterize how the peptide hormone, apelin, is processed and ii) to rationalize the pharmacological differences observed between apelin isoforms through biophysical means. This relied upon a variety of biochemical and biophysical techniques. These include recombinant protein production, liquid chromatography-mediated purification and assay development, and spectroscopy-based characterization of peptide conformations and dynamics.

To allow for an optimal flow of scientific discussion, the major techniques used in the thesis are detailed first (Chapter 2). Thus, the scientific background to my thesis (i.e., the apelinergic system) is introduced in Chapter 3, which describes the two peptide hormones, apelin and apela, and their class A G-protein-coupled receptor. This chapter summarizes the physiological roles of the apelinergic system, providing evidence that isoform-dependent effects are key for the function of both apelin and apela.

The next two chapters are devoted to studies characterizing apelin processing *in vitro* (Chapter 4) and *in situ* (Chapter 5). In these studies, I identify i) the first and, thus far, only endoprotease known to be involved in apelin processing (Chapter 4), and ii) show that apelin may be processed extracellularly in a cell-line-dependent manner (Chapter 5). The next two chapters focus on spectroscopy-based methods to compare and contrast conformations and dynamics of various apelin isoforms. My characterization allowed me to provide a direct biophysical rationale for the fact that apelin-55, previously presumed to be an inactive proprotein, is an active apelin isoform (Chapter 6). I then demonstrate that biomembranes have the potential for regulation of the pharmacological

properties of apelin isoforms (Chapter 7), particularly when compared to the behaviour of apela.

Finally, Chapter 8 revisits the work detailed. First, I examine the implications of my studies in terms of expanding the current understanding of the apelinergic system. Next, a number of future directions that I feel to be particularly valuable and relevant are outlined. Finally, I conclude by detailing the evidence I have developed to demonstrate that isoform-specific behaviour is a critical, but often neglected, aspect of apelinergic system function.

CHAPTER 2 OVERVIEW OF TECHNIQUES USED IN THIS STUDY

2.1 *ESCHERICHIA COLI*-BASED RECOMBINANT PROTEIN EXPRESSION

(Note: Section 2.1 is based on a segment of a review which I wrote. I was a co-author in this review, entitled "Small expression tags enhance bacterial expression of the first three transmembrane segments of the apelin receptor" by Pandey, Shin, Patterson and Rainey [1]. This was published in ***Biochemistry and Cell Biology*** (2016) 92(4): 269-278.)

The biophysical characterization of a protein typically requires the production of multi-milligram quantities of that protein. This subsequently must be purified to allow for the desired downstream characterization. To achieve this, the use of recombinant expression systems and fusion tags to enhance protein expression and purification have been highly successful. Of the many systems available, *Escherichia coli* has been the most widely used for expression of recombinant proteins for several reasons: (i) fast growth kinetics with a doubling time of 20 min in optimal conditions [2]; (ii) high achievable growth density and correspondingly high protein production [3]; (iii) cost-effectiveness and flexibility of growth medium without a significant loss in yield [4]; (iv) a vast number of available strains with specific advantages (e.g., [5-7]); and lastly, (v) an abundance of expression vectors to assist in production and purification [8]. In combination, these features of *E. coli* significantly reduce the time required for expression of the protein of interest (POI), while achieving large protein yield in an

inexpensive manner. Additionally, the flexibility of growth medium composition allows for efficient and cost-effective stable NMR-active isotope enrichment through simple manipulation of media contents, as has been instrumental throughout my research.

For recombinant protein production in *E. coli,* T7 RNA polymerase from *Enterobacteria phage λ* has often been a valuable tool in regulating expression of the POI [6]. There are several advantages of using this system. First of all, the exclusive recognition of the T7 promoter by T7 RNA polymerase allows for regulation of POI expression that is naturally absent in *E. coli*. In addition, T7 polymerase catalyzes a faster rate of mRNA synthesis than that of endogenous *E. coli* RNA polymerase with fewer incomplete transcripts (e.g. premature termination), which results in higher protein yield [9]. Furthermore, by putting T7 RNA polymerase expression under control of the *lac* operon, expression of the POI can be easily controlled by the exogenous addition of isopropyl β-D-thiogalactoside (IPTG) [6]. Another advantage of *E. coli*, as introduced above, is the ability to straightforwardly and cost-effectively produce isotope-labeled proteins for downstream NMR characterization [4]. Specifically, this involves growing bacteria and inducing POI expression in media supplemented with isotope-enriched precursors. In combination, induction of POI expression via addition of IPTG at the optimal time in the growth period of *E. coli* can enable significant POI overexpression.

Fusion tags can also greatly assist in production of a POI. In particular, for POI that are difficult to express such as membrane proteins, the use of tags has been instrumental in improving the POI yield through increased expression [10-12]. In addition, tags can be used to target expressed POIs to different cellular locations (e.g. inclusion bodies, media, periplasm) to prevent aggregation/degradation [13-15], and

increase solubility for efficient handling [16-18]. Some tags are fused to POI specifically for purification purposes. For example, hexahistidine-tagged proteins can be purified easily and efficiently through use of Ni^{2+} affinity resin [18] (discussed in detail in Section 2.2). In combination, fusion tags may provide a considerable enhancement in the yield of a POI by either increasing the overall yield and/or facilitating and enhancing the purification process.

Fusion tags can be combined in various configuration to provide the additive (or complementary) benefits of individual tag [11, 19-21] for potentially greater POI yield than is observed with a single fusion tag. However, the design of fusion tag-POI constructs still requires careful selection and consideration, as each tag may be accompanied by potential disadvantages. For example, the size of the fusion tag can play a major role as this may impose a heavy metabolic burden on the host system and may also interact with the POI structure and/or activity [22-24]. This, in turn, may reduce expression yield and hamper downstream purification and characterization. Thus, the use of fusion tags requires a variety of considerations alongside optimization of various conditions.

Fusion tags typically need to be removed prior to POI characterization, as the tag may interfere with the activity and/or perturb the structure of the POI. Notably, many choices are available for tag removal strategies, similar to the number of tags available for recombinant protein expression. These strategies include protease-mediated cleavage (e.g. tobacco etch virus (TEV) protease [25] and small ubiquitin modifier (SUMO) protease [26]), self-cleavage (e.g. intein-based methods [27]), and chemical cleavage (e.g. cyanogen bromide (CNBr)-mediated [28]). Although the mechanisms behind tag removal

can vary, all methods lead to a defined cleavage site between the tag and POI for their separation. This, in turn, has ramifications for construct design since the efficiency of tag removal for a given technique may vary dramatically between different target proteins, as was the case for one of the apelin isoforms characterized herein (Chapter 6). In summary, a variety of factors and conditions must be considered and optimized for efficient protein production, purification, and, potentially, fusion tag removal before carrying out biochemical and biophysical characterization of proteins.

2.2 LIQUID CHROMATOGRAPHY TECHNIQUES

Liquid chromatography techniques separate molecules by exploiting differences in their physical properties [29]. Solubility in water or organic solvents (normal or reverse phase chromatography), fusion tag (affinity chromatography), net charge (ion-exchange chromatography), and size (size-exclusion chromatography) of molecules are key examples of properties used to separate mixtures of peptides and proteins. Exploitation of differences in each of these properties has been instrumental in purifying numerous POIs upon production. In all instances, the impure sample containing the POI is dissolved in a solvent (liquid-phase) and is allowed to interact with solid particles (solid-phase) packed in a column that present chemical moieties that separate analyte through the physical properties mentioned. Variations in partitioning in the solid-phase, in response to differences in the physical properties between POI and contaminants, retard their motion through the column differentially.

Although the mechanism underlying separation is determined by choice of solid-phase, the choice of liquid-phase (the “mobile phase”) also has a major impact as the

retention times of the POI and contaminants will be determined by the favourability of partitioning of a given species between the mobile and solid-phases. As an example, Ni^{2+}-nitrilotriacetic acid (NTA) coupled to solid beads facilitates purification of polyhistidine-tagged proteins [30]. In several instances in my thesis, I have used this Ni^{2+}-NTA affinity-based mechanism to allow for initial purification of a hexahistidine-tagged POI from the bulk of *E. coli* proteins. The NTA forms a matrix on the solid support which securely coordinates Ni^{2+} ions through four coordination sites each, leaving two of the transition metal coordination sites exposed to interact with histidine imidazole rings [30]. Upon subjection to a column packed with these beads, histidine-tagged samples will bind to the Ni^{2+}-NTA matrix, while the vast majority of untagged proteins (i.e., most *E. coli* proteins) will freely pass through the column. Subsequently, application of a mobile phase containing an increasing concentration of free imidazole (competes with bound proteins for Ni^{2+} coordination sites) will initially release unselectively- or weakly-bound molecules and, eventually, release the POI once a sufficient imidazole concentration is reached.

Other chromatography techniques that were used for purification of my POIs were cation exchange and reverse-phase high performance liquid chromatography (RP-HPLC; see Section 2.2.1). Unlike Ni^{2+}-NTA column, the partitioning of molecules between the solid-phase and liquid-phase depends upon the charge state and hydrophobicity of a given molecule, respectively. Correspondingly, the desorption from the solid-state may then be effected by increasing the mobile phase salinity (e.g., increasing NaCl concentration) or the proportion of hydrophobic solvent in a mixed mobile phase (e.g., a greater proportion of acetonitrile in a water:acetonitrile mobile phase).

2.2.1 USING REVERSE-PHASE HIGH PERFORMANCE LIQUID CHROMAGRAPHY TO MONITOR PROTEIN PROCESSING

HPLC (defined above as high performance LC, but also referred to as high pressure LC), in particular the RP-HPLC variant, is a technique that was essential throughout the work described in my thesis. It was especially critical for Chapters 4 and 5. As stated earlier, reverse-phase chromatography separates molecules based on their hydrophobicity. The solid-phase, correspondingly, provides a hydrophobic environment for binding (e.g., octadecyl carbon chain (C_{18})-bonded solid silica beads) and the mobile phase is composed of a mixture of hydrophilic and hydrophobic solvents to provide the necessary competitive strength for disassociating the POI from the solid-phase. Consequently, RP-HPLC usually requires (i) a binary pump system to provide both solvents, ii) an HPLC column for separation, and iii) a detector for monitoring of elution and to allow for collection of the analytes.

The term high performance is based on the column efficiency [29], determined by the expression:

$$n = 16(t_r{}^2)/(t_w) \tag{2.1}$$

where n is the measure of efficiency, t_r is the retention time for a target protein, and t_w is the width of the peak (i.e., elution period). A typical value of n for normal column chromatography is ~500 while, in contrast, the value for n can easily exceed 10,000 for HPLC [29]. High column efficiency is obtained by use of small particle sizes (e.g., ≤ 5 μm particle diameter), which provides a large surface area to volume ratio to maximize sample interaction and a very low solvent volume between particles to significantly limit diffusion time. Thus, the use of small particle sizes increases the probability that a

molecule dissolved in the mobile phase will encounter the solid-phase rather than diffuse through the column, greatly improving spectral resolution. However, as particle beads become smaller, so does the space between them, which collectively causes a significant increase in the pressure within the portions of the instrument holding the mobile phase, giving rise to the term "high pressure" liquid chromatography. By using solid particles such as silica, which can withstand high pressures (~3.5 kPa), liquid chromatography may be carried out at high pressure and highly resolved peak separation results.

Sample elution can be monitored through number of different detectors (e.g., ultraviolet (UV)/visible absorption, fluorescence, refractive index, evaporative light scattering, etc.). In my thesis, I have used only one such detector, a UV absorption detector, to detect the elution of proteins through absorbance at 214 nm for peptide bond chromophores and at 280 nm for the aromatic tryptophan sidechain of the longer apelin isoforms. As will become evident in Chapters 4 and 5, the potential high resolution possible with HPLC allowed for differentiation between apelin isoforms. This was instrumental for studying apelin processing in two ways. First, the high resolution allowed for monitoring changes in the level of intact apelin-55 and shorter isoforms. Secondly, collection of distinct apelin processing products allowing for mass spectrometry (MS)-based protein identification was possible.

2.3 MASS SPECTROMETRY

MS is an analytical technique that can very accurately determine the mass of proteins contained in a biological sample, which can provide information on the identity of proteins, and can even identify and localize post-translational modifications on proteins [31, 32]. Generally, a mass spectrometer ionizes samples in the gaseous phase and determines the mass-to-charge (m/z) ratio of the ionized sample. The mass of the gas phase molecule can, in turn, be calculated based upon the number of charges it contains. Thus, a mass spectrometer minimally consists of i) an ionization source to produce charged particles in the gas phase, ii) a mass analyzer to separate the charged molecules, and iii) a detector to determine the m/z ratios.

2.3.1 MATRIX-ASSISTED LASER DESORPTION IONIZATION MASS SPECTROMETRY

Matrix-assisted laser desorption ionization (MALDI), developed by Karas and Hillenkamp [33], is one of the two most common ionization processes. This ionization process is based on the use of a large excess of matrix material which is co-precipitated with the molecule of interest. As the name indicates, the matrix, which is typically an organic molecule, assists in desorption of the sample from the solid to gas phases. Specifically, once the matrix-sample is co-precipitated, the resulting solid sample is irradiated with a laser at a wavelength that is efficiently absorbed by the matrix [31]. The photo-excited matrix can then promote desorption and ionization of sample molecules. The resulting gas phase molecule usually has a single charge (i.e., a single observable m/z ratio for a sample).

2.3.2 ELECTROSPRAY IONIZATION MASS SPECTROMETRY

Developed by Fenn *et al.* [34], electrospray ionization (ESI) is the other most common ionization process. In contrast to MALDI, ESI requires samples that are solubilized in a solvent. This solution is passed through a hypodermic needle held at high voltage, which electrostatically disperses (or "electrosprays") μm-sized multiply charged droplets. As these ionized droplets disperse, they rapidly undergo evaporation. This process imparts the charges of a droplet on the sample. As a result, the sample tends to have multiple charges, with a variety of observable m/z ratios for a given protein. Although multiple m/z ratios can complicate analysis, the distribution of m/z ratios can be helpful in identifying masses of unknown samples through deconvolution to determine the "parent mass" of the molecule in question.

2.3.3 TIME OF FLIGHT MASS ANALYZER

Once the samples are ionized using either the MALDI or ESI process, the masses of charged molecules must be determined for sample identification. Although there are a variety of mass analyzers available (e.g. triple quadrupole, ion-trap, etc.), all of the instruments employed in my thesis used a time-of-flight (TOF) mass analyzer. In TOF, the ionized sample is accelerated with fixed amount of kinetic energy and travels down a flight tube for a known distance [31]. Given the fixed kinetic energy, samples with smaller mass travel with greater velocity than heavier samples; thus, they are recorded on a detector earlier. The time of detection, in turn, can be used to determine the mass of each sample, given its relationship to velocity and, subsequently, energy.

2.4 CIRCULAR DICHROISM (CD) SPECTROPOLARIMETRY

Circular dichroism (CD) spectropolarimetry refers to the unequal absorption of right and left circularly polarized light at specific wavelengths due to molecular asymmetry. Thus, when linearly polarized light traverses a sample with circular dichroism, the resulting unequal absorbance gives rise to the observation of elliptically polarized light. The instrument, in turn, provides a measure of "ellipticity". For an observable CD phenomenon, the molecule needs to be intrinsically chiral, covalently linked to a chiral molecule, or placed in an asymmetric environment [35]. Although amino acids (except for glycines) are chiral at the α-position, the observable far- UV CD signal in proteins originates from ground to excited state electrical and magnetic dipole moment transitions of peptide bonds. This results in optically distinguishable features from secondary and tertiary structuring, making CD spectroscopy a powerful technique to study protein structure in solution and to monitor changes in conformation in response to environment factors.

Arguably, the most valuable aspect of CD spectroscopy for proteins is that different secondary structures in proteins give rise to clear and specific CD signals in the far-UV range. An α-helix has a positive CD band at 193 nm (a π to π* transition) and negative bands at 208 (π to π*) and 222 nm (an *n* to π* transition) [36]. In contrast, a β-sheet has a positive band at 196 nm (π to π*) and negative band at 218 nm (*n* to π*). Random coil structure has a strong negative band at 195 nm (π to π*) but no significant CD signal for its *n* to π* transition. Other structural units, such as β-turns or polyproline-II helices also give rise to distinct CD band patterns with a negative band near 189-195 nm and a positive band near 200-215 nm [37-39].

The CD signal at a given wavelength is given by the linear combination of the population-weighted CD signal for each type of secondary structure (e.g., α-helix, β-sheet, random coil, etc.) at that wavelength [39]. By examining the summed effect of convoluted CD signals over the far-UV regime (~180-250 nm, ideally), the secondary structure of protein can be quickly determined. Provided that an appropriate reference dataset is available, the CD spectrum can be deconvoluted to estimate the quantity (usually in percentage) of each secondary structuring in a sample [39]. Notably, deconvolution provides the most accurate results for helical structures as they are well-defined and tend to produce strong signals [40]. Other structures such as β-sheet tend to be more variable in their configurations and/or conformations (e.g., parallel and antiparallel), with accuracy lowered correspondingly. However, even without performing deconvolution, conformational changes in a protein in response to environment, intermolecular interaction, or other perturbing factors can often be readily characterized.

2.5 SOLUTION-STATE NUCLEAR MAGNETIC RESONANCE SPECTROSCOPY

Nuclear magnetic resonance (NMR) spectroscopy is a versatile biophysical technique that can provide information about protein structure and dynamics by exploiting the magnetic properties of the constituent nuclei [41]. In this thesis, this was particularly heavily used in the work described in Chapters 6 and 7. NMR spectroscopy requires i) nuclei with a non-zero nuclear spin angular momentum ("spin") and ii) an external magnetic field [41]. Nuclear spin is a fundamental property of a given nucleus, and is denoted by the quantum number I. Similar to other quantum numbers, it is

quantized to exist as an integer or as a half-integer. Examples of NMR-active nuclei with a spin of ½ are ^{1}H, ^{13}C and ^{15}N. Notably, some of the common nuclei in proteins, such as ^{12}C and ^{16}O, have nuclear spin of 0 while ^{14}N has a spin of 1. Nuclei with spin > ½ (e.g., ^{14}N) are quadrupolar, leading to complex interactions with the external magnetic field and, correspondingly, present spectra normally more difficult to interpret. In contrast, nuclei with spin ½ are ideal for solution-state NMR experiments, as they are NMR-active and provide more straightforward spectra. For these reasons, NMR-based experiments usually rely on proteins that are isotopically labeled with ^{13}C and ^{15}N using heterologous expression systems, such as *E. coli*, as discussed in Section 2.1.

If nuclei have non-zero spin angular momentum, they also have a magnetic moment [41]. When these nuclei are in the presence of an external magnetic field (B_0), the energy of a nucleus from the interaction between its magnetic moment and B_0 is given by the expression:

$$E = -\hbar\gamma m_I B_0 \tag{2.2}$$

where E represents the energy of the nucleus, ħ is the reduced Planck constant, γ is the gyromagnetic ratio (a constant for a given nucleus), and m_I is the secondary nuclear spin quantum number. This latter quantity, m_I, in turn is quantized. For a spin-½ nucleus, it may be ½ and -½, meaning that these nuclei can have two energy levels with an energy difference given by the expression:

$$\Delta E = -\hbar\gamma B_0 \tag{2.3}$$

This phenomenon of "splitting" of energy levels with a direct relation to B_0 is called the "Zeeman effect", and is responsible for providing the necessary energy difference for NMR spectroscopy. In case of nuclei with spin > ½, the increased number of m_I

(increasing in integer units from –I to +I) results in additional energy levels, and a more complex spectrum, as stated earlier. In contrast, nuclei with spin of 0 do not have any energy upon subjection to B_0, and cannot be observed by NMR spectroscopy. In the presence of B_0, the energy difference leads to the development of a bulk, or net equilibrium magnetization for a sample containing multiple nuclei along the direction of B_0. Using radiofrequency (RF) irradiation, torque can be produced on the bulk magnetization vector, causing it to rotate about the axis of the applied RF field. This occurs at a characteristic frequency called the Larmor frequency (ω_0), which is given by the expression:

$$\omega_0 = -\gamma B_0 \tag{2.4}$$

where ω_0 is in rad·s^{-1} and γ is the gyromagnetic ratio. As can be seen in equation 2.4, the Larmor frequency is dependent on the magnitude of B_0 and relates to ΔE (equation 2.3) through the reduced Planck constant.

It is important to note that while B_0, overall, depends upon the NMR spectrometer, typically in the form of a superconducting magnet in modern NMR spectrometers, the local magnetic field experienced by a particular nucleus will depend upon the environment around it (e.g., molecular structure). For example, electrons are able to partially shield the nucleus from the B_0 field, which will decrease the local magnetic field experienced by the nucleus and, consequently, produce a unique Larmor frequency (ω_{eff}) for that nucleus. This can be best visualized by the equation:

$$\omega_{eff} = -\gamma B_0(1 - \sigma) \tag{2.5}$$

where σ represents the degree of shielding. Due to these effects, each nucleus in a sample can have a chemically shifted Larmor frequency, which will vary with the chemical and

magnetic environment. Thus, NMR spectroscopy can provide details into the molecular environment for all nuclei with unique electron environment in a given sample.

In practice, the Larmor frequency of a given nucleus is represented by chemical shift (δ) [42], a value reported in parts per million and independent of B_0, as determined by:

$$\delta(ppm) = 10^6 \frac{\omega - \omega_{ref}}{\omega_{ref}} \quad (2.6)$$

where ω represents the frequency of the nucleus in question and ω_{ref} is the frequency of a defined reference compound such as 4,4-dimethyl-4-silapentane-1-sulfonic acid (DSS). In the case of DSS, its δ is usually set as 0 ppm for the ^{1}H dimension, which can then be used to indirectly reference nuclei other than ^{1}H [43].

To enable specific study of a given nucleus in the sample, its chemical shift must be assigned. In the case of a molecule such as a peptide with a small number of residues, the number of distinct NMR active nuclei (e.g., considering ^{1}H, ^{13}C, or ^{15}N) is small, and the number of chemical shifts arising will be correspondingly limited. Thus, chemical shift assignment for a sample of this nature would often be relatively straightforward using one-dimensional (1D), and/or two-dimensional (2D) experiments. However, with increasing molecular size (e.g., larger peptides or proteins), the number of distinct NMR-active nuclei becomes considerably greater. This will typically result in significant overlap of chemical shifts for a given type of NMR-active nucleus, meaning that dispersion in 1D and 2D experiments may not be sufficient to unambiguously assign all of the individual chemical shifts.

One solution to this signal overlap problem is to increase the dimensionality of experiments. For example, in the ^{1}H-^{15}N heteronuclear single quantum coherence

(HSQC) spectroscopy experiment, magnetization from a ^{1}H nucleus is transferred to a directly-bonded ^{15}N nucleus (e.g., a ^{1}H-^{15}N bond of an amide) and then back to the ^{1}H for signal detection [44]; thus, only ^{1}H nuclei covalently bonded to ^{15}N nuclei are detected. In addition, the detected signal is modulated by both associated ^{1}H and ^{15}N resonance frequencies. This, in turn, can be plotted as a 2D spectrum with the ^{1}H chemical shift as one dimension and the ^{15}N chemical shift as the other. A given ^{1}H-^{15}N bond will give rise to a cross-peak in this spectrum with chemical shifts associated with each of the bonded nuclei (i.e., considered as a graph in two dimensions, the horizontal position of the cross-peak would be at its ^{1}H chemical shift while the vertical position would be at its ^{15}N chemical shift (Fig. 2.1)). Since proteins have a limited number of distinct ^{15}N nuclei relative to either ^{1}H or ^{13}C, the resulting 2D spectrum has significantly less signals than either a 1D or 2D spectrum based upon either ^{1}H and/or ^{13}C. A 1D ^{15}N NMR spectrum would be similarly beneficial in its relative sparsity of resonances, but would be lacking in the capability to directly correlate the ^{15}N chemical shift to its directly bonded ^{1}H. It also has other experimental challenges including lowered natural abundance for ^{15}N (0.36%) compared to ^{1}H (99.98%), decreased energy difference compared to ^{1}H due to the ~10-fold difference in gyromagnetic ratios ($\gamma_N/\gamma_H = 0.10136$) resulting in lower net magnetization, and lowered sensitivity (~0.1% relative to ^{1}H) [45].

The dimensionality of NMR experiments is not limited to two and can expand further in order to both add nuclear correlation information and improve ability to resolve overlap (Fig. 2.1). For example, in the three-dimensional (3D) HNCO experiment, magnetization is transferred from ^{1}H (amide) to ^{15}N (amide) and then to a directly bonded ^{13}C (carbonyl). As in the HSQC, the magnetization is subsequently transferred back to

the ^{1}H for detection. Signals are modulated by each of these resonance frequencies, giving rise to cross-peaks with position in 3D space corresponding to each of the three associated chemical shifts. In a polypeptide, this will give rise to a cross-peak for each ^{1}H-containing peptide bond in the protein. Plotting the experiment in three dimensions thus further decreases signal overlap, since an additional separation relative to the ^{1}H-^{15}N HSQC is achieved through the ^{13}C' chemical shift dimension. Furthermore, the ^{13}C' chemical shift of a given peptide bond may be directly correlated to the associated ^{15}N and ^{1}H chemical shifts. A wide variety of other 3D NMR experiments relying on different correlations have also been developed, giving great versatility in both spectral dispersion and chemical correlation capabilities. For these reasons, the use of multi-dimensional NMR experiments has become common for structural characterization of proteins.

2.5.1 APPLICATIONS OF THE ^{1}H-^{15}N HSQC EXPERIMENT

The ^{1}H-^{15}N HSQC experiment was an especially useful NMR experiment for my thesis research, as will be evident in Chapters 6 and 7. To reiterate, the 2D ^{1}H-^{15}N HSQC spectrum provides cross-peaks that correlate the chemical shifts of ^{1}H nuclei to those of directly bonded ^{15}N nuclei (Fig. 2.2). Correspondingly, cross-peaks show chemical shift correlation for the amides of peptide bonds, asparagine and glutamine side chains and of amines in basic residue side chains [44]. Since NMR-active nuclei can act as probes to provide information on the chemical environment around them, the 2D ^{1}H-^{15}N HSQC cross-peak pattern is representative of the protein conformation under a specific condition (Fig. 2.2). For this reason, the ^{1}H-^{15}N HSQC cross-peak pattern may be referred to as a "finger print" of protein conformation [44]. In my thesis, comparative analysis of HSQC

spectra was instrumental in identifying conformational differences between proteins and isoforms (Chapter 6), and changes in response to environmental perturbation such as temperature modulation (Chapter 6) or direct interaction with membrane mimetics (Chapter 7).

As will become further evident in the relevant chapters, ^{1}H-^{15}N HSQC cross-peak patterns also directly represent processes of conformational sampling, and the equilibrium between states, with a dependence upon the rate of this sampling process relative to the NMR time-scale [46] (Fig. 2.3). This is based on the observation of cross-peak signal intensity, the number of observable cross-peaks, and/or chemical shift change for a given cross-peak. Specifically, fast-exchange in the NMR time-scale ($\leq \mu s$) is evidenced by the presence of a single cross-peak for multiple states, while the slow-exchange time-scale (~s) leads to separate cross-peaks being visible for each exchanging state. The intensity of these peaks represents the quantity of each conformer for the protein undergoing slow-exchange on the NMR time-scale. In contrast, when conformational change occurs under fast-exchange regime, the cross-peak is the weighted average of the chemical shifts, where the weighting is proportional to the population of each conformation sampled. Finally, for conformational exchange processes that occur on the intermediate-exchange time-scale (μs-ms), the result is actually a loss of observable NMR signal. Thus, detailed comparison of assigned ^{1}H-^{15}N HSQC spectra as a function of cross-peak pattern and peak intensities will be indicative of the number of different conformations sampled by a target protein and the equilibrium state. Changes in conformation that occur due to environmental factors such as binding to membrane-mimetics (Chapter 6 and 7) may also be directly monitored through the resulting change

in cross-peak pattern and intensities. This, in turn, may be applied to identify the specific residues responsible for binding alongside the equilibrium state (or affinity) of a target protein for a given binding partner.

2.5.2 SEQUENTIAL PROTEIN BACKBONE ASSIGNMENT USING 3D NMR EXPERIMENTS

In Chapters 6 and 7, Greek nomenclature will be used for protein backbone assignment, following the internationally-mandated standards [47]. In this nomenclature, backbone nitrogen and carbonyl carbons making up a peptide bond are referred to as N and C'. As in biochemical convention, the carbon to which the amino acid side chain is attached is referred to as the alpha carbon (C_α) and the side chain is annotated with an incremented Greek letter for each heavy atom away from C_α, starting with C_β. Protons are annotated according to the heavy nucleus that they are bonded to. Thus, H_N, H_α and H_β would represent a backbone amide proton, alpha carbon-bonded proton, and beta carbon-bonded protein, respectively.

There are multiple methods of assigning chemical shifts to each nucleus (e.g., C', C_α, and C_β) of a target protein. However, all methods share a similar underlying mechanism. These methods require i) correlation of the observed chemical shifts to those expected for a given type of amino acid for classification purposes, and ii) analysis of cross-peaks that provide connectivity between residues using either direct bonding or proximity of NMR active nuclei as a mechanism to produce inter-residue correlations. Unique patterns of backbone nuclei chemical shifts are produced for each amino acid [43]. These expected backbone chemical shift patterns are also affected by environmental

conditions (e.g., secondary structuring and solvent properties) [48], a phenomenon which has been characterized to better assist in protein assignment.

In my thesis, I used the main chain-directed approach (commonly known as the "backbone walk" approach [44], Fig. 2.4 and 2.5) to assign the protein backbone. This approach usually requires collection of 3 pairs of complementary triple-resonance experiments: i) HNCA [49] and HN(CO)CA [50], ii) HNCO [49] and HN(CA)CO [51], and iii) HNCACB [52] and HN(CO)CACB [52]. Each pair is anchored in the ^{1}H-^{15}N spin pair of a residue in position i and connects it to a ^{13}C nucleus (or nuclei) in residue in position i-1 (i.e., the residue N-terminal to i) with one of the two experiments in the pair also connecting to the same ^{13}C nucleus/nuclei in residue i. This connectivity anchored from the ^{1}H-^{15}N spin pairs allows for "walking" along the backbone (Fig. 2.4 and 2.5). All of these experiments rely on the direct transfer of magnetization to neighboring nuclei directly through chemical bonds. For example, in the HNCO experiment introduced above, the initial magnetization is passed from the H_N to N of residue i and then transferred specifically to C' of residue i-1, with a subsequent return back to H_N through N. As a result, a single observable cross-peak will show a correlation in 3D with each dimension corresponding to a single chemical shift: ^{1}H and ^{15}N for H_N and N of residue i, respectively, and ^{13}C for the C' of residue i-1. In the paired experiment, the HN(CA)CO, magnetization is transferred from H_N and N to the C_α of residues i and i-1 (a nucleus not directly observed in this experiment) and then on to the C' of both the residue. Following the return to the ^{1}H, the HN(CA)CO produces two observable cross-peaks having identical ^{1}H and ^{15}N frequencies, from residue i, but with distinct ^{13}C frequencies corresponding to the C' nuclei of (1) residue i and (2) residue i-1. By taking "slices" in

the ^{1}H and ^{15}N dimension (yellow squares in Fig. 2.4) and overlaying HNCO and HN(CA)CO spectra (Red and blue dots in Fig. 2.4), the order of H_N, N and C' chemical shifts with respect to the polypeptide sequence become apparent, allowing for the "backbone walk" to determine the sequential chemical shift assignment of these nuclei. Similarly, HNCACB:HN(CO)CACB correlate H_N and N of residue i to the C_α and C_β of i and i-1 while HNCA:HN(CO)CA correlate H_N and N of residue i to only C_α of i and i-1. Notably, in experiments such as HN(CA)CO, HNCA, and HNCACB, which show cross-peaks for residues i and i-1, the cross peak connecting to i-1 tends to be weaker due to poorer transfer of magnetization between nuclei compared to residue i (Fig. 2.4). This trend can be instrumental in the backbone assignment. In particular, I encountered this with studies of apela isoforms as some of the paired experiment sets acquired failed due to instrumental calibration issues with the spectrometer.

Finally, for sidechain assignment, experiments such as ^{1}H-^{1}H total correlation spectroscopy (TOCSY) [53], ^{13}C-/^{15}N-edited TOCSY-HSQC [44] and/or the HCCH-TOCSY [54] are required. In these experiments, magnetization is transferred from one ^{1}H to other ^{1}H nuclei that are connected through heavy atoms that are chemically bonded together. Effective ^{1}H-^{1}H TOCSY connectivity will be lost, for instance, at quaternary carbons. As an example of the flow of energy in this experiment, H_N can transfer its magnetization to the neighbouring H_α, which can then either transfer this back to H_N or on to H_β. This would result in cross-peaks with observable chemical shifts for all ^{1}H nuclei in a protein, for example at positions H_N-H_α, H_N-H_β, and H_α-H_β as well as the corresponding pairs with the x and y dimensions inverted. Given the relatively large number of ^{1}H nuclei in a protein, 3D experiments such as TOCSY-HSQC and HCCH-

TOCSY simplify the resulting spectra by directly correlating observable ^{1}H chemical shifts to a heteroatom (e.g., ^{13}C or ^{15}N), which decreases spectral overlap in the manner described earlier.

Assigned chemical shifts can be used to identify secondary structuring by comparing the observed chemical shifts to expected random coil chemical shifts (e.g., through the chemical shift index (CSI) [55, 56] or algorithms such as Dihedral Angles from Global Likelihood Estimates (DANGLE) [57] or Torsion Angle Likelihood Obtained from Shift and Sequence Similarity + (TALOS+) [58]). Comparison of chemical shifts can also highlight conformational changes that may not lead to canonical secondary structuring. In my thesis, I have employed the Euclidian combined chemical shift displacement (CSD) (frequently referred to as chemical shift perturbation) [59] for residue *j*:

$$CSD_j = \frac{1}{N}\sum_{i=1}^{N}\left|\frac{\gamma_i}{\gamma_H}\Delta\delta_{ji}\right| \tag{2.7}$$

where γ_i and γ_H are the gyromagnetic ratios of nucleus *i* and ^{1}H, respectively and $\Delta\delta$ is the difference in chemical shifts for nucleus *i* (e.g., H_N, N, C_α and C') in residue *j* between two different conditions. Thus, CSD combines chemical shift perturbations of different nuclei by normalizing them according to gyromagnetic ratio. This has the capability to provide more quantitative detail regarding structural changes in response to environment than simply comparing ^{1}H-^{15}N HSQC cross-peak displacement.

2.5.3 NMR RELAXATION

Proteins are inherently dynamic, which is often very important to allow the adoption of the various conformations required to carry a given function [60]. NMR

spectroscopy provides an ideal method to characterize biomolecules such as proteins as it is capable both of characterizing individual, site-specifically assigned nuclei within the molecule and is able to monitor processes that occur over a wide range of time-scales. For example, R_1 (the longitudinal relaxation rate constant), R_2 (the transverse relaxation rate constant), and the heteronuclear nuclear Overhauser effect (NOE) enhancement factor are all affected by motions that occur on the ps-ns time-scale. These are also influenced, in a less straightforward manner, by μs-ms chemical exchange [61]. R_1 is a first-order rate constant describing the re-establishment of thermal equilibrium (e.g., the net magnetization vector along B_0 at equilibrium introduced above) following perturbation away from equilibrium [41]. R_2 is a first-order rate constant describing the loss of coherence between nuclear spins, a process that results in the loss of any observable magnetic moment perpendicular to the B_0 field. Lastly, the heteronuclear NOE is a cross-relaxation process arising from a dipole-dipole interaction between nuclei in sufficiently close proximity. The NOE enhancement factor depends upon the distance between the nuclei and upon the rate at which they move relative to each other. All three of these NMR relaxation phenomena are affected by molecular dynamics or motion [44], and can be experimentally determined for each resolvable nucleus in a sample. Through appropriate consideration of the resulting relaxation parameters, NMR spectroscopy can thus provide valuable insight into the dynamics of a protein at the atomic-level scale.

In practice, ^{1}H-^{15}N heteronuclear correlation experiments are very commonly used to measure relaxation phenomena in proteins. As introduced in Section 2.5.1, the ^{1}H-^{15}N HSQC provides a decrease in spectral overlap relative to a 1D spectrum and is frequently less congested than a ^{1}H-^{13}C HSQC. Given that all residues have an amide

proton except for prolines, use of ^{1}H-^{15}N relaxation parameters provides at least one probe of molecular motion for nearly every residue. An additional benefit of this is that ^{1}H-^{15}N bond parameters in a peptide bond are well defined and quite uniform, meaning that the theoretical framework for consideration of these relaxation phenomena have been robustly worked out [62].

The experimental values of R_1, R_2, and heteronuclear NOE relaxation can be interpreted in number of different ways [61]. However, in my thesis, I have employed only the heteronuclear NOE enhancement factor as a probe of protein dynamics so I will focus on its interpretation. The enhancement factor of the heteronuclear NOE is dependent upon the signs of the gyromagnetic ratios of the nuclei observed [63]. Consequently, this "enhancement" may give rise to either an increase or decrease in the observed magnetization upon cross-relaxation, which is visualized by a proportional change in NMR signal intensity for the nucleus being enhanced. In a ^{1}H-^{15}N heteronuclear NOE experiment, the distance between the two nuclei is tightly constrained by the covalent bond. Hence, the primary contributor to the observed enhancement factor will be motion. Both the global tumbling of the molecule and local variation of backbone motion at each residue corresponding to segments of flexibility or rigidity will affect this (S^2 of Fig. 2.6). Assuming a relatively consistent global tumbling rate for a given protein means that local variations in dynamics may be inferred by comparing HSQC peak intensities from spectra with and without NOE enhancement. On another note, if global tumbling rate decreases due to changes in conditions such as interaction with other molecules (e.g., peptide-micelle binding; Chapter 7), the expected NOE enhancement changes in response (Fig. 2.6; blue vs. green vertical lines). Thus, comparison of ^{1}H-^{15}N

heteronuclear NOE enhancement values between two different peptide states (e.g., free vs. micelle-bound peptide) is indicative of local variation in backbone behaviour in response to varying conditions. In ^{1}H-^{15}N heteronuclear NOE enhancement experiments, due to the opposing signs for the gyromagnetic ratios of ^{1}H and ^{15}N, the NOE enhancement reduces cross-peak intensity for amides located in regions of internal flexibility and the peak intensity ratio cannot exceed 1. Depending upon the degree of local flexibility, the observed NOE enhancement can thus range from a theoretical maximum of 1 to negative values.

2.5.4 DIFFUSION ORDERED SPECTROSCOPY (DOSY)

Pulsed field gradient (PFG)-based diffusion ordered spectroscopy (DOSY) is a highly sensitive and accurate NMR spectroscopy technique for analyzing the hydrodynamics of molecules or supramolecular assemblies [64, 65]. Namely, the translational diffusion coefficients of each NMR observable component of the sample can be determined. DOSY was a key technique in my thesis for studying of apelin- and apela-micelle interactions, discussed in Chapter 7, as it allowed quantification of the population of micelle-bound relative to free proteins (Appendix B).

DOSY experiments depend upon a PFG with defined gradient strength (g) and duration (δ). In the simplest version of this experiment, an initial PFG pulse produces a phase shift in the resonance frequency of a nuclear spin that is dependent upon its position in the NMR tube. Then, the nuclear spins are allowed to diffuse for a set time period (the diffusion time, Δ), at which point a second PFG pulse is applied in a reversed manner relative to the first PFG pulse. If a given type of nuclear spin does not diffuse during Δ, then the second PFG pulse will refocus its phases perfectly and result in

practically no loss (other than R_2-based relaxation) in observable NMR signal. However, if diffusion occurs during Δ, magnetization will not be refocused perfectly upon application of the second PFG pulse due to differences in the phase offset as a function of position and an NMR signal with lower intensity will be observed. Actual DOSY experiments are typically more involved than this in terms of the number of PFG pulses applied and the manner in which the magnetization is manipulated between the first and second PFG pulses; however, the basis of the experiment remains identical in that greater translational motion will give rise to greater signal attenuation. Interpreting the translational diffusion coefficients determined from DOSY can then be used to estimate the quantity of interaction between molecules, such as protein and membrane mimetics (Chapter 7), using an appropriate model (Appendix B).

In DOSY, one of the signal attenuating parameters will be varied, and a series of experiments will be acquired and analyzed. The translational diffusion coefficients (*D*) for each diffusing species in a given DOSY experiment can then be calculated based on the Stejskal-Tanner relationship [66]:

$$I = I_0 \, e^{-D \, g^2 \gamma^2 \delta^2 \left(\Delta - \frac{\delta}{3}\right)} \tag{2.8}$$

where *I* is the observed intensity at a given value of gradient strength (g), I_0 is the intensity in the absence of attenuation (in practice, at 2% gradient strength), and γ is the gyromagnetic ratio of the nucleus. Since NMR relaxation (e.g., R_1 and R_2) also causes observable signal loss, these experiments are conducted with varying gradient strengths of fixed length (g) rather than varying the period of diffusion allowed (Δ) to maintain the same experimental time periods, meaning that the only variation in *I* relative to I_0 at a given value of g will be due to diffusional loss.

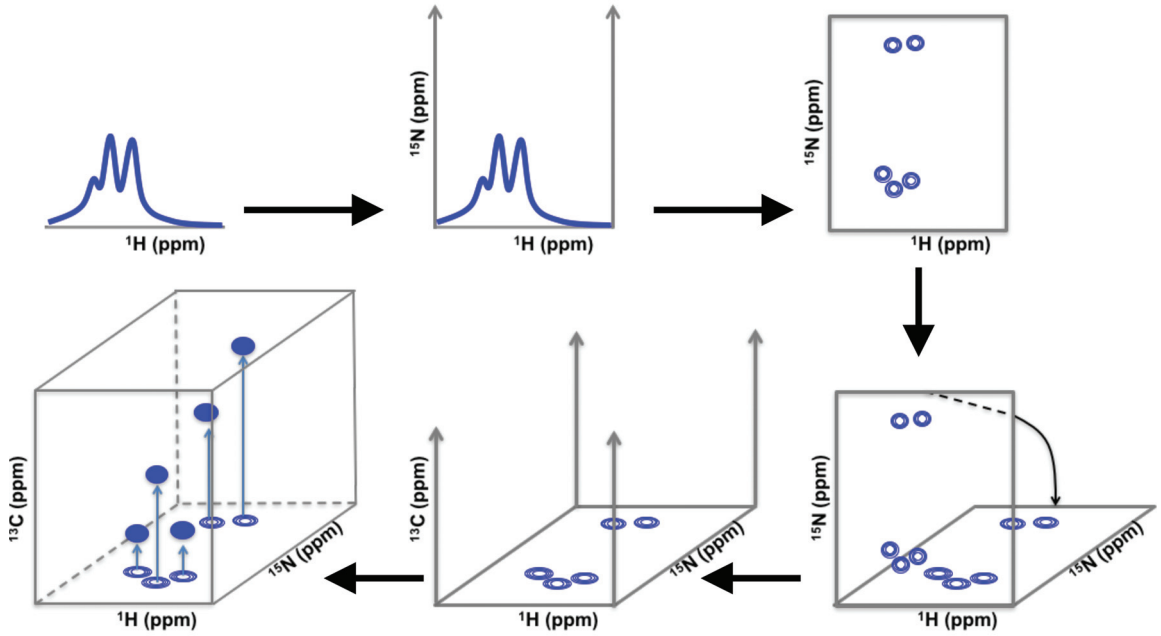

Figure 2.1: Schematic illustration of 1D vs. 2D vs. 3D NMR experiments. A 1D ^{1}H NMR spectrum is illustrated in the top left. Through addition of a second dimension correlating ^{1}H (x-axis) to ^{15}N (y-axis) and leading to cross-peaks having chemical shifts of both nuclei, signal overlap is further reduced (top right). Finally, a third dimension is added, which is visualized after flipping of the ^{15}N dimension from the y- to the z-axis, with correlation to ^{13}C (new y-axis) providing cross-peaks with distinct sets of ^{1}H, ^{15}N, and ^{13}C chemical shifts (bottom left).

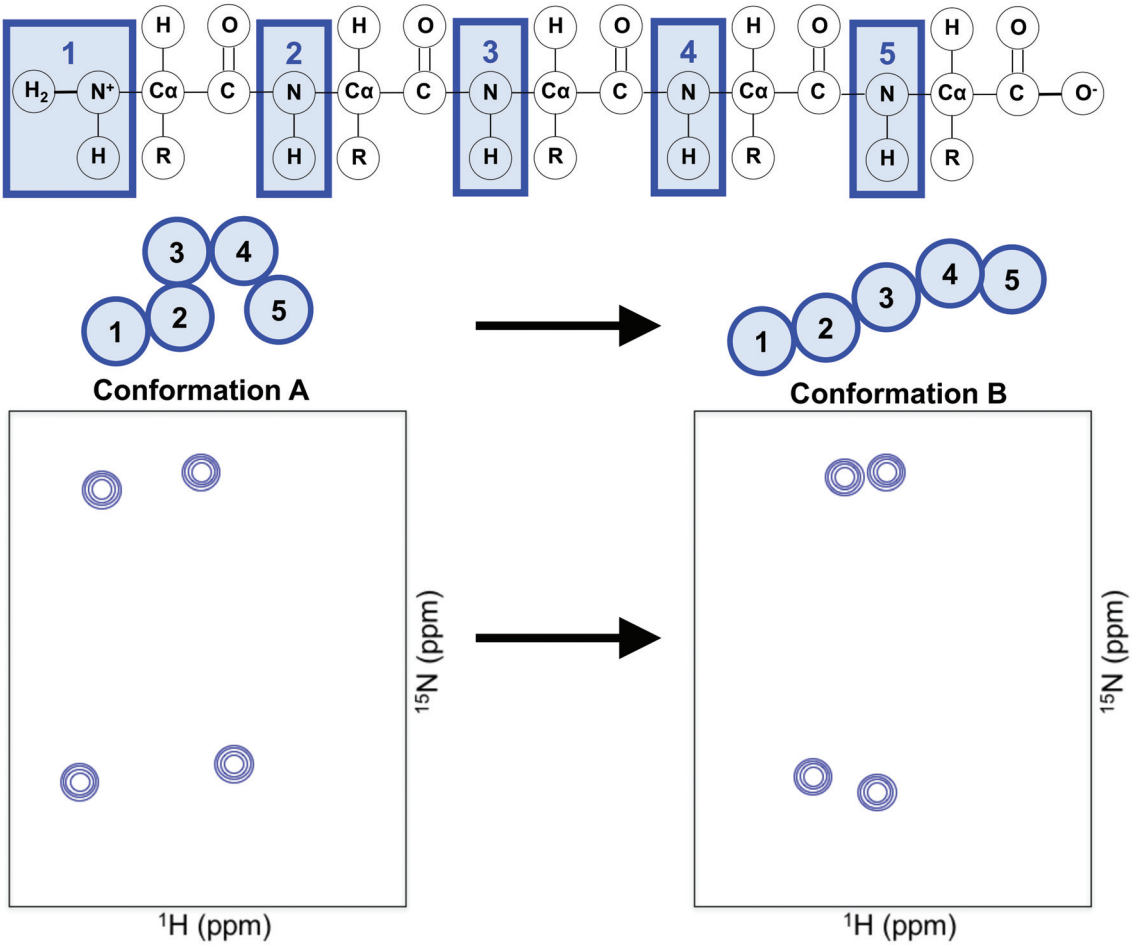

Figure 2.2: ^{1}H-^{15}N HSQC experiments as "fingerprints" of protein conformation. A pentapeptide is illustrated in two conformations (A and B). Each circle in a peptide represents a numbered residue having a ^{1}H-^{15}N bond, with the variation in polypeptide conformation illustrated schematically. A change from conformation A to B gives rise to a change in the resulting cross-peak pattern in the ^{1}H-^{15}N HSQC spectrum. Note that there are only four observable cross-peaks (from amides 2-5) on the sample ^{1}H-^{15}N HSQC spectra as protons in the N-terminal amine will undergo fast exchange, relative to the time-scale of the NMR observation, with those in solvent molecules (e.g., H_2O).

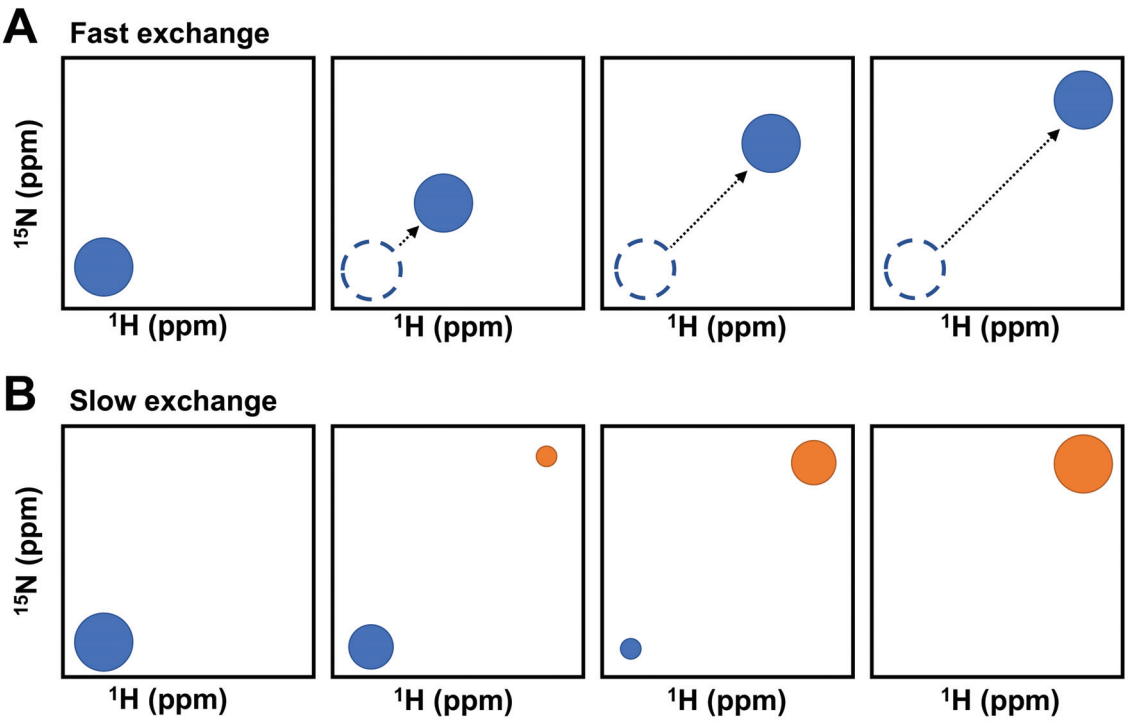

Figure 2.3: Effects of fast and slow exchange processes upon ^{1}H-^{15}N HSQC experiment A) A protein undergoing conformational change in fast-exchange will show a single cross-peak for a given residue, in which the position of the cross-peak is determined by the relative chemical shifts of various conformations weighted by population (two conformations in this figure). A scaled change in cross-peak position (i.e., in both ^{1}H and ^{15}N chemical shift) is observed if the equilibrium between states is tilted from strongly favouring one state (i.e., cross-peak in bottom left) to the other (top right). B) A protein undergoing slow-exchange on the NMR time-scale will exhibit two peaks for a single residue, assuming distinct chemical environments of the given residue in two different conformations (blue vs. orange cross-peaks). The relative intensities of each cross-peak represent a change in the proportion of one conformer relative to the other, with a direct relation between cross-peak intensity (or volume) and population.

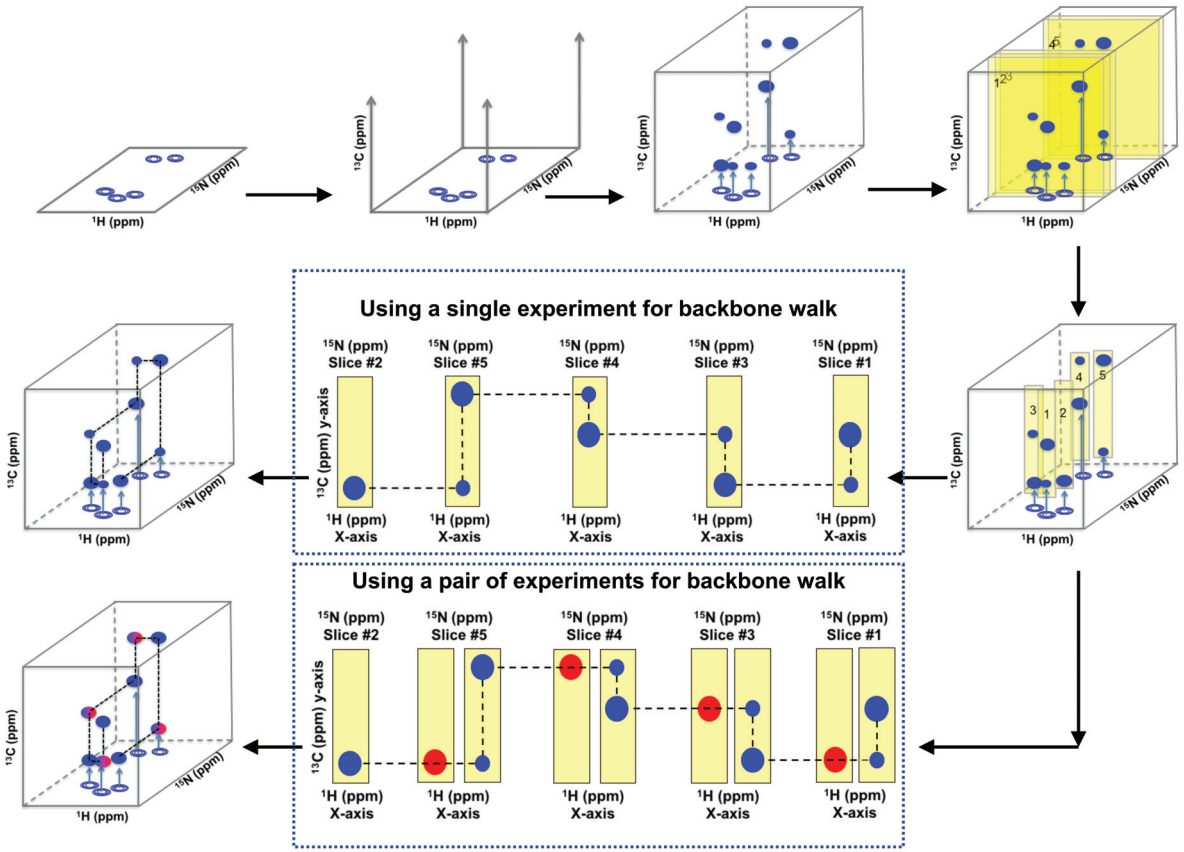

Figure 2.4: Illustration of triple-resonance NMR backbone walk sequential assignment strategy.
Backbone walk experiments rely either upon differences in intensity for one residue vs. another ("single experiment"), where the ^{13}C chemical shift a more intense peak in one $^{1}H/^{15}N$ "slice" pairs with the less intense peak in the slice from a neighbouring amine. In the paired experiment approach, one experiment provides a ^{13}C correlation only to a single amino acid (red peaks, bottom), while the other connects to both that residue and a neighbour (blue peaks, bottom; identical to experiment shown in middle). Comparison of $^{1}H/^{15}N$ slices having two "blue" vs. one corresponding "red" peaks allows a "walk" from one residue to the next along the backbone.

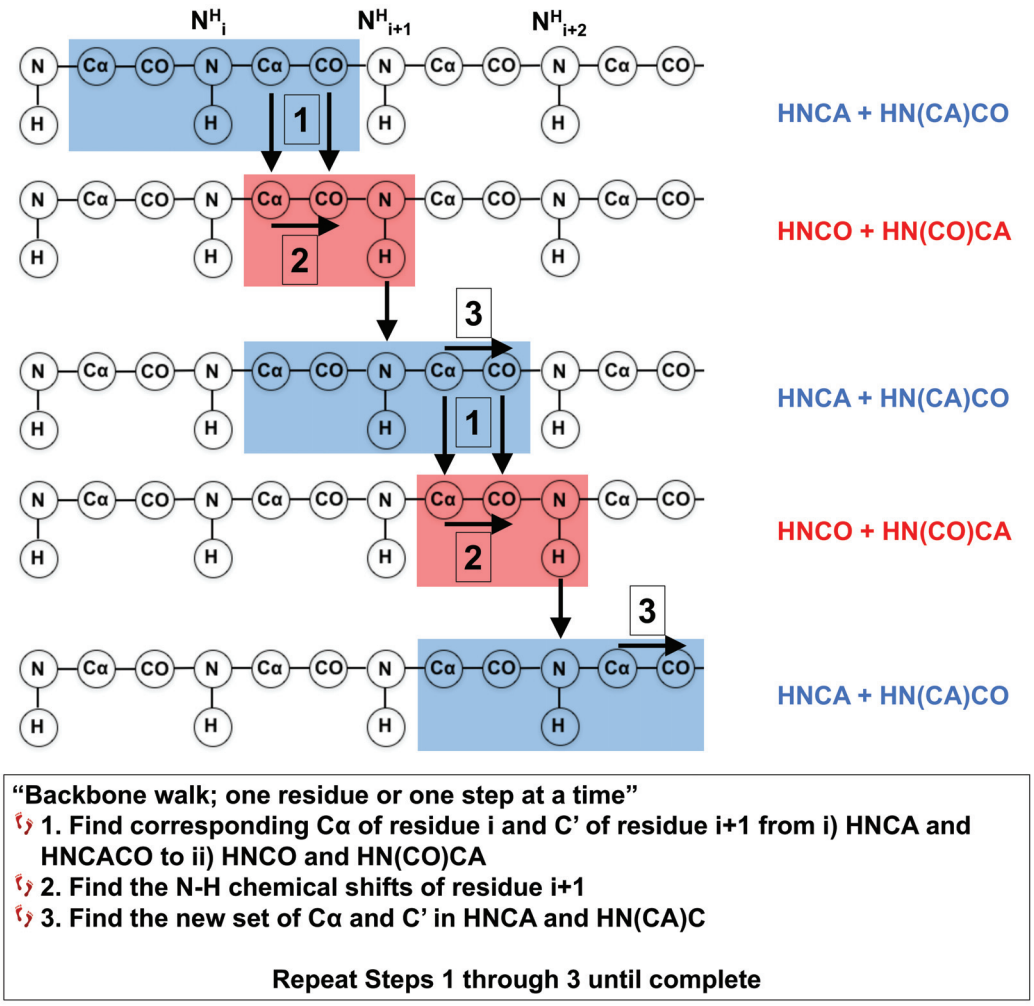

Figure 2.5: Backbone walk (or main chain directed) approach illustrated with respect to a polypeptide chain.
In the illustrated example, two paired sets of experiments are used to allow a complete backbone heavy atom and H^N chemical shift assignment. The HNCA correlates the ^1H and ^{15}N of residue i to the Cα of both i and i-1, pairing directly with the HN(CO)CA which correlates ^1H and ^{15}N of residue i only with i-1. In the HN(CA)CO, ^1H and ^{15}N of residue i are correlated to C' of i and i-1, pairing directly with the HNCO which correlates ^1H and ^{15}N of residue i to C' of i-1. Combined assessment of all four of these experiments will provide a full chemical shift assignment for all nuclei being correlated, broken only by a proline.

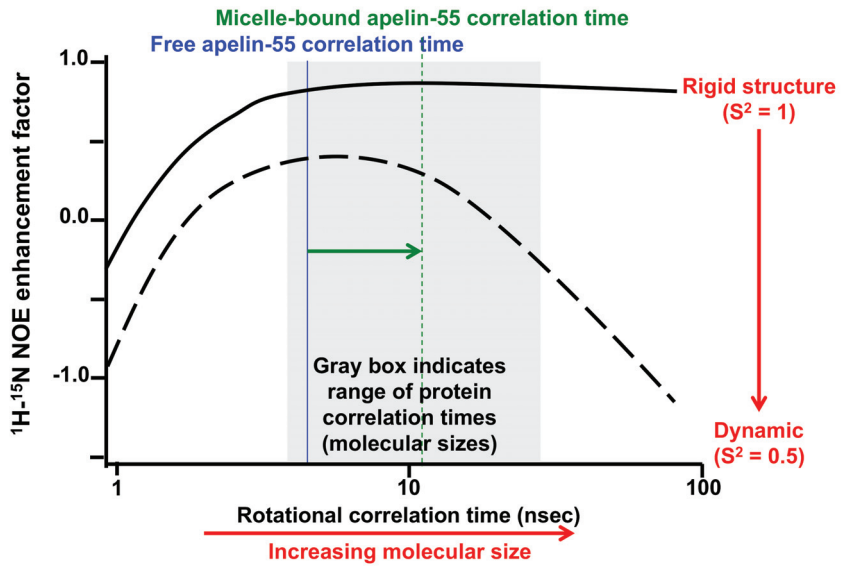

Figure 2.6: Relationship between tumbling, local flexibility in a protein, and the ^{1}H-^{15}N heteronuclear NOE enhancement.
Overall molecular tumbling is reflected in the rotational correlation time (τ_c), with a larger τ_c being consistent with larger size and the grey shaded box illustrating the typical range for proteins. Local flexibility is represented by the order parameter (S^2), which decreases from an absolute maximum of 1 as the degrees of dynamic behaviour increases. As illustrated in the solid line ($S^2 = 1$) vs. dashed line ($S^2 = 0.5$), the magnitude of the ^{1}H-^{15}N heteronuclear NOE enhancement factor directly depends upon both global tumbling and local polypeptide dynamics. In the specific case of a protein-micelle interaction, complex formation would result in an increase in τ_c. The illustrated blue line represents the predicted τ_c of a free apelin-55 molecule while the green line represents the increased τ_c in response to micelle binding, demonstrating the expected modulation of the heteronuclear NOE as a function of internal dynamics at a given site in the protein and as a function of protein-micelle binding. Figure is based on Figure 19.9 of reference [63].

CHAPTER 3 OVERVIEW OF THE APELINERGIC SYSTEM

(Note: parts of this chapter are based on sections, authored by me, of a paper entitled "Apelinergic system structure and function" in ***Comprehensive Physiology*** (2017), which was accepted on August 23 2017 for publication [67]. The paper presents multiple tables listing various roles of apelin and apela under both physiological and pathological settings. Furthermore, the tables indicate which apelin/apela isoform was used to study its role. However, only two of these tables were included as they were the most pertinent to the thesis.)

The focus of my thesis is characterizing ligand processing, functional behaviour, and biophysics of the apelinergic system. This system is composed of two peptide ligands (apelin and apela) and a single class A G-protein-coupled receptor (GPCR) called the apelin receptor (abbreviated herein as AR; also known as APJ). Each ligand has multiple endogenous bioactive isoforms with varying potencies (Table 3.1) and binding of these ligands to the AR may exert a variety of important functions, which include increasing heart muscle contractility, vasodilation, modulation of glucose and insulin homeostasis, and cardiovascular system development. Furthermore, the apelinergic system has been linked with number of pathological conditions, including chronic heart failure, diabetes, obesity, and human immunodeficiency virus (HIV) infection. For these reasons, the apelinergic system has been highlighted as having strong potential for therapeutic targeting. In this chapter, I highlight and summarize some of the important functions that the apelinergic system plays in both physiological and pathological conditions and the complexities that arise from the presence of multiple bioactive isoforms.

3.1 THE APELIN RECEPTOR

The AR is a class A rhodopsin-like GPCR that was identified in 1993 by O'Dowd *et al.* for its ~40-50% sequence identity with the angiotensin II receptor [68]. AR has 380-residues, which is arranged to present an extracellular N-terminus, seven α-helical transmembrane (TM) segments with three intracellular and extracellular loops connecting the TM segments, an intracellular membrane-associated eighth α-helix and a cytoplasmic C-terminus (Fig. 3.1) [69]. The AR is also highly homologous to the chemokine receptors CXCR4 and CCR5, and can similarly facilitate HIV infection [70, 71]. In addition, like CXCR4 and CCR5, the AR presents consensus sites for post-translational modifications such as phosphorylation, glycosylation, palmitoylation and sulfation [68, 72]. While phosphorylation of AR has been shown to regulate signalling bias [72], the roles of other modifications remain uncharacterized.

Although the AR presents high sequence similarities to angiotensin II receptor, the AR showed no interaction with angiotensin II [68, 73]. Instead, its ligands, apelin and apela, were identified in 1998 [74] and 2013 [75, 76], respectively. Since the discovery of AR ligands, much focus has been on identifying the physiological roles of apelin and apela and the signalling pathways that are activated. As will be further detailed in Sections 3.2 (apelin) and 3.3 (apela), ligand-AR interactions play important physiological roles in the body, including the central nervous system, cardiovascular system, and adipoinsular axis function. AR binding by apelin and apela activates various signalling molecules (e.g. ERK, Akt, and AMPK) through G-protein and β-arrestin-mediated

pathways. Some of these signalling pathways involved in AR signalling are shown in Table 3.2 for apelin and Table 3.3 for apela.

The AR crystal structure was recently determined in complex with an apelin-mimetic peptide agonist [69]. This structure shows an extracellular anionic surface groove, which is notable as it may facilitate interaction with the ligands, given their highly cationic nature. In support of this, mutations of acidic residues such as E20 and D23 in the N-terminus of AR obstructed apelin binding [77] and signalling [78]. Similar to other proteins, conformational variability is important for GPCR function (e.g., adenosine A_{2A} receptor [79]). Given the broad range of ligands with length-dependent pharmacological properties, the AR seems likely to adopt different conformations and dynamics to mediate ligand-dependent potency and efficacy. Specifically, the AR may adopt a different equilibrated conformation, or a set of conformations, in response to isoform binding. The isoform-mediated variance in AR conformation(s) will then alter the binding affinities of downstream signalling molecules to favour one signalling pathway over another (e.g., G-protein vs. β-arrestin), causing the differences observed in signalling/functional assays.

3.2 APELIN

In 1998, Tatemoto and coworkers identified a family of peptides from bovine stomach tissue extracts which acted as ligands for the orphan GPCR AR (APJ) [74]. On the basis of this interaction, the family of peptides was named ‘apelin’, short for APJ Endogenous Ligand, with a specific nomenclature of apelin-n specifying that a given isoform has “n” amino acids [74]. In this study, it was noted that the apelin (*APLN*) gene

encodes a 77-amino acid long protein, denoted as a preproprotein, with high sequence conservation exhibited in humans, cattle, mice, and rats (Fig. 3.2) [74]. Based upon our studies and as will be discussed in the subsequent chapters of my thesis, proapelin does not appear to be a strictly inactive proprotein. Therefore, in this thesis, this 77-residue form of apelin will be referred to as a pre(pro)protein to delineate this behaviour from that of a classical preproprotein, which produces an inactive proprotein upon signal peptide removal.

Closer examination of the pre(pro)apelin sequence demonstrates that its 23 C-terminal residues are completely conserved in human, cattle, mice and rats. Extending this analysis to non-mammalian species, the 12 C-terminal residues of the pre(pro)protein are identical over a wide range of fish as well as *Xenopus laevis* [80] (Fig. 3.2). Of importance throughout this thesis, these 12 C-terminal residues are essential for AR binding and activation. Following localization of the APLN gene on the X chromosome in humans [81], low levels of genetic variability have been observed in subsequent comparative genomics studies. These genetic variations have typically been isolated to single nucleotide polymorphisms and, consistent with the high level of amino acid conservation over numerous species, have been found only outside of the APLN coding regions [82-87].

3.2.1 APELIN PROCESSING

The 77-residue pre(pro)apelin comprises a putative N-terminal 22-residue signal peptide and a 55-residue C-terminal domain containing the receptor-binding site [74, 88]. Dimerization of pre(pro)apelin occurs by cystine-mediated disulfide bridge formation and has been shown to be impaired through reduction by dithiothreitol [89]. Both monomeric

and dimeric forms of pre(pro)apelin were observed in both whole-cell lysate of transiently transfected COS-7 cells and in heart tissue of transgenic mice, while only the dimeric form was observed *in vivo* in wildtype mice [89]. It should be noted that the only cysteines in pre(pro)apelin are located in the signal peptide domain (Table 3.1). Dimerization has previously been noted as a prerequisite step for proper processing in other prepropeptides, such as somatostatin-II [90], suggesting that dimerization may also be a prerequisite step for proper pre(pro)protein processing in the apelinergic system. Following signal peptide cleavage, exclusively monomeric apelin would, thus, be expected as the bioactive form.

Upon the discovery and first report of apelin by Tatemoto *et al.* [74], it was suggested that removal of the signal peptide by signal peptidases in the endoplasmic reticulum (ER) would produce a 55-residue isoform (apelin-55). Based on evidence (or, more accurately, lack of evidence) discussed below, this 55-residue isoform was presumed to be an inactive precursor (i.e., proprotein) and, thus, denoted as proapelin. Analysis of the apelin-55 sequence demonstrated the presence of multiple dibasic amino acid motifs [74], indicative of the potential for proprotein convertase subtilisin kexin (PCSK)-mediated proprotein processing [91] at multiple sites. Based on these predicted sites of processing, Tatemoto *et al.* synthesized apelin-36, -17, and -13 alongside the N-terminally pyroglutamate-modified apelin-13 (Pyr-apelin-13) and compared them to the peptide isolated from bovine stomach tissue by gel filtration chromatography and polypeptide sequencing [74]. From this analysis, they concluded that apelin-36 was the isoform isolated from bovine stomach tissue.

Despite identification of apelin-36 as the form of apelin isolated from stomach tissue, all four tested isoforms were shown to activate the receptor, as observed by a ligand-mediated acidification assay in CHO cells [74], and clearly indicated the importance of C-terminal residues in receptor binding and signalling (the essential residues/components of apelin are further detailed in our review paper, reference [67]). Interestingly, the shortest 13-residue isoforms (i.e., apelin-13 and Pyr-apelin-13) were the most active. Apelin-55, conversely, was not detected in bovine stomach extracts. This led to the conclusion that it was likely an inactive proprotein, with apelin-77 consequently labeled as a preproprotein [74]. The three processed isoforms introduced by Tatemoto *et al* [74]. (apelin-36, -17, and -13 alongside the pyroglutamate-modified form Pyr-apelin-13) have received by far the most attention, with by far the greatest emphasis being on apelin-13. This focus has likely arisen due to the relatively high potency of this isoform [74] and the cost-effectiveness of obtaining it.

Based on annotation of apelin-55 as proapelin, the hypothesis was made that only the N-terminally truncated versions of apelin-55 were bioactive, with length-dependent potency [74, 88]. This hypothesis led, in turn, to the suggestion that apelin processing occurred initially to produce apelin-36 from the 55-residue isoform, and apelin-36 acts as a precursor to be further processed to shorter and more potent isoforms, apelin-13 or -17 [88, 92]. In contrast to this theory, apelin-55 was detected in bovine colostrum and milk [93], and isoforms longer than apelin-36 was detected in plasma [94], which casts doubt on the accuracy of this theory. In further elaboration of this discrepancy, the next three chapters of my thesis will outline the evidence I have built to show that apelin processing mechanisms are more diverse than initially envisioned.

In addition to the various apelin isoforms that are obtained through proteolytic processing, apelin can be further post-translationally modified. One such modification, introduced above, is the spontaneous cyclization of the N-terminal glutamine of apelin-13 to pyroglutamate [95, 96], providing Pyr-apelin-13. This modified isoform has increased stability, as reflected in increased plasma half-life [97], likely through loss of the free primary N-terminal amine recognized by N-terminal exoproteases [98].

Another well characterized modification of apelin is the hydrolysis of C-terminal phenylalanine by angiotensin converting enzyme-2 (ACE2), a plasma metalloprotease, which removes the C-terminal phenylalanine of all apelin isoforms [99]. Notably, removal of this phenylalanine has been linked to decreased cellular response, with significant loss of hypotensive effects in mice for apelin-13 and -17 upon loss of their C-terminal phenylalanine [100]. Thus, this process has justly been attributed to be an apelin deactivation pathway. However, discrepancies exist as to whether C-terminal truncation leads to significant decrease in physiological function [101] and signalling biases [102].

In light of potential modulation, but not complete loss, of activity upon C-terminal truncation of apelin isoforms by ACE2, full deactivation processes likely involve more severe endo/exoprotease-mediated cleavage than the removal of a single amino acid. In support of this, the zinc-dependent metalloprotease, neprilysin, was recently identified to cleave after RPR or RPRL in the “RPRL” motif of the conserved C-terminal 12 residues required for activity [103]. This motif, which is discussed in more detail in Chapter 6 and 7, has been shown to be functionally essential and to present unique biophysical characteristics. Cleavage in this region would lead to inactive N- and C-terminal fragments, as peptides missing R, RP, or RPR residues of the RPRL motif have been

shown to be unable to decrease arterial blood pressure [104]. C-terminal truncations also resulted in inactivation of apelin peptides. Specifically, apelin peptides truncated beyond the three C-terminal residues (MPF) showed ~2000-fold reduction in activity, while truncation of one or two C-terminal residues resulted in an ~20-fold loss, as demonstrated with Ca^{2+} mobilization assays [105]. Thus, endo/exoproteases other than neprilysin are likely to be involved in the deactivation process.

Supporting the likelihood of other, as yet unidentified, post-translational processing, shorter apelin fragments lacking various numbers of N-terminal residues were detected in bovine colostrum and milk (e.g., apelin-35, -18, and -15) [93]. This provides a much wider variety of potential bioactive apelin isoforms than those first identified by Tatemoto *et al*. [104]. In addition, isoforms lacking up to three C-terminal residues (i.e., the C-terminal MPF) have also been detected in colostrum and milk [93] as well as in plasma [106], suggesting that there are likely exoproteases other than ACE2 that are responsible for complete deactivation. Finally, additional degradation patterns are evident [105, 106], all of which provide clear evidence of a complex pathway modulated by numerous enzymes.

3.2.2 APELINERGIC SYSTEM EXPRESSION IN THE BODY

Since the initial discovery of the apelin receptor [68] and then apelin [74] in the brain and stomach, respectively, the known tissue distribution of both the ligand and the receptor in the body have expanded to include the central nervous system, cardiovascular system, circulatory system, digestive system, reproductive system, and various peripheral tissues including adipose and skeletal muscles [71, 81, 92, 107-109] (Fig. 3.3A). The wide tissue distribution of the apelinergic system in rats, mice, and humans has been

well-reviewed by O'Carroll *et al.* [110]. In contrast to apelin, apela has thus far been found to have a relatively limited distribution. Chng *et al*., in the first report on apela, noted the presence of mRNA in adult human prostate and kidney [75]. Since then, apela has been detected in adult hearts [111, 112], kidneys [113], and pluriopotent stem cells [114]. Although there are some differences between apelin and apela localization, as a whole, this is indicative of broad functionality for the apelinergic system.

In addition to expression in diverse tissues, the levels of the apelinergic system ligands and their receptor can change with developmental state. During embryogenesis, apela and AR mRNA expression are enhanced, leading to apela-AR signalling which facilitates the migration of progenitor cells to the anterior lateral plate mesoderm for cardiovascular development in zebrafish [75, 76]. However, the levels of apela quickly drop subsequent to this, and apelin mRNA levels are enhanced.

Interestingly, dominant isoforms of apelin have been associated with various tissues, using detection methods such as enzyme immunoassays (EIA) and radioimmunoassays (RIA) in combination with separation techniques such as gel exclusion chromatography (GEC) or high-performance liquid chromatography (HPLC) (Fig. 3.3B). Through techniques of this nature, Pyr-apelin-13 was identified as the predominant isoform in heart [115] and brain [116] while apelin-36 was predominant in lungs, testis, and uterus [108]. Conversely, multiple dominant isoforms were shown to be present in or secreted from other tissues. For example, both Pyr-apelin-13 and apelin-36 are present at similar levels in mammary glands [108] and colostrum and milk contain apelin-55, -36, -17, -13 and many other modified isoforms [93]. Therefore, tissues and

organs demonstrate specificity in which, or even whether one, apelin isoform is predominantly produced and secreted over the others.

At present, confidently stating the major form that is found in circulation is not straightforward due to discrepancies in the literature. Specifically, nearly all major isoforms have been identified in plasma by various combinations of techniques. The dominant plasma apelin isoform(s) have specifically been identified as: i) Pyr-apelin-13 using HPLC-MS [97]; ii) Pyr-apelin-13 and -17 by GEC-RIA [116] and HPLC-RIA, with significantly less apelin-36 in comparison [117]; iii) apelin-13 by GEC-HPLC-RIA [118]; and, iv) isoforms longer than apelin-36 by GEC-RIA [94]. It is interesting to note that identification of various isoforms in plasma is consistent with the results from colostrum and milk [93], which also demonstrated multiple isoforms. Thus, the discrepancies in the dominant form observed in plasma from study-to-study, and technique-to-technique, suggest that apelin can be secreted into biofluids other than milk without a requirement for intracellular processing.

The conflicting results observed in plasma apelin isoform levels likely stem from several possible causes, including as yet unknown physiological mechanisms such as the location of processing enzymes and regulatory molecules involved. However, these discrepancies may also arise from the technical limitations in the assay employed and/or physiological conditions in a given study. For example, the concentration of apelin can vary considerably over the range of picograms to nanograms per millilitre in the plasma of healthy subjects, as assessed through immunoassays [119]. Alternatively, another study using HPLC-MS did not detect any apelin isoforms in plasma [88, 120]. In combination, the development of novel techniques or improvements in current techniques

in terms of both accuracy and precision are greatly warranted to reliably determine the predominant isoforms of apelin or, looking forward, apela in plasma and other tissues/organs.

3.2.3 ROLE OF APELIN IN PHYSIOLOGICAL SYSTEMS

Apelin was initially discovered in bovine stomach extracts, and its effects in the gastrointestinal system include regulating acid secretion [121]; gastric and pancreatic enzyme activity [122]; and stimulating proliferation of gastric cells [123]; and, gut contraction [124]. However, consistent with its diverse expression profile, apelin has also been shown to play various physiological roles. As an example, multiple studies have examined the effects of intracerebroventricular (ICV) injection of apelin peptides, given the initial detection of AR in the brain. Apelin treatment caused changes in the level of fluid [81, 113, 125-127] and food intake [95, 127-135], implying that apelin-AR interaction centrally regulates physiological homeostasis. In addition, apelin has demonstrated neuroprotective [136-143] and analgesic [143-146] effect, indicating its diverse role in the nervous system. It is notable that role of apelin in fluid and food intake is controversial, since apelin treatments have demonstrated both positive and negative regulatory effects.

Since the discovery of apelin, the study of this bioactive peptide has most extensively focused around its roles in the cardiovascular system and associated diseases (recently reviewed by Yang *et al.* [147]). Apelin is considered be one of the most potent endogenous positive inotropes, as evidenced by its effects upon cardiac contractility and developed cardiac tension [148]. In addition, apelin exhibits regulatory effects on blood pressure through endothelium- and nitric oxide synthase-dependent mechanisms[104,

149-153]. In cardiovascular diseases, such as myocardial infarction, heart failure, and hypertension, apelin has a significant demonstrated protective effect. For example, apelin treatment resulted in improved cardiac parameters (e.g., cardiac output and contractility) [154-164] and increased cell viability[156, 164-169]. Thus, apelin has been justly implicated as a potential therapeutic target for multiple cardiovascular diseases.

The role of apelin in regulating adipoinsular axis function and ameliorating diabetes parameters has also been actively characterized, as detailed in recent reviews by Chaves-Almagro *et al.* [170] and Hu *et al.* [171]. In one primary example, apelin has been shown to regulate glycemia, likely through controlling glucose uptake, gluconeogenesis, and glycogenolysis. In addition, apelin can modulate both insulin and insulin receptor levels [172-176]. The effects of apelin have also been extensively characterized in adipocytes, with apelin treatment significantly inhibiting white adipogenesis, decreasing free fatty acid release, and increasing brown adipogenesis [140, 177-179]. All of these functional effects implicate apelin as a potential therapeutic target for diabetes. Correspondingly, apelin treatments in diabetic models decreased fat mass [180, 181], hyperinsulinemia [180-183], and glycemia [124, 152, 181, 183, 184] while increasing pancreatic islet mass [185], mitochondrial biogenesis [181], and glucose uptake [124, 186]. Thus, apelin may also have a protective role against diabetes similar to cardiovascular diseases.

It is important to note that the discrepancies in physiological functions mentioned above may be due to the location of injection. For example, Reaux *et al.* and Cheng *et al.* employed an intravenous (IV) mode of injection, resulting in increased heart rate by apelin [126, 187]. Dai *et al.*, conversely, observed a decrease in heart rate with

intracerebroventricular (ICV) apelin treatment [188]. In contrast, Kagiyama *et al.* observed an opposite trend with ICV treatment in their experimental conditions, with the result being an increase in heart rate [189]. Similar discrepancies have also been described in terms of hypotensive effects, where apelin treatments have been shown to both increase and decrease blood pressure. Furthermore, apelin dosage-dependent changes have been demonstrated in cardiac contractility [157, 158], adding an additional layer of complication.

In functional modulation of the adipoinsular axis, the role of apelin is also convoluted, with a variety of opposing and dosage-dependent effects having been noted for apelin. Specifically, Duparc *et al.* showed that low dose ICV (20 fmol) apelin treatment decreased glycemia and improved glucose tolerance [190]. Conversely, high dose ICV (40 fmol) treatment increased glycemia [190]. These findings illustrate the importance of dosage. Drougard *et al.* subsequently showed that a high dose treatment of apelin stimulated gluconeogenesis and glycogenolysis to cause hyperglycemia [191] and decreased energy expenditure and thermogenesis [192], which occurred in parallel to increased levels of reactive oxygen species [191] and inflammatory cytokines [192] in the hypothalamus. These studies, thus, indicated that central apelin administration at a high dose contributed to diabetes progression, while the opposite was true for low dosages. Furthermore, Ringstrom *et al.* observed that while high dose (1 μM) apelin treatment resulted in a moderate increase in glucose-stimulated insulin secretion, low dose (10-100 nM) treatment robustly decreased insulin secretion [174].

The conflicting role of apelin in the adipoinsular axis and in diabetes also translates to related diseases, such as diabetic nephropathy. As observed by Day *et al*. and

Chen *et al.*, apelin can suppress diabetes-induced glomerular hypertrophy, inflammation, and proteinuria [193, 194]. This implies that apelin protects against the development of diabetes nephropathy. However, Guo *et al.* and Zhang *et al.* observed an opposite trend, where apelin treatment aggravated the disease through abnormal glomeruli angiogenesis and increased proteinuria and glomerular permeability [195, 196]. Regardless, given the opposing effects of apelin observed in various diseases models, apelin has been suggested to play a "switch"-role in preventing or promoting disease progression.

3.2.4 PHARMACOLOGICAL DIFFERENCES BETWEEN APELIN ISOFORMS

Although all apelin isoforms share the identical C-terminal residues and likely share similar C-terminal conformations [197] as will become clear in Chapter 6, the initial report by Tatemoto *et al*. demonstrated length-dependent potency, with apelin-13 and Pyr-apelin-13 being the most potent isoforms, as determined using extracellular acidification assays in AR expressing Chinese hamster ovary (CHO) cells [74]. Since then, numerous studies have identified shorter isoforms, typically apelin-13, as being more potent in activating various signalling pathways. As an example, apelin-13 was shown to be more potent than apelin-36 in stimulating gastric cell proliferation in murine enteroendocrine cancer cell line (STC-1) [123]. Furthermore, only apelin-13 enhanced proliferation of choroids-retina endothelial cell line (RF/6A) while apelin-36 did not [198], demonstrating that isoforms can differ in both potency and efficacy.

Although length-dependent potencies and/or efficacies were observable through various assays, many also showed discrepancies, bringing controversy into the concept of ligand-dependent properties. For example, in terms of inhibition of forskolin-stimulated cAMP production, Pyr-apelin-13 was identified as a more potent isoform than apelin-36

[88, 108], while no difference in potency was observed between Pyr-apelin-13 and -17 [199]. Conversely, Medhurst *et al*. identified no significant differences in potencies between apelin-13, Pyr-13, -17, and -36 [109]. In chemotaxis, both Pyr-apelin-13 and apelin-36 could cause cell migration in CHO cells expressing AR, with increased potency of Pyr-apelin-13 in comparison to its longer counterpart. For RF/6A cells and lymphatic endothelial cells, however, apelin-13 and Pyr-apelin-13 showed comparable potency to apelin-36 in terms of enhancing cell migration [198, 200]. In terms of ERK signalling, we demonstrated that Pyr-apelin-13 to be significantly more potent in its capacity to phosphorylate the signalling molecule in comparison to its longer counterparts (-17, -36, and -55) as will be shown in Chapter 6. However, Gerbier *et al.* observed no significant differences between Pyr-apelin-13 and apelin-17 under their ERK assay conditions [201]. Furthermore, despite the potential for potency differences, all isoforms have been shown to exhibit similar efficacy in terms of ERK signalling [202]. As a whole, this implies that both assay conditions and the reported parameters must be chosen with care.

Length-dependent properties observed at the cellular level also translate to physiological function. For example, in the cardiovascular system, apelin-13 was shown to be more potent than apelin-36 in decreasing blood pressure [104]. However, the discrepancies observed in cellular assays also translate to organism-level studies. In terms of hypotensive action, apelin-17 was shown to be more potent than Pyr-apelin-13 [116], demonstrating that shorter isoforms are not necessarily more potent. Further complicating things, apelin-13 and -36 were shown to have a comparable hypotensive effect in rats alongside a similar inotropic effect [115].

Regardless of the discrepancies observed between assays, the demonstration of isoform-dependent pharmacological and physiological properties indicates that apelin processing may serve as a potential mechanism for the regulation of apelin function. On this note, Adam *et al.* showed that both apelin-13 and -36 could inhibit thrombosis, but that an apelin-36 mutant that was incapable of being processed could not [203]. This finding suggests that apelin-36 must be processed in order to inhibit thrombosis. However, it is important to note that the effect of apelin on thrombosis is actually somewhat controversial as apelin-13 treatments result in increased tissue factor expression, which is consistent with a prothrombotic role for apelin [204]. Despite this complication, it seems plausible that differential apelin processing is a potential underlying cause for the discrepancies between the isoforms mentioned above.

Another cause for discrepancy may involve AR-independent mechanisms. Picault *et al*. showed that apelin-13, Pyr-13, and -36 could all inhibit apoptosis in human colon cancer cell line (LoVo) through deactivation of caspase-dependent pathways [205]. However, in retinal ganglion cells, N-methyl-D-aspartic acid (NMDA)-induced cell death could be inhibited by apelin-36, but not by apelin-13 [206]. Interestingly, in this study, Sakamoto *et al*. noted that inhibition of cell death was likely through a mechanism independent of the AR, as inhibitors of AR and various protective signalling pathways of the AR did not impair apelin-36 activity [206]. Based on these results, Sakamoto *et al.* suggested that apelin-36 may protect against neuronal cell death by directly influencing a non-AR receptor (i.e., the NMDA receptor in their case). Although the potential for apelin interaction with the NMDA receptor remains uncharacterized, involvement of AR-

independent mechanisms may also be a plausible source of the discrepancies in apelin function as reported in literature.

Adding support for another receptor for apelin, Galon-Tilleman *et al.* also showed that apelin-36, introduced through use of adenovirus to achieve lasting systemic expression, reduced cholesterol levels, glycemia, and body weight [184]. Conversely, systemic expression of apelin-13 or -17 resulted in low or negligible effect using the same model. Thus, this study implicated the potential for another membrane receptor that recognizes, and is activated by, the N-terminal residues of apelin-36. However, the presence of another receptor is rather controversial since treatment with apelin-13 or -17 peptides has been shown to similarly reduce glycemia [152] through increased uptake of glucose [124, 152, 181, 183] and also to decrease body weight [182]. Galon-Tilleman *et al.*, rightly, highlight that differences in AR oligomerization state or other intermolecular interactions may be modulated differently by apelin-36 vs. by shorter isoforms [184], which in turn will cause the differences observed.

In short, although there are potential discrepancies in the function of the apelin isoforms, the number of publications that have relied upon the use of one isoform (usually either apelin-13 or Pyr-apelin-13) is significantly greater than the number of publications that have compared the properties or effects of multiple isoforms. Given that there may be pharmacological differences – in some cases quite dramatically so – between these isoforms, the exclusive use of one isoform is worrisome. Serious critical thought should be given to the importance of comparison of multiple isoforms, particularly if the relative levels of physiologically-relevant isoforms in a given setting are unclear.

3.2.5 DIFFERENCES IN RECEPTOR REGULATION BY APELIN ISOFORMS

The differences between the pharmacological properties of apelin isoforms are difficult to rationalize in terms of their affinities for the AR (Table 3.2). Theoretically, if the N-terminal residues impeded binding, then the affinity of longer isoforms should decrease with a corresponding decrease in potency. Conversely, the observed increased affinity upon N-terminal extension of apelin to longer isoforms should suggest that the longer isoforms would show increased potency. However, experimental data are suggestive of a perplexing combination of these two hypotheses. Some studies have noted a more stable interaction [107, 108] and higher affinity [108, 207] between the longer apelin isoforms and the AR, compared to the shorter isoforms, whereas potency has been noted to be greater for the shorter isoforms, as observed through the various assays as introduced above. As a whole, these findings indicate that potency is likely not limited to interaction between ligand and receptor, and that another mechanism (or more than one alternative mechanism) exists to regulate the activity of the apelinergic system.

Although it is not exactly clear what mechanisms underlie the variation observed between isoforms, one of these may rely upon variation in ligand-dependent receptor internalization and regulation. This was clearly demonstrated by Hosoya *et al*., who showed that apelin-36 remained strongly associated with the AR [107]. They demonstrated that radiolabeled apelin-13 did not displace AR-bound apelin-36 in CHO cells whereas AR pretreated with apelin-13 readily bound radiolabeled apelin-13 [107]. This study indicated that the interaction between the longer apelin-36 and the AR is stronger than that between apelin-13 and the AR. This, logically, led to the hypothesis that a stable complex formed between apelin-36 and the AR would be likely lead to

receptor internalization, with subsequent regulation of signalling. Conversely, weak binding between apelin-13 and the AR would allow for rapid disassociation of the ligand from the receptor, allowing for receptor recycling to the cell surface.

In support of this hypothesis, using HEK cells stably expressing fluorescently tagged AR, Lee *et al.* clearly showed that receptor regulation (i.e., the balance of cell surface recycling vs. degradation) is ligand-mediated (summarized in Fig. 3.4) [208]. Specifically, treatment with apelin-13 treatment resulted in agonist-mediated internalization of the AR to intracellular vesicles. However, upon agonist washout, the activated AR reappeared at the cell surface within 1 hour. Apelin-36 treatment resulted in similar internalization of AR. In contrast to apelin-13, however, apelin-36 treatment did not result in AR recycling back to the cell surface even after agonist washout. Analysis of the receptor regulation pathway demonstrated that apelin-13 activation resulted in recruitment of β-arrestin to the cell surface, but that the arrestin molecules did not internalize as a complex with the AR. Apelin-36 also recruited β-arrestin, but β-arrestin remained associated with the receptor during internalization. Similarly, Evans *et al.* demonstrated that the AR recruited β-arrestin to the cell surface upon activation by apelin-13 [209]. Notably, they detected internalization of apelin peptides, but did not observe significant alterations in the distribution of β-arrestins. This supports the concept that AR activated by apelin-13 undergoes endocytosis but dissociates promptly from β-arrestin close to the cell surface, thereby facilitating rapid recycling of the receptor back to the cell surface.

In addition to relying on β-arrestin, AR internalization has been shown to be clathrin-dependent [116, 210], since pretreatment with hypertonic sucrose, to block

clathrin-mediated endocytosis, inhibited receptor internalization. Furthermore, clathrin-mediated internalization also likely involves the transferrin receptor, since co-localization of the AR and transferrin receptors were observed intracellularly [211]. Like other GPCRs, the AR depends on Rab proteins for receptor regulation, where the receptor is internalized with Rab5 for endosomal trafficking as observed by co-localization of fluorescent AR and Rab5 by confocal microscopy. Interestingly, Rab4 was required for recycling of agonist-activated AR from intracellular vesicles [208]. This was evident as cells expressing an inactive Rab4 mutant could not recycle the AR back to the cell surface even for apelin-13 treated cells. In contrast, Rab7 was recruited for receptor trafficking to the lysosome for degradation, as constitutive Rab7 expression directed the AR to lysosomes while inactive Rab7 expression resulted in no co-localization with the AR.

Notably, the differential internalization observed between ligands also translates to receptor desensitization [212, 213]. By probing for cAMP inhibition and ERK phosphorylation, Masri *et al*. showed that apelin-36 treatment resulted in significantly diminished level of inhibition in response to repeated exposure in CHO cells expressing the AR [212]. Conversely, a similar loss in signal with repeated exposure was not observable when treated with apelin-13 [212]. Furthermore, a similar desensitization was observed through a Ca^{2+} response assay in human NT2.N neurons [213].

It is important to note that the four N-terminal residues of apelin-17 (KFRR) may also play a major role in controlling the downstream effects of apelin. Using internalization assays, El Messari *et al.* observed significant differences between the potencies of apelin-13 and -17 toward induction of AR internalization [214], suggesting

that the KFRR motif regulates receptor internalization. Given the similar conformation shared for the 12 core C-terminal residues as will be observed in Chapter 6 and previous work in the Rainey lab [197] and the two-site binding mode detailed above, these N-terminal residues may be responsible for stabilizing the ligand-receptor interaction. Furthermore, the stabilization likely arises from electrostatic interactions between positively charged N-terminal residues of apelin isoforms and key acidic residues in the AR [77, 78, 215, 216], as mutations of these key residues on the receptor results in loss of binding. This is consistent with some of the observed AMG3054 interactions with the AR N-terminus and ECL2 segments, with the presence of anionic grooves on the receptor surface to provide additional sites for electrostatic stabilization of apelin-AR binding [69]. Furthermore, given the isoform-dependent affinity and variable regulatory binding partners, it is possible that both ligand-induced receptor conformation through allosteric effects and the resulting receptor dynamics would vary as a function of isoform. Such variation offers biophysical justification for isoform-dependent interaction with regulatory molecules.

In summary, the longer apelin isoforms lead to β-arrestin binding to the AR, causing internalization and degradation of the AR (Fig. 3.4). Apelin-13, conversely, allows for disassociation of the receptor from β-arrestin and subsequent recycling of the receptor following internalization. Based on these findings, Lee *et al.* hypothesized that the levels of different apelin isoforms that are available may control the level of AR on the target cell surface, i.e., the level of receptor desensitization [208]. Correspondingly, isoform-dependent potencies may in part be affected by this differential regulation, since receptor desensitization will result in a higher dose requirement for apelin in order to

function. Conversely, the potencies of the isoforms may increase with longer peptides for β-arrestin signalling. Given that a more stable interaction is promoted with arrestin molecules, potency will be improved to reflect increased binding. In support of this, El Messari *et al.* demonstrated that apelin-17 was more potent in causing the β-arrestin-mediated decrease in blood pressure in comparison to Pyr-apelin-13 [214]. In combination, isoform-mediated differences are likely due to their inherent differences in receptor interaction, leading to differential downstream effects upon receptor binding and the resultant-activation of signalling cascades. It is also interesting to note that if the ratio of long to short apelin isoforms can determine the level of AR desensitization, then this ratio will directly determine whether apelin treatment plays a physiological or pathological role in the target tissues.

3.3 APELA

My thesis mainly focuses on apelin, which is only one of the two peptide ligands for the AR. However, apela is an important component of the apelinergic system, and I characterized a number of apela isoforms with a former Honour's student, Ms. Shuya Kate Huang. As it should become evident in Chapter 7, a comparison of apela to apelin isoforms showed very interesting and striking conformational variations between ligands and their isoforms, and in response to environmental factors. Furthermore, the implications of the differences between the AR ligands are discussed in Chapter 8. Thus, I have opted to include an introduction to apela in this chapter to emphasize the similarities and differences between the two ligands of the apelinergic system.

For 15 years, apelin was considered to be the only ligand for the AR. During this period, the receptor was even renamed after the ligand (i.e., apelin) which had, in turn, been initially named for APJ (former name for the AR). However, one clear line of evidence had always suggested that there was more to the story. Specifically, AR knockdown caused impairments in cardiovascular development during the embryonic stages; however, these impairments were not observed upon apelin knockout [217-220]. Based on these discrepancies, AR signalling was speculated to occur through either an apelin-independent mechanism or to be mediated by an alternative ligand during embryonic development. Using zebrafish as a model, two research groups independently identified a new ligand for the AR nearly simultaneously in 2013. This ligand was named differently by the two groups, as ELABELA [75] and Toddler [76]. The recommended name for the ligand (as used herein) is now "apela", coming from Apelin Receptor Early Endogenous Ligand [221].

The *apela* gene, located on chromosome 4, was initially identified as producing a non-coding RNA [75, 76]. However, analyses by Chng *et al.* [75] and Pauli *et al.* [76] independently identified the gene as encoding a 54-residue long preprotein in humans (58-aa in zebrafish), with an N-terminal α-helical hydrophobic 22-residue signal peptide [75, 76, 222] (Table 3.1 and Fig. 3.5). Upon removal of the signal peptide, the longest bioactive isoform, apela-32, is produced. Apela-32 has an N-terminal glutamine, as in apelin-13. This residue, similarly to apelin-13, spontaneously converts to pyroglutamate [222, 223], which likely increases the stability of this isoform. As in apelin-55, analysis of the amino acid sequence of apela-32 demonstrates the presence of multiple dibasic sites, indicating potential proprotein convertase-mediated processing to yield 22, 21 or

11-residue isoforms (apela-22, -21 and -11) (Table 3.1). All isoforms contain a highly conserved set of 7 C-terminal residues (Fig. 3.5). Notably, only apela-11 has, thus far, been observed endogenously via mass spectrometry in embryos expressing apela mRNA [76]. However, other isoforms likely do exist *in vivo*, as incubation of apela-32 in rat plasma produced an N-terminal domain containing the first 9 residues and apela-22 [223]. Corresponding to the relatively recent identification of apela, no enzymes have yet been implicated in apela processing and/or deactivation.

One feature that clearly differentiates apelin and apela is the absence vs. presence, respectively, of cysteine residue(s) following signal peptide cleavage. In apelin, as detailed above, cysteines are located only in the signal peptide, resulting in dimer formation potentially important for signal peptide processing [89]. In apela, conversely, the putative 22-residue signal peptide does not have any cysteines. Rather, apela-54 contains two highly conserved cysteines at positions 39 and 44 [75, 76] (Fig. 11). This allows for potential intra- (for apela-32) and inter-molecular disulfide bridge formation. In support of this, apela-11 spontaneously dimerizes [222]. However, it is unclear at present what role, if any, dimerization plays in apela peptide function, as substitutions that prevent disulfide bridge formation resulted only in minor conformational differences in apela-11 [222] and did not significantly affect the potency of apela-14 analogues via AR-mediated G-protein-dependent or independent pathways [223]. It is also unclear whether disulfide linkages occur physiologically. *In vitro*, neither HPLC nor mass spectrometry showed evidence of intramolecular or intermolecular disulfide bridge formation in apela-32 in recombinant production and purification [222], but minor differences by far-UV CD spectropolarimetry were observable between reducing and

oxidizing conditions suggestive of disulfide bridge formation. Thus, further studies are required to characterize the dimerization state of endogenous apela isoforms and the physiological purpose that these cysteine residues may play.

3.3.1 PHYSIOLOGICAL EFFECTS OF APELA

As introduced above, apela was initially discovered as a second ligand for the AR that is expressed during embryogenesis and is important for cardiovascular development. Specifically, finely regulated control of apela levels was shown to be essential as its absence or overproduction led to inappropriate migration of mesendodermal cells during zebrafish gastrulation [76]. Its expression was also noted to be tied directly to developmental stage in zebrafish, as apela expression was upregulated during embryogenesis and development, whereas in adults where apelin expression was upregulated [75, 76]. Furthermore, supplementation of apelin in apela knockout zebrafish could rescue the mutant phenotype [76], suggesting that apelin and apela have overlapping functions mediated by the AR during embryogenesis and that their difference in bioavailability is the reason for discrepancies in phenotypes between apelin and AR knockout models.

Exogenous treatment using apela peptides results in similar downstream physiological effect to apelin, which is perhaps expected as both ligands activate the AR. For example, apela can regulate blood pressure [223]; fluid homeostasis [113]; food intake [224]; cardiac contractility [111]; and, angiogenesis and vasodilation [114]. In addition to these functions, apela activates the canonical downstream signalling molecules that have been associated with apelin-mediated signalling, including G-proteins [113, 223], ERK [113], and β-arrestin [223]. Thus, it is likely that apela activates

signalling pathways in a similar manner to apelin to exert the corresponding physiological effect. Consistent with this, apela-11, the isoform with the lowest potency for β-arrestin recruitment, showed the lowest capacity to decrease mean arterial pressure (MAP) [223]. This corresponds to previous work showing that β-arrestin activation and the resulting AR internalization regulate MAP [89, 116].

Despite these apparent similarities in apelin and apela function, some clear differences are also apparent. For example, apela triggers vascular relaxation in a nitric oxide-independent manner [114]. This was clearly evident as relaxation still occurred even when blood vessels were treated with the nitric oxide inhibitor L-NAME [114]. Apela and apelin also differ in their potencies with respect to particular physiological effects. Apela-32, for example, bound to the AR with increased affinity, increased ERK phosphorylation response, and had a greater impact on fluid homeostasis than apelin-13 [113]. Similarly, Yang *et al.* demonstrated that apela-32 was more potent than apelin-13 in inducing cardiac contractility and output [112].

3.4 RATIONALE AND OBJECTIVES

As indicated above, the apelinergic system has important functions in the body. Furthermore, the two ligands, apelin and apela, are complex hormones due to the existence of numerous isoforms that exhibit length-dependent variations in efficacies, binding affinities, and receptor trafficking. The observation of ligand-dependent pharmacological properties is a clear indication that apelin processing can have regulatory roles in both physiological and pathological settings. Furthermore, the biophysical mechanisms underlying ligand-dependent variations in activity (i.e.,

differences in conformations and dynamics between ligands and/or receptor) remain uncharacterized but are highly conceptually interesting and, potentially, valuable as a means for therapeutic targeting of the apelinergic system.

Despite the known ligand-dependent variations in apelinergic system activity, the field has typically been focused on determining the physiological effects of apelin (specifically apelin-13/Pyr-13) and upon developing agonists and/or antagonists for therapeutic purposes. Thus, through a combination of structural biology, biochemistry, biophysics, and endocrinology techniques, I have set out to better elucidate both apelin processing mechanisms and the biophysical phenomena giving rise to the observed differences in isoform behaviour.

Table 3.1: Apelin and apela isoform amino acid sequence

Identity	Amino acid sequence*	Net charge (pH 7)[#]	Hydrophobic residues[‡]
Preapelin	MNLRLCVQALLLLWLSLTAVCGGSLMPLPDGNGLEDGNVRHLVQPRGSRNGPGPWQGGRRKFRRQRPRLSHKGPMPF	9.1	26
Apelin-55	GSLMPLPDGNGLEDGNVRHLVQPRGSRNGPGPWQGGRRKFRRQRPRLSHKGPMPF	8.2	12
Apelin-36	LVQPRGSRNGPGPWQGGRRKFRRQRPRLSHKGPMPF	10.1	6
Apelin-17	KFRRQRPRLSHKGPMPF	6.1	4
Apelin-13	QRPRLSHKGPMPF	3.1	3
Pyr-apelin-13	<ERPRLSHKGPMPF	3.1	3
Preapela	MRFQQFLFAFFIFIMSLLLISGQRPVNLTMRRKLRKHNCLQRRCMPLHSRVPFP	10.1	25
Apela-32	QRPVNLTMRRKLRKHNCLQRRCMPLHSRVPFP	9.1	9
Pyr-apela-32	<ERPVNLTMRRKLRKHNCLQRRCMPLHSRVPFP	9.1	9
Apela-22	KLRKHNCLQRRCMPLHSRVPFP	6.1	6
Apela-21	LRKHNCLQRRCMPLHSRVPFP	5.1	6
Apela-11	CMPLHSRVPFP	1.0	4

*Underlined residues represent the signal peptide for each respective ligand; <E represents pyroglutamate

[#]Net charge was determined using the equation $Z=\sum_i N_i \frac{10^{pKa_i}}{10^{pH}+10^{pKa_i}} - \sum_j N_j \frac{10^{pH}}{10^{pH}+10^{pKa_j}}$, where N_i are the number, and pKa_i the pKa values [225], of the N-terminus and the basic side chains. The j-index refers to the C-terminus and side chains of Asp, Glu, Cys, and Tyr.

[‡]Aromatic and aliphatic residues.

Table 3.2: Pharmacological comparison of apelin isoforms

Function	-13	Pyr-13	-17	-36	Other isoforms	References
Ligand-receptor binding (competitive radioligand assay)	✓ (+/++)	✓ (+/++)	✓ (+)	✓ (+)		[107, 113, 201, 207, 215, 223, 226-229]
Ligand-receptor disassociation (inhibition of radioligand binding)	✓ (+)	✓ (+)	✓ (+)	✓ (+/++)	-12 (+), -11 (–)	[107-109, 116]
G-protein interaction	✓	✓				[72, 223, 228, 230]
G-protein-mediated effect (inhibitor-mediated)	✓	✓ (+)		✓ (+)		[231]
β-arrestin recruitment	✓ (+)	✓ (+)	✓ (++)	✓ (+)		[201]
Receptor internalization	✓ (+)	✓ (+)	✓ (+/++)	✓ (+/++)	-16, -12(+), -11(–), -10(–)	[201]
→Receptor recycling	✓ (+)			✓ (–)		[208]
→→Rab4-dependent recycling	✓ (+)			✓ (–)		[208]
→Rab7-dependent lysosome trafficking	✓ (–)			✓ (+)		[208]
→Receptor desensitization	✓ (+)		✓ (+)	✓ (+/++)		[210, 212, 213]
Inhibited intracellular cAMP production	✓ (+)	✓ (+/++)	✓ (+/++)	✓ (+)	-12(+), -11(–), -10(–)	[72, 88, 101, 108, 109, 116, 126, 173, 184, 199, 201, 205, 207, 215, 227, 228, 232-234]
Akt activation	✓ (+)	✓ (+)	✓ (+)	✓ (+)	-12 (+)	[137, 138, 140, 152, 156, 161, 165, 185, 186, 202, 205, 212, 235-264]
AMP-activated protein kinase (AMPK) activation	✓	✓				[140, 152, 177, 181, 185, 244, 247, 254, 255, 265-269]
Acetyl-CoA carboxylase (ACC) activation	✓	✓				[152, 177, 181, 244, 267]
ERK (p44/42) activation	✓ (+)	✓ (+/++)	✓ (+)	✓ (+)	-55 (+), -16	[72, 113, 138, 156, 161, 178, 185, 201, 202, 212, 233, 235, 237, 238, 242, 243, 245-247, 249, 252, 254, 257, 260-264, 270-278, 279##]
Protein Kinase C (PKC) activation	✓	✓		✓	-16	[235, 251, 257, 270, 272, 275, 280-283]
Extracellular pH acidification	✓ (+++)	✓ (+++)	✓ (++)	✓ (+)		[74, 107, 284]
Inhibit apoptosis	✓ (+/–)	✓ (+)		✓ (+)		[205, 206, 239-242, 247, 249, 252, 263, 272, 285-295]
Decrease caspase-3, -8, -9, -12 activation and levels	✓ (+)	✓ (+)		✓ (+)		[136, 205, 239-241, 247, 249, 263, 286, 291, 293, 296]
Increase cell proliferation	✓ (+/++)	✓ (+/–)		✓ (+/–)	-12 (–)	[123, 198, 236, 243, 271, 273, 285, 297-301] [162, 196, 255, 256, 274, 276, 277, 290, 291, 295, 302-304]
Regulate chemotaxis	✓ (+)	✓ (+/++)		✓ (+)		[107, 162, 196, 198, 200, 252, 255, 259, 285, 288, 289, 291, 293, 299, 302, 303, 305-309]

- ✓ represents which isoform was used.
- (+/++/+++) represents potency and/or efficacy differences between isoforms compared in a single publication where additional + represent increased pharmacological properties.

Table 3.3: Pharmacological comparison of apela isoforms

Function	-32	Pyr-32	-21	-11	Other isoforms	References
Receptor binding	✓ (++)	✓ (++)	✓ (++)	✓ (+)	-16 (++) -14 (++)	[111-113, 223]
Receptor internalization	✓ (++)		✓ (++)	✓ (+)		[76, 112, 114, 310]
Inhibit cAMP production	✓ (+)		✓ (+)	✓ (+)	-14(+)	[112-114]
G-protein interaction		✓ (++)		✓ (+)	-16 (++) -14 (++)	[223]
β-arrestin interaction	✓ (++)	✓ (++)	✓ (++)	✓ (+)	-16 (++) -14 (++)	[112, 223]
G-protein activation	✓					[113]
Akt activation	✓					[310]
ERK activation	✓					[111-114]
eNOS activation	✓					[112]
SMAD3 activation	✓					[310]
p70-S6K activation	✓					[310]
Increase cell proliferation	✓					[310]
Inhibit apoptosis	✓					[310]
Regulate cell migration			✓			[76]
Increase diuresis	✓	✓ (+)			-14(++)	[113, 223]
Increase c-Fos expression in the brain			✓			[224]
Increase Ca^{2+} mobilization	✓		✓			[114, 224]
NO-mediated effect	✓					[114]

- ✓ represents which isoform was used.
- (+/++) represents potency and/or efficacy differences between isoforms compared in a single publication where additional + represent increased pharmacological properties.

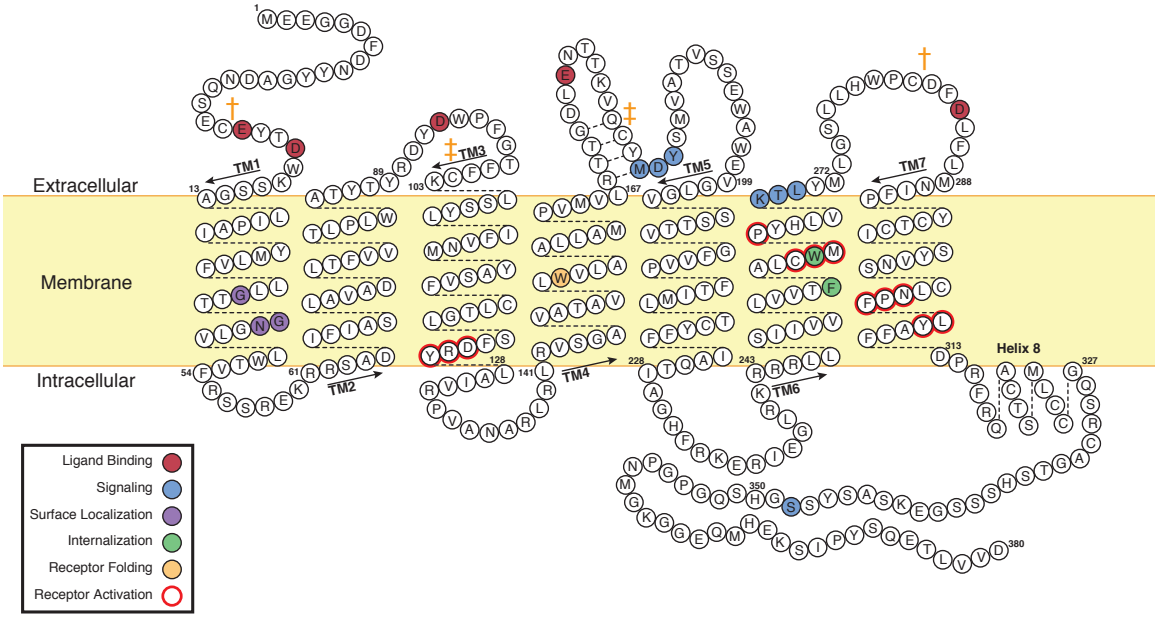

Figure 3.1: "Snake plot" showing human apelin receptor (AR) sequence.
The seven transmembrane helices (denoted TM1-TM7) are delineated and additional structural features observed in the AR crystal structure [69] are also illustrated. These include a short β-sheet in the second extracellular loop; the 8th helix, immediately C-terminal to TM7; and, two extracellular domain disulfide linkages (denoted by distinct dagger symbols to link †) C19 to C281 and ‡) C102 to C181). Filled coloured circles represent functionally important residues, as identified by mutagenesis. Red circles mark important motifs common to class A GPCRs [311, 312]: the Trp toggle (CWXP) in helix 6; the ionic lock (DRY) in helix 3; and, the NPXXY motif in TM7. This figure was made with Dr. Jan K Rainey and Mr. Calem Kenward and is taken from Shin *et al.* (accepted) ***Comprehensive Physiology*** [67].

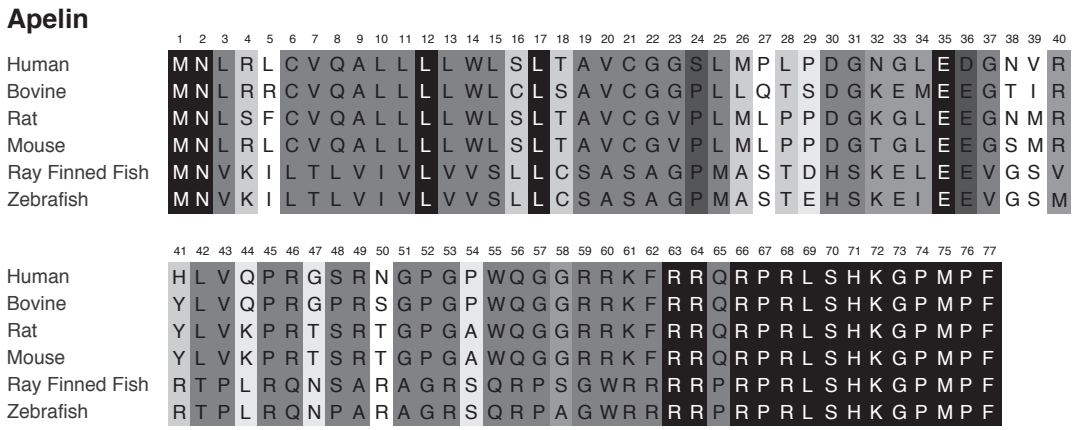

Figure 3.2: Sequence conservation of apelin.
Residues that are fully conserved over the six illustrated species are indicated with a black background; partially conserved residues with varying shades of grey; and, variable positions with white. This figure was made with Mr. Calem Kenward and is taken from Shin *et al.* (accepted) ***Comprehensive Physiology*** [67].

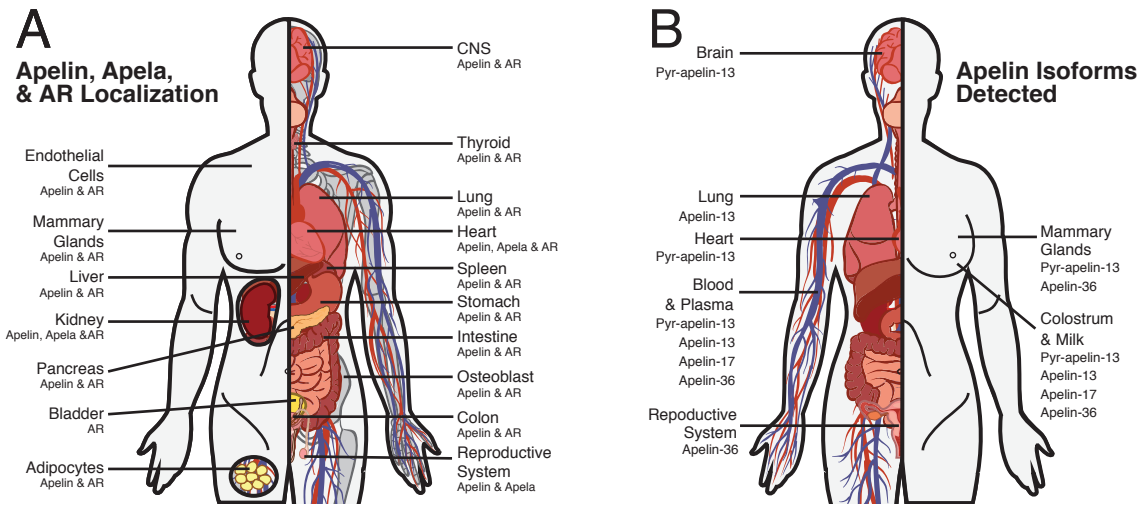

Figure 3.3: Apelinergic system expression and isoform localization profile.
A) Apelin, apela, and AR localization as a function of tissue/organ system. B) Predominant apelin isoform(s) detected, to date, in specific organs or body fluids. This figure was made with Mr. Calem Kenward and is taken from Shin *et al.* (accepted) ***Comprehensive Physiology*** [67].

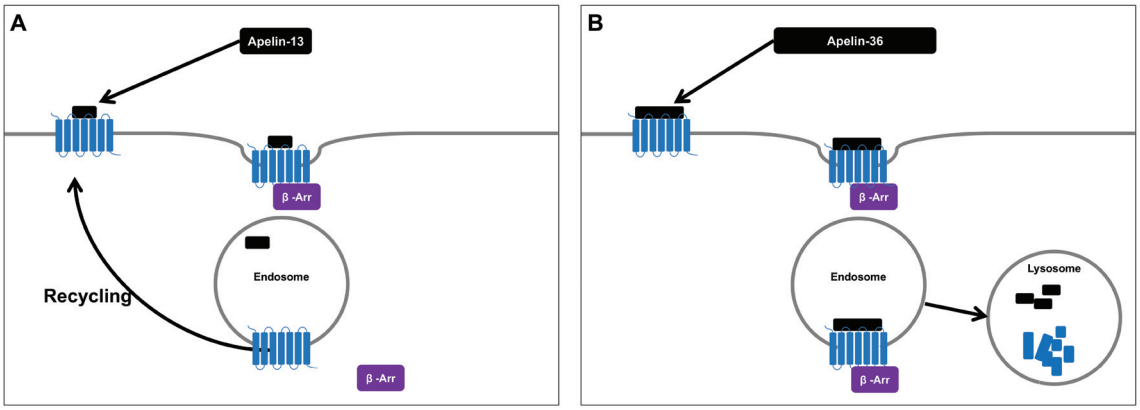

Figure 3.4: Apelin isoform-dependent AR regulation.
A) Apelin-13 causes internalization of the AR through β-arrestin-mediated mechanism, but upon internalization, ligand and receptor disassociate to allow receptor recycling. B) Apelin-36 causes internalization of the receptor through β-arrestin-mediated mechanism, but does not disassociate from the receptor upon internalization. This causes trafficking of the ligand-receptor complex to the lysosome for degradation. The figure is based on Lee *et al.* [208].

Figure 3.5: Sequence conservation of apela.
Residues that are fully conserved over the five illustrated species are indicated with a black background; partially conserved residues with varying shades of grey; and, variable positions with white. Hyphens indicate residues absent from a given species. This figure was made with Mr. Calem Kenward and is taken from Shin *et al.* (accepted) ***Comprehensive Physiology*** [67].

CHAPTER 4 *IN VITRO* PROCESSING OF APELIN-55

(Note: The majority of this chapter has been published in a paper entitled "Preferential apelin-13 production by the proprotein convertase PCSK3 is implicated in obesity" in ***FEBS Open Bio*** 3: 328-333. Dr. Aditya Pandey, a past PhD graduate from the Rainey lab, cloned apelin-55 into the pEXPT-NT vector and developed an initial optimized procedure for the expression and purification of apelin-55 in *E. coli* C41 (DE3) strain. All other experimental work was carried out by me.)

4.1 INTRODUCTION

As mentioned in Chapter 3, apelin is initially expressed as a 77-residue pre(pro)protein, which is cleaved to a 55-residue isoform (apelin-55) following removal of an N-terminal signal peptide [74, 88]. Upon the discovery and first report of apelin by Tatemoto *et al.* [74], it was presumed that the 55-residue isoform was an inactive protein precursor and denoted as "proapelin". Notably, and as will become clear in Chapter 6, apelin-55 does not appear to be an inactive proprotein. Thus, for sake of clarity, proapelin will be referred to as apelin-55 in all chapters of my thesis. Regardless of nomenclature, this 55-residue isoform can be processed into shorter bioactive isoforms, all of which retain at least the 12 C-terminal residues of their precursor protein [104]. Through these shared C-terminal residues, all bioactive apelin isoforms bind to the AR to cause similar cellular effects; however, isoform potencies, efficacies, and receptor recycling kinetics differ [74, 208].

As discussed in Section 3.2.1, the prevailing mechanism of apelin processing prior to this work suggested that an inactive apelin-55 was first N-terminally truncated to form apelin-36 intracellularly. Apelin-36 would then be further processed to shorter apelin isoforms that retain the C-terminus, predominantly apelin-13 and -17 [92]. These shorter isoforms were presumed to be more bioactive. Spontaneous cyclization of the N-terminal glutamine of apelin-13 would also be expected to occur, producing the more stable [313] pyroglutamate-modified form, Pyr-apelin-13.

Studies had also demonstrated that there is tissue specificity in apelin isoform production (Section 3.2.2). For example, Pyr-apelin-13 is the dominant isoform present throughout the brain, hypothalamus, and heart, but the predominant isoform in the lungs, testes, and uterus is apelin-36 [108, 115, 199]. Despite this variability in isoform potency, activity, and localization, no studies had yet directly investigated apelin processing or the endoproteases involved [74, 92].

4.1.1 INDICATIONS OF PROPROTEIN CONVERTASE SUBTILISIN/KEXIN-MEDIATED PROCESSING

For most secreted hormones, such as apelin, regulatory mechanisms are required to maintain bodily homeostasis in response to internal and external challenges [314]. These mechanisms rely upon a broad group of regulatory molecules, including enzymes that post-translationally process hormones for activation/deactivation. The proprotein convertase subtilisin/kexin (PCSK) enzyme family has a number of key roles in regulation of secreted hormones. Namely, this family of eukaryotic Ca^{2+}-dependent serine endoproteases is recognized for roles in activating proproteins in the secretory

pathway (i.e., ER, Golgi apparatus, secretory vesicles, endosomes, lysosomes, and cell surface) [315, 316].

Named for their structural similarities to the yeast and bacterial enzymes kexin and subtilisin, PCSKs have been shown to be important for homeostasis. For example, many physiologically important proteins (e.g., insulin) require activation by means of post-translational cleavage by PCSKs. As might be anticipated, given the general potential for any important system to misfunction, this family of enzymes has conversely also been shown to be responsible for a diverse array of pathological states, including endocrinopathies, neoplastic diseases, infectious diseases, atherosclerosis, and neurodegenerative diseases.

The PCSK family consists of 9 subtypes, named PCSK1 through PCSK9 (Table 4.1). PCSK subtypes 1 through 7 have similar domain structures and biochemical properties to both kexin and subtilisin. The domains of these enzymes include a signal peptide, a pro domain, a catalytic domain that contains the catalytic triad, and a P domain, which is important for catalytic activity, but absent in bacterial proprotein convertases [317] (Fig. 4.1). In some instances, extensions are found, including cysteine-rich and serine/threonine-rich regions, transmembrane domains, and cytosolic domains. The other two enzymes (i.e., PCSK8 and 9) were more recently discovered and are distinct from the rest, as evident from their distinct substrate recognition sites. Despite being part of the same family, these PCSK subtypes differ in substrate specificity, size, pH optimum, salt concentration tolerance, cellular localization, and tissue distribution (Table 4.1).

Given their presence in the secretory pathway and the ubiquitous expression of some of the PCSKs, unprocessed apelin is likely to encounter at least one of the PCSK subtypes as it moves through the secretory pathway. For example, PCSK subtypes 3 and 7 are ubiquitously expressed and present in the trans-Golgi network. Assuming that apelin is trafficked through the Golgi, apelin will encounter these enzymes. If apelin is trafficked to secretory granules without processing, it would, alternatively, encounter PCSK subtypes 1 and 2. Regardless of the trafficking or secretion pathway, the potential commonality in intracellular localization for apelin and a variety of PCSKs imply the possible involvement of PCSKs in apelin processing.

One particularly notable indicator of PCSK involvement is the presence of primary and secondary structure recognition motifs in apelin. The first seven PCSK subtypes recognize substrates with basic residues and, in some cases, a β-turn at or near the substrate cleavage site [318]. Notably, apelin-55 has dibasic motifs directly N-terminal to the cleavage sites for apelin-36, -17, and -13 (Table 3.1), as first noted by Tatemoto *et al.* [74]. In addition, previous structural characterization by the Rainey group of apelin-17 in buffer identified β-turn structuring at the cleavage site of apelin-13 [197]. Considering these factors, I hypothesized that PCSKs were, at least partly, responsible in the production of apelin isoforms.

To test this hypothesis, I developed an *in vitro* apelin-55 processing assay to assess commercially available PCSK subtypes. This assay utilized RP-HPLC (Section 2.2.1) in conjunction with MALDI-TOF-MS (Section 2.3.1 and 2.3.3) to monitor processing and identify the cleavage products, respectively. Using this *in vitro* assay, I

demonstrate for the first time that apelin-55 can be processed into a shorter isoform by a PCSK enzyme.

4.2 MATERIALS AND METHODS

4.2.1 APELIN ISOFORM PRODUCTION AND PURIFICATION

Apelin-12, -13 and -17 (*Homo sapien*s) were chemically synthesized and purified by Dr. Rainey or by previous students in the lab using the procedure outlined previously [197]. Apelin-36 was purchased from AnaSpec. To produce apelin-55, a synthetic gene with *Escherichia coli* (*E. coli*) codon bias (BioBasic) coding for apelin-55 with an N-terminal hexahistidine (His_6) tag and TEV protease cleavage site was cloned into the pEXP5-NT vector (ENLYFQS; Invitrogen) and expressed in *E. coli* C41 (DE3) (Lucigen). Cells expressing His-tagged apelin-55 (His-apelin-55) were initially grown overnight in 250 ml baffled flask containing 15 ml of lysogeny broth (LB) growth medium that was used to inoculate 2 L flask containing 1 L of LB medium. The expression was induced by addition of 0.5 mM isopropyl β-D-1-thiogalactopyranoside (IPTG) to the culture in approximately mid-log phase (Absorbance at 600 nm; A_{600} = 0.6-0.8). Cells were grown for 4 h at 37 °C after induction and then harvested by centrifugation (6,000 *g* at 4 °C for 20 min). Pelleted cells were re-suspended in lysis buffer (50 mM NaH_2PO_4, 300 mM NaCl, 10 mM imidazole, pH 8.0). The cells were lysed in buffer containing 50 mM NaH_2PO_4, 300 mM NaCl, 10 mM imidazole, pH 8 using French Pressure Cell Press (Dalhousie University). The soluble and insoluble fractions were separated by centrifugation (7,500 *g* at 4 °C for 2 h or 14,000 *g* at 4 °C for 1 h).

The soluble fraction was applied to a column packed with Ni-NTA agarose beads (Qiagen Inc. or Roche) for His_6-based affinity chromatography. The column was then washed with a buffer containing a slightly higher imidazole content (50 mM NaH_2PO_4, 300 mM NaCl, 20 mM imidazole, pH 8.0). Finally, bound proteins were eluted using buffer at much higher imidazole content (50 mM NaH_2PO_4, 300 mM NaCl, 250 mM imidazole, pH 8.0). Fractions containing proteins were identified based upon the observation of absorbance at 214 nm (i.e., peptide bond) and 280 nm (i.e., tryptophan and, more weakly, tyrosine). Any fractions identified in this manner were pooled, dialyzed against distilled water (dH_2O) at 4 °C, and then lyophilized. To remove the His_6 tag, the lyophilized His-apelin-55 was dissolved in TEV protease buffer (50 mM Tris-HCl, 0.5 mM EDTA, pH 8.0) and then cleaved overnight using TEV protease (produced in-house using vector obtained from Addgene). Any insoluble precipitate that formed during cleavage was separated from the soluble fraction by centrifugation (14,000 *g* at 4 °C for 2 h). The resulting apelin-55 obtained after cleavage has 55 residues and an extra Ser at the N-terminal due to use of TEV protease, which leaves a Ser or Gly.

Apelin-55 is highly basic (pI of 12.11) and was purified using cation exchange chromatography following the manufacturer's guidelines (S Ceramic HyperD F column, PALL Life Science). Subsequently to TEV protease cleavage, the resulting solution was applied to cation exchange column. The column was then washed with buffer (80 mM Na_2HPO_4, 100 mM NaCl, pH 7.0) and all column-bound proteins were eluted with 1 M NaCl containing buffer (80 mM Na_2HPO_4, 1 M NaCl, pH 7.0). Fractions containing protein content (again, on the basis of absorbance at 214 and 280 nm) were pooled, dialyzed against dH_2O, and then lyophilized.

4.2.2 *IN VITRO* ENZYMATIC DIGESTIONS

Active recombinant PCSKs (2 μg; RnD Systems) were mixed with apelin-55 (750 nmol) in appropriate buffer (PCSK1: 25 mM acetate or 2-(*N*-morpholino) ethanesulfonic acid, 5 mM $CaCl_2$, 1% Brij-35, pH 6; PCSK3: 25 mM Tris or acetate, 1 mM $CaCl_2$, 1% Brij-35, pH 5-7; PCSK7: 25 mM Tris, 0.4-1.5 mM $CaCl_2$, 0.5% Brij-35, pH7). In each case, the reaction was monitored at various time points by reverse phase high performance liquid chromatography (RP-HPLC) separation (Varian ProStar HPLC) using an analytical column C18-AR-II (4.6 x 250 mm, Cosmosil). The mobile phase components were Type II water (A) and acetonitrile (B), both containing 0.1% trifluoroacetic acid (v/v). Elution was carried out at a flow rate of 1 ml/min using a linear gradient from 2-100% B in A (2-20% in 5 min, 20-40% in 20 min, 40-100% in 15 min, and 100-2% in 2 min) or 2-40% (2-20% in 3 min, 20-40% in 20 min, and 40-2% in 2 min). UV chromatograms were recorded at 214 and 280 nm simultaneously and eluent masses determined by MALDI-TOF MS (C-CART Facility at Memorial University, St. John's, Newfoundland).

4.3 RESULTS AND DISCUSSION

4.3.1 *IN VITRO* ENZYMATIC ASSAY OPTIMIZATION

To characterize apelin processing, apelin-55, with an N-terminal His_6 tag linked with a TEV protease cleavage recognition motif (referred to as "His-apelin-55"), was recombinantly expressed in an *E. coli*-based system. Overexpressed His-apelin-55 remained highly soluble in *E. coli*, did not significantly perturb cell viability, and exhibited high affinity in Ni^{2+}-NTA purification (Fig. 4.2). Subsequent tag removal and

cation exchange purification yielded apelin-55, extended by an additional Ser at the N-terminus following TEV protease cleavage, at ~90% purity.

Elution times of pure apelin isoform samples (apelin-12, apelin-13, pyr-apelin-13, apelin-17, apelin-36, and apelin-55) were then characterized to determine whether the different apelin isoforms could be differentiated using RP-HPLC separation with an analytical C_{18} column. Initially, a method using a gradient of 2-100% solvent B over 49 min was employed to determine approximate elution time points. Based upon observed elution times, an optimized method was then determined, using a gradient of 20-40% solvent B over 20 min with a flow rate of 1 ml/min. This allowed for determination of accurate elution times for each apelin isoform (Table 4.2). Using this chromatographic method, relatively similar elution times were observed for the shorter isoforms, while apelin-55 demonstrated a significantly later elution time point, indicating the potential to study apelin-55 processing by RP-HPLC.

Notably, the spontaneous production of Pyr-apelin-13 was observed during determination of apelin-13 elution time. This follows previous reports of spontaneous conversion of the N-terminal glutamine of apelin-13 to pyroglutamate [313], a process since indicated to be important for increased stability in plasma [97], likely through loss of the free primary N-terminal amine recognized by N-terminal exoproteases [98]. Prior to studying the role of PCSKs in apelin processing, stability of apelin-55 was also determined over 5 h, for which 90-97% stability in PCSK3 buffer was noted (Fig. 4.3).

To test for the potential of apelin-55 being cleaved into multiple apelin isoforms or to produce an unknown product that may elute outside the range of 20-40%, each enzyme reaction mixture was initially analyzed using an RP-HPLC method of 2-100%.

The initial 20-40% in 20 min method was incorporated into 2-100% method, since the apelin isoforms eluted between 20-40% and could easily be identified at the 1%/min gradient. Once it was confirmed that no eluents were detected at >40% acetonitrile, a revised 2-40% method was used to decrease the time required for each RP-HPLC analysis.

4.3.2 PCSK3 PREFERENTIALLY PROCESSES APELIN-55 INTO APELIN-13

We initially studied the PCSK-mediated apelin processing with PCSK3 (also known as furin) because it is the most well-studied PCSK subtype that cleaves C-terminally to dibasic sites. In addition, expression of PCSK3 is detected in tissues secreting apelin, such as the heart [319] and adipose tissue [320], suggesting the possibility for apelin processing by PCSK3.

Recombinantly produced apelin-55 was incubated with PCSK3 *in vitro* to test its propensity for cleavage by PSCK3. *In vitro* apelin processing assays were conducted at 37 °C and at pH 5, 6, and 7 to investigate the process across the pH gradient found along the secretory pathway [321]. Crude reaction mixture samples at given time points were subjected to RP-HPLC using the mobile phase gradient optimized for separation of apelin isoforms detailed in Section 4.3.1. The constituents of all resulting peptide/protein-containing fractions were then identified by MALDI-TOF-MS.

As shown in Figure 4.4, incubation of apelin-55 (6243 m/z, aa 1-56, Fig. 4.5) with PCSK3 resulted in production of two polypeptide species with distinct RP-HPLC elution properties at all tested pH conditions. These species were unambiguously identifiable as apelin-13 (1550 m/z, aa 44-56, Fig. 4.6) and the resulting N-terminal segment of apelin-55 (apelin-55Δ13, 4693 m/z, aa 1-43) (Fig. 4.7A). This observation fits the concept of

apelin-55 as a proprotein (albeit not an *inactive* proprotein, as detailed in Chapter 6), in which PCSK3 removes the N-terminal pro-domain (i.e. apelin-55Δ13) to produce the bioactive apelin-13. In support of this, neither of these eluents was observed when apelin-55 was incubated in the absence of PCSK3 (Fig. 4.3). Notably, oxidized products of both uncleaved apelin-55 (~6259 m/z; Fig. 4.5) and apelin-55Δ13 (~4709 m/z; Fig. 4.7) were observed, each exhibiting an additional ~16 amu over the expected masses of each. Following a 5 h incubation, the concentrations of apelin-13 and the pro-domain consistently exceeded that of apelin-55 at both pH 6 and 7. Consistent with the behaviour of apelin-13 during elution time determination (Section 4.3.1), at the 5 h time point, another product became visible with mass corresponding to Pyr-apelin-13 (1533 m/z, Fig. 4.8), presumably arising from spontaneous cyclization of the apelin-13 N-terminal glutamine [313]. At pH 5, PCSK3 showed decreased enzymatic activity similar to previous studies [322], but decreased activity did not affect preferential production of apelin-13 (Fig. 4.4D). In no instance were cleavage products observed corresponding to production of any of the longer apelin isoforms.

Many PCSK3 substrates have a β-turn at their cleavage site and a four residue consensus amino acid sequence N-terminal to the cleavage site of R-(X)-K/R-R, with X representing any amino acid other than Cys [315]. Exceptions to the consensus sequence are also observed, and it is the last two basic amino acids that are believed to be most critical for cleavage [323]. Strikingly, previous structural investigations of apelin-17 in the Rainey group demonstrated a β-turn over the residues R↓Q-R-P (with the apelin-13 cleavage site indicated by ↓) [197]. Furthermore, the sequence immediately N-terminal to

the cleavage site is K-F-R-R, similar to the consensus sequence required by PCSK3 in terms of basic residues (Fig. 4.4A).

Interestingly, apelin-17, which also has two Arg residues immediately N-terminal to its cleavage site, was not produced by PCSK3. This may simply be due to much lower affinity of PCSK3 to cleave following the G-G-R-R sequence N-terminal to apelin-17 vs. the K-F-R-R N-terminal to apelin-13. Alternatively, the absence of apelin-17 production may be due to the presence of ordered structures such as α-helices or β-strands upstream of apelin-17 cleavage site since structuring is associated with non-cleaved sites [323]. Based upon this hypothesis, characterization of apelin-55 conformation is reported in Chapter 6 of this thesis as no atomic-level structural data were available for any apelin isoform longer than apelin-17 and CD spectroscopy studies of apelin-36 implied that extensive secondary structuring was not present [197, 226]. The observation of specific and preferential production of apelin-13 from the 55-residue isoform demonstrates that not all putative cleavage sites are processed by PCSKs and implies that recognition by endoproteases is not correlated with the existence of a single consensus primary sequence around cleaved sites.

4.3.3 PCSK1 AND PCSK7 DO NOT CLEAVE APELIN-55 *IN VITRO*

As introduced earlier, PCSK1 and PSCK7 were also likely candidates of apelin processing. Thus, we investigated the capability of the neuroendocrine system-specific PCSK1 and ubiquitously expressed PCSK7 to process apelin. During screening for cleavage by PCSK1 and PCSK7, various Ca^{2+} concentrations and buffer compositions were employed, following previously reported optimized reaction conditions [322, 324, 325]. In the case of PCSK1, lower specific activity than PCSK3 was expected based on

previously reported specific activity values [326]. However, no processing to bioactive apelin isoforms was evident even after 3 days of incubation of apelin-55 with PCSK1 (Fig. 4.9A). PCSK7, alternatively, has similar specific activity to PCSK3, is expressed ubiquitously, and is known to process some of the same substrates [327]. Thus, PCSK7 was expected to yield similar results as PCSK3. Despite this, no evidence of apelin processing by PCSK7 was observed after 2 days of incubation (Fig. 4.9B).

It is important to note that the PCSK subtypes used herein were commercially available, recombinantly produced, enzymes. Their activities are tested for quality control using a small fluorescent substrate by the manufacturers. Thus, we cannot ignore the possibility for these enzymes to be misfolded and impaired in terms of cleaving physiological substrates. In support of my results, however, Adam *et al.* presented similar lack of apelin processing by PCSK7 using LoVo cells that were transiently transfected to express both apelin and PCSK7 [203].

4.3.4 A NEW PROPOSED MECHANISM FOR APELIN ISOFORM PRODUCTION

Apelin is present in the body as many bioactive isoforms with potential tissue specific processing with ligand-dependent pharmacological properties. However, the mechanism of apelin processing existing prior to this work was highly speculative. The contents of this chapter are, therefore, noteworthy as they detail the first demonstration of apelin-13 production by a specific endoprotease, namely PCSK3. As introduced in Section 3.2.1, the prior proposed mechanism of apelin processing required the initial processing of apelin-55 to apelin-36 prior to any of the shorter isoforms [92]. However, here I demonstrate that PCSK3 specifically and preferentially produces apelin-13 directly from apelin-55 without evidence of any apelin-36 or apelin-17 production. Furthermore,

neither PCSK1 nor PCSK7 could cleave apelin-55, suggesting a specificity, hard to rationalize as this may be, of PCSK3 for apelin-13 production. Therefore, at this point, we can propose a new mechanism of apelin processing in which the presumed-to-be inactive apelin-55 is cleaved to produce various bioactive isoforms directly from the inactive 55-residue state by disparate endoproteases, including PCSK3.

This addition of apelin-55 as a direct precursor of multiple isoforms in the apelin processing pathway expands the potential routes by which apelin can be cleaved, indicating the likelihood of many regulators and enzymes being involved. Subsequent to my report of PCSK3 processing of apelin-55 to apelin-13, apelin-36 was shown to be processed by PCSK3 [203]. Although other regulators and/or enzymes involved in apelin processing still remain unknown, the identification of PCSK3 as one of the proteases involved in apelin processing is a key initial step in unraveling the mechanisms of isoform-level and length-dependent activity of apelin as a function of both tissue type and physiological (or pathological) condition.

4.4 MOTIVATION AND BASIS FOR CHAPTER 5

The previously proposed apelin processing theory of Kleinz and Davenport stated that “apelin-36 may function as a precursor with limited biological activity until undergoing further proteolysis and post-translational modification to yield the more biologically active of peptides” [92]. Following this theory, apelin-55 must be processed intracellularly into apelin-36, which can subsequently be released or processed into shorter isoforms. However, the subsequent processing steps are unclear in this proposal. Specifically, it is not stipulated (nor speculated upon) whether the additional processing

of apelin-36 to apelin-13 or -17 occurs strictly intracellularly or if it can occur extracellularly. Supporting the possibility of extracellular processing, most members of PCSK family, including PCSK3, have a transmembrane domain which serves to anchor the enzyme to the cell surface on the extracellular face. Furthermore, many PCSK subtypes can be secreted or, when cell-anchored, shed from the cell surface. Both of these processes would, in turn, allow for extracellular processing of proproteins (or, in the context of my work, longer apelin isoforms) at the cell surface, in the extracellular matrix, or in body fluids. It is this possibility that is directly tested in the next chapter.

Table 4.1: Summary of PCSK subtypes and their properties

PCSK	Generic name	Subcellular location	Secretion	Optimal pH	Optimal Ca^{2+} (mM)	Tissue distribution	Recognition site
PCSK1	PC1/3	Secretory granules	Secreted	5.5-6.5	2.5	Neuroendocrine	(R/K)-$[X]_{0,2,4,6}$-(R/K)↓
PCSK2	PC2	Secretory granules	Secreted	5.5-6.0	10	Neuroendocrine	(R/K)-$[X]_{0,2,4,6}$-(R/K)↓
PCSK3	Furin	TGN, cell surface, endosomes	Shed	6.0-8.5	1-2	Ubiquitous	(R/K)-$[X]_{0,2,4,6}$-(R/K)↓
PCSK4	PC4	Not described	Shed	7.0	2	Germ cells	(R/K)-$[X]_{0,2,4,6}$-(R/K)↓
PCSK5A (isoform)	PC5/6A	TGN, secretory granules	Secreted	6.5	5	Ubiquitous	(R/K)-$[X]_{0,2,4,6}$-(R/K)↓
PCSK5B (isoform)	PC5/6B	TGN, cell surface, endosomes	Shed	6.5	5	Ubiquitous	(R/K)-$[X]_{0,2,4,6}$-(R/K)↓
PCSK6	PACE4	TGN, cell surface, ECM	Secreted	7.5-8.5	2	Ubiquitous	(R/K)-$[X]_{0,2,4,6}$-(R/K)↓
PCSK7	PC7	TGN, cell surface, endosomes	Not secreted	6.0-7.0	1-2	Ubiquitous	(R/K)-$[X]_{0,2,4,6}$-(R/K)↓
PCSK8	SKI-1/S1P	TGN, cell surface, endosomes	Not secreted	6.5	2	Ubiquitous	R-X-(L/V)-X↓
PCSK9	None	TGN, cell surface, endosomes	secreted	8.0-11.0	Not dependent	Liver, intestine, kidney, central nervous system	V-F-A-Q↓

Table data summarized from Artenstein and Opal [328], Seidah [315], and Seidah and Prat [91]; TGN = trans-Golgi network; ↓ represents cleavage site

Table 4.2: Apelin isoform elution properties.

Apelin isoform	% Acetonitrile in H_2O	Elution time (min)
Apelin-55	30.98	10.98
Apelin-12	27.87	7.87
Apelin-13	27.60	7.60
Pyroglutamate-apelin-13	28.35	8.35
Apelin-17	27.70	7.70
Apelin-36	28.08	8.08

Method: Linear gradient; 20-40% solvent B over 20 min

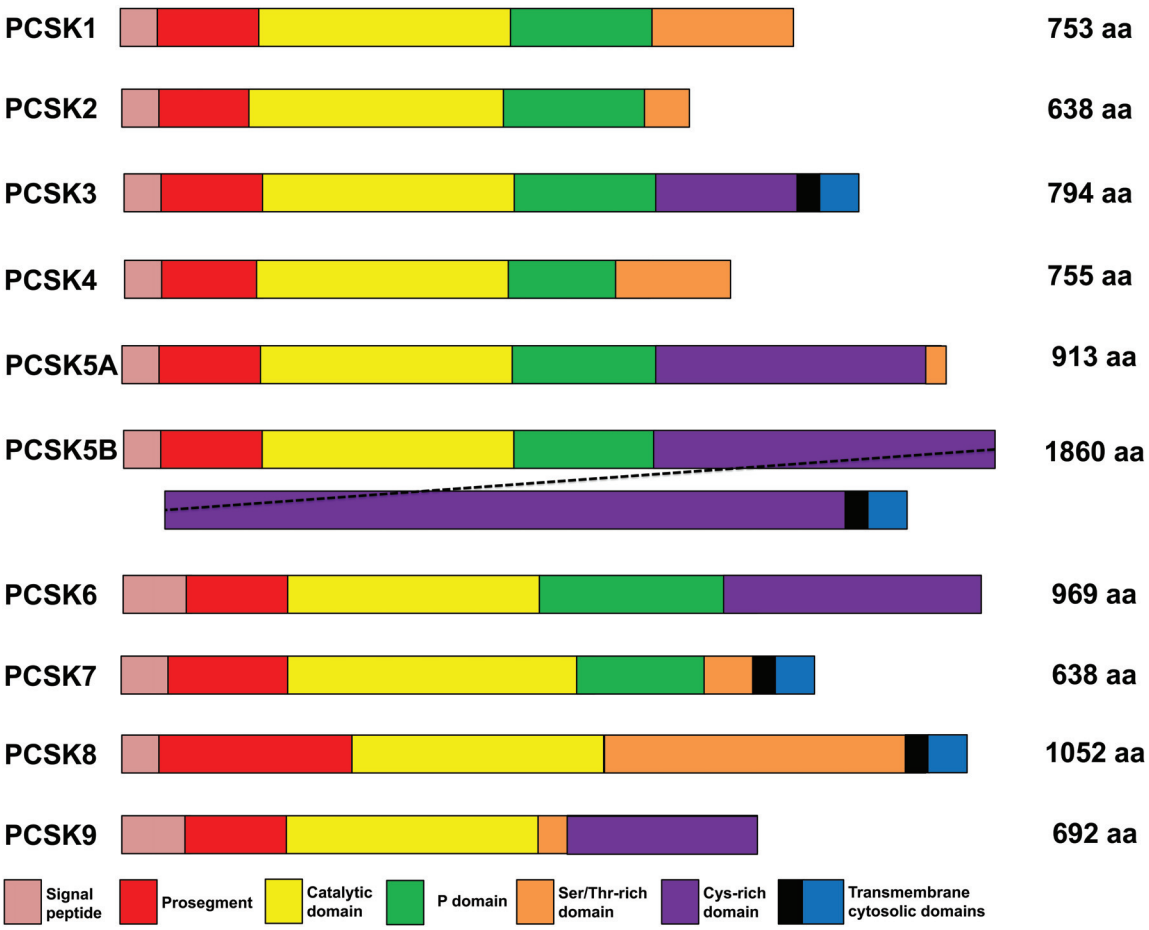

Figure 4.1: The structural organization of PCSK family members.

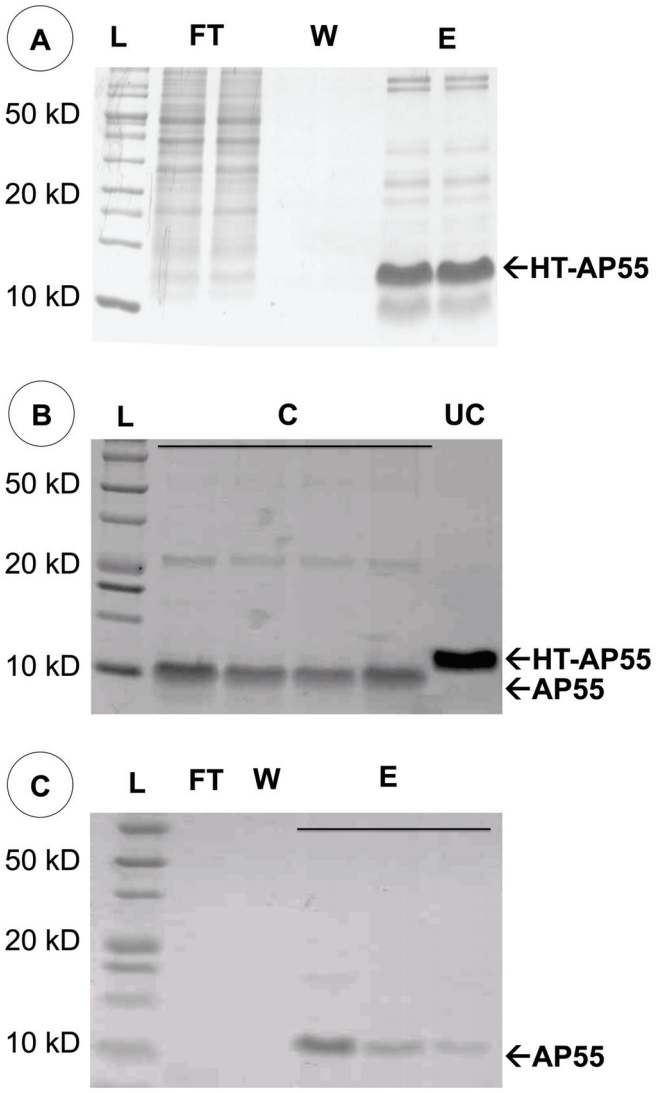

Figure 4.2: Apelin-55 expression and purification.
A) Ni-NTA affinity purification of His-TEV-apelin-55 (HT-AP55) after cell lysis. B) TEV protease-mediated removal of His tag from fusion protein, providing apelin-55 (AP55). C) Cation exchange purification of AP55 upon protease-mediated tag removal. Abbreviations: L-ladder (with key molecular weights annotated), FT-flowthrough, W-wash, E-elution, C-cleaved, and UC-uncleaved.

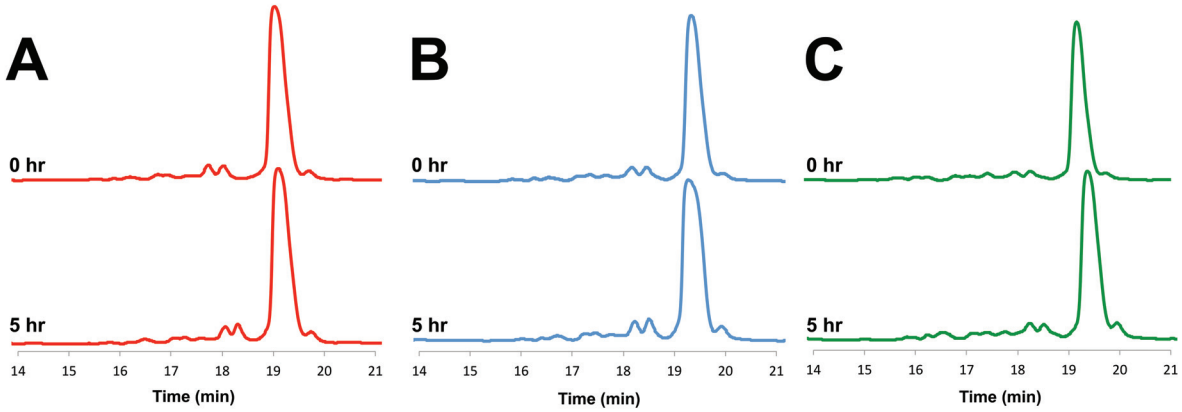

Figure 4.3: Apelin-55 does not undergo spontaneous processing.
RP-HPLC chromatograms show 0 h vs. 5 h timepoints for incubation of apelin-55 at A) pH 5, B) pH 6, and C) pH 7. Apelin-55 was incubated in PCSK3 assay buffer without enzyme. 90-97% stability was observed, based on integration of apelin-55 peak area at 5 h vs. 0 h.

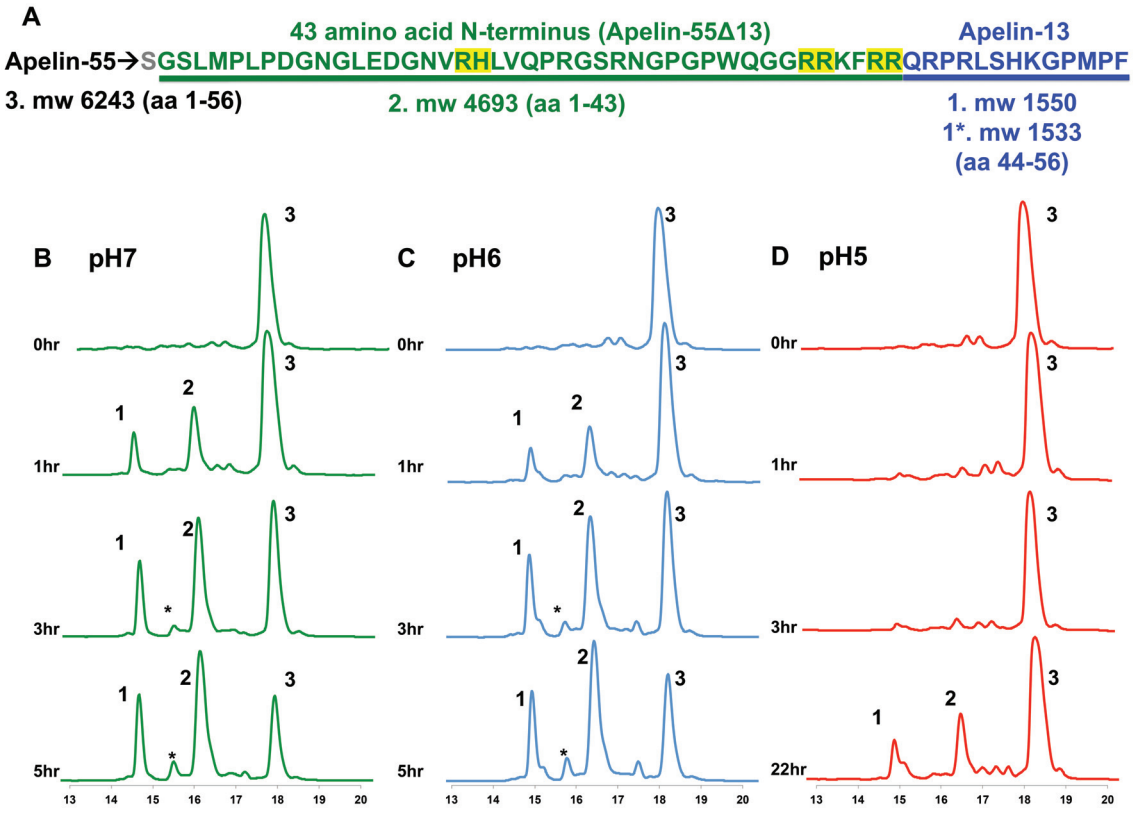

Figure 4.4: PCSK3 preferentially cleaves apelin-55 into apelin-13.
Apelin-55 produced and purified from *E. coli* was incubated with recombinant PCSK3. A) Apelin-55 and its fragments alongside predicted molecular weights; numbered 1-3, corresponding to RP-HPLC elution times shown in panels B-D. The grey Ser at the N-terminus is not found in human apelin-55 but is retained residue following TEV protease cleavage; the green residues represent the endogenous 42 amino acid N-terminal domain (apelin-55Δ13); blue represents the 13-residue apelin-13, with peptide 1* being Pyr-apelin-13. B-D) RP-HPLC chromatograms (monitored through absorbance at 214 nm) demonstrating time-dependent result of incubating apelin-55 with PCSK3. The production of 3 new products corresponding to apelin-13, Pyr-apelin-13, and the 43-residue N-terminal domain were observed at B) pH 7, C) pH 6, and D) pH 5.

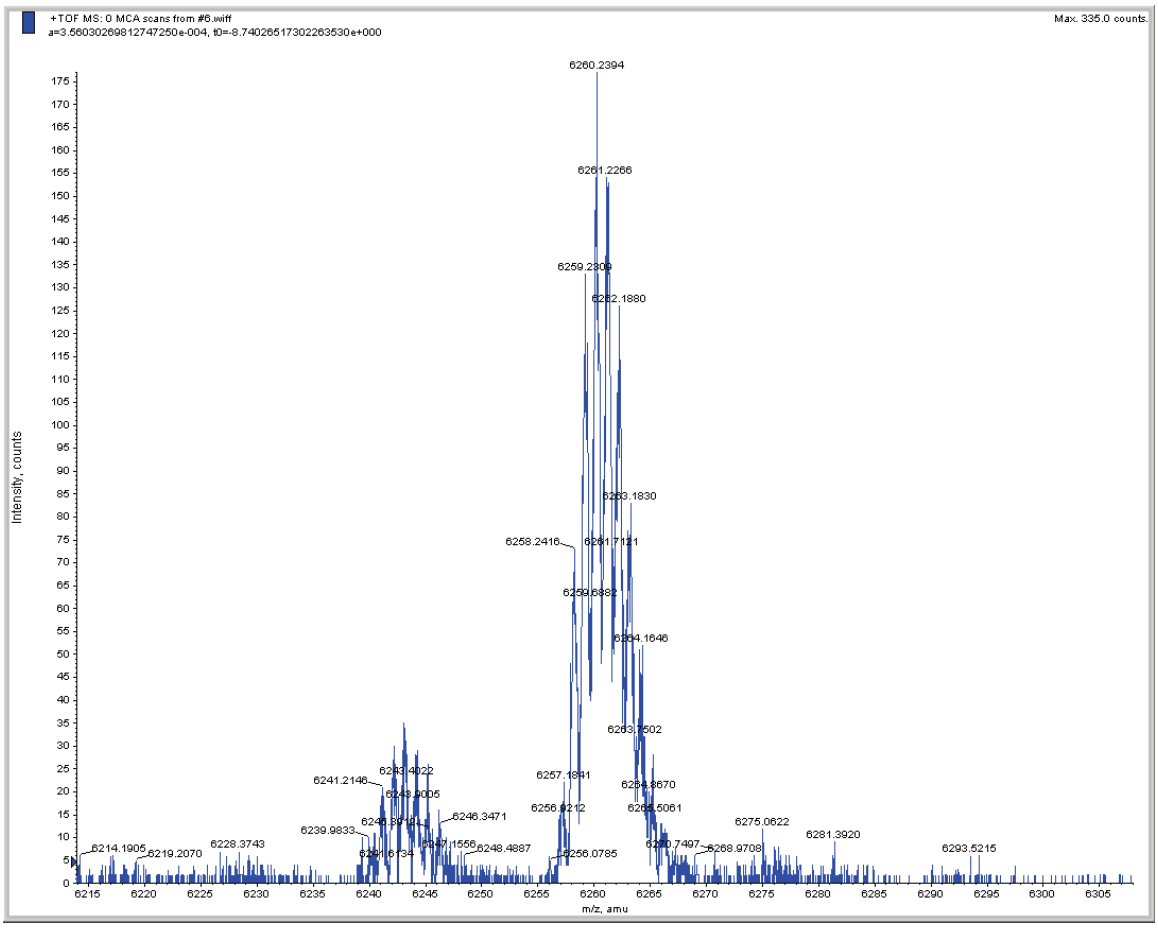

Figure 4.5: MALDI-TOF-MS confirmation of mass of apelin-55 in PCSK3 reaction mixture (peak 3, Figure 4.4).

Oxidized form of apelin-55 with additional ~16 amu is observable (~6259 m/z).

Isotopic distribution is also present for both forms.

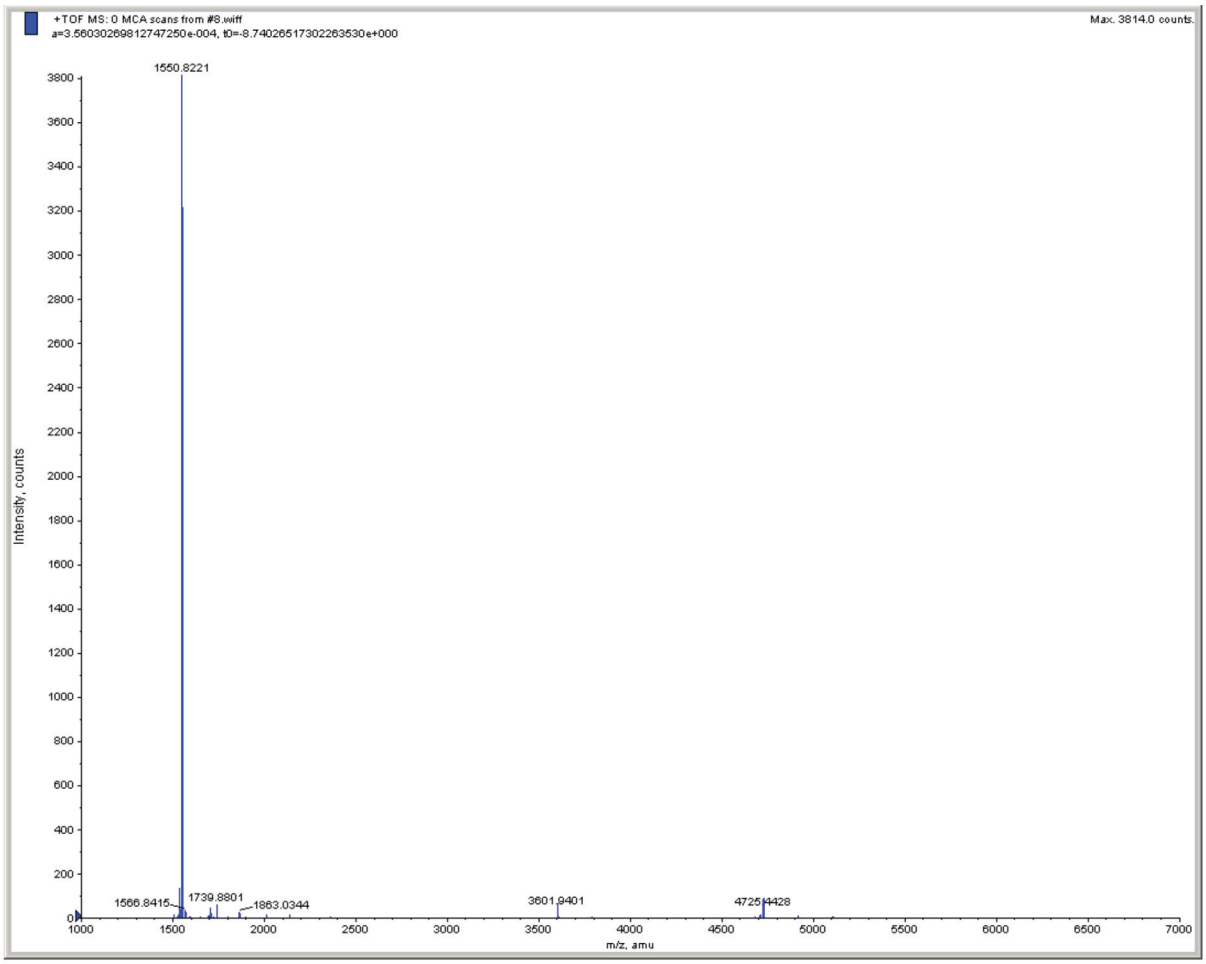

Figure 4.6: MALDI-TOF-MS confirmation of apelin-13 mass in PCSK3 reaction mixture (peak 1, Figure 4.4).

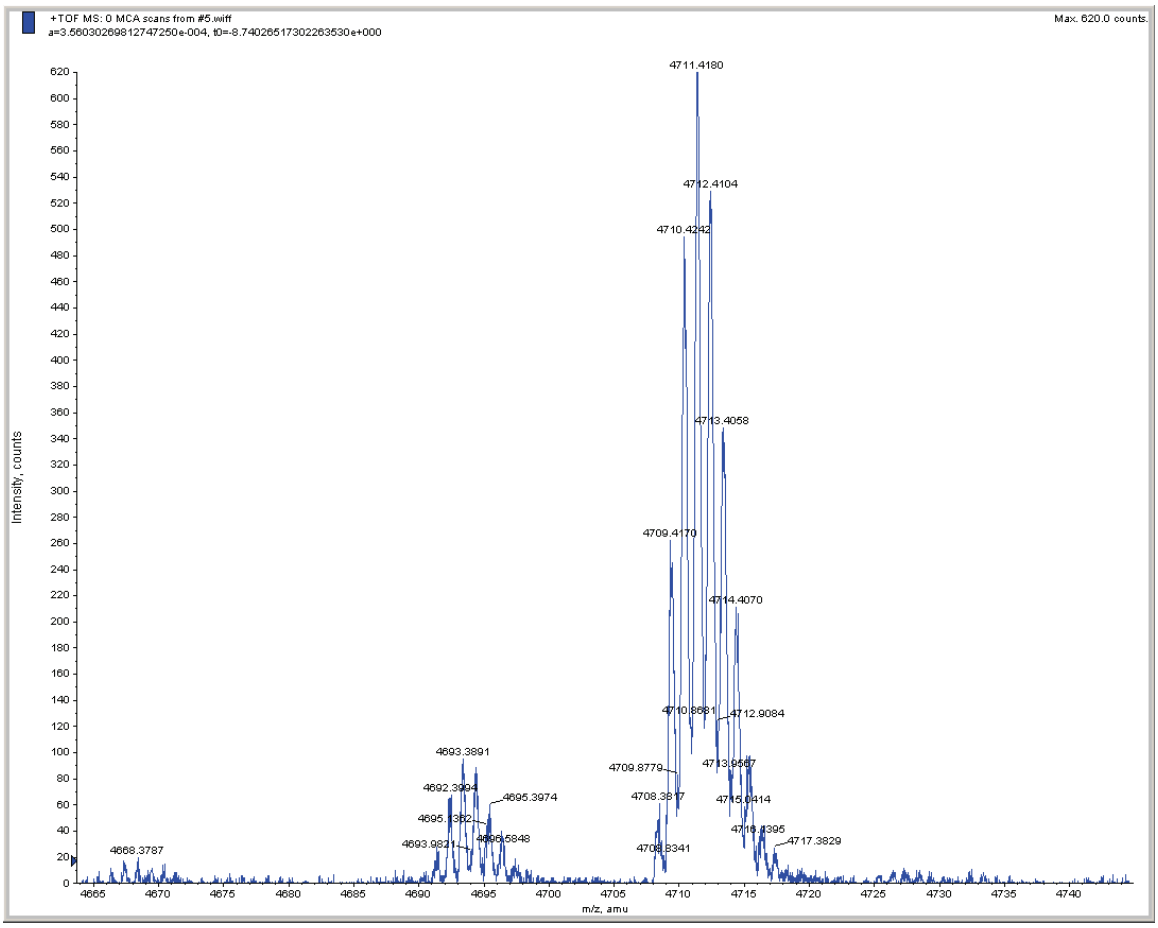

Figure 4.7: MALDI-TOF-MS confirmation of apelin-55Δ13 mass, or the putative pro-domain, in PCSK3 reaction mixture (peak 2, Figure 4.4).

Oxidized form of apelin-55Δ13 with additional ~16 amu is observable (4709 m/z). Isotopic distribution is also present for both forms.

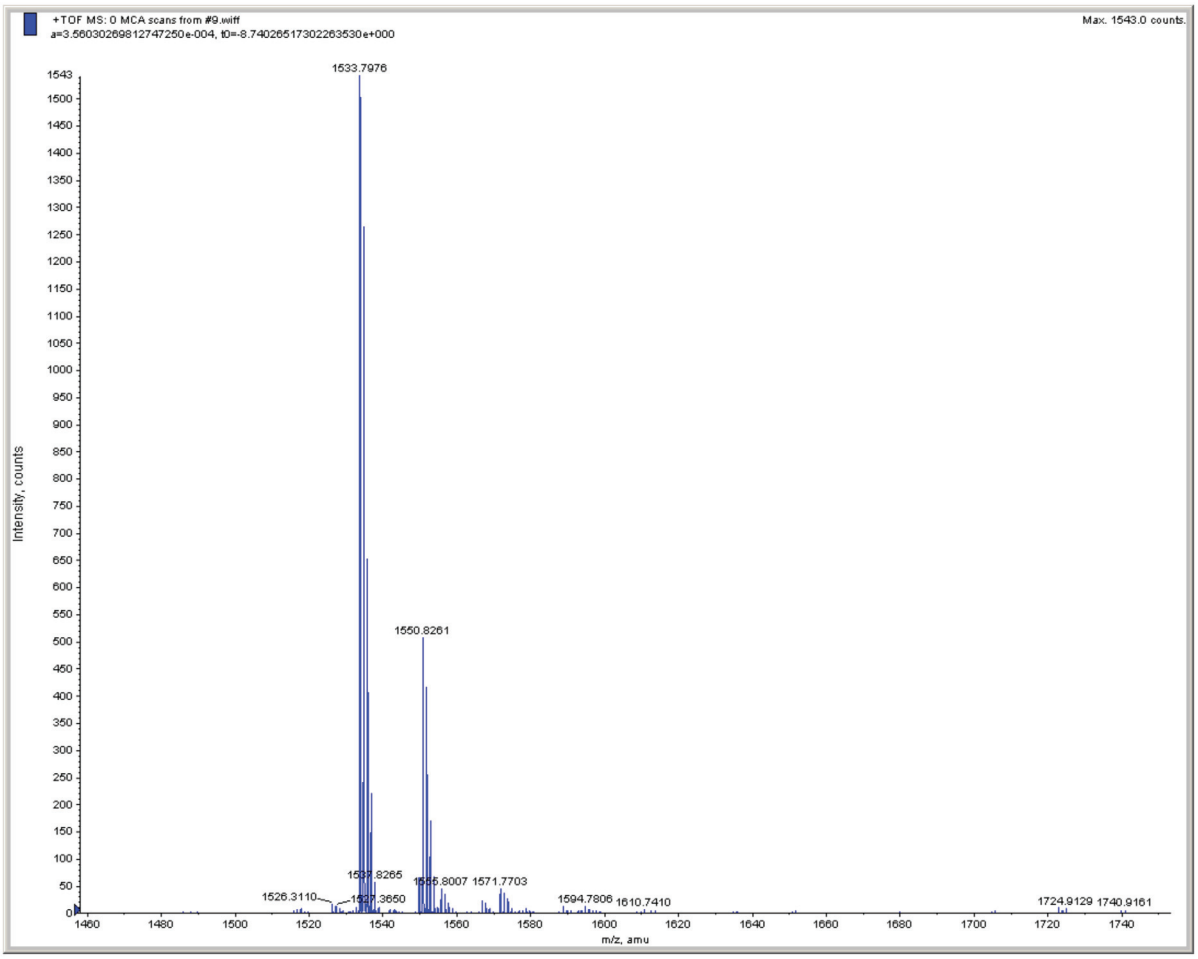

Figure 4.8: MALDI-TOF-MS confirmation of Pyr-apelin-13 mass in PCSK3 reaction mixture (peak 1*, Figure 4.4).

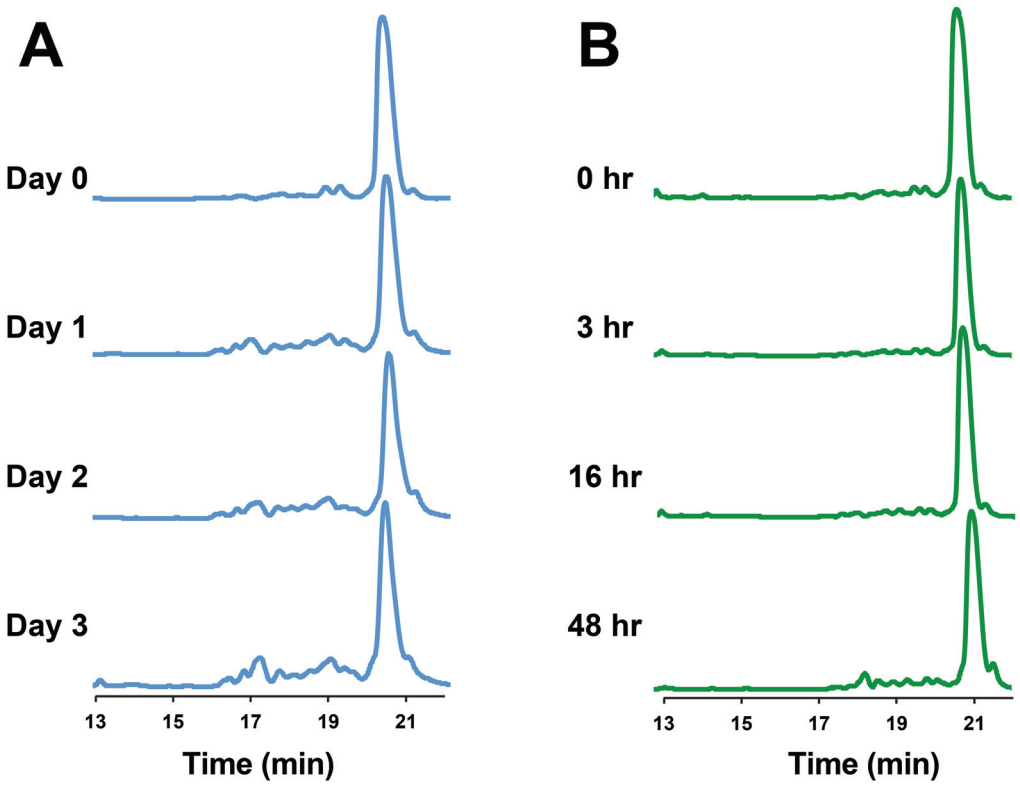

Figure 4.9: Apelin-55 is not processed by PCSK1 and PCSK7.
Apelin-55 is not cleaved in over 48 h by A) PCSK1 or B) PCSK7. Apelin-55 was incubated with PCSK1 or 7 in appropriate reaction buffer, with reactions monitored (absorbance at 214 nm) at indicated discrete time points by RP-HPLC.

CHAPTER 5 *IN SITU* (EXTRACELLULAR) PROCESSING OF APELIN-55

(Note: This chapter has been prepared as a manuscript entitled "Extracellular apelin processing occurs and gives rise to cell line-dependent preferences in isoform production" for ***Endocrinology***, which requires a separate results and discussion sections for a primary article. Thus, unlike other chapters of this thesis, Chapter 5 has separate results and discussion sections. This work was supported by two undergraduate mentees. Mr. Michael Landsman was an undergraduate student volunteer who assisted me in nearly all aspects of the project. Mrs. Stephanie Pelletier was another undergraduate student who assisted in the development of the extracellular assay. Dr. Bader Alamri helped to maintain and differentiate 3T3-L1 adipocytes.)

5.1 INTRODUCTION

As introduced in Chapter 3, apelin-55 was not initially detected in the first report of apelin identification in bovine stomach tissues [74]. Instead, apelin-36 was the longest isoform identified and apelin-55 was labeled as an inactive proprotein as a consequence. These inferences collectively led to the hypothesis that apelin processing occurred initially intracellularly to produce apelin-36 from the 55-residue isoform [88, 92]. In support of the potential for intracellular apelin processing, co-expression of apelin and PCSK3 demonstrated observable cleavage of apelin into shorter isoforms upon analysis of cell extracts [203].

In contrast to this, intact apelin-55 was detected in both colostrum and milk [93] while isoforms having a mass larger than that of apelin-36 were detected in plasma [94].

Thus, apelin-55 secretion into the extracellular fluid appears entirely possible without an explicit requirement for intracellular processing. Following from the discussion in Section 4.4, processing enzymes such as PCSK3 may be cell surface-anchored, in the extracellular matrix, and/or in body fluids [315]. Thus, it is fully possible for apelin-55 to encounter endoproteases on the cell surface or in the extracellular fluid and to undergo enzymatic processing. In support of this contention, while apelin-36 was detected in the mixture of bioactive peptides purified from bovine stomach tissues [74], only Pyr-apelin-13 was detected in glucose-stimulated gastric secretion in mice [268]. Hence, if apelin-36 is the isoform secreted from stomach cells, the detection of only a shorter isoform in gastric secretions indicates that processing should be occurring extracellularly, assuming that the source of apelin is the stomach tissue.

Although it is probable that multiple proteases are capable of processing apelin, only PCSK3 has, thus far, been demonstrated to process apelin [96, 203]. Due to the presence of a transmembrane domain, PCSK3 is membrane-anchored, both in the secretory pathway and on the cell surface [315], giving rise to the possibility that this enzyme is responsible, at least in part, for extracellular processing of apelin. Notably, apelin also binds to membrane-mimetic micelles [329] (see Chapter 7), further increasing the likelihood of apelin-PCSK3 interactions on the cell surface through the combination of a variety of factors associated with increasing the favourability of peptide-receptor interactions in the "membrane catalysis" model [330] detailed in Chapter 7.

There is a strong potential, therefore, for apelin to be processed extracellularly by cell surface enzymes such as PCSK3. To test for this, we initially exposed exogenous His_6-tagged apelin-55 to PCSK3-overexpressing human embryonic kidney (HEK) cells,

providing the best probability of observing extracellular processing. In addition, apelin processing was probed in differentiated 3T3-L1 adipocytes, which express both apelin and PCSK3 endogenously [96] and which have been extensively used to study the role of apelin in adipoinsular axis at both cellular and molecular level [140, 177-179]. Culture media from each cell line were initially characterized through western blotting (probing for the His_6 tag). Then, following a similar method optimized for the *in vitro* apelin processing assay discussed in Chapter 4, culture media were characterized through RP-HPLC and ESI-TOF-MS to determine both the extent and isoform-specificity of extracellular apelin processing that were taking place.

5.2 MATERIALS AND METHODS

5.2.1 APELIN-55 PRODUCTION AND PURIFICATION

Following the method detailed in Section 4.2.1, human apelin-55 with an N-terminal His_6 tag and TEV protease cleavage site (total 75 residues) was expressed in *Escherichia coli* C41 (DE3) and purified using Ni-NTA affinity and cation exchange chromatographies. Unlike the work detailed in Chapter 4, the protein was purified by cation exchange chromatography without TEV protease cleavage to allow for downstream detection through use of the His_6 tag. The His_6-tagged peptide was further purified using RP-HPLC using a ProStar HPLC (Varian Canada Inc.), a preparative C_{18} column (20 mm I.D. x 250 mm, Cosmosil, Nacalai USA Inc. San Diego, CA), with a binary solvent system (A: H_2O with 0.1% trifluoroacetic acid (TFA) and B: acetonitrile with 0.1% TFA; flow rate 8 mL/min). Gradients were as follows: i) 2 to 20% solvent B in 5 min, ii) 20 to 45% solvent B in 25 min, iii) 45% to 2% solvent B in 1 min. Eluent peaks

were collected, lyophilized, and analyzed by ESI-TOF-MS (Mass Spectrometry Laboratory, Department of Chemistry, Dalhousie University). Lyophilized, purified His-apelin-55 aliquots were prepared based upon the Beer Lambert law ($c=A\cdot\varepsilon^{-1}\cdot l^{-1}$, where A is absorbance at a given wavelength (280 nm, here), $\varepsilon_{280\ nm} = 6990\ M^{-1}\ cm^{-1}$ is the molar absorptivity at 280 nm for the fusion protein calculated as described by Gill and von Hippel [331], and *l* is the pathlength).

5.2.2 CELL CULTURE

HEK293A cells (ATCC) were cultured at 37 °C in 5% CO_2 in DMEM containing 10% fetal bovine serum (FBS, Invitrogen, USA), 1% penicillin/streptomycin (P/S, P4333, Sigma Aldrich). 3T3-L1 preadipocytes (ATCC) were grown at 37 °C in 5% CO_2 in high glucose Dulbecco's modified Eagle's medium (DMEM, Sigma Aldrich) containing 10% new calf serum (NCS, Invitrogen) and 1% P/S. The medium for both cell lines was refreshed every second day, with transfer accomplished by 10% trypsin digest when cells were at ~70% confluence.

5.2.3 HEK293A CULTURE AND TRANSFECTION

HEK293A cells were seeded in 12-well plates and cultured in high glucose DMEM containing 1% P/S and 10% FBS. At ~80% confluency, cells were transfected by addition of serum-free Opti-MEM (High Glucose, Gibco) containing 1 μg of the PCSK3 coding pIRES2-EGFP plasmid (gift of Drs. Janice Mayne and Michel Chrétien, University of Ottawa) and 5 μL of Lipofectamine 2000 (Invitrogen, Thermo Fisher Scientific) per well. Exposure to transfection medium was carried out for 4 h, then medium was replaced with high glucose DMEM containing 10% FBS. Transfected cells

were allowed to express the PCSK3 gene for 48 h prior to use in the extracellular processing assay. To check the efficiency of transfection, total RNA was extracted from HEK293A cells using Aurum™ Total RNA Fatty and Fibrous Tissue Kit (Bio-Rad) according to the manufacturer's protocol. Total RNA was reverse transcribed using the iScript™ cDNA Synthesis Kit (Bio-Rad) and PCSK3 mRNA was amplified by polymerase chain reaction (PCR) (primers; forward: 5'-AACAACGGTGTCTGTGGTGTAGGT-3'; reverse: 5'-AGCTGGCACTGTAGATGTGGATGT-3').

5.2.4 3T3-L1 PREADIPOCYTE DIFFERENTIATION

3T3-L1 preadipocytes were seeded in 12-well plates and grown to confluence. At 2 days post-confluence (day 0), the medium was changed to induction medium (DMEM, 10% FBS, 1% P/S, 1 µM dexamethasone (DEXA, D2915, Sigma Aldrich), 0.5 mM 3-isobutyl-1-methylxanthine (IBMX, I7018, Sigma Aldrich), and 1 µg/ml human insulin (HI-210, Eli Lilly and Company)). After 2 days of incubation (day 2), the medium was replaced with insulin medium (DMEM supplemented with 10% FBS, 1% P/S, and 10 µg/ml human insulin). Thereafter, the medium was replaced every day with FBS medium (DMEM supplemented with 10% FBS and 1% P/S). Once full differentiation was observed (day 8-10), adipocytes were used for extracellular apelin-55 processing assays.

5.2.5 EXTRACELLULAR APELIN-55 PROCESSING ASSAY

Following the final step of cell setup (HEK293A transfection or 3T3-L1 differentiation), His-apelin-55 was dissolved (3 µg/µL) in phenol red-free DMEM (High Glucose, Sigma Aldrich). Medium was replaced with serum-free and phenol red-free

DMEM (High Glucose, 400 µL/well). Each well of the plate was supplemented with dissolved protein (50 µL) at a final concentration of 0.333 µg/µL per well. Cells were exposed to His-apelin-55 for designated time points. For inhibition studies, cells were exposed to decanoyl-RVKR-CMK (Biomol International) in serum-free and phenol red-free DMEM (High Glucose, 400 µL/well) at concentrations of 25, 2.5, or 0.25 µM for 1 h prior to supplementation with His-apelin-55 based on the manufacturer's guidelines. For 0 h (control) samples, the culture medium was collected promptly upon addition of His-apelin-55; thus, exposure to His-apelin-55 was short (≤ ~1 min). For all other treatments, the culture medium was collected at the designated incubation periods, and cells were resuspended in 150 µL of lysis solution (Cytobuster protein extraction reagent, Novagen) supplemented with protease (Roche) and phosphatase (Roche) inhibitors. All treatments were carried out in triplicate and all experiments were at least in duplicate. A high inhibitor treatment (25 µM) was used as a control for all inhibitor experiments.

5.2.6 WESTERN BLOTTING/COOMASSIE STAINING-MEDIATED DETECTION

For detecting intracellular His-apelin-55, cells were homogenized through sonication, followed by centrifugation at 10,000 *g* for 10 min at 4 °C. Supernatants were collected and protein concentration determined using bovine serum albumin (BSA) protein standard assay (Bio-Rad). Resulting cell lysate samples (~60 µg) were resolved by SDS-PAGE (20% polyacrylamide gel, 120 V, 2 h) and visualized with Coomassie blue.

For detection of extracellular His-apelin-55, culture media were collected and 30 µL (~10 µg protein load, based on initial His-apelin-55 concentration prior to cell exposure) aliquots were resolved by SDS-PAGE (20% polyacrylamide gel, 120 V, 2 h).

The resulting gel was either stained with Coomassie blue or transferred to a polyvinylidene difluoride membrane (Bio-Rad) at 100V for 45 min. Membranes were blocked in Tris-buffered saline with 0.1% Tween-20 (TBST) containing 25 mg/ml BSA for 60 min at room temperature and then washed twice with TBST for 10 min each before incubation with HisProbe-HRP (Thermo Fisher Scientific; 1:5000 dilution in TBST with 25 mg/ml BSA) for 60 min. Subsequently, membranes were washed with TBST four times for 5 min each then incubated in Clarity Western ECL Blotting Substrates (Bio-Rad). Chemiluminescence was detected and quantified through densitometry using a molecular imager (Gel Doc^{TM} XR+, Bio-Rad). Quantified values were standardized to unprocessed control lane (i.e., 0 h) for the respective membrane blots prior to statistical analyses. Results were then presented as means ± SEM and were analyzed using the t-test to compare each inhibitor treatment to the control at 0 h (a significance of $P < 0.05$ was applied).

5.2.7 RP-HPLC-BASED DETECTION

Media samples were resolved using a ProStar HPLC (Varian Canada Inc., Mississauga, ON) employing a C_{18} analytical column (4.6 mm I.D. X 150 mm, Grace Alltech, Columbia, MD) and a binary solvent system (A: H_2O with 0.1% trifluoroacetic acid (TFA) and B: acetonitrile with 0.1% TFA; flow rate 1 mL/min) with gradient elution as follows: i) 2 to 20% solvent B in 5 min, ii) 20 to 40% solvent B in 20 min, iii) 40% to 100% solvent B in 15 min, iv) 100% to 2% solvent B in 1 min. UV chromatograms were recorded at 213 and 280 nm simultaneously. Non-culture media eluents were collected and pooled for each experiment then lyophilized. Eluent masses were then determined

using ESI-TOF-MS (Dalhousie University) and compared to all masses that could theoretically result from post-translational processing of His-apelin-55 for identification.

5.3 RESULTS

5.3.1 HIS-APELIN-55 IS PROCESSED UPON EXTRACELLULAR INTRODUCTION TO HEK293A CELLS.

Exposure of exogenous His-apelin-55 (His_6+TEV cleavage site-tagged apelin-55; total 75 residues; ~8380 Da) to HEK293A cells resulted in clear changes, as observed by western blotting for His_6. Specifically, a band at ~10 kDa (consistent with intact His-apelin-55) decreased in intensity after 24 h exposure to cells (Fig. 5.1A). This decrease in intensity was dependent upon exposure, as incubation in cell-free culture medium did not result in a similar behaviour (Fig. 5.2). In addition, a new His_6-reactive product was observed at lower intensity and mass (Fig. 5.1A). Since this assay could only detect unprocessed peptides and any N-terminal domains containing the tag, as it probed for the N-terminal His_6 tag, Coomassie blue staining was also employed to test for the potential to detect any other products in this manner (Fig. 5.3). However, no additional bands were detected using Coomassie stain relative to western blotting that would be representative of other processing products.

To better identify potential products of exogenous His-apelin-55 processing, culture media constituents were evaluated by RP-HPLC. Notably, comparison of HPLC chromatograms of culture media with and without exogenous His-apelin-55 demonstrated elution over a distinct time range (~15-20 min using the applied gradient) for His-apelin-55 and its processed products (Fig. 5.1B and C). This elution period is consistent with the

fraction of acetonitrile required for elution of apelin isoforms (Table 4.2). Consistent with western blotting, HPLC chromatograms demonstrated a significant loss in the level of intact His-apelin-55 at both 4 h and 24 h incubation time points (depletion of eluent peak at ~18 min, Fig. 5.1B and C; peptide identity confirmed by ESI-TOF-MS, Fig. 5.4-6). Processing was also implied, given the appearance of multiple new observable peaks, with this being more evident after 24 h of incubation than at the 4 h time point (Fig. 5.1B and C). Thus, the 24 h incubation period was chosen for subsequent experiments.

ESI-TOF-MS analysis of these potential processing products was carried out (Table 5.1 lists all masses considered). The second largest peak in the chromatogram (eluting at ~17 min) had a mass of 6535 Da (Fig. 5.7), corresponding directly to the expected mass of His-apelin-55Δ15 (i.e., the product following cleavage of 15 C-terminal residues). The peak at ~17.5 min corresponded to a peptide with mass ~4640 Da (Fig. 5.6), consistent with His-apelin-55Δ32 (i.e. the product resulting from release of C-terminal 32 residues) and increasing in intensity as a function of incubation period (Fig. 5.5 and 5.6). Masses determined for eluents over the 15-16.5 min period exhibited convoluted m/z ratios corresponding to various processed products (Table 5.1 and Fig. 5.8 and 5.9). Similar to the eluent at 17 min, the predicted cleavage product consistent with many of these corresponded to release of 15 C-terminal residues, but with additional N- and, in some cases, up to 16 C-terminal truncations (Table 5.1).

A similar processing pattern was observed in non-transfected HEK293A cells. Upon transfection (Fig. 5.10), however, processing was increased, as the level of processed products consistently exceeded that of intact-His-apelin-55 with transfection, while opposite trend was observed without transfection (Fig. 5.1). Thus, to improve the

yield of observable extracellular apelin processing, transfected HEK293A cells were used for subsequent experiments. On another note, although the quantity of unprocessed His-apelin-55 changed with transfection, the quantities of processed products observed did not change proportionally (Fig. 5.1B and C). Analysis of intracellular contents using SDS-PAGE optimized to separate low molecular weight species and visualized by Coomassie blue staining did not demonstrate any bands of similar mass to His-apelin-55 (Fig. 5.11). Furthermore, in contrast to culture media, comparison of cellular contents did not show any observable differences between treated and untreated cells.

5.3.2 PCSK INHIBITOR TREATMENT DECREASES THE QUANTITY OF PROCESSING.

To better elucidate the role of PCSK3 in exogenous His-apelin-55 processing, decanoyl-RVKR-CMK was applied. This compound acts as a PCSK inhibitor and is not specific to PCSK3 [332]. Pretreatment with decanoyl-RVKR-CMK significantly decreased processing of exogenous His-apelin-55 (Fig. 5.12), as was evident by western blotting (Fig 5.13A) and HPLC elution profiles (Fig 5.13B and C). Densitometry demonstrated that statistically significant inhibition was achieved in response to both 25 and 2.5 μM doses; however, pretreatment with the inhibitor even at the higher of these doses did not completely block processing. HPLC chromatograms also exhibited a prominent peak eluting at ~16 min with the addition of inhibitor. ESI-TOF-MS analysis identified a mass of 8233 Da for this prominent eluent, matching the expected mass of His-apelin-55Δ1 (i.e., His-apelin-55 missing the C-terminal phenylalanine) (Fig. 5.14; and Table 5.2 lists all masses). Addition of the inhibitor also decreased the production of His-apelin-55Δ32, as observed by a single apparent peak eluting at ~19 min by HPLC;

however, an m/z ratio corresponding to 4640 Da could still be detected by ESI-TOF-MS (Fig. 5.15), implying that this processing product is still present even though it was not visible through monitoring of UV absorption.

5.3.3 HIS-APELIN-55 IS PROCESSED BY 3T3-L1 ADIPOCYTES

The potential for His-apelin-55 processing was also examined in 3T3-L1 adipocytes, a cell line with more potential physiological relevance to natural apelin processing. Given that mRNA expression of PCSK enzymes (PCSK1, 3, and 7) are increased in 3T3-L1 cell line upon differentiation [96], fully differentiated 3T3-L1 adipocytes were employed to characterize extracellular apelin-55 processing to increase the likelihood of PCSK-mediated apelin processing. Introduction of His-apelin-55 to differentiated adipocytes exhibited similar behaviour to that observed in HEK293A cells by western blotting (Fig. 5.16A). Namely, the level of exogenous His-apelin-55 decreased upon 24 h incubation with cells. In addition, pretreatment of 3T3-L1 adipocytes with the inhibitor decanoyl-RVKR-CMK reduced, but did not completely block, processing (Fig. 5.17). In contrast to HEK293A cells, where a 2.5 μM dose of inhibitor was required, a dose of 0.25 μM was also capable of inhibiting processing in 3T3-L1 cell medium. As a final contrast to HEK293A cells, bands at lower molecular weights were not observed by western blotting in adipocyte culture medium (Fig. 5.16A).

HPLC analysis of adipocyte culture media samples demonstrated further striking differences relative to chromatograms observed for HEK293A cell media. Specifically, the elution profile of His-apelin-55 and its processed products widened to a range of ~13-20 min (Fig. 5.16B and C), the overall chromatographic resolution was lowered, and the number of distinguishable peaks decreased. Analysis of the resulting eluents by ESI-

TOF-MS also demonstrated distinct products from those observed in HEK293A culture medium. In particular, the product eluting at ~16 min consistently presented a mass of 4202 Da (Fig. 5.18; and Table 5.3 shows all masses considered for adipocytes), matching the expected mass of His-apelin-55Δ36, N-terminal domain produced upon release of apelin-36. Consistent with this, the eluents from 13-15 min exhibited m/z ratios corresponding to peptides with masses of 3602 and 4196 Da, matching apelin-31 and -36, respectively (Fig. 5.19).

5.4 DISCUSSION

When incubated with HEK293A cells overexpressing PCSK3, His-apelin-55 was processed to shorter isoforms, as observed by HPLC and by western blotting (Figs. 5.1, 5.13, and 5.22). The major product correlated to the mass of His-apelin-55Δ15. While the peak for this N-terminal domain did not significantly change in intensity upon pretreatment with a PCSK inhibitor, the ratio of the processed N-terminal product to intact His-apelin-was significantly increased upon transfection. These observations suggest that while His-apelin-55Δ15 production is mediated by PCSKs, the N-terminal product likely undergoes further processing by protease(s) other than PCSKs leading to a steady-state in its concentration.

One possible source of this N-terminal domain would be the direct processing of His-apelin-55 to release apelin-15. Consistent with this, apelin-15 has been detected in both colostrum and milk [93]. However, based on *in vitro* demonstration of apelin-13 production from apelin-55 by PCSK3 as shown in Chapter 4 and the increased level of PCSK3 being effected through transfection and overexpression, it is also quite likely that

apelin-13 was produced. The resulting N-terminal domain may have then been further processed by Arg exoproteases (Fig. 5.23), such as carboxypeptidase M which is membrane-anchored on the surface of kidney cells [333]. These possibilities are difficult to distinguish as neither apelin-13 nor -15 were detected in the medium.

The other processing product produced upon incubation with PCSK3-overexpressing HEK293A cells is consistent with His-apelin-55Δ32. This domain would couple with production of apelin-32. However, this is not an isoform observed under physiological settings, even in milk where the largest variety of isoforms has been identified [93]. Rather, the isoform most comparable to this in milk and colostrum was apelin-31, which would result in an N-terminal apelin cleavage product with an arginine at its C-terminus (i.e., His-apelin-55Δ31). Thus, similar to the rationale above for His-apelin-55Δ15 production from His-apelin-55Δ13, His-apelin-55Δ32 may also be a product of additional processing of His-apelin-55Δ31 by Arg exoproteases (Fig. 5.23). The levels of this N-terminal processing product detected were modulated both by transfection and through pretreatment with a PCSK inhibitor. This alternative processing product may, therefore, arise from a proprotein convertase other than PCSK3 and/or from subsequent processing of His-apelin-55Δ15 to a shorter product.

Analysis of other minor eluents showed masses corresponding to N-terminally truncated His-apelin-55 products. Although the amount of N-terminal truncation varied, all observed products were missing the N-terminal His_6 tag. The cleavage of the His_6 tag is consistent with the lack of visualization of these apelin processing products by western blotting. The level of absorption observed in the HPLC chromatogram for these products is also consistent with other products that are below the detection level of Coomassie blue

staining following SDS-PAGE. Notably, these products also demonstrated the loss of 15-16 C-terminal residues, consistent with His-apelin-55Δ15 production and with either apelin-16 release from apelin-55 or with further C-terminal processing of His-apelin-55Δ15. It is unclear whether one or both of these processes occurred; however, observation of these N- and C-terminally truncated products is a further indication of the involvement of additional endo and/or exoproteases.

Pretreatment of HEK293A cells with the PCSK inhibitor decanoyl-RVKR-CMK resulted in visualization of a distinct processing product correlating to His-apelin-55Δ1 (i.e., His-apelin-55 missing the C-terminal Phe). Angiotensin-converting enzyme 2 (ACE2) has previously been linked to apelin deactivation processes and/or regulation of signalling [99, 100, 102]. This enzyme is also membrane-anchored similarly to PCSK3, and has been detected in kidney cells [334]. Hence, ACE2 is likely responsible for the observed processing upon PCSK inhibition. The ability to observe this processed form of apelin-55 only in the presence of PCSK inhibitor suggests that His-apelin-55Δ1 would be readily processed by PCSKs into other isoforms undetectable in our experimental conditions as with the shorter, intact apelin isoforms.

One alternative possibility is that His-apelin-55 is internalized and processed intracellularly, rather than extracellularly, following the demonstration of intracellular apelin processing when co-expressed with processing enzymes [203]. This mechanism would be energy intensive and is difficult to reconcile with the observation of cleaved N-terminal processing products in the culture medium, since the secreted product would presumably be the bioactive C-terminal apelin isoform. Correspondingly, under my assay conditions, I did not detect any His-apelin-55 in the intracellular fraction of HEK293A

cells or any bands upon SDS-PAGE visualization that differed between His-apelin-55 treated and untreated cells. His-apelin-55 is, thus, unlikely to be internalized for processing. Coupling these findings to those of Adam *et al*. [203], alongside the observation of high levels of apelin-55 in extracellular fluid [93], apelin processing appears possible either intracellularly or extracellularly.

3T3-L1 adipocyte cell-line has previously been employed for characterization of physiological roles of apelin such as adipogenesis, lipolysis, and glucose homeostasis [178, 186]. Thus, it is highly notable that incubation of His-apelin-55 with 3T3-L1 adipocytes resulted in a clearly distinct processing pattern relative to HEK293A cells (Figs. 5.16 and 5.22). Specifically, the primary product observed was His-apelin-55Δ36, the N-terminal domain corresponding to cleavage of apelin-36. Although lesser in intensity in the HPLC chromatogram, apelin-36 was also directly observed. In addition, apelin-31 was detected, suggesting that additional processing takes place. As in HEK293A cells, processing in adipocytes was modulated upon addition of PCSK inhibitor. Given the lack of observation of N-terminal His-apelin-55 domains corresponding to shorter isoforms, processing of apelin in 3T3-L1 medium seems inconsistent with the reported production of apelin-13 by PCSK3 in Chapter 4 and others [203], implying that other PCSK(s) may be responsible (Fig. 5.23).

Perplexingly, the detectable levels of some N-terminal apelin processing products in HEK293A (e.g., His-apelin-55Δ15) and 3T3-L1 adipocytes (e.g., His-apelin-55Δ36) did not change significantly with either transfection or inhibitor, while His-apelin-55Δ1 was only detectable with inhibitor treatment. As stated earlier, one possible explanation of this phenomenon is that the level of each of the processed products is regulated and

maintained at a steady-state by enzyme(s) or protein(s) other than PCSKs. Unfortunately, beyond the noted evidence of ACE2 processing, the roles and implications of any additional enzymatic processing, or other regulatory mechanisms, remain unclear. It should be emphasized, however, that the observation of steady-state levels of N-terminal products (i.e., His-apelin-55Δ15 and -55Δ36) should not be taken as evidence to discount the involvement of PCSKs. The observation of a 10-fold increase in minimum inhibitory concentration for HEK293A cells over 3T3-L1 adipocytes is a clear demonstration of PCSK involvement, given the increased level of PCSK3 expected in the former case through transfection and overexpression. Thus, apelin processing likely occurs extracellularly not only through the involvement of PCSKs but also of other enzymes.

Under our assay conditions, we detected processing products with masses directly correlated to N-terminal pro-domains that would result from apelin-15, -16, -32, and -36 production. As noted above, we detected apelin-31 and -36 in 3T3-L1 adipocytes, with no products having masses appropriate for the C-terminal bioactive apelin segments observed in HEK293A cells. Beyond the potential for these bioactive peptides to be proteolytically processed [335], the differences in capability to observe processed bioactive apelin peptides may stem from isoform-dependent receptor internalization and regulation [208, 209, 214, 215]. Supporting this, the AR is expressed in both kidney cells and adipocytes [110], allowing for ligand-receptor complex formation. If apelin-13 is the most abundant isoform formed (i.e., with HEK293A cells overexpressing PCSK3), the findings of Lee *et al.* [208] suggest that AR will be recycled to the cell surface to allow for internalization of additional apelin-13 in the extracellular fluid. This would prevent detection of apelin-13 in the medium. Alternatively, if apelin-36 is the primary product

(i.e., in 3T3-L1 adipocytes), the ligand-AR complex will be trafficked for degradation and prevent internalization of other apelin-36 from the cell surface, resulting in accumulation of apelin-36 in the culture medium and allowing its detection.

The observed variation in the major apelin-55 cleavage product between cell lines seems likely to arise from differences in the levels of various membrane-anchored processing enzymes in each cell line. Furthermore, the difference in processing observed between HEK293A cells and 3T3-L1 adipocytes is a clear indication that tissue-dependent preferential apelin processing would be expected – for kidney vs. adipose tissue, in this case. In support of this contention, predominant apelin isoforms have been previously associated with specific tissues [108, 116].The physiological purpose of having differential processing between cell lines is not yet clear. One hypothetical role is that differential processing may be important for controlling the physiological impact downstream. Receptor regulation, as noted above, is known to be isoform-dependent [208]. Conversely to this receptor-centric viewpoint, the production of a given apelin isoform may itself be physiologically important. As an example of this, Galon-Tilleman *et al.* showed that treatment by apelin-36, but not apelin-13, resulted in an improved blood glucose tolerance and lipid profile, with lowered body weight and blood glucose in diet-induced obese mice [184]. Production of apelin-36 may thus be favoured in adipocytes to control glucose homeostasis.

In conclusion, extracellular apelin processing is both possible and highly likely. Through this mechanism, longer apelin isoforms (e.g., apelin-55 or apelin-36) may be processed to specific isoform(s) at an appropriate location to exert a required physiological response. Given the known differences in potency, efficacy, and in

downstream effects, controlling apelin processing through the presence of the required enzymes at the cell surface would serve to provide an additional level of regulation in directing the downstream effects. Apela may, logically, be regulated similarly. In combination with the previously demonstrated potential for intracellular processing of apelin, extracellular processing of apelinergic system ligands is indicative of the involvement of diverse mechanisms and proteases in regulation of the apelinergic system.

5.5 MOTIVATIONS AND BASIS FOR CHAPTER 6

In summary, apelin-55 is differentially processed between HEK293A cells and 3T3-L1 adipocytes, presumably through cell-line specific cell-anchored or secreted processing enzymes. If apelin-55 is secreted and interacts with a known binding partner extracellularly, then it is quite possible that it may interact with another cell surface protein, namely its cognate GPCR. In support of this, apelin-55 contains the necessary 12 C-terminal residues required for receptor activation. At this point, however, it is unclear whether the N-terminal residues in apelin-55 have the potential to obstruct receptor binding and/or activation. Thus, we tested whether or not apelin-55 could activate the AR. These functional studies were directly correlated to NMR spectroscopy-based characterization of the biophysical properties of apelin-55, allowing direct comparison to the shorter isoforms already known to be bioactive.

Table 5.1: Masses detected and considered for analysis from HEK293A media purification

Elution period (min)	Mass detected (Da)	Mass predicted (Da)	Most likely amino acid sequence (His_6 motif bolded)
15-16.5	3182	3181.5	GLEDGNVRHLVQPRGSRNGPGPWQGGRRK
	3922	3922.3	PLPDGNGLEDGNVRHLVQPRGSRNGPGPWQGGRRKF
	4254	4253.8	SLMPLPDGNGLEDGNVRHLVQPRGSRNGPGPWQGGRRKF
	6388	6387.9	SGS**HHHHHH**GSSGENLYFQSGSLMPLPDGNGLEDGNVRHLVQPRGSRNGPGPWQGGRRK
16.5-17.5	6535	6535.1	SGS**HHHHHH**GSSGENLYFQSGSLMPLPDGNGLEDGNVRHLVQPRGSRNGPGPWQGGRRKF
17.5-18.5	4640	4639.9	SGS**HHHHHH**GSSGENLYFQSGSLMPLPDGNGLEDGNVRHLVQP
	6535	6535.1	SGS**HHHHHH**GSSGENLYFQSGSLMPLPDGNGLEDGNVRHLVQPRGSRNGPGPWQGGRRKF
	8380	8380.3	SGS**HHHHHH**GSSGENLYFQSGSLMPLPDGNGLEDGNVRHLVQPRGSRNGPGPWQGGRRKFRRQRPRLSHKGPMPF

Table 5.2: Masses detected and considered for analysis of HEK293A cells media pretreated with inhibitor purification

Elution period (min)	Mass detected (Da)	Mass predicted (Da)	Most likely amino acid sequence (His_6 motif bolded)
16-17	4252	4250.7	SGSLMPLPDGNGLEDGNVRHLVQPRGSRNGPGPWQGGRRK
	8233	8233.1	SGS**HHHHHH**GSSGENLYFQSGSLMPLPDGNGLEDGNVRHLVQPRGSRNGPGPWQGGRRKFRRQRPRLSHKGPMP
17-17.5	6535	6535.1	SGS**HHHHHH**GSSGENLYFQSGSLMPLPDGNGLEDGNVRHLVQPRGSRNGPGPWQGGRRKF
17.5-18.5	8380	8380.3	SGS**HHHHHH**GSSGENLYFQSGSLMPLPDGNGLEDGNVRHLVQPRGSRNGPGPWQGGRRKFRRQRPRLSHKGPMPF

Table 5.3: Masses detected and considered for analysis of 3T3-L1 cells media

Elution period (min)	Mass detected (Da)	Mass predicted (Da)	Most likely amino acid sequence (His_6 motif bolded)
13-15	3602	3602.1	GSRNGPGPWQGGRRKFRRQRPRLSHKGPMPF
	4196	4195.9	LVQPRGSRNGPGPWQGGRRKFRRQRPRLSHKGPMPF
15-16.5	4202	4202.4	SGS**HHHHHH**GSSGENLYFQSGSLMPLPDGNGLEDGNVRH
17.5-19	8380	8380.3	SGS**HHHHHH**GSSGENLYFQSGSLMPLPDGNGLEDGNVRHLVQPRGSRNGPGPWQGGRRKFRRQRPRLSHKGPMPF

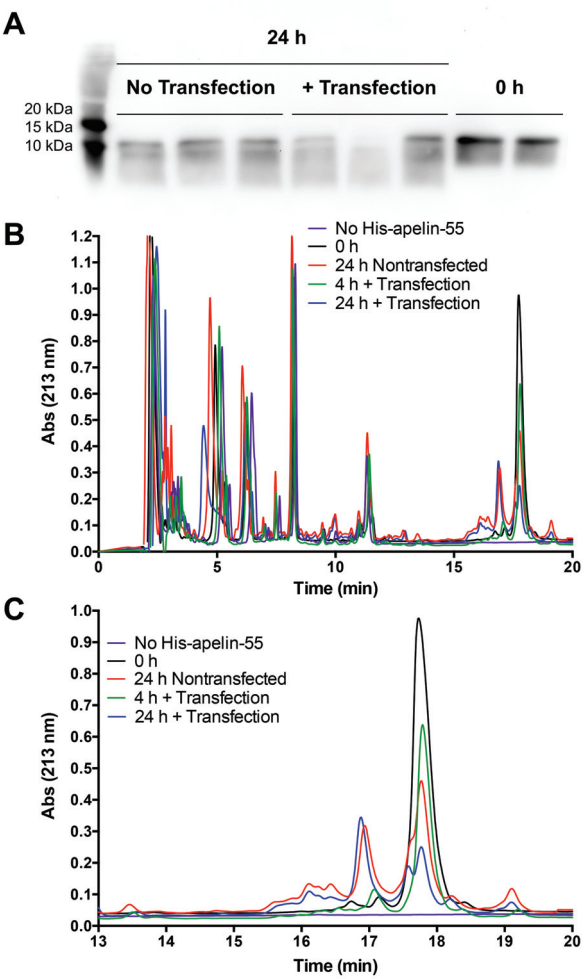

Figure 5.1: Extracellular His-apelin-55 processing by HEK293A cells is increased with PCSK3 overexpression and as a function of incubation period.
Representative A) western blot analysis and B-C) RP-HPLC chromatogram of His-apelin-55 processing.

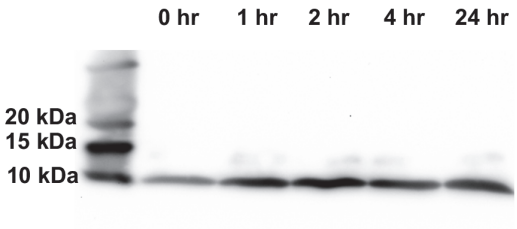

Figure 5.2: His-apelin-55 is stable in culture media over the processing assay period. Monitored by western blotting.

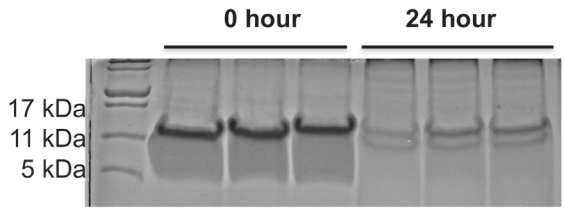

Figure 5.3: Extracellular His-apelin-55 is processed by HEK293A cells as observed by Coomassie blue staining.

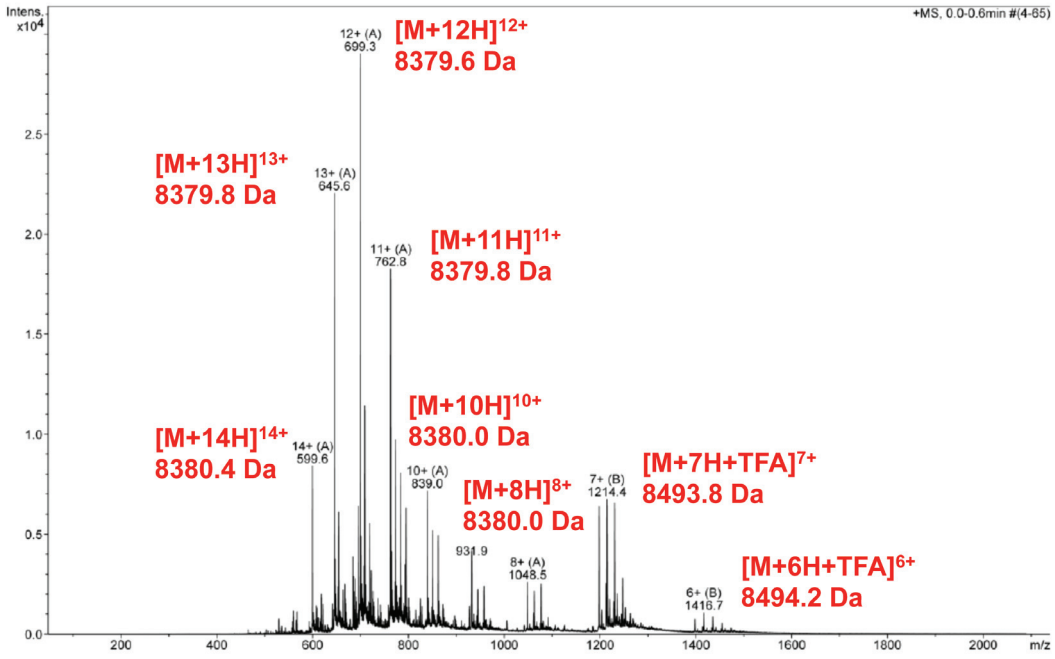

Figure 5.4: ESI-TOF-MS confirmation of His-apelin-55 mass (8380 Da; RP-HPLC elution time ~18 min) prior to incubation (i.e., at 0 h).
His-apelin-55 with TFA adducts (~114 Da) can be visualized. Isotopic distribution is also observable.

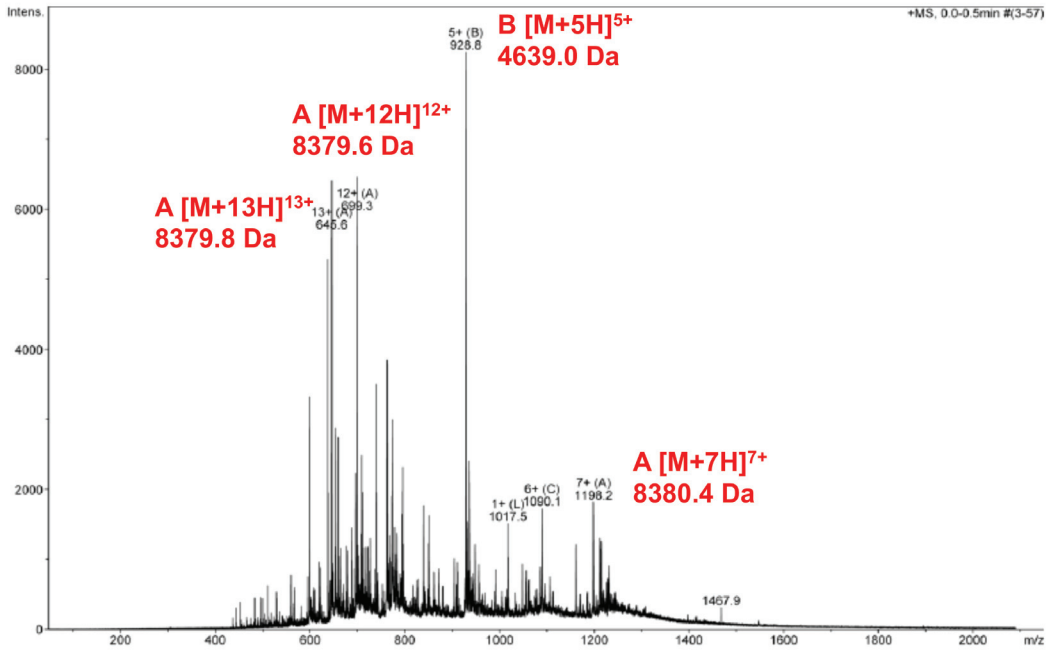

Figure 5.5: ESI-TOF-MS confirmation of His-apelin-55 (~8380 Da) and His-apelin55Δ32 (~4640 Da; HPLC elution time ~17.5 min) observed after 4 h incubation in PCSK3 overexpressing HEK293A cell medium.
Isotopic distribution is observable.

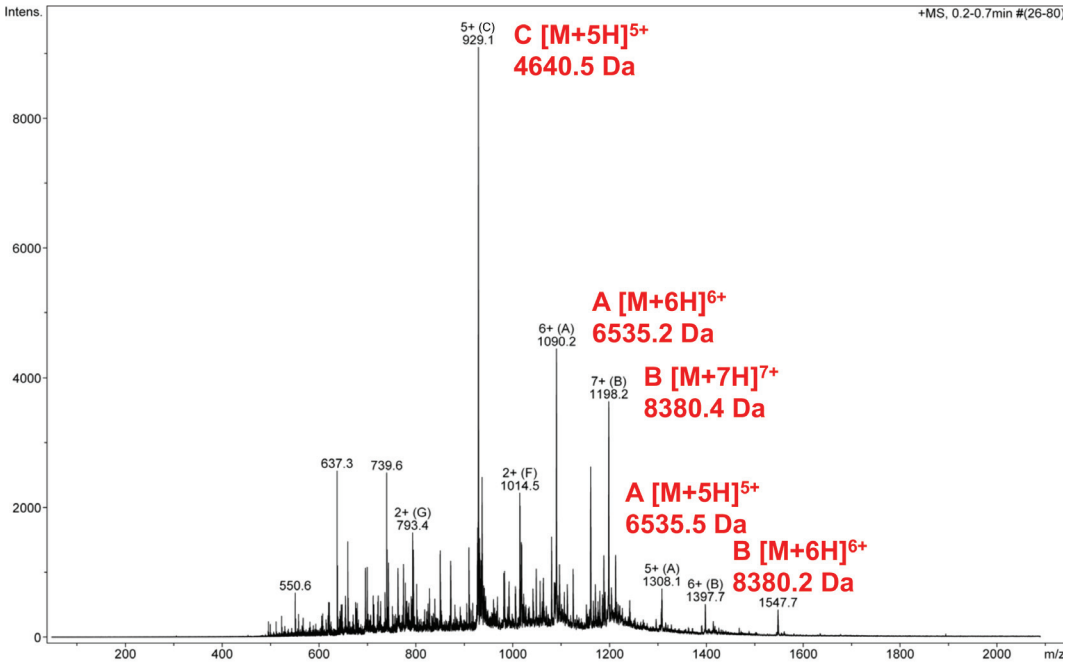

Figure 5.6: ESI-TOF-MS confirmation of His-apelin-55 (~8380 Da) and His-apelin55Δ32 (~4640 Da; HPLC elution time ~17.5 min) observed after 24 h incubation in PCSK3 overexpressing HEK293A cell medium.
His-apelin-55Δ15 (~6535 Da) is also observable, likely due to fraction collection overlap.
Isotopic distribution is observable.

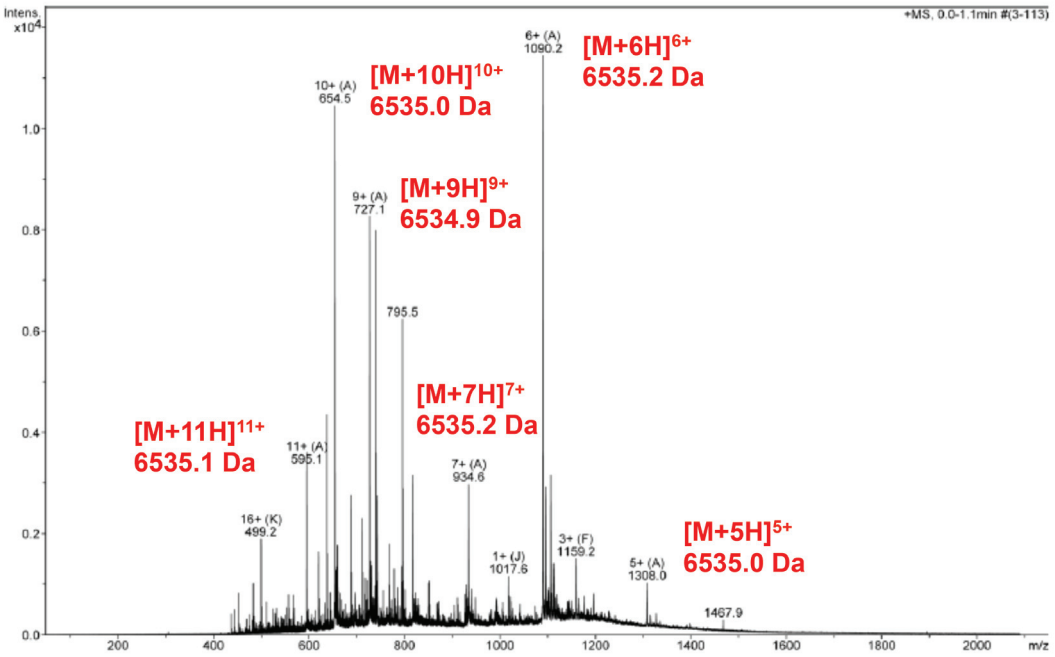

Figure 5.7: ESI-TOF-MS confirmation of His-apelin-55Δ15 mass (~6535 Da; HPLC elution time ~17 min) observed after 24 h incubation in PCSK3 overexpressing HEK293A cell medium.
Isotopic distribution is observable.

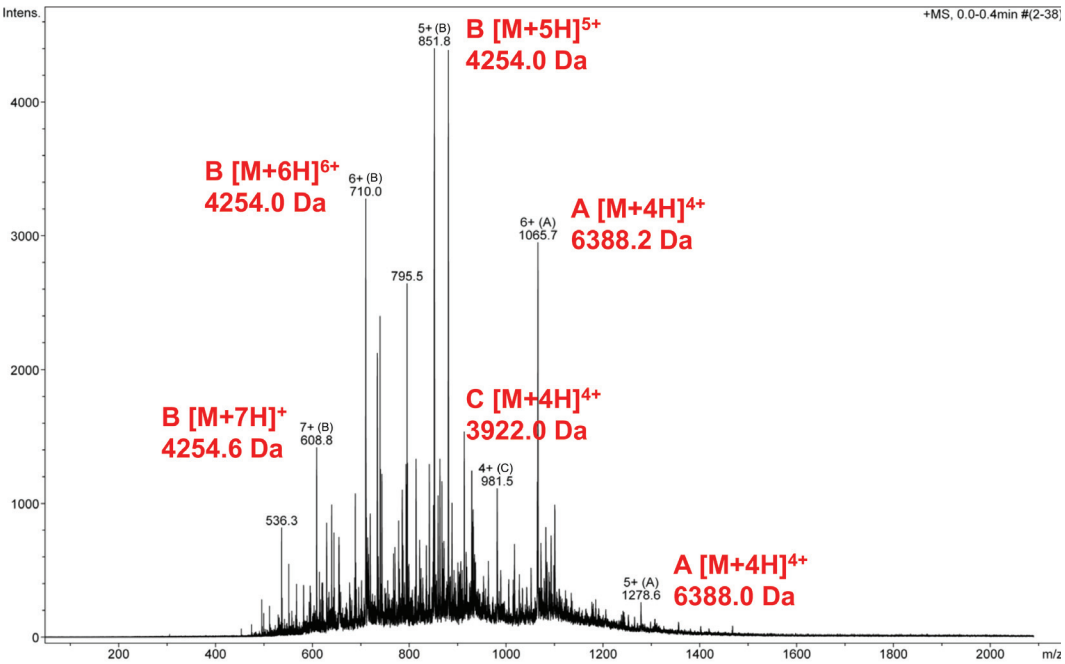

Figure 5.8: ESI-TOF-MS analysis of His-apelin-55 processing products (~3922, 4254, and 6388 Da; eluting over 15-16.5 min) observed after 24 h incubation in PCSK3 overexpressing HEK293A cell medium.
Isotopic distribution is observable.

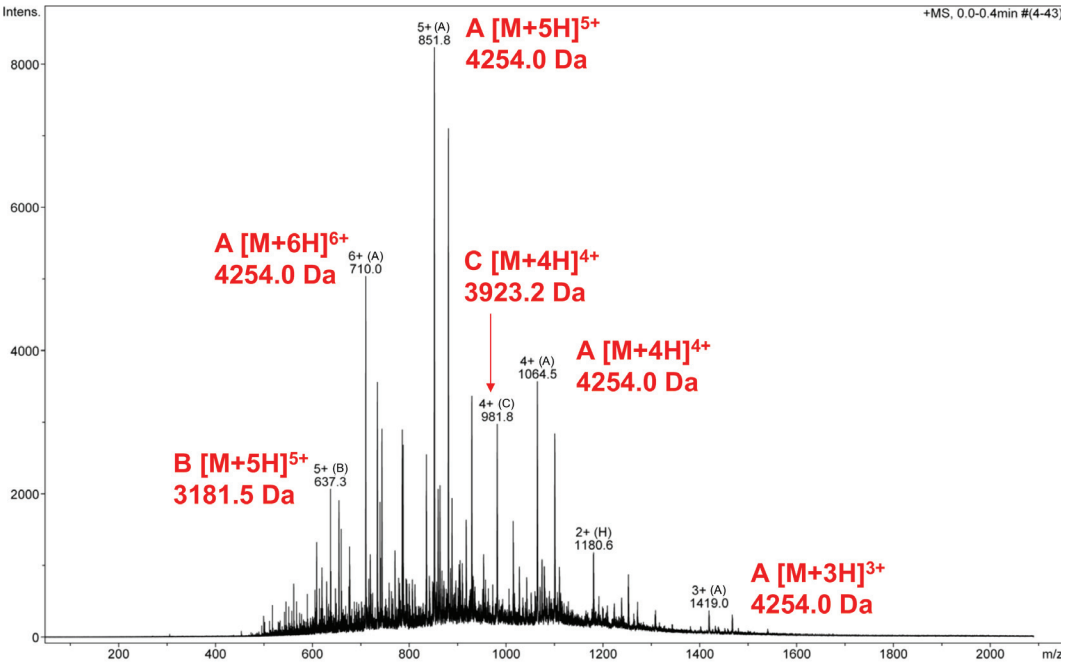

Figure 5.9: ESI-TOF-MS analysis of His-apelin-55 processing products (~3182, 3923, and 4254 Da; eluting over 15-16.5 min) observed after 24 h incubation in PCSK3 overexpressing HEK293A cell medium.
Isotopic distribution is also observable.

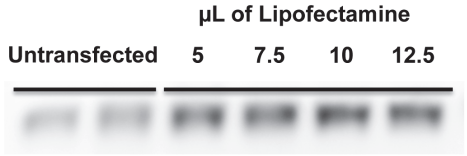

Figure 5.10: PCSK3 expression is increased in HEK293A cells upon lipofectamine-mediated transfection with pIRES2-EGFP plasmid containing the PCSK3 gene.

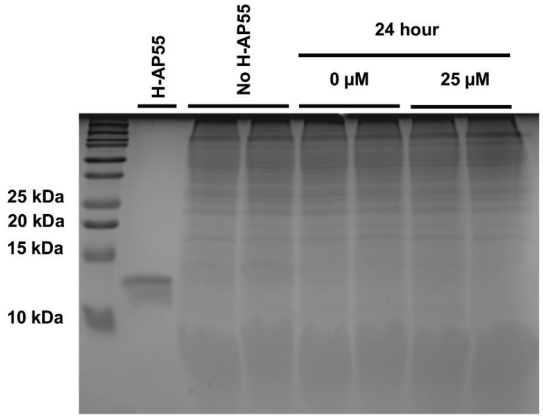

Figure 5.11: His-apelin-55 (H-AP55) is not detected intracellularly in PCSK3 overexpressing HEK293A cells.
Gel staining by Coomassie did not yield any differential band pattern in response to HEK293A cells with or without RVKR-CMK inhibitor.

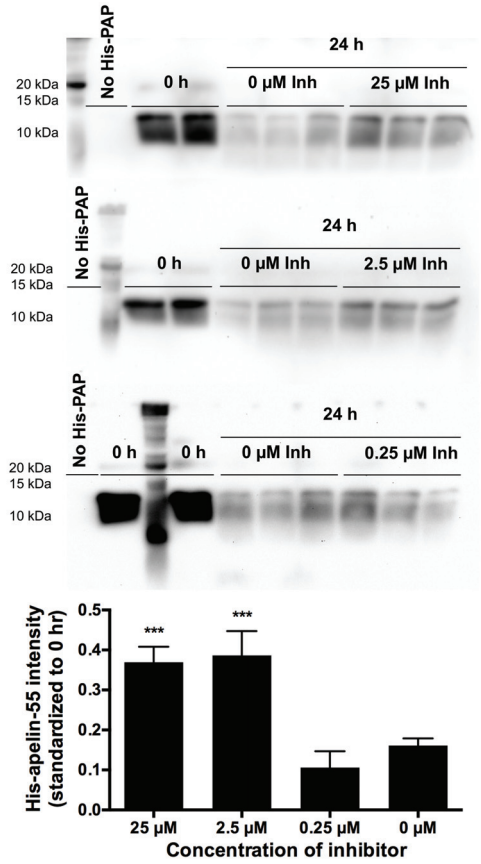

Figure 5.12: Pretreatment of HEK293A cells with the PCSK inhibitor decanoyl-RVKR-CMK reduces His-apelin-55 processing.
Cells were pretreated with the inhibitor for 1 h prior to supplementing culture media with exogenous His-apelin-55. ***: $P < 0.0001$ by t-test in comparison to 0 μM control.

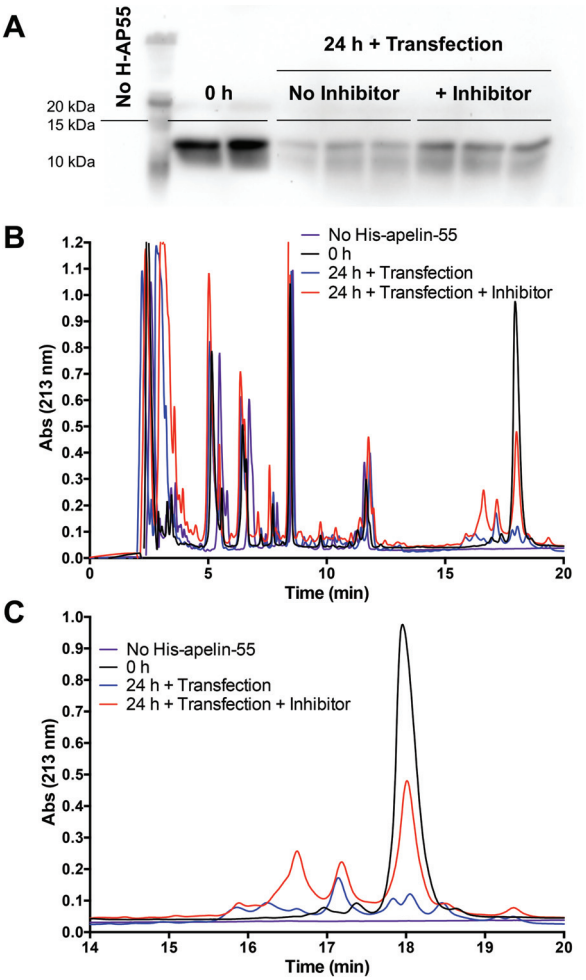

Figure 5.13: HEK293A-mediated extracellular processing of His-apelin-55 is reduced by the PCSK inhibitor decanoyl-RVKR-CMK.
Representative A) western blot analysis and B-C) RP-HPLC chromatograms following apelin-55 processing in presence vs. absence of inhibitor (as indicated).

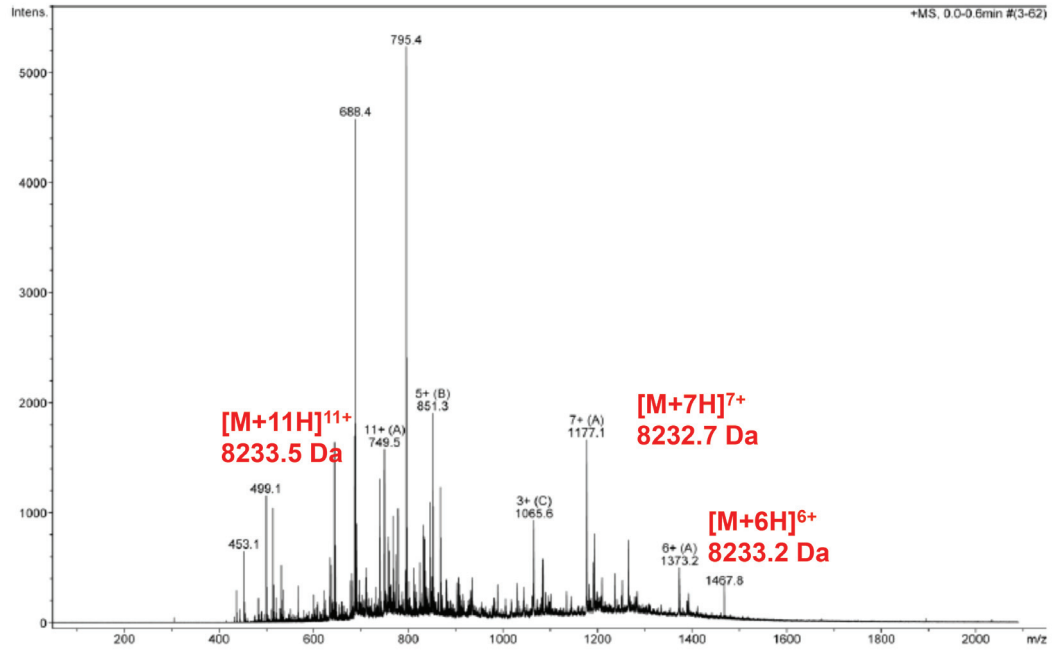

Figure 5.14: ESI-TOF-MS confirmation of His-apelin-55Δ1 mass (~8233 Da; HPLC elution time ~16 min) observed after 24 h incubation in PCSK3 overexpressing HEK293A cell medium pretreated with PCSK inhibitor decanoyl-RVKR-CMK. Isotopic distribution is also observable.

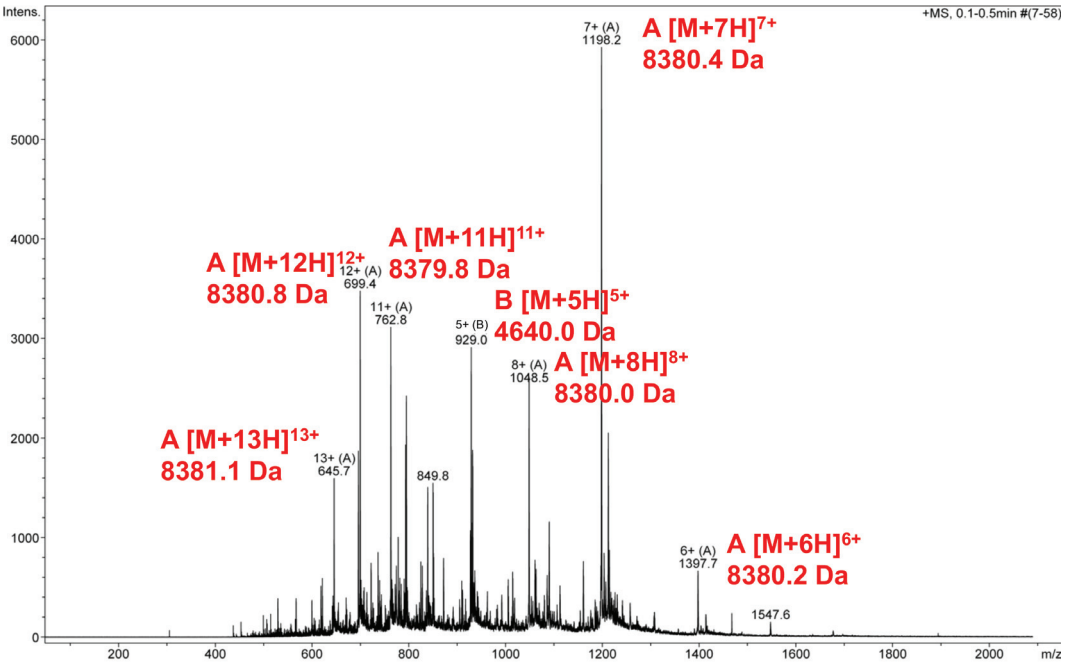

Figure 5.15: ESI-TOF-MS confirmation of His-apelin-55 (~8380 Da) and His-apelin55Δ32 (~4640 Da; HPLC elution time ~17.5 min) observed after 24 h incubation in PCSK3 overexpressing HEK293A cells pretreated with the PCSK inhibitor decanoyl-RVKR-CMK.
Isotopic distribution is also observable.

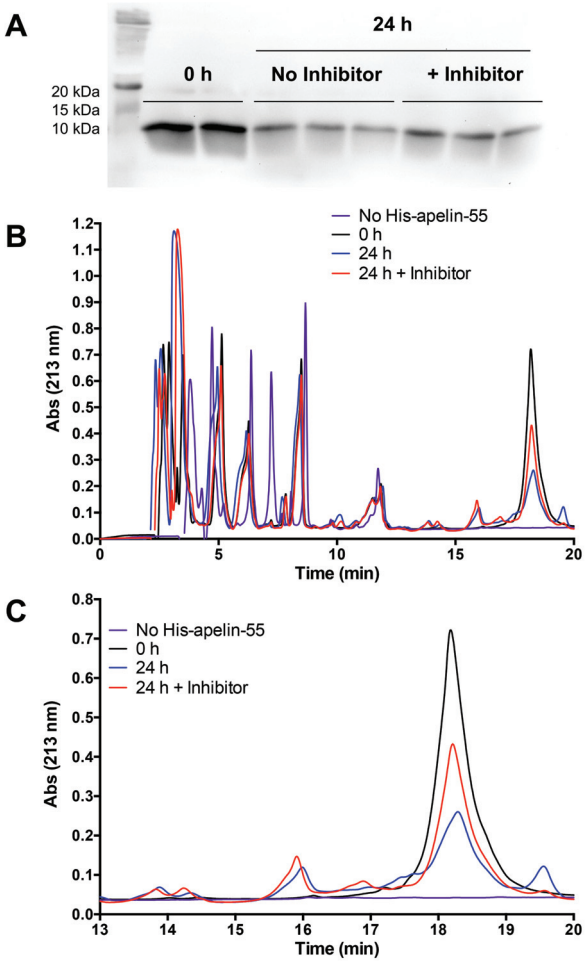

Figure 5.16: His-apelin-55 is processed extracellularly by 3T3-L1 adipocytes and processing is inhibited with PCSK inhibitor decanoyl-RVKR-CMK.
Representative A) western blot analysis and B-C) HPLC chromatograms tracking apelin-55 processing in 3T3-L1 adipocytes in presence vs. absence of inhibitor (as indicated).

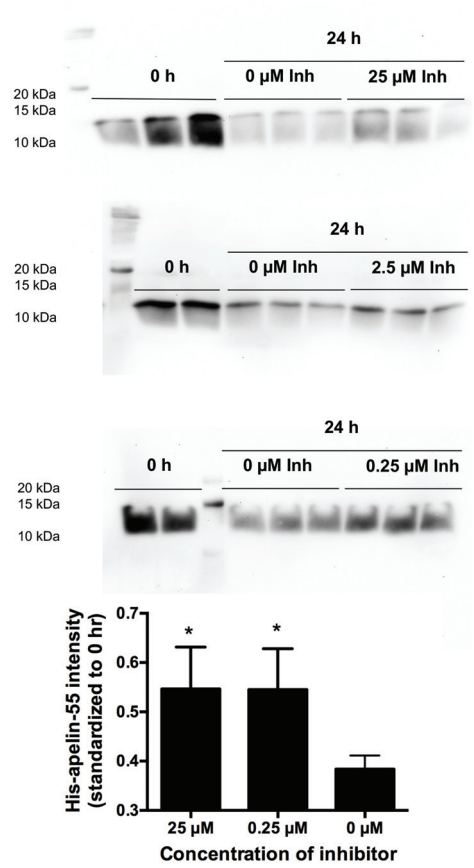

Figure 5.17: Pretreatment of 3T3-L1 adipocytes with the PCSK inhibitor decanoyl-RVKR-CMK reduces His-apelin-55 processing.
Cells were pretreated with the inhibitor for 1 h prior to supplementing culture media with exogenous His-apelin-55. Representative western blots for each dose is shown. *: $P <$ 0.05 by t-test in comparison to 0 µM control.

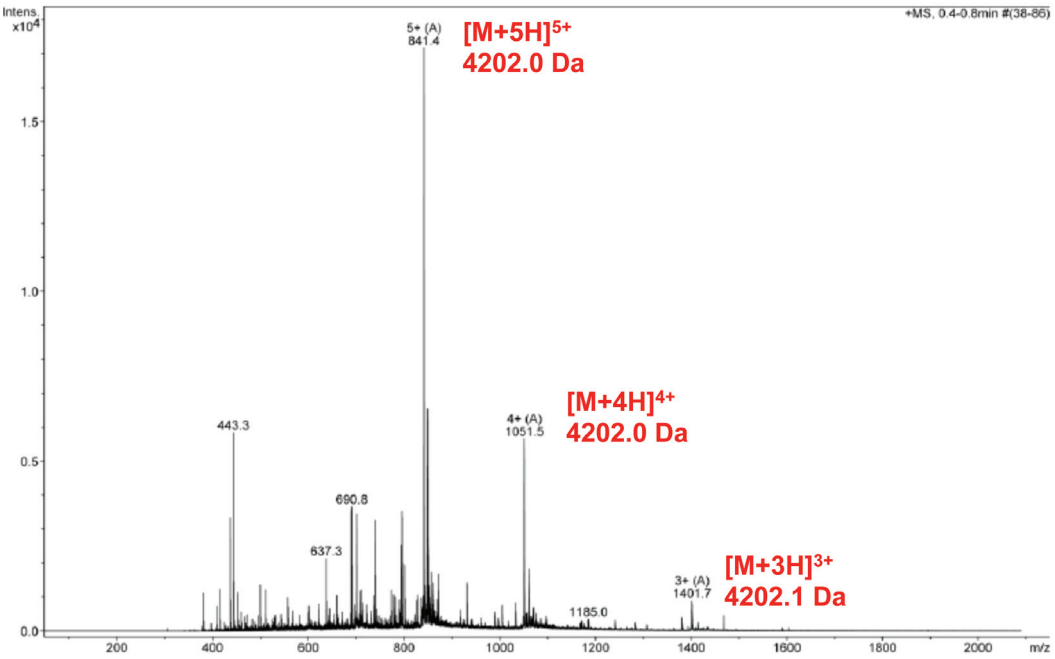

Figure 5.18: ESI-TOF-MS confirmation of His-apelin-55Δ36 mass (4202 Da; HPLC elution time ~17 min) observed after 24 h incubation in 3T3-L1 adipocyte medium Isotopic distribution is also observable.

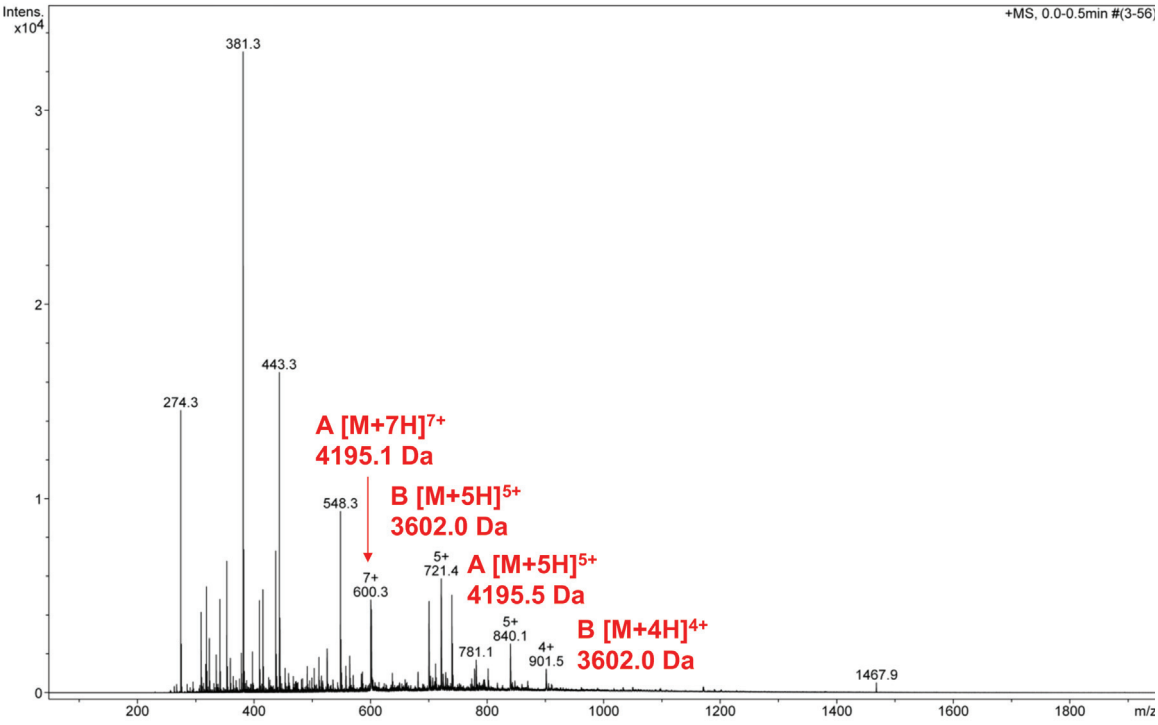

Figure 5.19: ESI-TOF-MS confirmation of apelin-36 (A, 4195 Da) and apelin-31 (B, 3602 Da; HPLC elution time 13-15 min) masses observed after 24 h incubation in 3T3-L1 adipocyte medium.
Isotopic distribution is also observable.

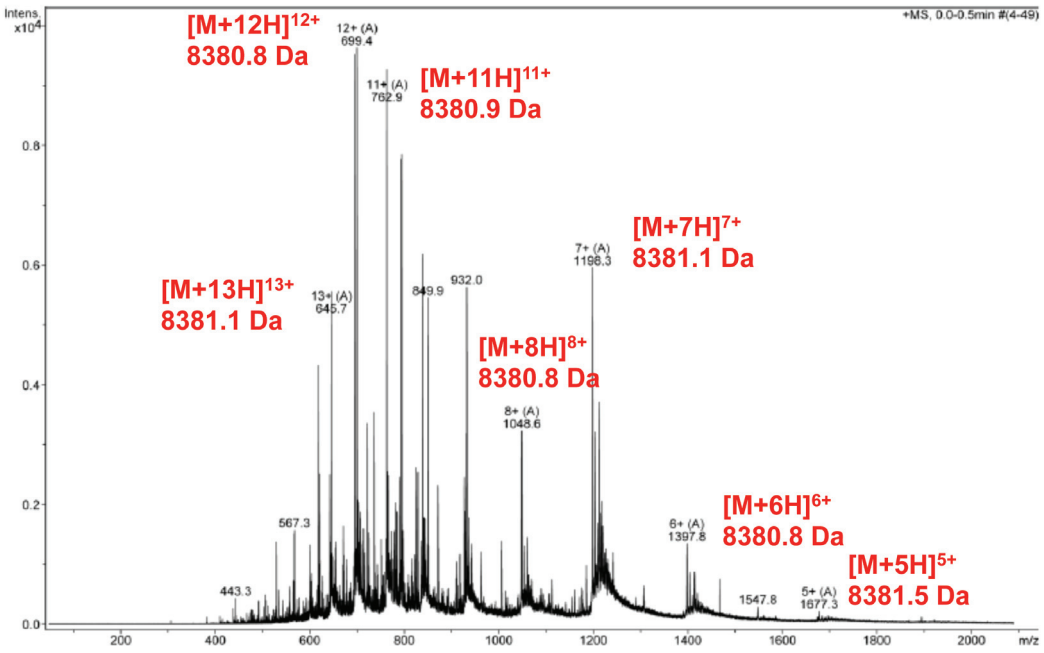

Figure 5.20: ESI-TOF-MS confirmation of His-apelin-55 mass (8380 Da) after incubation with 3T3-L1 adipocytes for 24 h.
Isotopic distribution is also observable.

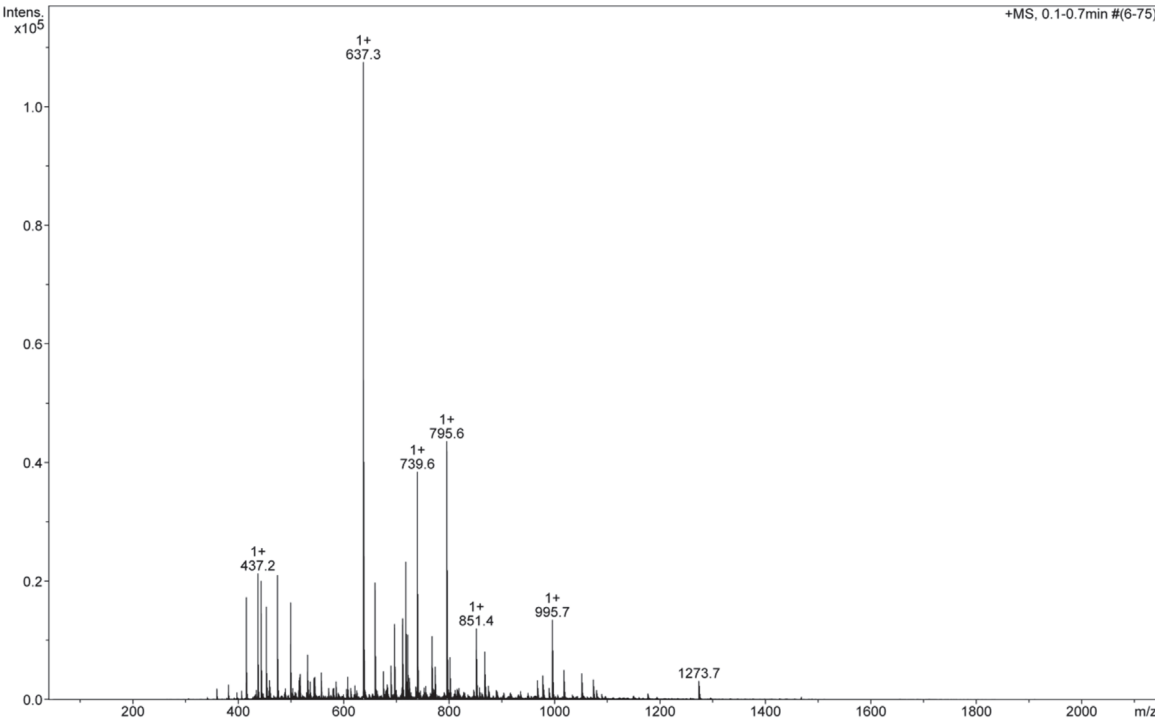

Figure 5.21: Background ESI-TOF-MS, demonstrating lack of any detectable protein

Figure 5.22: Visual summary of His-apelin-55 processing by HEK293A cells and 3T3-L1 adipocytes. Bolded residues represent apelin-55.

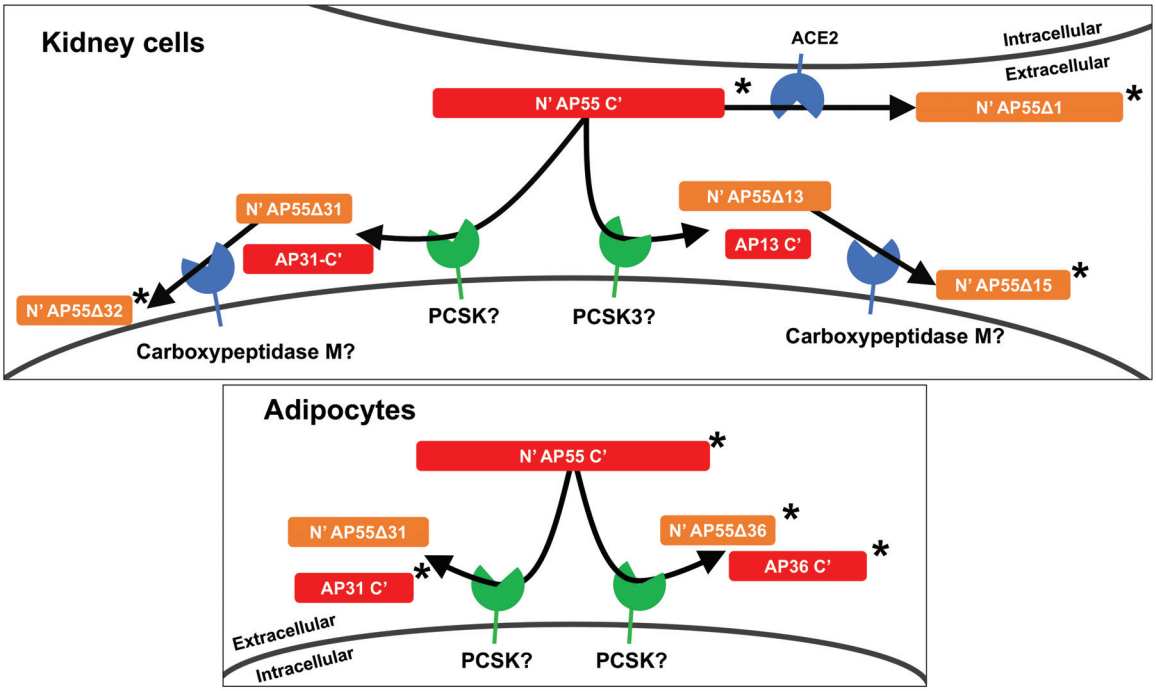

Figure 5.23: Hypothetical tissue-dependent extracellular processing of apelin-55 in kidney cells (i.e. HEK293A) and adipocytes (i.e. 3T3-L1).
N' and C' represents processed products containing the N- (orange) and C-terminal (red) domains of His-apelin-55, respectively. * represents that this product mass was detected by HPLC coupled to ESI-TOF-MS.

CHAPTER 6 IDENTIFICATION OF APELIN-55 AS THE LONGEST BIOACTIVE ISOFORM AND DECLASSIFICATION FROM PROAPELIN

(Note: This chapter is based on a paper entitled "Bioactivity of the putative apelin proprotein expands the repertoire of apelin receptor ligands" in ***BBA General Subjects*** (2017) 1861: 1901-1912 [279]. See Appendix C for permissions from Elsevier. Mr. Nigel Chapman (M.Sc. from the Rainey lab) and Dr. Aditya Pandey (PhD from the Rainey lab) cloned apelin-36 for recombinant expression. Mr. Calem Kenward (former Honours student in the Rainey lab) identified the optimal apelin-36 production conditions under my mentorship. Dr. Aditya Pandey carried out site-directed mutagenesis of F55A mutant apelin-55. Mr. Nigel Chapman developed the In-Cell Western technique discussed below and exclusively carried out the identification of EC_{50} values for all isoforms except apelin-36 in which I assisted in conducting additional experiments. Mr. Nathan Weatherbee-Martin (former M.Sc. from the Rainey lab) chemically synthesized apelin-13 and -17 used in this work. Ms. Shuya Kate Huang (former Honours student in the Rainey lab) assisted in CD-based characterization of apelin-55 and -36 under my mentorship. I acquired the majority of NMR data under the mentorship of either Dr. Muzaddid Sarker (former post-doctoral fellow in the Rainey lab) and/or my supervisor Dr. Jan K. Rainey)

6.1 INTRODUCTION

As stated at the end of Chapter 5, the detection of apelin-55 in extracellular fluid (e.g., colostrum and milk [93]) implies the potential for apelin-55 to interact with binding

partners in the extracellular fluid and/or cell surface. Chapter 5 focused on one of these potential partners (i.e., processing enzymes), but the cell surface is also the location for the cognate GPCR for apelin, the AR. The interaction between apelin-55 and processing enzymes evidenced by its extracellular processing further implies that apelin-55 should be capable of directly binding to and activating the AR. Thus, this chapter will focus on demonstrating the role of apelin-55 as the longest bioactive isoform, rather than the inactive proprotein it was initially presumed to be.

The 12 C-terminal residues of apelin isoforms are required for receptor binding [104]. Therefore, apelin-55 theoretically contains all of the functionality required for binding to the AR and activating downstream signalling pathways. At the time of this work, only the shorter apelin isoforms (i.e., apelin-17, -13, and -12) had been characterized in solution by NMR spectroscopy [197], while very limited biophysical characterization had been reported for the longer apelin-36 isoform and none for apelin-55. The prior NMR-based characterization demonstrated a similar conformation in solution for all of the short apelin isoforms, indicating the potential for a similar mode of receptor activation. However, apelin isoforms have length-dependent differences in their pharmacological properties as described in Section 3.2.4 and 3.2.5. The cause of this is unknown, but one hypothesis is that this may originate from structural differences between isoforms. Specifically, I hypothesized that longer apelin isoforms had i) differing C-terminal conformation relative to shorter isoforms and/or ii) that the N-terminal domain excluded in shorter isoforms occluded the primary receptor binding site. These hypotheses were developed in advance of the crystal structure by Ma *et al.* [69] (Section 3.1), which demonstrated the presence of two distinct sites of apelin analogue-

AR interaction. Either of these mechanisms would hamper AR interaction and the subsequent activation process for longer isoforms, resulting in the differences in potency observed.

To test these hypotheses, all of the common endogenously-produced apelin isoforms (apelin-55, -36, -17 and -13) were initially examined for AR activity by In-Cell Western-based assay. Subsequently, they were characterized by far-UV CD and NMR spectroscopy to identify the structural basis for receptor binding and activation. This was facilitated using a recombinant *E. coli* expression system for both apelin-55 and -36, which allowed for isotope enrichment for heteronuclear NMR experiments.

6.2 MATERIALS AND METHODS

(Note: HEK293A cells used in this chapter were cultured using the standard protocols followed in Dr. Denis Dupré's laboratory at Dalhousie University.)

6.2.1 APELIN-55 AND -36 EXPRESSION AND PURIFICATION

Human apelin-55 (C-terminal 55-residues of pre(pro)apelin with N-terminal serine from TEV cleavage; total 56 residues) was expressed in *E. coli* C41(DE3) and purified using Ni-NTA affinity and cation exchange chromatography, as outlined previously in Section 4.2.1, and further purified by RP-HPLC using the procedure outlined in Section 5.2.1. The purity of apelin-55 was analyzed by analytical RP-HPLC (C_{18} column, 5 µm, 5 mm x 250 mm, AAPPTec), with the same binary system as for preparative column purification (2 to 40% solvent B in 30 min, followed by 40% to 2% in 5 min).

The C-terminal phenylalanine of apelin-55 was mutated to alanine through site-directed mutagenesis using the Phusion® High-Fidelity DNA Polymerase (NEB), as confirmed by sequencing (Bio Basic). The vector expressing the mutant gene was electroporated into the *E. coli* C41 (DE3) strain, F55A-apelin-55 protein expression was induced, and the resulting mutant protein purified using the same protocol as the wildtype detailed in Sections 4.2.1 and 5.2.1 with identity confirmed by ESI-TOF-MS.

An open reading frame coding for N-terminally hexahistidine SUMO (His-SUMO)-tagged human apelin-36 (bacterial codon optimized) was cloned into the pET-HN vector (gift from Dr. Xiang-Qin Liu, Dalhousie University) and transformed into the BL21 (DE3) strain of *E. coli*. Protein expression was induced through addition of 0.5 mM IPTG once cells reached logarithmic growth phase (optical density=0.6) and protein expression was carried out for 4 h. The cells were lysed through French Press in buffer containing 50 mM NaH_2PO_4, 300 mM NaCl, 10 mM imidazole, pH 8.0. Soluble proteins were applied to a column packed with Ni-NTA beads (Roche Diagnostics, Indianapolis, IN). The column was washed with a buffer containing higher imidazole content (50 mM NaH_2PO_4, 300 mM NaCl, 20 mM imidazole, pH 8.0) and any bound proteins were subsequently eluted using buffer with 250 mM imidazole (50 mM NaH_2PO_4, 300 mM NaCl, 250 mM imidazole, pH 8.0). The resulting solution was dialyzed against dH_2O and then diluted until the total protein concentration reached ≤15.0 μM (identified through A_{280} and $\epsilon_{280} = 6980$ for fusion protein calculated using the method outlined by Gill and von Hippel [331]). SUMO protease (produced in-house; reaction in 50 mM Tris-HCl, 150 mM NaCl, pH 8.0) was added to reach ~1:100 molar ratio to its substrate. SUMO proteolysis was allowed to occur overnight and monitored by SDS-PAGE. The resulting

reaction mixture was dialyzed against dH_2O and lyophilized. Apelin-36 was then purified by RP-HPLC (Varian ProStar) using the same gradient method, preparative column, and solvents as for apelin-55. Purity and peptide identity were confirmed identically to apelin-55 by analytical RP-HPLC and ESI-TOF-MS, respectively.

Apelin-17 and apelin-13 were chemically synthesized and purified as detailed previously [197]. Pyroglutamate-modified apelin-13 (Pyr-apelin-13) was purchased from AnaSpec. Apelin-17 and -13 purity were determined using the same analytical RP-HPLC protocol as for apelin-55.

The concentration (c) of each apelin peptide was determined using the Beer-Lambert law (detailed in Section 5.2.1). For apelin-36 and -55, absorbance at 280 nm was employed (ε of 5,500 $M^{-1}cm^{-1}$); for apelin-13 and -17, absorbance at 214 nm was employed (ε of 30,893 $M^{-1}cm^{-1}$ for apelin-13 and 40,030 $M^{-1}cm^{-1}$ for apelin-17), as estimated by the method described by Kuipers and Gruppen [336]).

6.2.2 ISOTOPICALLY LABELED PEPTIDE PRODUCTION

For uniformly ^{15}N and ^{13}C-labeled apelin-55 and apelin-36 production, *E. coli* cells were grown in LB medium to optical density of 0.6-0.8. Pelleted cells were re-suspended in a ½-equivalent volume of minimal medium (100 mM NaH_2PO_4, 40 mM K_2HPO_4, 4 mM $MgSO_4$, 1.8 μM $FeSO_4$, 2 g/L $^{13}C_6$ D-glucose, 1 g/L $^{15}NH_4Cl$ and 100 mg/L ampicillin, adjusted to pH 7.3 with NaOH [4]) and allowed to express isotopically labeled proteins for 4 h at 37 °C. Proteins were purified as detailed above and the incorporation of NMR-active isotopes was confirmed by ESI-TOF-MS. The mass gain of the major protein species was used to estimate isotope labeling efficiency.

6.2.3 ERK PHOSPHORYLATION ASSAY FOR TRANSIENTLY TRANSFECTED HEK293A

Human Embryonic Kidney (HEK) 293A cells were cultured in 10 cm dishes and grown in DMEM (High Glucose, Sigma Aldrich) containing 5% P/S (Sigma Aldrich) supplemented with 10% FBS (Sigma Aldrich). At ~70% confluency, cells were transfected by addition of serum-free DMEM (High Glucose, Sigma Aldrich) containing 10 µg of the AR-coding pcDNA 3.1 plasmid (cDNA Resource Center) and 100 µg of polyethylenimine (PEI, Sigma Aldrich). Cells were incubated with the transfection mixture for 24 h, at which time the medium was aspirated and refreshed with serum-free DMEM. After an additional 24 h, plates of cells were stimulated with Pyr-apelin-13 or apelin-55 or non-stimulated (DMEM, no apelin), respectively, for 5 minutes. Immediately after stimulation, the medium was aspirated and cells were harvested with cold PBS, treated with DNase I (10 mg/mL) then resuspended in radioimmuno-precipitation assay (RIPA) buffer with added protease inhibitor cocktail (50 mM Tris/HCl, pH 7.5, 10 mM $MgCl_2$, 150 mM NaCl, 0.5% sodium deoxycholate, 1% Nonidet P-40, 0.1% SDS, Complete Protease inhibitors (Roche). To aid in separation of a protein fraction free from cellular debris, 30 µL of a suspension of Protein A Sepharose beads (100 mg/mL, Sigma Aldrich) in RIPA containing bovine serum albumin (BSA) were added to each sample. The samples were vortexed and nutated for 20 minutes at 4 °C. Lysates were centrifuged (13 000 *g*, 15 min, 4 °C) and the supernatant protein fractions were collected. Finally, the supernatant was added to Laemmli sample buffer and boiled prior to SDS-PAGE loading.

Immunoblots were probed with primary antibodies for extracellular signal-regulated kinase (ERK; 1:1000 rabbit polyclonal ERK2; Santa Cruz Biotech, sc-154) and pERK (1:500 mouse monoclonal pERK; Santa Cruz Biotech, sc-7383) and fluorophore-conjugated secondary antibodies (Dylight 549, donkey anti-rabbit, 1:2000; and Dylight 649, donkey anti-mouse, 1:1000; Rockland). The membranes were then imaged by fluorescent excitation and detection using a VersaDoc imaging system (Bio-Rad). Digital images were analyzed using Bio-Rad's Image Lab software. Apparent molecular weights were inferred from the migration distance of a given band relative to the BLUeye prestained protein ladder (Froggabio). Ratios between pERK and ERK values were determined, averaged between datasets, and statistically significant differences between the resulting values were determined using unpaired Student's t-tests.

6.2.4 DEVELOPMENT OF STABLY-AR TRANSFECTED HEK293A CELL LINE

Untransfected HEK293A cells were seeded into a 10 cm dish. Upon reaching 80% confluency, cells were transfected (treated with a transfection mixture containing 20 µg plasmid DNA and 60 µL PEI for 24 h) with a pIRES2-EGFP plasmid (gift of Drs. Janice Mayne and Michel Chrétien, University of Ottawa) containing the WT AR gene (Clontech), which was first linearized using the AflII restriction enzyme (NEB). This plasmid encodes both the protein of interest and a second separate open reading frame for eGFP expression on the same mRNA transcript, allowing for verification of successful transfection without fluorescent modification of the protein of interest. After 24 h, the antibiotic G418 (Sigma Aldrich) was added to the growth medium at a concentration of 400 mg/mL, and maintained at this concentration during subsequent passages. After 3-5

passages, an individual colony of green cells was isolated and seeded onto a new 10 cm dish.

6.2.5 IN-CELL WESTERN™ ASSAY

HEK293A cells stably expressing the WT-AR gene were seeded into 96-well microplates in the growth media (High Glucose DMEM, 10% FBS and 5% P/S, 100 µL/well). After 24 h, the growth medium was removed and replaced with serum-free DMEM (50 µL/well). After an additional 24 h, cells were stimulated: i) for 5 minutes at 37 °C with a range of doses of apelin (Pyr-13, -17, -36, -55; 10^{-11} M to 10^{-5} M); ii) with 1 µM dose of apelin isoforms for various times (0 to 30 min); or, iii) with a 50% FBS positive control. In each case, 50 µL of stimulation solution was added to the 50 µL already in each well. Subsequently, the medium was removed and replaced with 100 µL/well of fixation solution (4% paraformaldehyde in PBS), for 10 minutes. Next, the cells were washed with buffer (0.01% Tween-20 in PBS, 100 µL/well) and then treated with blocking buffer (20% Odyssey Blocking Buffer (LI-COR) in PBS with 0.4% Triton X-100, 40 µL/well) for 1 h on a shaker at RT. Blocking buffer was removed and replaced with primary antibody solution (1:500 mouse monoclonal pERK (Santa Cruz Biotech) and 1:500 rabbit polyclonal ERK2 (Santa Cruz Biotech) in blocking buffer), and cells were incubated overnight on a shaker at 4 °C. The next day, cells were again washed for 5 x 3 min on a shaker at RT. Wash buffer was removed and replaced with secondary antibody solution (1:500 Goat anti-Mouse IgG Dylight-680, Cross Adsorbed (Thermo Fisher) and 1:500 Donkey anti-Rabbit IgG Dylight-800, Cross Adsorbed (Thermo Fisher) in blocking buffer), and cells were incubated for 1 h on a shaker at RT, in the dark. Finally, cells were again washed (5 x 3 min on a shaker at RT), in the dark, and

subsequently imaged using the LI-COR Odyssey scanner (LI-COR). The signal from the 700 nm (pERK) and 800 nm (ERK) channels was quantified using the LI-COR Odyssey scanning software. Dose-response data were collected as pERK/ERK ratios, normalizing against total ERK. The averaged ratios were then plotted as percentages of the maximum response induced by the positive control FBS stimulation. For each individual microplate, a non-linear regression was performed, yielding EC_{50} (dose at which a half-maximal pERK response was reached) and E_{max} (maximum achievable response) values. The determined values were then averaged across at least 3 separate experiments. Statistically significant differences between the resulting values were determined using unpaired Student's t-tests.

6.2.6 FAR-UV CD SPECTROPOLARIMETRY

Each apelin isoform was re-suspended in an appropriate volume of CD buffer (1 mM NaN_3, 1 mM $CaCl_2$, 25 mM Na_2HPO_4/NaH_2PO4 buffer, pH 6.00±0.05) to reach a final peptide concentration of 250 μM. Far-UV CD spectra were acquired (J-810 spectropolarimeter, Jasco) at 37 °C with a data pitch of 0.1 nm from 260 to 190 nm at 100 nm/min. Cuvettes of 0.1 mm path length (Hellma) were employed. All spectra were acquired in triplicate, and experiments were carried out in duplicates using independently prepared samples. All data acquired were averaged, blank subtracted, and reported as mean residue ellipticity (MRE). Finally, MRE values were subjected to a sliding window average over 3 nm stretches.

6.2.7 APELIN-55 STABILITY

The stability of apelin-55 was assessed in CH_3COONa (pH 5), 2-(N-morpholino) ethanesulfonic acid (MES; pH 6), NaH_2PO_4/Na_2HPO_4 (pH 6 and 7), Bis Tris (pH 6 and 7), and HEPES (pH 7) buffers. Solutions contained 25 mM buffer salt, 1 mM $CaCl_2$, and 1 mM NaN_3. Apelin-55 samples were prepared in the appropriate volume to reach a final concentration of 0.2 mM. Samples were incubated at 5 °C, room temperature (~23 °C), or 37 °C for 1 week, and analyzed by SDS-PAGE and Coomassie staining.

6.2.8 NMR SPECTROSCOPY

Each apelin isoform was re-suspended in appropriate volume of NMR buffer (1 mM DSS, 1 mM NaN_3, 25 mM Na_2HPO_4/NaH_2PO4 buffer, pH 6.00±0.05, 90%/10% H_2O/D_2O) to reach a final protein concentration of 0.2 mM for isotope-labeled apelin-55 and -36, 2.1 mM for unlabeled apelin-17, and 2.5 mM for unlabeled apelin-13. Sensitivity enhanced ^{1}H-^{15}N HSQC experiments were acquired at 37 °C for each apelin isoform; for isotopically labeled apelin-36, an Avance 500 MHz spectrometer equipped with a room temperature 5 mm broadband fluorine observe (BBFO) SmartProbe with a z-axis gradient (Bruker Canada; NMR^3 facility, Dalhousie University) was employed; for all other apelin isoforms an Avance-III 700 MHz spectrometer with 5 mm triple resonance inverse (TCI) cryoprobe with a z-axis gradient (Bruker Canada; Biomolecular Magnetic Resonance Facility, National Research Council (NRC)) was employed. Chemical shifts for the C', C_α, C_β, H_N, and N nuclei of apelin-55 were assigned through the main chain-directed approach [44] at 37 °C and at 5 °C using HNCA; HN(CO)CA; HN(CA)CO; HNCO; CBCANH (37 °C) or HNCACB (5 °C); and, CBCA(CO)NH (37 °C) triple-resonance experiments employing an Avance-III 700 MHz spectrometer (NRC)). Side chain ^{1}H

chemical shifts were assigned using a ^{15}N-edited total correlation spectroscopy (TOCSY)-HSQC experiment. At 5 °C, ^{15}N-edited nuclear Overhauser effect (NOE) spectroscopy (NOESY; mixing time: 150 ms) experiment was also acquired to both assist in side chain ^{1}H assignment and to validate sequential assignment. Finally, the signal enhancement from the heteronuclear NOE at both 37 °C and 5 °C was determined using paired ^{1}H-^{15}N HSQC experiments acquired in an interleaved manner with or without ^{1}H saturation during the recycle delay. All experiments were carried out using the standard pulse programs available in the TopSpin 2.1 library (Bruker Canada; Table 6.1 details experimental parameters).

Spectra were processed using TopSpin 3.1 and NMRPipe [337]. ^{1}H frequencies were referenced to DSS (0 ppm) and ^{15}N and ^{13}C frequencies indirectly referenced based on ^{1}H [43]. Sequential assignment, secondary chemical shifts (Δδ), CSI [55, 56], Bayesian algorithm DANGLE [57], and heteronuclear NOE intensity ratios (intensity of saturated relative to unsaturated interleaved experiments) were analyzed using CcpNmr Analysis 2.3.1 [338]. The identified ^{1}H and ^{15}N chemical shifts of apelin-55 at 37 °C were, in turn, used to assign ^{1}H-^{15}N heteronuclear HSQC spectra for the shorter isoforms. CSD [59] values between isoforms were determined using N and H_N chemical shifts (Section 2.5.2).

6.3 RESULTS AND DISCUSSION

6.3.1 PRODUCTION AND PURIFICATION OF APELIN-36 AND APELIN-55

For apelin-55, the optimized *E. coli*-based expression method followed by TEV protease cleavage (detailed in Chapter 4) allowed for cost-effective production of both

isotope-labeled (~2 mg/L, ^{15}N and ^{13}C enriched) and natural abundance (~3-4 mg/L) apelin-55 with purity greater than 95% (Fig. 6.1), making apelin-55 highly amenable to biophysical characterization. Following from this success, an *E. coli*-based system was developed to produce apelin-36 both at natural abundance and isotopically-labeled. Specifically, an N-terminal His-SUMO fusion tag was used, as is frequently employed to enhance target protein expression and purification [1]. Overexpressed His-SUMO-apelin-36 remained highly soluble in *E. coli* and did not significantly perturb cell viability. In addition, it exhibited high affinity in Ni-NTA purification (Fig. 6.1A). Interestingly, nearly complete His-SUMO tag removal could only be achieved when the total protein concentration was less than ~15 μM (Fig. 6.1A). The final apelin-36 yield, following SUMO cleavage, was ~2 mg/L for apelin-36 at greater than 95% purity (Fig. 6.2C). For NMR spectroscopy, ^{15}N incorporation of ~≥90% efficiency was achieved for apelin-36 with a final yield of ~1-1.5 mg/L. Finally, apelin-13 and -17 were synthesized and purified, following previous outlined methods by the Rainey lab [197], at greater than 95% purity (Fig. 6.2A-B).

6.3.2 APELIN-55 CAN ACTIVATE THE AR

Apelin-55–AR activation was initially tested using the previously developed method by the Rainey lab. Specifically, this involved testing for ERK phosphorylation upon apelin treatment in HEK293 cells transiently transfected with AR [78]. Based upon this previous protocol and upon literature precedents [78, 270], a 5 min apelin treatment period with 1 μM dose was employed and the response to apelin-55 and -13 was compared. Notably, treatment with either apelin-55 or -13 led to a significant increase in ERK phosphorylation (pERK) in comparison to the non-stimulated control (Fig. 6.3). To

our knowledge, this was the first report identifying unprocessed apelin-55 as an isoform capable of activating the AR implying that apelin-55 is a longer bioactive isoform rather than strictly an inactive proprotein.

6.3.3 APELIN-55 HAS A SIMILAR POTENCY TO APELIN-17 AND -36

To better characterize the bioactivity of apelin-55, given that a 1 μM dose is not likely to correspond to the physiological condition [339], the potency (EC_{50}) of apelin-55 was directly compared to those of the other bioactive isoforms. The N-terminally pyroglutamate modified apelin-13 isoform (Pyr-apelin-13) was employed for these assays to reduce potential variability between experiments given that Pyr-apelin-13 spontaneously forms from apelin-13 as observed in Chapter 4 (Fig. 4.4) and others [95]. Pure Pyr-apelin-13 was thus used to avoid uncertainty about the relative quantities of apelin-13 and Pyr-apelin-13 employed. Testing of only Pyr-apelin-13 is expected to provide values of E_{max} and EC_{50} representative of both apelin-13 isoforms, since previous studies have shown apelin-13 and Pyr-apelin-13 to maintain highly similar backbone conformations [197] and to induce ERK phosphorylation with near identical potency [74] and efficacy [88].

Apelin isoform potencies were directly compared through development of a microplate-based In-Cell Western™ assay using stably AR-transfected HEK 293A cells. Prior to determining EC_{50} values for each isoform, activation of ERK by 1 μM apelin treatment was monitored for 30 min to determine the optimal treatment period. Time-course analysis of ERK phosphorylation showed a maximum response at 5 min for all isoforms (Fig. 6.4A-D), similar to previous reports by standard western blotting [78, 270], which progressively decreased to a near basal level by 30 min.

Under the In-Cell-Western™ assay conditions, all isoforms showed similar maximum pERK response (i.e., E_{max}) at 5 min (Fig. 6.4E). Furthermore, apelin-17, -36, and -55 exhibited no significant difference in EC_{50} (Fig. 6.4E and Table 6.2). Thus, our results indicate that apelin-55 is as active as the shorter isoforms. In contrast, the EC_{50} of apelin-13 was ~8 fold lower than the other isoforms, suggesting a significantly higher potency (Table 6.2: apelin-13 vs. apelin-17; $P<0.01$, vs. apelin-36; $P<0.05$, vs. apelin-55; $P<0.001$). A similarly increased potency for apelin-13 compared to longer isoforms has been reported previously [74, 104, 107, 123, 198]. In summary, these results clearly demonstrate that apelin-55 can bind to the AR and induce a transient pERK response similar to apelin-17 and -36.

One alternative to direct AR activation by apelin-55 would be extracellular processing prior to activation by a resulting shorter apelin isoform as introduced in the previous chapter. This is unlikely under the assay conditions detailed in this chapter for three primary reasons. First, apelin-55 processing only occurs in the presence of processing enzymes, and does not spontaneously undergo proteolysis or degradation over hours in buffer or cell culture media (Fig. 4.3 and 5.2), let alone within the 5 min assay period. Second, production of the shorter apelin-13 isoform to an appreciable level requires a significantly longer time period than 5 min, even under optimal *in vitro* and *in situ* proteolysis conditions (Fig. 4.4B, C, D and 5.1), suggesting that apelin-55 is the predominant isoform during the treatment period. Third, the level of cell surface AR was increased by transfection and, thus, would likely far outweigh the level of cell surface processing enzymes. In combination, it is more probable that apelin-55 will encounter and interact with an AR molecule than an endogenous processing enzyme during the 5

min incubation period. The observed ERK phosphorylation, thus, is most likely to result from a direct apelin-55—AR interaction rather than the processing of apelin-55 to a shorter isoform prior to activation.

6.3.4 CONFORMATIONAL COMPARISON OF APELIN ISOFORMS BY CD SPECTROPOLARIMETRY

Given that all apelin isoforms activated the AR and they share C-terminal residues required for the AR binding and activation [74], I hypothesized that they shared a similar conformation in the C-terminal region. Comparison of the secondary structure of apelin-55 and -36 by far-UV CD spectroscopy (Fig. 6.5), the latter exhibiting spectra consistent with previous studies of synthetic apelin-36 [197, 226], did not imply any significant α-helical or β-sheet content. Rather, each isoform exhibits a strong negative band at ~200 nm consistent with random coil conformation [340].

In the shorter apelin-13 and -17 isoforms, previous work by the Rainey lab students reported distinctive positive bands at ~194 nm and ~218 nm directly attributed to the C-terminal phenylalanine side chain, as they were eliminated by alanine substitution (i.e., in F13A-apelin-13) [197]. Interestingly, the F55A-apelin-55 mutant exhibited an increased magnitude of ellipticity relative to both apelin-55 and -36 over the ~190-220 nm range (Fig. 6.5), suggesting that residual band structure from the phenylalanine is still convoluting the backbone ellipticity in the longer isoforms. Apelin-36 also showed minor increases in ellipticity at ~194 nm and ~218 nm in comparison to apelin-55. Thus, these results imply that the negative band at ~200 nm in the longer isoforms (apelin-36 and -55) is accentuated by the increased number of backbone amide chromophores in comparison to the shorter isoforms (apelin-13 and -17), additively increasing in

magnitude to outweigh the positive bands from the phenylalanine side chain. In combination, the CD results are consistent with the presence of bands from C-terminal phenylalanine regardless of the number of N-terminal residues.

6.3.5 STRUCTURE AND DYNAMICS OF APELIN-55 AT 5 °C AND 37 °C

To allow characterization of apelin-55 at the atomic-level, sequential assignment was carried out. Prior to conducting the heteronuclear NMR experiments required for the main chain-directed assignment approach, stability of apelin-55 was tested in various NMR buffer conditions ($NaCH_3COO$ (pH 5), MES (pH 6), NaH_2PO_4/Na_2HPO_4 (pH 6 & 7), Bis Tris (pH 6 & 7), and HEPES (pH 7)). The analysis showed that apelin-55 was stable in all potential NMR buffer conditions for at least one week at 37 °C, room temperature, and 5 °C, as analyzed through SDS-PAGE similar to the observations made in Chapter 4 and 5 (Fig. 4.3 and 5.2). The stability of apelin-55 in NaH_2PO_4/Na_2HPO_4 buffer at pH 6 was further demonstrated by a lack of perturbation to the ^{1}H-^{15}N HSQC peak pattern following 9 days of triple-resonance experiments.

Triple-resonance NMR experiments allowed sequential assignment in NaH_2PO_4/Na_2HPO_4 buffer (pH 6) using uniformly ^{15}N- and ^{13}C-labeled apelin-55 at both 5 and 37 °C. H_N, N, C_α, C_β, and C' alongside asparagine N_δ-H_δ and glutamine H_ε-N_ε chemical shifts were assigned for all residues except 0S (remaining residue from TEV cleavage), 1G, 49H and 50K at 37 °C (Table 6.3 and Table A.1). In contrast, H_N, N, C_α, C_β, C', asparagine N_δ-H_δ, and glutamine H_ε-N_ε chemical shifts were assigned for all residues except 0S at 5 °C (Table 6.3 and A.2). Interestingly, cross-peaks with chemical shifts suggestive of asparagine H_δ-N_δ and/or glycine H_N-N could be detected quite downfield relative to the typical values expected for ^{15}N (glycine) or ^{1}H (asparagine)

chemical shifts at both 5 °C and 37 °C (Fig. 6.6A; green annotations) [341]. Using a ^{15}N-edited TOCSY-HSQC experiment, H_α and the majority of side chain H_β, H_γ, and H_δ ^{1}H chemical shifts were also assigned. For reference, H_N-N resonance assignments are annotated on ^{1}H-^{15}N HSQC spectra (Fig. 6.6A at 37 °C and Fig. 6.7 at 5 °C).

The lack of assignable resonances for residues 0S and 1G was expected due to fast exchange with solvent molecules at 37 °C [342], given the reliance upon H_N in the triple-resonance experiments and the TOCSY-HSQC experiment. In the case of 49H and 50K, previous structural characterization of apelin-17 in the Rainey lab demonstrated that these residues were located in a highly dynamic region [197]. Specifically, the region encompassing 10S, 11H, and 12K in apelin-17 (equivalent to 48S, 49H, and 50K in apelin-55) could not be superposed over the ensembles of NMR structures calculated at either 5 °C or 35 °C in buffer, indicating that it is effectively acting as a flexible linker between two relatively more structured regions. The lack of assignable spin-systems for residues 49H and 50K in apelin-55 is, thus, consistent with poor structural convergence similar to apelin-17 with the implication that this region is undergoing dynamics on the intermediate time scale from an NMR perspective ([44] and refer to Section 2.5.1). In support of this, spin systems for 1G, 49H, and 50K could clearly be identified upon decreasing the temperature from 37 °C to 5 °C (Fig. 6.7 and Table A.2). This is consistent with a temperature-dependent modulation of the exchange rate upon cooling, likely from the intermediate (ms) towards the slow (s) exchange regime.

Although apelin-55 only contains one tryptophan (33W), three cross-peaks attributable to the side chain $H_{\varepsilon 1}$-$N_{\varepsilon 1}$ spin-pair were visible in the HSQC spectrum (Fig. 6.6B; one major, two minor cross-peaks). These additional cross-peaks imply the

sampling of conformational states in the slow exchange regime [44]. In support of this, additional distinct sets of backbone ^{1}H and ^{15}N chemical shifts were assignable for 33W and for a variety of other amino acids (Fig. 6.8A). These additional assignments were predominantly localized to the region of apelin-55 N-terminal to apelin-17 and to the C-terminal GPMPF region. Despite evidence of slow exchange in these regions of the backbone, it was not possible to sequentially assign any additional chains of multiple amino acids that would be consistent with a second major conformation of the apelin-55 backbone.

In further support of chemical exchange giving rise to the additional chemical shifts observed, apelin-55 at 5 °C exhibited a different pattern of potential assignments on a residue-by-residue basis in comparison to those observed at 37 °C (Fig. 6.8). This modulation in exchange may arise from a temperature-dependent change in the equilibrium populations of different states. Specifically, lowering of the temperature will proportionally reduce the entropic contribution to Gibbs free energy. This would, in turn, increase the relative contribution of enthalpic components to the Gibbs energy, increasing the propensity of observing a lower populated entropically disfavoured but enthalpically favoured state [343]. Alternatively, or in concert, lowering of temperature may slow the rate of an exchange process from the intermediate toward the slow exchange regime. Interestingly, increased evidence of slow exchange was especially clear at 5 °C for residues near 33W. Correspondingly, 33W $H_{\varepsilon 1}$-$N_{\varepsilon 1}$ presented an altered HSQC peak pattern, both with respect to chemical shifts and through the presence of one additional major cross-peak relative to 37 °C (Fig. 6.6C). Unlike at 37 °C, where only one set of chemical shifts could be assigned sequentially corresponding to one major conformation,

additional sets of chemical shifts could be sequentially assigned at 5 °C (Fig. 6.8B, yellow highlights; Table A.2). In combination, these results indicate that apelin-55 undergoes exchange at the intermediate through slow time scales.

All proline residues except 23P and 45P exhibit multiple sets of chemical shifts at both 5 °C and 37 °C, indicative of slow exchange. Correspondingly, multiple sets of chemical shifts were frequently observed for residues N-terminal to or flanked by prolines. One likely source of conformational exchange for proline arises from its altered *cis*-*trans* isomerization equilibrium relative to other amino acids [344]. This may result in a significant population of *cis* peptide bonds in slow exchange with the *trans* isomer. Correspondingly, previously characterized conformation of apelin-17 presented two major conformers in the C-terminal GPMPF region of apelin-17, one with both proline residues having *trans* peptide bonds and the other with both *cis* alongside less populated conformers with one residue *trans* and one *cis* [197]. The C_β chemical shift of proline is diagnostic of the presence of either a *cis* (av. 34.8 ppm) or *trans* (av. 32.2 ppm) peptide bond, even in disparate environments [48, 345]. The presence of both *cis* and *trans* isomers is clear for 52P and 54P at both 5 °C and 37 °C (*trans/cis* ratio of ~9:1), while *cis* isomers are also clear for 5P at 37 °C (*trans/cis* ratio of ~9:1) and 32P at 5 °C (*trans/cis* ratio of ~3:1) (Table A.1 and A.2). Correspondingly, the proline-induced conformers identified as being in slow exchange in apelin-17 may also exist in the C-terminal region of apelin-55.

The reason that residues in the N-terminal half of apelin-55 exhibit multiple sets of chemical shifts independent of proline is not as clear-cut. Whether this is the result of proline-mediated isomerization being propagated along the backbone or simply less

stringent degree of backbone conformational restriction remains to be determined. However, N-terminal flexibility may hypothetically be required to facilitate interaction with diverse binding partners (e.g., the AR, proprotein processing enzymes, or as-yet unidentified partners) or other cellular factors that regulate the rate of receptor interaction.

Interestingly, the lowest degree of conformational variation was observed over 37R-48S at both 5 °C and 37 °C. This region encompasses the 39K-42R and 43R-46L segments, which were converged in apelin-17 (apelin-17 numbering 1K-4R and 6R-9L) [197]. Decreased conformational variation in this region, similar to apelin-17, further bolsters the hypothesis that apelin-55 may have a similar pool of converged conformations in the shared C-terminal region facilitating receptor interaction.

Chemical shift analysis of apelin-55 implied no extended segments of secondary structure according to either the CSI (Fig. 6.9) or the Bayesian algorithm DANGLE (data shown in Chapter 7 Fig. 7.8) at both 37 and 5 °C. Furthermore, a comparison of chemical shifts to expected random coil chemical shifts only showed minor differences throughout the majority of the peptide backbone (Fig. 6.9). These results correlate well with the random coil CD spectral characteristics observed (Fig. 6.5). It should be noted that β-turn character may still be present, as previously observed in apelin-17 [197]. Neither DANGLE [57] nor CSI [55, 56] unambiguously identifies β-turns, despite their utility for more extended secondary structures.

At higher temperature, analysis of the ^{1}H-^{15}N heteronuclear NOE enhancement factor on a residue-by-residue basis also implies that apelin-55 is highly dynamic along the entire backbone at the ps-ns time scale, further supporting the random coil

conformation suggested by CD and the lack of extended secondary structuring predicted by DANGLE and CSI (Fig. 6.9A). In contrast, analysis of the ^{1}H-^{15}N heteronuclear NOE enhancement factor at 5 °C showed decreased dynamics throughout apelin-55 (Fig. 6.9B). This may simply be due to the expected increase in viscosity of water at this temperature [346], as no extended secondary structuring was predicted by DANGLE and CSI similar to 37 °C (Fig. 6.9B). Interestingly, NOE analysis identified the greatest dynamics in the N-terminal end of the protein at both temperatures, corresponding to the lack of assignable resonances for N-terminal residue(s). Similar to apelin-55, the shorter isoforms were also highly dynamic in buffer at higher temperature [197]. Their dynamics at 35 °C were only decreased upon interaction with membrane mimetic detergents, which also resulted in striking conformational changes [197, 329]. On this note, interactions between membrane mimetic detergents and longer apelin isoforms (i.e., -55 and -36) were studied and are discussed in Chapter 7.

6.3.6 ATOMIC-LEVEL COMPARISON OF APELIN ISOFORMS BY NMR SPECTROSCOPY

The potential conformational similarities between apelin-55 and the shorter apelin isoforms were probed using ^{1}H-^{15}N HSQC experiments at 37 °C for ^{15}N-labeled apelin-55 and -36 and for apelin-17 and -13 at natural abundance (Fig. 6.10A). Comparison of the HSQC spectra of all apelin isoforms showed near perfect spectral overlay for any cross-peaks shared between longer and shorter isoforms, with a greater number of cross-peaks corresponding directly to increased isoform length. Furthermore, inference of the amino acids giving rise to the correlations observed in the ^{1}H-^{15}N HSQC for each of the shorter apelin isoforms corresponded directly to the shared amino acids assigned in

apelin-55. The observed chemical shifts were practically indistinguishable from apelin-55, with only very minor CSD perturbation (CSD ≤ ~0.02 ppm; Fig. 6.11).

Additional sets of chemical shifts assigned to 51G, 53M and 55F (likely arising from multiple conformations in the C-terminal region of apelin) were observable in all of the shorter apelin peptides, inferring that all isoforms maintain a similar pool of *cis*/*trans* isomers in the C-terminal GPMPF motif (Fig. 6.10C-E). The observation of similar chemical shifts between apelin isoforms extends from previous work on shorter isoforms by the Rainey lab, where highly similar chemical shifts between apelin-12, -13, Pyr-13, and -17 was observed [197]. Inferring chemical shift assignments from apelin-55 did not allow for unambiguous identification for 1K-4R (equivalent to 39K-42R) in apelin-17. This may be due to increased dynamics near the N-terminus and the low natural abundance of ^{15}N (0.37%). Spectral comparison of tryptophan $H_{\varepsilon 1}$-$N_{\varepsilon 1}$ spin-pairs for apelin-55 vs. -36 also showed minor differences in conformational biases. In particular, one additional cross-peak was observed for apelin-36 (Fig. 6.10B), which was visible near the noise level for apelin-55.

In summary, the results clearly indicate that the common C-terminal residues (Table 3.1) share a highly similar set of conformations, and provide a structural rationale to explain the observation of receptor activation by all apelin isoforms, including the putative proprotein (summarized in Fig. 6.12). Furthermore, the NMR spectroscopic results imply that the critical C-terminal residues remain conformationally unhindered by the N-terminal residues in all isoforms, which is likely fundamental to the processes of receptor binding and activation. Conversely, N-terminal residues remain unobstructed by

C-terminal residues to interact with either the AR and other binding partners such as PCSK3.

6.3.7 STRUCTURE-FUNCTION CORRELATION OF APELIN ISOFORMS

Practically identical ^{1}H-^{15}N chemical shift patterns across all apelin isoforms from apelin-13 to -55 imply nearly identical backbone conformations and conformational sampling, leading to the hypothesis that all isoforms are recognized by, bind to, and activate the AR through their shared C-terminal conformational behaviour. This is further exemplified by the fact that all isoforms were capable of activating downstream signalling *via* the AR. One significant distinction was, however, clear in that apelin-13 was observed to be ~8× more potent that the longer isoforms (-17, -36, and -55), all of which displayed comparable potency.

It is interesting to note that the near identical conformations between apelin isoforms are also in contrast to the other ligand of the AR, apela [222]. Although apelin and apela have relatively similar amino acid composition and bind to the same receptor, apela isoforms (-32 and -11) presented differences in their conformations by ^{1}H-^{15}N HSQC [222] and ability to activate various signalling pathways [223], suggesting the potential of ligand conformation-dependent potencies for apela isoforms.

For apelin, one possible explanation for isoform-dependent potency is interference in receptor binding arising from the additional N-terminal residues of the longer isoforms, specifically by the KFRR that falls immediately N-terminal to apelin-13 in the longer isoforms. In contrast to this, however, several studies have shown longer isoforms to have greater affinity for the receptor than apelin-13 [107, 208, 214]. This has been proposed to be the result of electrostatic interactions between positively charged N-

terminal residues of apelin isoforms and key negatively charged surface residues of the AR [77, 78, 215, 216]. This may relate to the conformational flexibility observed in the N-terminal region of apelin-55, allowing partner-dependent folding upon binding [347], including to the AR. Furthermore, the observed lack of interaction between N- and C-terminal regions of apelin-55 would provide additional freedom for favourable ligand-receptor interactions to increase affinity.

Perplexingly, the observed increased affinity for longer isoforms seems counterintuitive with respect to their lower potency relative to apelin-13. Although the isoforms may vary in their biophysical and pharmacological properties *in vivo,* significant isoform-dependent variation was not detected between E_{max} or conformational sampling under our experimental conditions. Thus, it seems likely that the difference in potency stems from as yet unknown intricacies in ligand-receptor interactions, which would ultimately result in isoform-dependent modulation of receptor conformation and/or dynamics [79, 348, 349].

6.3.8 ISOFORM-MEDIATED IMPACT ON PHYSIOLOGICAL RESPONSES

As detailed in Sections 3.2.4 and 3.2.5, and mentioned in previous chapters, isoforms can have different AR signalling and regulation, and the ratio of apelin isoforms has been proposed to be an important regulatory method *in vivo* as a result [208]. With the introduction of apelin-55 as a significantly longer bioactive isoform, these *in vivo* ligand-dependent phenomena are likely not limited solely to apelin-36 and -13. Furthermore, this implies that the level of various isoforms or their half-lives will need appropriate regulation to modulate the final physiological response(s). Based on results from Chapter 5, this regulation may be conducted extracellularly to provide an additional

layer of control. Intriguingly, an alternative as-yet unidentified receptor has also been implicated for apelin-36 [184]. The effect of N-terminal extension to apelin-55 upon this alternative signalling pathway remains uncharacterized. Regardless, the identification of apelin-55 as an additional bioactive isoform indicates greater complexity and considerably expands the apelinergic system than previously recognized.

6.4 MOTIVATIONS AND BASIS FOR CHAPTER 7

In this chapter, I demonstrated that apelin-55 is not an inactive proprotein, as many have speculated since the discovery of apelin in 1998. Rather, through western blotting techniques (both traditional and In-Cell Western™ by me and in collaboration with Mr. Nigel Chapman), I show herein that apelin-55 is an additional, longer bioactive apelin isoform. NMR spectroscopy demonstrated similar shared C-terminal conformations for apelin-55 and all of the shorter isoforms, suggesting similar modes of AR recognition, binding, and activation, and providing a clear biophysical justification for the AR activation observed for all isoforms. In addition, the N-terminal domain showed increased flexibility and conformational dynamics that may be necessary for interaction with its extracellular binding partners, whether in the context of AR activation or in that of cleavage by processing enzymes.

As was stated in Section 6.3.7, the increased affinity observed for longer apelin isoforms appears to contrast with the decreased potency of these isoforms and this may stem from ligand-mediated changes in receptor conformations and/or the occlusion of the ultimate binding site for the apelin C-terminal located in the AR transmembrane domain. An additional mechanism may serve to regulate ligand-receptor interactions, following

the “membrane catalysis” mechanism proposed by Sargent and Schwyzer [330]. In this mechanism, interaction of a bioactive peptide with a biological membrane may act to modulate the potency and efficacy of the ligand through changes in favourability of receptor encounter, recognition, and binding. In support of this mechanism being a potential regulator of apelin function, previous studies of apelin-17 in the Rainey lab showed that this isoform exhibited preferential interactions with micelles having anionic headgroups, leading to structuring upon binding [329]. Thus, longer apelin isoforms may present different biophysical behaviour in the presence of and binding to membranes, leading to the observable pharmacological differences between ligands through distinct membrane-catalyzed interactions with AR.

Table 6.1: NMR experimental details

Experiment	Pulse program (Bruker)	Delay (s)	# of scans	Acquisition time (s)	# of complex points	Sweep width (ppm)	Center position (ppm)	^{1}H frequency (MHz)	Note
Apelin-55 in buffer at 37 °C									**^{15}N- and ^{13}C-labeled**
HNCO	hncogp3d	1	8	^{1}H: 0.1216512 ^{15}N: 0.0183830 ^{13}C: 0.0262114	^{1}H: 2048 ^{15}N: 48 ^{13}C: 48	^{1}H: 12.0224 ^{15}N: 18.4000 ^{13}C: 5.2000	^{1}H: 4.709 ^{15}N: 117.200 ^{13}C: 172.600	700	
HN(CA)CO	hncacogp3d	1	24	^{1}H: 0.1216512 ^{15}N: 0.0183830 ^{13}C: 0.0262114	^{1}H: 2048 ^{15}N: 48 ^{13}C: 48	^{1}H: 12.0224 ^{15}N: 18.4000 ^{13}C: 5.2000	^{1}H: 4.709 ^{15}N: 117.200 ^{13}C: 172.600	700	
HNCA	hncagp3d	1	16	^{1}H: 0.1216512 ^{15}N: 0.0183830 ^{13}C: 0.0059268	^{1}H: 2048 ^{15}N: 48 ^{13}C: 48	^{1}H: 12.0224 ^{15}N: 18.4000 ^{13}C: 23.0000	^{1}H: 4.709 ^{15}N: 117.200 ^{13}C: 51.000	700	
HN(CO)CA	hncocagp3d	1	16	^{1}H: 0.1216512 ^{15}N: 0.0183830 ^{13}C: 0.0059268	^{1}H: 2048 ^{15}N: 48 ^{13}C: 48	^{1}H: 12.0224 ^{15}N: 18.4000 ^{13}C: 23.0000	^{1}H: 4.709 ^{15}N: 117.200 ^{13}C: 51.000	700	
CBCANH	cbcanhgp3d	1	16	^{1}H: 0.1216512 ^{15}N: 0.0183830 ^{13}C: 0.0048279	^{1}H: 2048 ^{15}N: 48 ^{13}C: 68	^{1}H: 12.0224 ^{15}N: 18.4000 ^{13}C: 40.0000	^{1}H: 4.709 ^{15}N: 117.200 ^{13}C: 44.000	700	
CBCA(CO)NH	cbcaconhgp3d	1	16	^{1}H: 0.1216512 ^{15}N: 0.0183830 ^{13}C: 0.0048279	^{1}H: 2048 ^{15}N: 48 ^{13}C: 68	^{1}H: 12.0224 ^{15}N: 18.4000 ^{13}C: 40.0000	^{1}H: 4.709 ^{15}N: 118.000 ^{13}C: 44.000	700	
^{1}H-^{15}N HSQC	hsqcetf3gpsi2	1	16	^{1}H: 0.1044480 ^{15}N: 0.0490214	^{1}H: 2048 ^{15}N: 128	^{1}H: 14.0025 ^{15}N: 30.0000	^{1}H: 4.709 ^{15}N: 117.200	700	
^{1}H-^{15}N TOCSY-HSQC (TOCSY mixing time 60 ms)	dipsihsqcf3gpsi3d	1	8	^{1}H: 0.1216512 ^{15}N: 0.0183830 ^{1}H: 0.0106289	^{1}H: 2048 ^{15}N: 48 ^{1}H: 128	^{1}H: 12.0224 ^{15}N: 18.4000 ^{1}H: 8.6000	^{1}H: 4.709 ^{15}N: 117.200 ^{1}H: 4.709	700	TOCSY mixing time 60 ms
^{1}H-^{15}N Het. NOE HSQC	hsqcnoef3gpsi	5	28	^{1}H: 0.1044480 ^{15}N: 0.0949467	^{1}H: 2048 ^{15}N: 128	^{1}H: 14.0025 ^{15}N: 19.0000	^{1}H: 4.707 ^{15}N: 117.200	700	With NOE (interleaved)
^{1}H-^{15}N Het. NOE HSQC	hsqcnoef3gpsi	5	28	^{1}H: 0.1044480 ^{15}N: 0.0949467	^{1}H: 2048 ^{15}N: 128	^{1}H: 14.0025 ^{15}N: 19.0000	^{1}H: 4.707 ^{15}N: 117.200	700	Without NOE (interleaved)
Apelin-55 in buffer at 5 °C									**^{15}N- and ^{13}C-labeled**
HNCO	hncogp3d	1	8	^{1}H: 0.1216512 ^{15}N: 0.0169124	^{1}H: 2048 ^{15}N: 48	^{1}H: 12.0224 ^{15}N: 20.0000	^{1}H: 4.698 ^{15}N: 117.000	700	

				^{13}C: 0.0194713	^{13}C: 48	^{13}C: 7.0000	^{13}C: 173.700		
HN(CA)CO	hncacogp3d	1	24	^{1}H: 0.1216512 ^{15}N: 0.0169124 ^{13}C: 0.0194713	^{1}H: 2048 ^{15}N: 48 ^{13}C: 48	^{1}H: 12.0224 ^{15}N: 20.0000 ^{13}C: 7.0000	^{1}H: 4.698 ^{15}N: 117.000 ^{13}C: 173.700	700	
HNCA	hncagp3d	1	16	^{1}H: 0.1216512 ^{15}N: 0.0169124 ^{13}C: 0.0059268	^{1}H: 2048 ^{15}N: 48 ^{13}C: 48	^{1}H: 12.0224 ^{15}N: 20.0000 ^{13}C: 23.0000	^{1}H: 4.698 ^{15}N: 117.000 ^{13}C: 50.500	700	
HN(CO)CA	hncocagp3d	1	8	^{1}H: 0.1216512 ^{15}N: 0.0183830 ^{13}C: 0.0059268	^{1}H: 2048 ^{15}N: 48 ^{13}C: 48	^{1}H: 12.0224 ^{15}N: 20.0000 ^{13}C: 23.0000	^{1}H: 4.698 ^{15}N: 117.000 ^{13}C: 50.500	700	
HNCACB	hncacbgp3d	1	16	^{1}H: 0.1216512 ^{15}N: 0.0169124 ^{13}C: 0.0048279	^{1}H: 2048 ^{15}N: 48 ^{13}C: 96	^{1}H: 12.0224 ^{15}N: 20.0000 ^{13}C: 41.0000	^{1}H: 4.698 ^{15}N: 117.000 ^{13}C: 42.500	700	
^{1}H-^{15}N HSQC	hsqcetf3gpsi2	1	16	^{1}H: 0.1044480 ^{15}N: 0.0300664	^{1}H: 2048 ^{15}N: 128	^{1}H: 14.0025 ^{15}N: 30.0000	^{1}H: 4.698 ^{15}N: 118.000	700	
^{1}H-^{15}N NOESY-HSQC	noesyhsqcf3gpsi3d	1	8	^{1}H: 0.1216512 ^{15}N: 0.0169124 ^{1}H: 0.0085536	^{1}H: 2048 ^{15}N: 48 ^{1}H: 144	^{1}H: 12.0224 ^{15}N: 20.0000 ^{1}H: 12.0224	^{1}H: 4.698 ^{15}N: 117.000 ^{1}H: 4.698	700	Mixing time 150 ms
^{1}H-^{15}N TOCSY-HSQC	dipsihsqcf3gpsi3d	1	8	^{1}H: 0.1216512 ^{15}N: 0.0169124 ^{1}H: 0.0079717	^{1}H: 2048 ^{15}N: 48 ^{1}H: 96	^{1}H: 12.0224 ^{15}N: 20.0000 ^{1}H: 8.6000	^{1}H: 4.698 ^{15}N: 117.000 ^{1}H: 4.698	700	TOCSY mixing time 60 ms
^{1}H-^{15}N Het. NOE HSQC	hsqcnoef3gpsi	5	28	^{1}H: 0.1044480 ^{15}N: 0.1002215	^{1}H: 2048 ^{15}N: 128	^{1}H: 14.0025 ^{15}N: 18.0000	^{1}H: 4.698 ^{15}N: 117.500	700	With NOE (interleaved)
^{1}H-^{15}N Het. NOE HSQC	hsqcnoef3gpsi	5	28	^{1}H: 0.1044480 ^{15}N: 0.1002215	^{1}H: 2048 ^{15}N: 128	^{1}H: 14.0025 ^{15}N: 18.0000	^{1}H: 4.698 ^{15}N: 117.500	700	Without NOE (interleaved)
Apelin-36 in buffer at 37 °C									**^{15}N-labeled**
^{1}H-^{15}N HSQC	hsqcetfpgpsi2	1	64	^{1}H: 0.1703936 ^{15}N: 0.0526138	^{1}H: 2048 ^{15}N: 160	^{1}H: 12.0160 ^{15}N: 30.0000	^{1}H: 4.709 ^{15}N: -261.500	500	
Apelin-17 in buffer at 37 °C									**Unlabeled**
^{1}H-^{15}N HSQC	hsqcetf3gpsi2	1	768	^{1}H: 0.0909312 ^{15}N: 0.0225499	^{1}H: 2048 ^{15}N: 64	^{1}H: 16.0840 ^{15}N: 20.0000	^{1}H: 4.704 ^{15}N: 117.000	700	
Apelin-13 in buffer at 37 °C									**Unlabeled**
^{1}H-^{15}N HSQC	hsqcetf3gpsi2	1	768	^{1}H: 0.0909312 ^{15}N: 0.0225499	^{1}H: 2048 ^{15}N: 64	^{1}H: 16.0840 ^{15}N: 20.0000	^{1}H: 4.708 ^{15}N: 117.000	700	

Table 6.2: Pharmacological properties of apelin isoforms (mean ± SEM).

	Pyr-apelin-13	Apelin-17	Apelin-36	Apelin-55
EC_{50} (nM, 5 min)[a]	2.05 ± 0.65	16.35 ± 3.73**	16.54 ± 6.51*	16.91 ± 2.86***

[a]The EC_{50} values (based on Fig. 6.4E) for each isoform were extrapolated and averaged from the curves of individual experiments. Statistical significance compared to Pyr-apelin-13 was determined using one-tailed unpaired Student's t-test (*$P < 0.05$, **$P < 0.01$, and ***$P < 0.001$).

Table 6.3: Assignment report for apelin-55 in indicated conditions

Atom type	37 °C	5 °C
H_N*	44/47 (94%)	47/47 (100%)
N‡	44/47 (94%)	47/47 (100%)
C'	54/56 (96%)	56/56 (100%)
C_α	54/56 (96%)	56/56 (100%)
C_β	44/46 (95%)	44/46 (96%)

*N-terminal H_N was excluded
‡Proline residues and N-terminal N were excluded

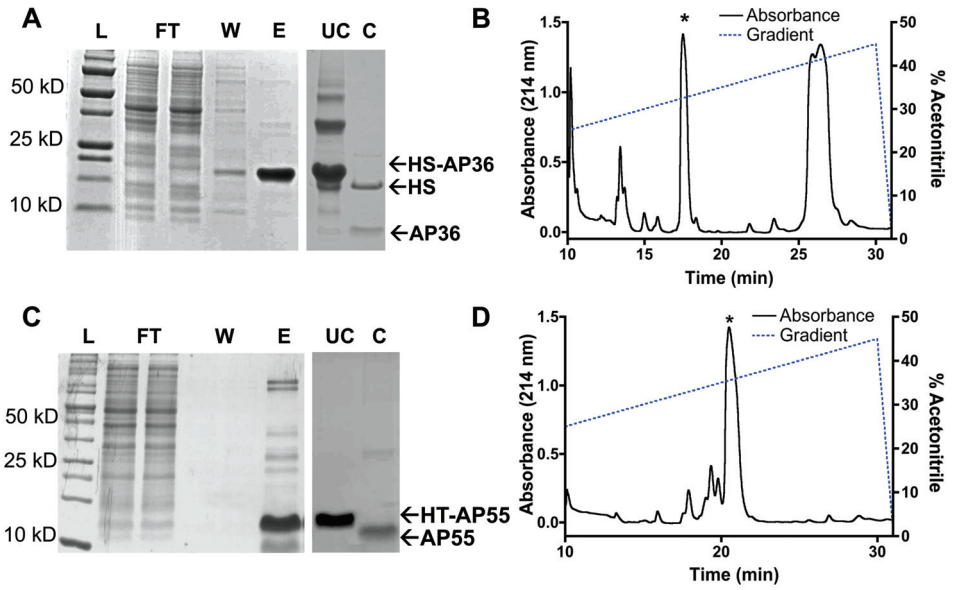

Figure 6.1: Apelin-36 and-55 expression, fusion protein cleavage, and purification. SDS-PAGE gels demonstrating Ni-NTA column purification of (A) His-SUMO-apelin-36 (HS-AP36) and (C) His-TEV-apelin-55 (HT-AP55) and subsequent cleavage reaction by (A) SUMO protease to produce His-SUMO (HS) tag and apelin-36 (AP36) and (C) TEV protease-mediated His tag removal to produce apelin-55 (AP55). Preparative RP-HPLC chromatograms of (B) apelin-36 and (D) apelin-55 (confirmed product elution denoted by asterisks (*)). Acronyms: L-ladder, FT-flow through, W-wash, E-elution, UC-uncleaved, C-cleaved.

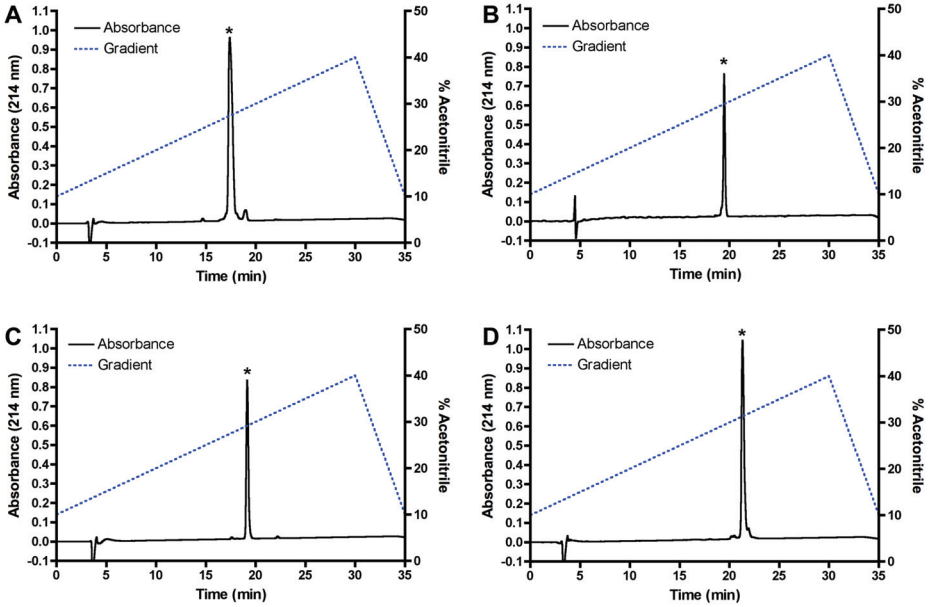

Figure 6.2: Analytical HPLC chromatograms of purified apelin isoform samples. A) apelin-13, B) apelin-17, C) apelin-36, and D) apelin-55. All samples were resolved using an analytical C_{18} column with a binary system (A: H_2O with 0.1% trifluoroacetic acid (TFA) and B: acetonitrile with 0.1% TFA; flow rate 1 mL/min). Gradients followed i) 10 to 40% solvent B in 30 min and ii) 40% to 10% in 5 min.

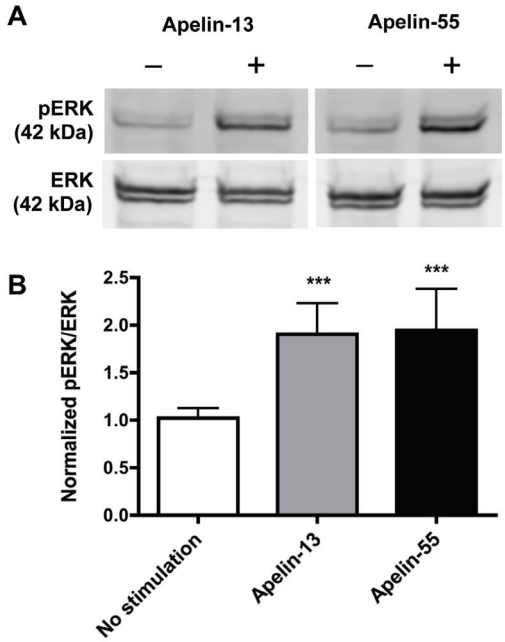

Figure 6.3: Apelin-55 and -13-mediated ERK phosphorylation in HEK293A cells transiently expressing the AR.
HEK293A cells transfected with an AR-encoding plasmid were treated (+) with 1 μM of given apelin isoform for 5 min. (A) Levels of pERK and ERK were determined by western blot analysis, as illustrated for representative experiments carried out on the same membrane. (B) pERK/ERK levels were quantified by densitometry and compared to controls without stimulation (–). Statistical significance was determined by one-tailed unpaired Student's t-test (mean ± SEM, N=4, ***P < 0.001 compared to no stimulation control).

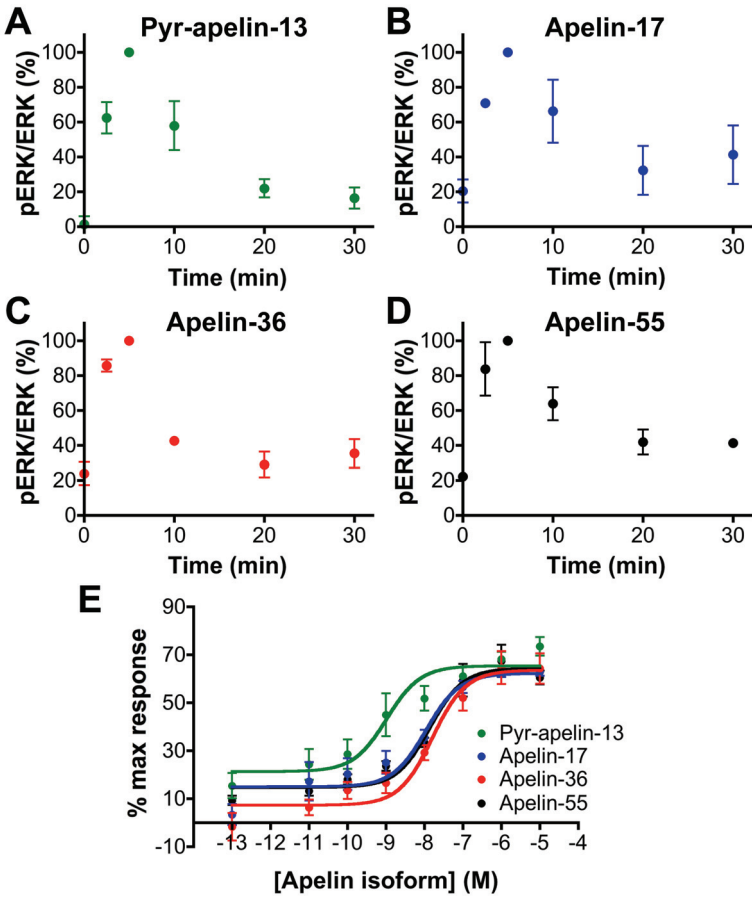

Figure 6.4: Apelin isoform-mediated ERK phosphorylation.
(A) Pyr-apelin-13, (B) apelin-17, (C) apelin-36, and (D) apelin-55 (1µM for each isoform) show time-dependent ERK phosphorylation by In-Cell Western™ assay (mean ± SEM, N=3). (E) Non-linear regression analysis of apelin isoform dose-response.

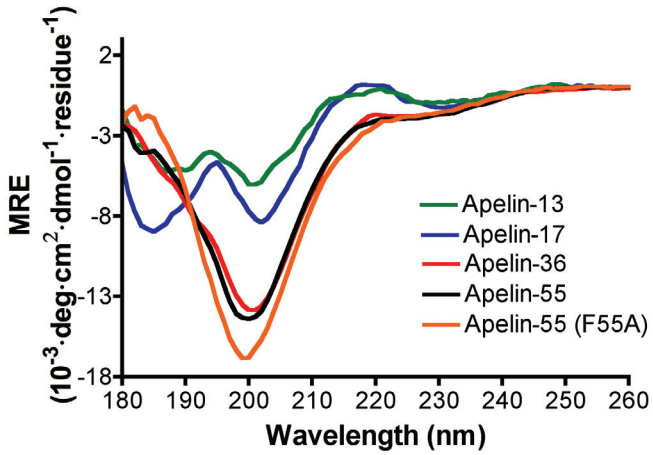

Figure 6.5: Comparison of apelin isoforms by far-UV CD spectropolarimetry.
Apelin-13 and -17 data are re-plotted from Langelaan *et al.* [197].

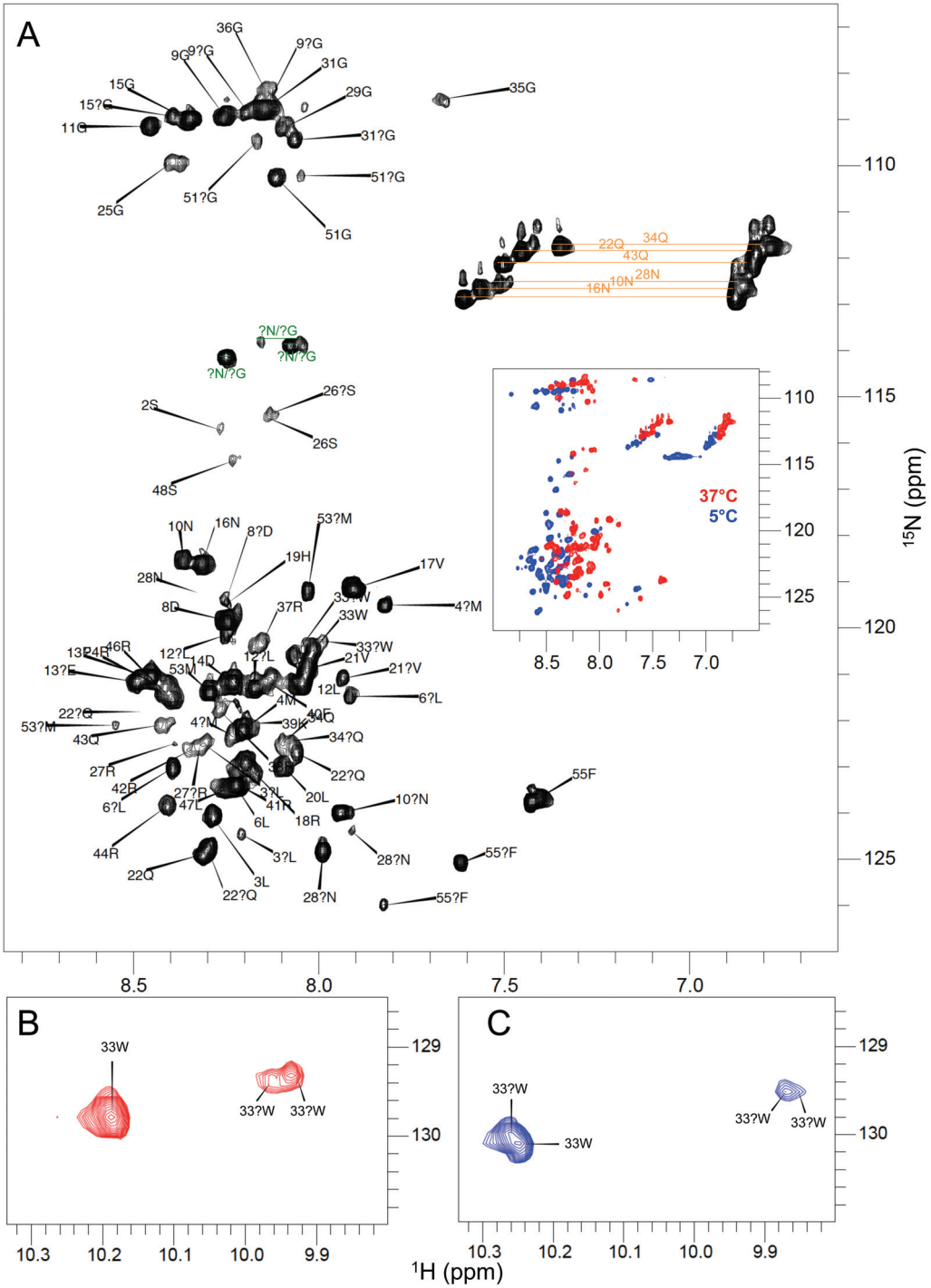

Figure 6.6: Comparison of apelin-55 at 37 °C and 5 °C.
(A) ^{1}H-^{15}N HSQC spectrum at 37 °C, with cross-peaks annotated with by residue number in the sequence and one-letter amino acid code. Additional resonance assignments from alternative conformations are differentiated by a question mark. Orange lines connect asparagine and glutamine side chain amides and green lines connect potential asparagine side chain amides. Inset shows overlay of apelin-55 at 5 °C (blue) on 37 °C (red). 33W $H_{\varepsilon 1}$-$N_{\varepsilon 1}$ side chain amides are also compared between (B) 37 °C and (C) 5 °C.

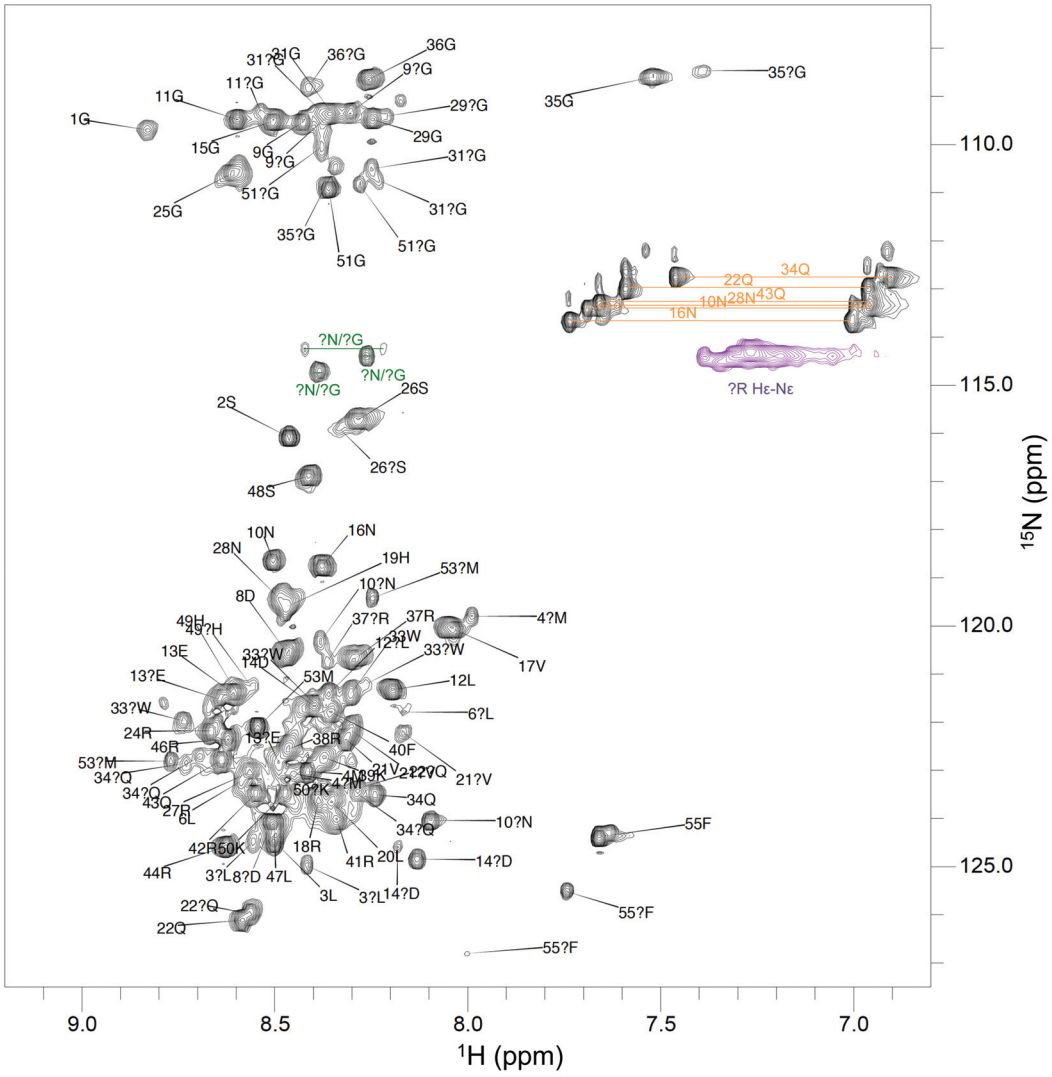

Figure 6.7: Assigned ^{1}H-^{15}N HSQC spectrum of apelin-55 at 5 °C.
Additional potential peak assignments with similar chemical shifts are marked by a question mark. Purple contours are non-specific arginine H_{ε}-N_{ε} resonances. Orange lines connect asparagine and glutamine side chain amides and green lines connect potential asparagine side chain amides.

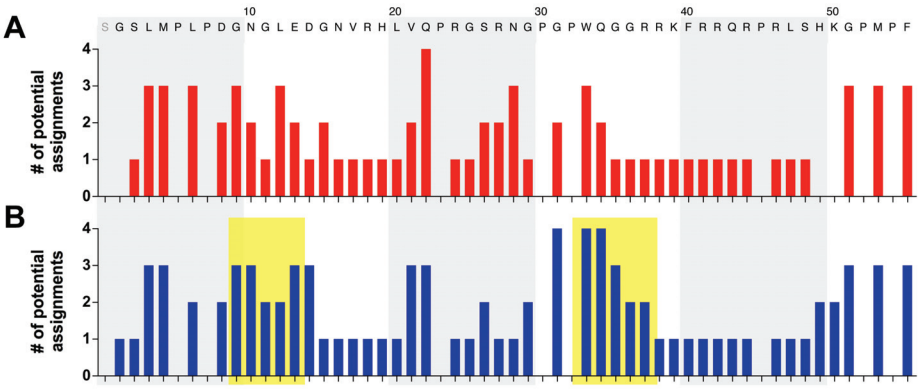

Figure 6.8: Number of potential spin-system assignments per residue of apelin-55 based upon sequential assignment at (A) 37 °C and (B) 5 °C.
The yellow boxes identify chains of more than three residues exhibiting more than one sequentially assigned series of chemical shifts at 5 °C (detailed in Table A.2).

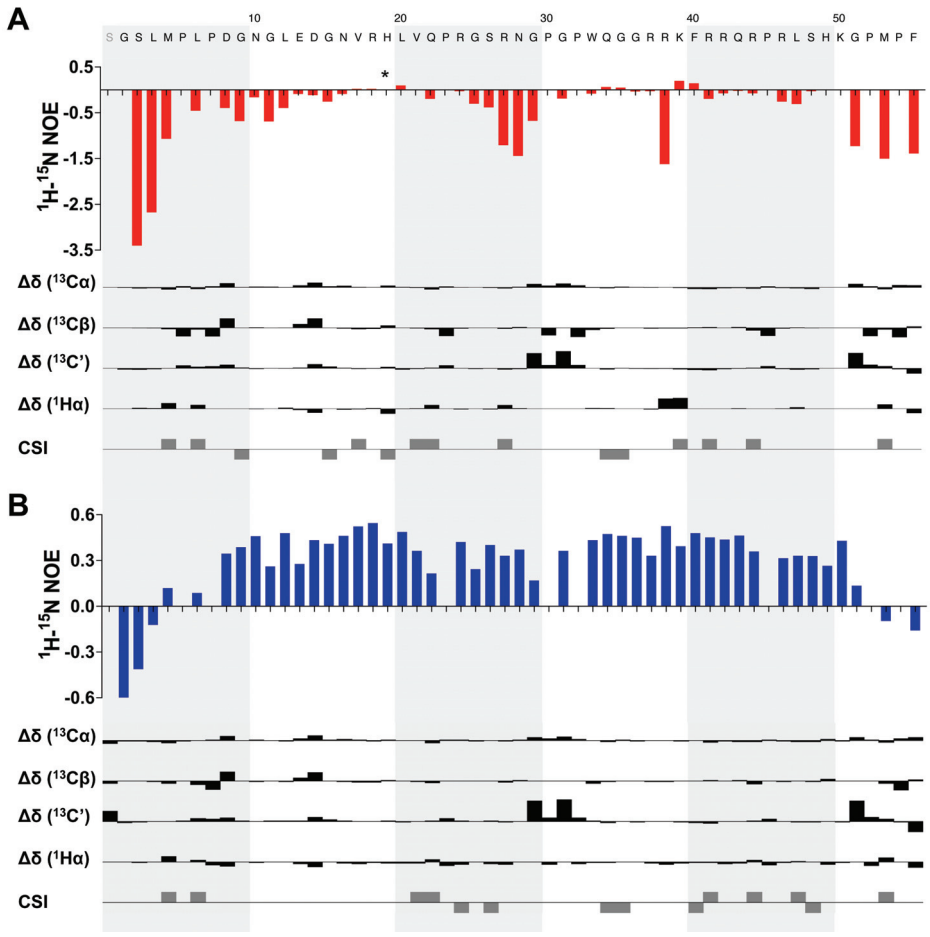

Figure 6.9: ^{1}H-^{15}N heteronuclear NOE enhancement factor, secondary chemical shift (Δδ), and CSI for apelin-55 at (A) 37 °C and (B) 5 °C.
* Residue not observable in the heteronuclear NOE-modulated ^{1}H-^{15}N HSQC experiment.

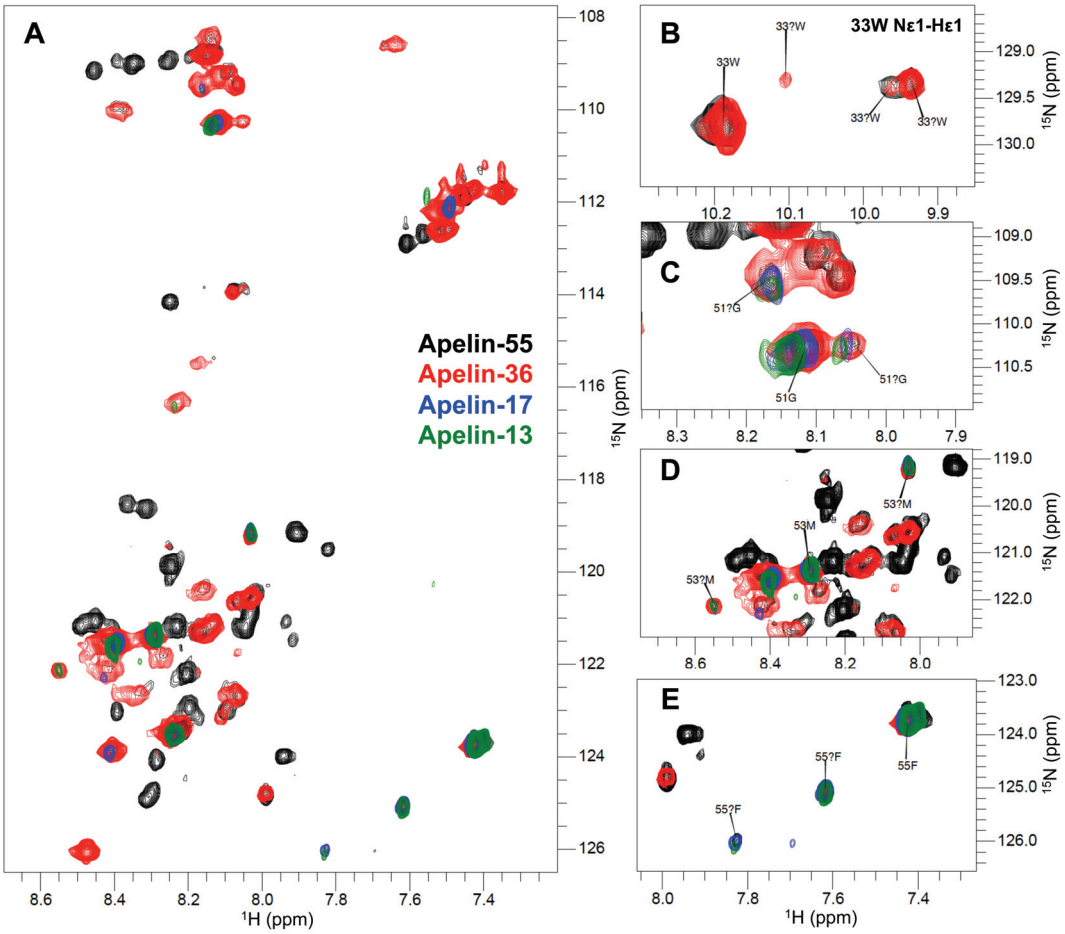

Figure 6.10: Apelin isoform atomic-level conformational comparison. (A) Overlay of ^{1}H-^{15}N HSQC spectra for each indicated isoform. (B) Expansion of HSQC region for tryptophan $H_{\varepsilon 1}$-$N_{\varepsilon 1}$ spin-pairs of apelin-55 and -36. (C-E) Overlays of HSQC regions corresponding to (C) 51G, (D) 53M, and (E) 55F in the C-terminal GPMPF motif shared between all apelin isoforms.

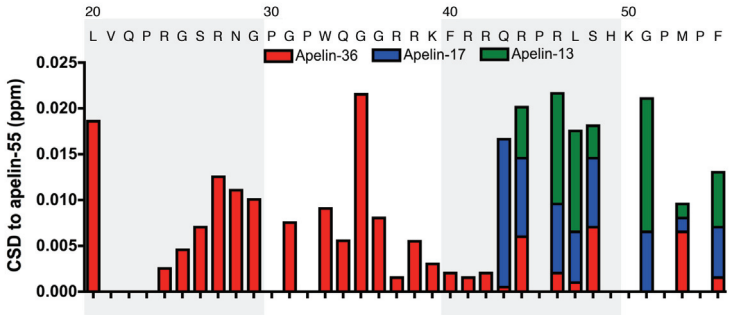

Figure 6.11: Euclidian combined chemical shift displacement (CSD) of apelin isoforms relative to apelin-55 in buffer at 37 °C.

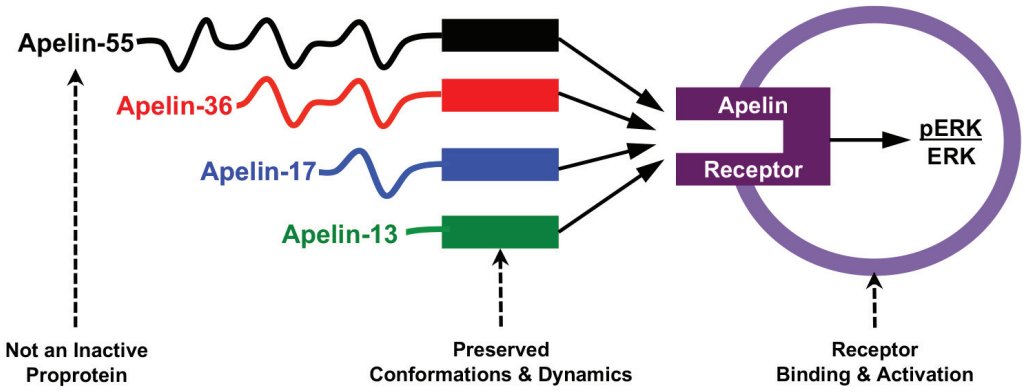

Figure 6.12: Graphical summary of structure-function analyses of apelin isoforms.

CHAPTER 7 APELIN ISOFORMS AND MEMBRANE-MIMETIC INTERACTIONS

(Note: this chapter is based upon a manuscript entitled "Apelin conformational and binding equilibria upon micelle interaction primarily depend on membrane-mimetic headgroup" submitted to ***Scientific Reports*** (under review). In the work described in this chapter, Ms. Shuya Kate Huang assisted in CD-based characterization of apelin-55 and -36 under my mentorship, and I acquired NMR data under the mentorship of postdoctoral fellow Dr. Muzaddid Sarker and/or my supervisor Dr. Jan K. Rainey.)

7.1 INTRODUCTION

In Chapter 6, apelin-55 was shown to have similar C-terminal conformational behaviour to the shorter apelin isoforms leading to the likelihood of similar modes of receptor activation for all bioactive apelin isoforms. However, as noted in Section 6.3.7, this is difficult to justify given differences in the ligand-dependent potencies and receptor regulation, detailed in Sections 3.2.4 and 3.2.5, respectively. These results indicate involvement of an additional biophysical mechanism beyond ligand structuring to regulate receptor activation. According to membrane catalysis theory [330], peptide interaction with the biological membrane may be a critical biophysical mechanism that regulates ligand-receptor interactions.

7.1.1 MEMBRANE CATALYSIS THEORY

The membrane catalysis theory, developed for peptide-receptor interactions by Sargent and Schwyzer [330], states that peptide-receptor recognition and binding is

preceded by binding of the ligand to the plasma membrane (Fig. 7.1). This initial peptide-membrane interaction "catalyzes" the rate of ligand-receptor complex formation by confining the ligand to a two-dimensional diffusion space, subsequently improving the diffusional encounter probability of the ligand-receptor pair. Furthermore, localization onto the membrane increases the local concentration of the ligand, while interaction can induce a structural change within the ligand to provide for optimal receptor recognition and binding. Thus, biological membranes have the potential to regulate ligand potency and efficacy, making the membrane a factor of particular relevance for ligand-receptor interactions. In support of the membrane catalysis theory, numerous peptide hormones, including apelin [329] and apela [222], have demonstrated binding to membrane-mimetics such as micelles and bicelles, leading to structural changes within the peptide, as reviewed in some detail by Langelaan and Rainey [350].

7.1.2 INDICATIONS OF MEMBRANE INVOLVEMENT IN THE APELINERGIC SYSTEM

Previous work in the Rainey lab demonstrated apelin-membrane interactions with a focus on the apelin-17 isoform [329]. Specifically, apelin-17 interactions were characterized with zwitterionic detergent micelles composed of dodecylphosphocholine (DPC); and anionic micelles composed of either sodium dodecyl sulfate (SDS) or 1-palmitoyl-2-hydroxy-*sn*-glycero-3-[phospho-*rac*-(1-glycerol)] (LPPG) (Fig. 7.2). A preferential interaction was demonstrated with anionic detergent micelles. It is important to note that DPC most closely mimics phosphatidylcholine, the most abundant phospholipid headgroup on the outer leaflet of eukaryotic plasma membranes [351]. SDS and LPPG, in contrast, are mimetic of either anionic lipids or glycolipids (with

modifications conferring the negative charge) that may accumulate near the receptor [352-354]. In addition to demonstrating a preferential interaction with negatively charged micelles, the NMR spectroscopy-based characterization demonstrated direct interaction between apelin-17 and anionic SDS micelle headgroups via the basic RPRL motif (Table 3.1), which adopted a type I β-turn conformation [329]. In addition, micelle binding led to highly converged structuring of the three C-terminal residues (MPF; Table 3.1) in apelin-17, despite this region being completely solvent exposed. Other work in the Rainey lab examined micellar interactions of fluorophore-conjugated apelin-36, -17 and -12. However, direct conclusions about apelin-36 relative to the shorter isoforms could not be drawn because each conjugate was non-trivially distinct in its behaviour relative to either peptide alone or fluorophore alone [355].

We also recently characterized apela-32 and -11 in the presence of DPC, SDS, and LPPG micelles [222]. Interestingly, apela demonstrated both isoform- and detergent headgroup-dependent changes in conformation and dynamics. Notably, while both apela isoforms efficiently bound to SDS and LPPG micelles, they showed clear differences in their binding with DPC. Specifically, apela-32 readily bound to any of the three types of detergent micelles, while apela-11 demonstrated a significant preference for binding to anionic over zwitterionic micelles. Further elaboration came from the fact that zwitterionic headgroup binding was localized to the N-terminal half of apela-32, which adopted an α-helical conformation in response to binding.

A number of studies have also demonstrated length-dependent potency and efficacy for apela, similar to apelin. For example, apela-32 is significantly more potent than apela-11 with regard to both receptor binding and signalling [113, 223], in contrast

to apelin where potency is generally inversely correlated with increasing isoform size (Tables 3.2 and 3.3). The observed differences in potency for apela may be explained by differences in interaction with membranes. Specifically, the favourable interaction with zwitterionic headgroups may increase apela-32 levels on a typical cell surface more than apela-11, consequently leading to a higher probability of apela-32-AR binding and increasing potency.

To date, the longer apelin isoforms in their natural state remain uncharacterized in the presence of membrane-mimetics. As a consequence, it is unknown whether these isoforms differ in membrane interaction preferences. Furthermore, it is unknown whether longer apelin isoforms will interact similarly to shorter isoforms in a strictly headgroup-dependent manner or if the increased hydrophobic content of these peptides will allow for significant peptide interaction with the hydrophobic micelle core and, by extension, lipid tailgroups in a bilayer. Any, or all, of these potential discrepancies in interaction could give rise to the observed variation in potencies. Thus, I hypothesized that apelin isoforms may have distinct membrane binding preferences. To test this hypothesis, I expanded characterization to the two longest apelin isoforms, apelin-55 and -36, in the presence of DPC, SDS, and LPPG micelles. Apelin secondary structuring as a function of environment was characterized by far-UV CD spectropolarimetry alongside NMR spectroscopy to characterize both relative prevalence of micellar interactions and changes in conformations and dynamics at the atomic-level.

7.2 MATERIALS AND METHODS

7.2.1 MATERIALS

Ampicillin, SDS, acetonitrile (high performance liquid chromatography (HPLC) grade), and reagents to make lysogeny broth (LB) medium were purchased from Fisher Scientific. DPC and LPPG were purchased from Anatrace and Avanti Polar lipids (Alabaster, AL), respectively. $^{15}NH_4Cl$, $^{13}C_6$-D-glucose, SDS-d_{25}, and DPC-d_{38} were purchased from Cambridge Isotope Laboratories. Deuterium oxide (D_2O; 99.8 atom % D) and D_2O containing 1% (w/w) sodium 2,2-dimethyl-2-silapentane-5-sulfonate (DSS) were obtained from C/D/N Isotopes. All other reagents were purchased from Sigma-Aldrich Canada.

7.2.2 APELIN-55 AND -36 PREPARATION

Human apelin-55 was expressed in *E. coli* C41 (DE3) and purified using Ni-NTA affinity and cation exchange chromatography, as outlined in Section 4.2.1, and purified by RP-HPLC as detailed in Section 5.2.1. Human apelin-36 was expressed in *E. coli* BL21 (DE3) and purified using Ni-NTA affinity and RP-HPLC, as detailed previously in Section 6.2.1. Aliquots of purified peptides at a given concentration (c) were quantified prior to lyophilisation using the Beer-Lambert law (detailed in Sections 5.2.1 and 6.2.1).

7.2.3 CD SPECTROPOLARIMETRY

Far-UV CD spectra of apela-55 and -36 were recorded at 37 °C using a J-810 spectropolarimeter (Jasco, Easton, MD) with 0.1 mm quartz cuvettes (Hellma). Lyophilized peptide samples were diluted in an appropriate volume of CD buffer (1 mM NaN_3, 1 mM $CaCl_2$, 25 mM Na_2HPO_4/NaH_2PO_4 buffer, pH 6.00±0.05) to obtain a final concentration of 0.2 mM. For micelle interaction studies, lyophilized aliquots of apelin-

55 or apelin-36 were resuspended in CD buffer containing 32 mM SDS, 38 mM DPC, 76 mM LPPG, or 16 mM Brij-35 to achieve a 1:2 protein:micelle ratio based on aggregation numbers and critical micelle concentrations previously reported [356-358]. CD spectra were acquired in triplicate from 260 nm to 180 nm at 100 nm/min with a data pitch of 0.1 nm, with each experiment performed in duplicate using independently prepared samples. Ellipticity values were averaged, blank-subtracted, converted to mean residue ellipticity, and subjected to a 3 nm sliding window average.

7.2.4 DOSY AND PEPTIDE-MICELLE BINDING ANALYSIS

For DOSY, uniformly ^{15}N-labeled apelin-55 and -36 were prepared at 0.2 mM in NMR buffer (1 mM DSS, 1 mM NaN_3, 25 mM Na_2HPO_4/NaH_2PO_4 buffer, pH 6.00±0.05, 90%/10% H_2O/D_2O). For micelle interaction, lyophilized aliquots were dissolved in NMR buffer containing 32 mM SDS (SDS-d_{25} for apelin-36), 38 mM DPC (DPC-d_{38} for apelin-36), 76 mM LPPG, or 16 mM Brij-35 similar to CD spectroscopy conditions to achieve a 1:2 protein:micelle ratio. Identically prepared micelle samples without apelin incorporation were also analyzed. All experiments were conducted at 37 °C using an Avance 500 MHz spectrometer equipped with a room temperature 5 mm broadband fluorine observe (BBFO) SmartProbe with a z-axis gradient (Bruker Canada; NMR^3 facility at Dalhousie University). Table 7.1 details experimental parameters. All samples for DOSY analysis were prepared in symmetrical susceptibility-matched NMR microtubes (Shigemi). Stimulated echo ^{1}H and ^{31}P DOSY experiments with bipolar gradients and longitudinal eddy-current delay [65] were employed to collect pseudo two-dimensional data (F1: one-dimensional ^{1}H/^{31}P NMR spectra; F2: corresponding diffusion coefficient) with individually optimized gradient length (δ) and diffusion time (Δ) (Table

7.2). A DOSY-HSQC experiment was also employed to allow for straightforward and unambiguous characterization of ^{15}N-labeled protein diffusion (led1dhsqc2d.jkr; Bruker TopSpin pulse program available upon request). Specifically, a 1D diffusion-editing experimental block using stimulated echo and longitudinal eddy-current delay with bipolar gradient pulses (Bruker pulse program ledbpgp2s1d [65]) was inserted in place of the initial 90° ^{1}H pulse of a sensitivity enhanced ^{1}H-^{15}N HSQC acquired with water flip back pulses and ^{15}N decoupling during acquisition (Bruker pulse program hsqcetfpgpsi2 [359-362]. To perform DOSY, a series of 1D ^{1}H-^{15}N HSQC experiments were carried out with increasing diffusion measurement gradient amplitude (parameters detailed in Table 7.2). Translational diffusion coefficients for each diffusing species in a given DOSY experiment were determined using the diffusion module of Dynamics Centre (Bruker) based on the equation 2.8. The observed diffusion coefficients for peptide or micelle populations (D_{ob}) were obtained by integrating two to three separate regions of the NMR spectrum for DOSY or DOSY-HSQC experiments, with two replicates averaged for the higher sensitivity ^{1}H- and ^{31}P-DOSY experiments.

As detailed in Appendix B [222], the determined diffusion coefficients were used to quantify population of micelle-bound apelin using a two-state model. Briefly, assuming an excess of micelles (i.e., ~2:1 stoichiometry of micelle to peptide), peptide-micelle binding was considered as an equilibrium between free and bound peptide states in fast exchange, allowing the diffusion coefficient of the bound complex (D_b) to be estimated from diffusion coefficients of free protein (D_p) and free micelle (D_m) (equation B.4 in Appendix B). D_{ob} is then given by the sum of the fraction of peptide in the micelle-bound state (f_b) and free states (1 - f_b) with respect to the appropriate diffusion

coefficient [363]. For D_{ob}, D_p, and D_m, the diffusion coefficients obtained over all spectral regions and/or replicates were averaged and normalized for viscosity variation using the equation:

$$D_{ob,p,m} = D_{sample} \cdot \frac{\eta_{sample}}{\eta_{buffer}} \quad (7.2)$$

where η_{sample} and η_{buffer} are the viscosities of a given sample and of buffer alone, respectively. Viscosities were determined at 37 °C using a temperature controlled *micro*Visc HVROC-L microviscometer (RheoSense).

7.2.5 TRIPLE-RESONANCE NMR SPECTROSCOPY AND ISOFORM COMPARISON ANALYSIS

For triple-resonance NMR experiments, uniformly ^{13}C- and ^{15}N-labeled apelin-55 samples were prepared at 0.4 mM in NMR buffer with 64 mM SDS-d_{25}, 76 mM DPC-d_{38}, or 152 mM LPPG. Samples were prepared in symmetrical susceptibility-matched NMR microtubes shaped for CryoProbe usage (Bruker). NMR experiments for apelin-55 in each micelle conditions (e.g., backbone assignment and ^{1}H-^{15}N HSQC with/without heteronuclear NOE enhancement) were acquired, processed, and analyzed as detailed in Section 6.2.8 with the experimental details summarized in Table 7.1. For isoform comparison, uniformly ^{15}N-labeled apelin-36 were prepared in the same experimental conditions as DOSY experiments detailed in Section 7.2.4 and ^{1}H-^{15}N HSQC spectra were acquired using an Avance 500 MHz spectrometer equipped with a BBFO SmartProbe (Bruker Canada). Table 7.2 details experimental parameters.

7.3 RESULTS AND DISCUSSION

7.3.1 PROBING APELIN-MEMBRANE INTERACTIONS BY CD SPECTROPOLARIMETRY

Far-UV CD spectropolarimetry was used to test for perturbation to overall apelin peptide structuring in the presence of excess micelles (~2:1 micelle:protein stoichiometry, as was maintained throughout). Both apelin-55 (Chapter 6) and -36 [197, 226] have been demonstrated to have a random coil conformation in buffer, as indicated by a strong negative band at ~200 nm (Fig. 7.3A-B). In the presence of zwitterionic DPC micelles, apelin-55 showed negligible spectral difference in comparison to buffer. However, apelin-36 showed an increase in ellipticity from 190-214 nm relative to its longer counterpart. This difference is clear upon spectral subtraction (Fig. 7.3C-D). Despite this minor difference, however, the minimal perturbation in the presence of DPC observed for both apelin-55 and -36 is highly similar to the behaviour of both apelin-17 [329] and apela-11[222].

Contrasting with the behaviour in DPC, and echoing previous findings with shorter apelin isoforms [329], both apelin-55 and -36 exhibited a significant increase in ellipticity over 190-214 nm in the presence of anionic micelles. Difference spectra obtained in the presence of anionic micelles relative to buffer demonstrated a strong positive band at ~198 nm and a broad negative band at ~220 nm (Fig. 7.3C-D), which may be indicative of β-turn conformations [35, 37] or another non-canonical secondary structuring convolution. In support of induced β-turn structuring, however, spectral comparison of apelin-17 in anionic micelles relative to buffer showed similar positive

band at ~198 nm and broad negative band at ~225 nm with unambiguous demonstration of β-turn induction by NMR spectroscopy [329].

Notably, the structural perturbation observed for apelin-36 was more pronounced than that of apelin-55 in both anionic micelles (Fig. 7.3). Given units of mean residue ellipticity, where spectral magnitude is normalized by the number of peptide bond chromophores, this may result from a situation where the 36 C-terminal residues of apelin-55 undergo a disproportionally greater conformational change than the 19 N-terminal residues present only in apelin-55. Regardless of minor differences in the magnitude of ellipticity perturbation, both apelin-55 and -36 clearly exhibit preferable and more structurally perturbing interactions with anionic micelles relative to zwitterionic micelles, as was the case with apelin-17 [329]. This contrasts with apela, where isoform-dependent behaviour was observed [222].

7.3.2 COMPARISON OF APELIN-MICELLE BINDING PROPENSITIES

Although apelin-micelle interactions are implied by CD spectroscopy, a more direct examination of binding is desirable. This was carried out by DOSY [65], which allows the determination of the translational diffusion coefficients. Under the assumption that a given apelin-micelle complex will diffuse more slowly than either the free ligand or micelle, the D_{ob} values of apelin-55 and -36 in both the presence and absence of micelles, alongside those of each micelle in the absence of apelin, were determined and analysed (Table 7.2; See appendix B for DOSY fits). Notably, a decrease in D_{ob} was observed for both apelin-55 and -36 in all micelle conditions. The f_b was determined in each case using a two-state model (Fig. 7.4), as previously employed for apelin-17 [329] and apela-32 and -11 [222] micelle interaction studies. Consistent with the degree of perturbation

evident from CD spectroscopy, the D_{ob} values were most severely reduced and the corresponding f_b values were greatest in the presence of anionic micelles.

DOSY-based D_{ob} determination relies upon quantification of diffusion-mediated signal decay. It is important to note, however, that signal decay may also occur through additional processes such as transverse relaxation. The rate of transverse relaxation (R_2) increases with rotational correlation time (τ_C) [44]. In the two-states of apelin being considered, the bound-state would thus be likely to experience a greater τ_C, leading to a more rapid R_2 for the bound-state vs. the free state. As this is unaccounted for in the model we have employed, the interaction between apelin isoforms and micelles is likely underestimated, with a greater degree of underestimation for the larger LPPG micelles vs. the similarly sized DPC and SDS micelles. Regardless of this underestimation, similar to shorter isoforms, the estimated f_b values demonstrate that both apelin-55 and -36 preferentially interact with anionic relative to zwitterionic micelles.

To test the potential for interaction with non-ionic detergent micelles, biophysical characterization of apelin-55 was also carried out in the presence Brij-35, the detergent employed in PCSK3 cleavage of apelin-55 in Chapter 4. Apelin-55 was practically unperturbed in the presence of non-ionic Brij-35 micelles according to CD (Fig. 7.5) and a correspondingly lower f_b than zwitterionic DPC micelles was observed (Table 7.2). It is important to note that for larger micelles such as LPPG [356] and Brij-35[364], a decreased diffusion coefficient due to collision between ligands and micelles may become more apparent [365] due to relative crowding. However, despite this potential error, the disproportionate decrease in D_{ob} of apelin-55 in response to LPPG relative to

Brij-35 clearly indicates that apelin-membrane interaction is dependent on charge of detergent headgroups.

Comparison of the micellar interaction behaviour of apela-32 and -11 relative to apelin-55 and -36 reveals striking differences. The most notable difference is between apelin-36 and apela-32 in DPC micelles. Specifically, although these isoforms are comparable in size and net charge (Table 3.1), they show large differences in f_b to zwitterionic micelles, while sharing relatively similar f_b values for anionic micelles. In addition, the variability in f_b for zwitterionic micelles indicates that the hydrophobic effect and corresponding partitioning into the micelle interior is likely a minimal mediator of apelin-micelle interaction, as the f_b values observed in all micelle types for apelin-55 with the largest hydrophobic content (Table 3.1) and apela-11 with the lowest hydrophobic content were very similar (Fig. 7.4). Interestingly, for both apelin and apela, increasing isoform size resulted in an increase in f_b. Collectively, these results indicate that electrostatic interactions are likely the main contributor to apelin-micelle interaction with favourable interaction occurring between positively charged residues of apelin isoforms and negatively charged micelle headgroups.

7.3.3 CHEMICAL SHIFT ASSIGNMENT OF APELIN-55 IN MICELLAR ENVIRONMENTS

The chemical shifts of nearly all apelin-55 backbone (N, H_N, C_α, and C′) and C_β nuclei (Table 7.3) alongside asparagine N_δ and H_δ and glutamine H_ε and N_ε were assigned in DPC, SDS, and LPPG micelle conditions using standard triple-resonance NMR experiments (chemical shifts shown in Table A.3-7). For reference, H_N-N resonance assignments are annotated on the corresponding ^1H-^{15}N HSQC spectra (Fig.

7.6). Despite the spectral perturbations observed by CD spectroscopy, chemical shift analysis of apelin-55 in each of the three micelle conditions showed only minor differences to expected random coil chemical shifts. Furthermore, analysis of assigned chemical shifts by the CSI [56] or DANGLE [57] did not indicate any segments of extended secondary structuring in any of the experimental conditions (Fig. 7.8).

In all three micelle conditions, 0S (the additional residue at the N-terminus of our apelin-55 following TEV protease cleavage) was unassignable, likely due to fast exchange of the H_N with solvent [342]. 1G was only assignable in the presence of SDS, potentially due to a micelle headgroup-dependent protection from exchange with solvent. In the presence of SDS and LPPG, but not DPC, arginine side chain H_ε-N_ε resonances were also observed; these could not be unambiguously assigned.

Beyond these N-terminal residues, three other regions exhibited headgroup-dependent variations in behaviour. 49H and 50K were not assignable in DPC, as was also the case in our characterization of apelin-55 in buffer (Chapter 6). The lack of assignable resonances for these residues was attributed to increased conformational flexibility in this region of apelin, thus falling within NMR timescale of intermediate exchange, as observed in our characterization of apelin-17 [197]. This finding is, thus, indicative of similar dynamics over this segment being experienced by apelin-55 in DPC micelles and in buffer, corresponding to a low degree of micellar interaction. 39K was, conversely, not assignable in either DPC and LPPG micelles, although this residue was assignable in buffer and in SDS micelles. The lack of assignable resonances for 39K for these micelle conditions is likely the result of a localized change in dynamics into the intermediate exchange regime on the NMR timescale in response to DPC and LPPG micelle binding.

Lastly, 20L could not be assigned in LPPG, potentially due to differences in local dynamics in response to this micelle.

As discussed in Chapter 6, additional spin-system assignments were achieved for a number of residues for apelin-55 in buffer, indicating sampling of multiple conformational states in the slow exchange regime. Interestingly, the number of potential assignments per residue changed as a function of micelle type (Fig. 7.7), suggesting alterations in both the number and equilibria of the conformations being sampled in the slow exchange NMR time-scale. Similar to the buffer state at 37 °C (Chapter 6), there were no stretches of additional sequential assignments possible (> 2 residues) for all three micelle conditions consistent with additional major conformations.

7.3.4 MEMBRANE HEADGROUP-DEPENDENT CONFORMATIONAL AND DYNAMIC CHANGES FOR APELIN-55

Although there were only minor perturbations relative to expected random coil chemical shifts and no indication of extended secondary structural elements in each micellar condition (Fig. 7.8), the CSD based upon N, H_N, C_α, and C′ for apelin-55 varied as a function of micelle type (Fig. 7.9A), with the lowest magnitude observed for DPC micelles and higher magnitudes observed for SDS and LPPG micelles. As described in Section 2.5.1, this is consistent with a fast exchange between bound and free states. Hence, the observed correlation between the magnitude of CSD and f_b of apelin-55, with ~27% bound in DPC relative to 73% and 84% bound in SDS and LPPG, respectively, is indicative of a fast exchange process rather than a slow exchange process.

Restriction in ps-ns timescale dynamics was also clearly observed in each of the micellar conditions along the apelin-55 backbone, as evidenced by increases in the ^{1}H-

^{15}N heteronuclear NOE enhancement factors relative to buffer. Both anionic micelles exhibited similar increases in heteronuclear NOE enhancement factor that were more pronounced than DPC, with DPC exhibiting enhancement factors falling between those with anionic micelles and those in buffer (Fig. 7.9A).

These CSD and heteronuclear NOE enhancement data are both, therefore, consistent with the CD spectroscopy and DOSY data indicating a greater degree of apelin-55 structural perturbation by and interaction with anionic micelles than by/with DPC. It should be noted that although both anionic micelles caused significant changes of similar magnitude in both CSD (Fig. 7.9A) and heteronuclear NOE enhancement (Fig. 7.9B) for apelin-55, distinct ^{1}H-^{15}N HSQC cross-peak patterns were observed (Fig. 7.5). This suggests that the conformations and/or local chemical environments resulting from micelle interaction are dependent on the detergent headgroup properties.

Comparison of apelin-55 chemical shifts in all three micelles relative to buffer suggest a number of regions are likely involved in micellar interaction, with the magnitude of CSD approximately scaling with f_b in each of these regions. Specifically, the 3L-6L, 17V-22Q, 29G-34Q, and 37R-48S regions all demonstrate comparatively large CSD values relative to other residues of apelin-55 (Fig. 7.9A). All of these regions contain aromatic and/or basic residue(s), providing the potential for micellar interaction through the hydrophobic tailgroup (for aromatics) and/or polar/charged detergent headgroups (aromatic or basic). Notably, the apelin-55 N-terminal regions which showed interactions may explain the increased f_b for apelin-55 in DPC and LPPG relative to apelin-36. As apelin-55 encompasses more micelle-interacting segments than its shorter counterpart, the bound population may increase accordingly.

Given the relatively overlapped nature of the ^{1}H-^{15}N HSQC spectra (Fig. 7.5), ^{1}H and ^{15}N resonance assignments for residues in each of the perturbed regions were plotted individually as a function of micelle condition (Fig. 7.10). Notably, these regions appear to exhibit similar patterns of CSD but with differing magnitudes. The majority of these perturbed residues exhibit behaviour consistent with two-state fast exchange [46], where the observed chemical shift is a weighted function of the relative proportion of peptide bound in a given micellar condition as detailed in Section 2.5.1. This is not uniformly observed. Such disparate behaviour would be fully expected if a given amide bond is in closer proximity to the detergent headgroup in the bound state or in a dissimilar interfacial or hydrophobic core regions of the micelle. This could, in turn, be influenced by an altered conformational equilibrium in response to size and/or fluidity of the micelle or by a change in partitioning coefficient of hydrophobic segments into the micelle interior with a change in the hydrophobic core. Given the disparate dipole moments, charge distributions, and steric bulk, and tailgroups of the three detergents employed (detailed, e.g., by Patterson *et al*.[355]), such residues would experience different and additional chemical shift perturbations. These data are, thus, consistent with a situation where there is a similar bound-state conformation (or, likely more accurately, equilibrated set of conformations) undergoing fast exchange with the free state regardless of the micelle type. It should be noted that this interpretation was only feasible through sequential chemical shift assignment in each condition, allowing comprehensive analysis of H_N and N chemical shift modulation at each residue as a function of both f_b and headgroup.

7.3.5 BACKBONE-LEVEL INDEPENDENCE OF APELIN-36

In examination of apelin-55 interactions with DPC, SDS, and LPPG micelles, segregation of the N-terminal and C-terminal regions is apparent, where the average CSD observed for the 36 C-terminal residues (common to apelin-36) is greater than that of the 19 N-terminal residues exclusive to apelin-55. The heteronuclear NOE enhancement is also indicative of a lesser degree of ps-ns timescale dynamics in the C-terminal region relative to the N-terminal region. This corresponds well to the observed greater perturbation in mean residue ellipticity for apelin-36 vs. apelin-55, with more conformational change being observed in the 36 C-terminal residues shared between isoforms than in the 19 N-terminal residues present only in apelin-55.

To test the hypothesis that the apelin-36 segment behaves similarly whether in the context of apelin-55 or in isolation, apelin-36 was also characterized by NMR spectroscopy. ^{1}H-^{15}N HSQC spectra exhibited nearly identical perturbation patterns between the two isoforms in all three micelles (Fig. 7.11). Cross-peak assignments for apelin-36 were thus inferred, based on the longer 55-residue counterpart (Fig. 7.12). The only exception to this was the four N-terminal residues, for which no assignable spin-systems were observed, likely as a result of increased exchange with solvent and, potentially, intermediate exchange [46] on the NMR timescale.

Direct quantitative comparison of H_N and N chemical shifts between apelin-55 and apelin-36 demonstrates that the vast majority of residues exhibit a CSD of less than 0.04 ppm (Fig. 7.12). This echoes the fact that all of the bioactive apelin isoforms (i.e., apelin-13, -17, -36, and -55) maintain identical conformations of the shared region in buffer (Chapter 6). The minimal CSD values observed are consistent not only with the

adoption of highly similar pool of conformations by both isolated apelin-36 and the corresponding segment in apelin-55 in response to each micelle but, more strikingly, with highly comparable fast exchange regime sampling of bound and free states. Notably, despite being the least perturbed overall relative to the buffer state, apelin-36 in DPC exhibits the highest CSD compared to apelin-55 of the three micellar conditions. Given that f_b is most disparate between apelin-36 and -55 in DPC (Fig. 7.4), this modestly larger CSD is logical as this would lead to a perturbation to the free vs. bound state equilibrium underlying the observed average chemical shift.

The highly similar conformation sampling behaviour of both apelin isoforms in all three micelle conditions is in striking contrast to apela isoforms. Specifically, apela-11 showed chemical shift differences in comparison to apela-32, impeding H_N-N resonance assignment through chemical shift inference [222]. This implied that apela-32 and -11 have differing conformations due to interaction between the N-terminal region of apela-32 and the C-terminal region corresponding to apela-11. In addition, this difference in behaviour was further exemplified in the presence of zwitterionic DPC micelles. The α-helical segment induced in the N-terminal region of apela-32, a region absent in apela-11, likely serves to stabilize its interaction with DP. Converse to this, the high degree of chemical shift similarity between apelin-55 and -36 in buffer (Chapter 6) and in all three micellar environments (Fig. 7.11) suggests that there are no apparent stabilizing interactions between N- and C-terminal domains in the longer apelin isoforms, even in the presence of micelles.

7.3.6 IMPLICATIONS OF MEMBRANE CATALYSIS IN APELIN-MEDIATED AR ACTIVATION

Membrane catalysis may explain the increased potency for apela-32 in comparison to apela-11 and apelin-13 [113], given the relatively high propensity for apela-32 interaction with DPC micelles (Fig. 7.4 [222]) that serve as a mimic for the most prevalent lipid in typical eukaryotic cells. The isoform-dependent differences in potency between apelin isoforms cannot be similarly explained. Although apelin-17 [329], -36, and -55 all preferentially interact with anionic over zwitterionic micelles, the data presented herein show that peptide behaviour in the bound state is similar regardless of headgroup properties, with the NMR observables being scaled by the proportion of bound vs. free peptide.

Notably, the relatively large CSD observed in the 37R-48S region is consistent with the previous characterization of apelin-17, suggesting that longer apelin isoform may also bind to anionic detergent headgroup through the RPRL motif [329]. If so, the three C-terminal residues (MPF) are likely structurally converged in apelin-55 upon anionic micelle binding. In support of this, a significant loss in dynamics by heteronuclear NOE enhancement was observed for 53M and 55F (Fig. 7.9), while clearly exhibiting behaviour consistent with fast exchange between free and micelle-bound state proportional to f_b (Fig. 7.10). These findings collectively imply that the functionally critical C-terminal RPRL and MPF motifs adopt a similarly converged structuring as apelin-17, translating to a similar mode of membrane-catalysed receptor activation.

Clear observation of fast exchange between the free and bound states of apelin for all micelles indicates that binding and unbinding rates are on the order of 10^5 s^{-1} or faster

[366], with a similar bound-state conformation being sampled by the proportion of ligand molecules on the membrane. A lower proportion of peptide bound to zwitterionic headgroups at any given time would allow for a less hindered diffusional search for the receptor, while also maintaining a high local concentration proximal to the membrane. Hence, one could envision a situation where the ligand rapidly traverses the predominantly zwitterionic extracellular face of the membrane, frequently sampling the bound state conformation, with an increased propensity for membrane binding and association in areas of elevated anionic character. Given the shared C-terminal region of all apelin isoforms and membrane interaction behaviour, highly similar membrane-catalysed receptor recognition and binding would be facilitated regardless of either the length of the isoform or the local lipid environment. Correspondingly, apelin isoform-dependent differences in potency may not be directly regulated by membrane interaction. Instead, these seem likely to be mediated by changes in the receptor conformational equilibrium in response to ligand, following membrane-catalysed binding, potentially through interaction with recently identified [69] anionic grooves on the AR surface that are unoccupied by an apelin-17 analogue (Fig. 7.13). Thus, future experiments should focus on delineating the common structural and dynamic features of apelin and apela isoforms that are involved in the membrane-catalysed ligand-receptor recognition step vs. features that are involved in activation and downstream regulation.

Table 7.1: NMR experimental details

Experiment	Pulse program (Bruker)	Delay (s)	# of scans	Acquisition time (s)	# of complex points	Sweep width (ppm)	Center position (ppm)	^{1}H frequency (MHz)	Note
Apelin-55 in DPC at 37 °C									**Backbone assignment**
HNCO	hncogp3d	1	8	^{1}H: 0.1216512 ^{15}N: 0.0182837 ^{13}C: 0.0227165	^{1}H: 2048 ^{15}N: 48 ^{13}C: 48	^{1}H: 12.0224 ^{15}N: 18.5000 ^{13}C: 6.0000	^{1}H: 4.705 ^{15}N: 117.250 ^{13}C: 173.000	700	
HN(CA)CO	hncacogp3d	1	16	^{1}H: 0.1216512 ^{15}N: 0.0182837 ^{13}C: 0.0227165	^{1}H: 2048 ^{15}N: 48 ^{13}C: 48	^{1}H: 12.0224 ^{15}N: 18.5000 ^{13}C: 6.0000	^{1}H: 4.705 ^{15}N: 117.250 ^{13}C: 173.000	700	
HNCA	hncagp3d	1	16	^{1}H: 0.1216512 ^{15}N: 0.0182837 ^{13}C: 0.0126805	^{1}H: 2048 ^{15}N: 48 ^{13}C: 96	^{1}H: 12.0224 ^{15}N: 18.5000 ^{13}C: 21.5000	^{1}H: 4.705 ^{15}N: 117.250 ^{13}C: 51.250	700	
HN(CO)CA	hncocagp3d	1	8	^{1}H: 0.1216512 ^{15}N: 0.0182837 ^{13}C: 0.0126805	^{1}H: 2048 ^{15}N: 48 ^{13}C: 48	^{1}H: 12.0224 ^{15}N: 18.5000 ^{13}C: 21.5000	^{1}H: 4.705 ^{15}N: 117.250 ^{13}C: 51.250	700	
HNCACB	hncacbgp3d	1	16	^{1}H: 0.1216512 ^{15}N: 0.0182837 ^{13}C: 0.0086550	^{1}H: 2048 ^{15}N: 48 ^{13}C: 128	^{1}H: 12.0224 ^{15}N: 18.5000 ^{13}C: 42.0000	^{1}H: 4.705 ^{15}N: 117.250 ^{13}C: 43.500	700	
^{1}H-^{15}N HSQC	hsqcetf3gpsi2	1	8	^{1}H: 0.1044480 ^{15}N: 0.0450997	^{1}H: 2048 ^{15}N: 128	^{1}H: 14.0025 ^{15}N: 20.0000	^{1}H: 4.705 ^{15}N: 117.000	700	
^{1}H-^{15}N Het. NOE HSQC	hsqcnoef3gpsi	5	32	^{1}H: 0.1216512 ^{15}N: 0.1066547	^{1}H: 2048 ^{15}N: 280	^{1}H: 12.0224 ^{15}N: 18.5000	^{1}H: 4.705 ^{15}N: 117.250	700	
Apelin-55 in SDS at 37 °C									**Backbone assignment**
HNCO	hncogp3d	1	8	^{1}H: 0.1216512 ^{15}N: 0.0180399 ^{13}C: 0.0136299	^{1}H: 2048 ^{15}N: 48 ^{13}C: 48	^{1}H: 12.0224 ^{15}N: 18.7500 ^{13}C: 10.0000	^{1}H: 4.707 ^{15}N: 116.350 ^{13}C: 174.500	700	
HN(CA)CO	hncacogp3d	1	16	^{1}H: 0.1216512 ^{15}N: 0.0180399 ^{13}C: 0.0136299	^{1}H: 2048 ^{15}N: 48 ^{13}C: 48	^{1}H: 12.0224 ^{15}N: 18.7500 ^{13}C: 10.0000	^{1}H: 4.707 ^{15}N: 116.350 ^{13}C: 174.500	700	

HNCA	hncagp3d	1	16	^{1}H: 0.1216512 ^{15}N: 0.0180399 ^{13}C: 0.0054526	^{1}H: 2048 ^{15}N: 48 ^{13}C: 48	^{1}H: 12.0224 ^{15}N: 18.7500 ^{13}C: 25.0000	^{1}H: 4.707 ^{15}N: 116.350 ^{13}C: 51.000	700	
HN(CO)CA	hncocagp3d	1	16	^{1}H: 0.1216512 ^{15}N: 0.0180399 ^{13}C: 0.0054526	^{1}H: 2048 ^{15}N: 48 ^{13}C: 48	^{1}H: 12.0224 ^{15}N: 18.7500 ^{13}C: 25.0000	^{1}H: 4.707 ^{15}N: 116.350 ^{13}C: 51.000	700	
HNCACB	hncacbgp3d	1	16	^{1}H: 0.1216512 ^{15}N: 0.0180399 ^{13}C: 0.0070683	^{1}H: 2048 ^{15}N: 48 ^{13}C: 112	^{1}H: 12.0224 ^{15}N: 18.7500 ^{13}C: 45.0000	^{1}H: 4.707 ^{15}N: 116.350 ^{13}C: 40.500	700	
^{1}H-^{15}N HSQC	hsqcetf3gpsi2	1	16	^{1}H: 0.1216512 ^{15}N: 0.0481064	^{1}H: 2048 ^{15}N: 128	^{1}H: 12.0224 ^{15}N: 18.7500	^{1}H: 4.707 ^{15}N: 116.350	700	
^{1}H-^{15}N Het. NOE HSQC	hsqcnoef3gpsi	5	32	^{1}H: 0.1044480 ^{15}N: 0.1080234	^{1}H: 2048 ^{15}N: 256	^{1}H: 14.0025 ^{15}N: 16.7000	^{1}H: 4.699 ^{15}N: 115.650	700	
Apelin-55 in LPPG at 37 °C									**Backbone assignment**
HNCO	hncogp3d	1	8	^{1}H: 0.1216512 ^{15}N: 0.0187916 ^{13}C: 0.0170374	^{1}H: 2048 ^{15}N: 48 ^{13}C: 48	^{1}H: 12.0224 ^{15}N: 18.0000 ^{13}C: 8.0000	^{1}H: 4.705 ^{15}N: 116.750 ^{13}C: 174.000	700	
HN(CA)CO	hncacogp3d	1	16	^{1}H: 0.1216512 ^{15}N: 0.0187916 ^{13}C: 0.0170374	^{1}H: 2048 ^{15}N: 48 ^{13}C: 48	^{1}H: 12.0224 ^{15}N: 18.0000 ^{13}C: 8.0000	^{1}H: 4.705 ^{15}N: 116.750 ^{13}C: 174.000	700	
HNCA	hncagp3d	1	16	^{1}H: 0.1216512 ^{15}N: 0.0187916 ^{13}C: 0.0079024	^{1}H: 2048 ^{15}N: 48 ^{13}C: 48	^{1}H: 12.0224 ^{15}N: 18.0000 ^{13}C: 23.0000	^{1}H: 4.705 ^{15}N: 116.750 ^{13}C: 51.000	700	
HN(CO)CA	hncocagp3d	1	16	^{1}H: 0.1216512 ^{15}N: 0.0187916 ^{13}C: 0.0079024	^{1}H: 2048 ^{15}N: 48 ^{13}C: 64	^{1}H: 12.0224 ^{15}N: 18.0000 ^{13}C: 23.0000	^{1}H: 4.705 ^{15}N: 116.750 ^{13}C: 51.000	700	
HNCACB	hncacbgp3d	1	16	^{1}H: 0.1216512 ^{15}N: 0.0187916 ^{13}C: 0.0080781	^{1}H: 2048 ^{15}N: 48 ^{13}C: 128	^{1}H: 12.0224 ^{15}N: 18.0000 ^{13}C: 45.0000	^{1}H: 4.705 ^{15}N: 116.750 ^{13}C: 40.500	700	
^{1}H-^{15}N HSQC	hsqcetf3gpsi2	1	16	^{1}H: 0.1044480 ^{15}N: 0.0450997	^{1}H: 2048 ^{15}N: 128	^{1}H: 14.0025 ^{15}N: 20.0000	^{1}H: 4.705 ^{15}N: 116.750	700	
^{1}H-^{15}N Het. NOE HSQC	hsqcnoef3gpsi	5	32	^{1}H: 0.1216512 ^{15}N: 0.0939578	^{1}H: 2048 ^{15}N: 240	^{1}H: 12.0224 ^{15}N: 18.0000	^{1}H: 4.707 ^{15}N: 116.750	700	

Apelin-55 in buffer at 37 °C									**^{15}N-labeled/ Diffusion**
^{1}H DOSY	ledbpgppr2s	1	128	^{1}H: 0.8579424	^{1}H: 12016 16 points	^{1}H: 14.0019	^{1}H: 4.706	500	
^{15}N-DOSY	led1dhsqc2d.jkr	1	2560	^{1}H: 0.1462272	^{1}H: 2048 9 points	^{1}H: 14.0019	^{1}H: 4.706	500	
^{1}H-^{15}N HSQC	hsqcetfpgpsi2	1	64	^{1}H: 0.1462272 ^{15}N: 0.0507348	^{1}H: 2048 ^{15}N: 144	^{1}H: 14.0019 ^{15}N: 28.0000	^{1}H: 4.706 ^{15}N: -261.500	500	
Apelin-55 in Brij-35 at 37 °C									**^{15}N-labeled/ Diffusion**
^{1}H-DOSY	ledbpgppr2s	1	32	^{1}H: 0.8579424	^{1}H: 12016 16 points	^{1}H: 14.0019	^{1}H: 4.705	500	
^{1}H-DOSY (water)	ledbpgp2s	1	8	^{1}H: 0.9997428	^{1}H: 14002 16 points	^{1}H: 14.0019	^{1}H: 4.706	500	
^{15}N-DOSY	led1dhsqc2d.jkr	1	2560	^{1}H: 0.1462272	^{1}H: 2048 13 points	^{1}H: 14.0019	^{1}H: 4.705	500	
^{1}H-^{15}N HSQC	hsqcetfpgpsi2	1	64	^{1}H: 0.1462272 ^{15}N: 0.0507347	^{1}H: 2048 ^{15}N: 144	^{1}H: 14.0019 ^{15}N: 28.0000	^{1}H: 4.705 ^{15}N: -261.000	500	
Apelin-55 in DPC at 37 °C									**^{15}N-labeled/ Diffusion**
^{1}H-DOSY	ledbpgppr2s	1	32	^{1}H: 0.8579424	^{1}H: 12016 16 points	^{1}H: 14.0019	^{1}H: 4.705	500	
^{15}N-DOSY	led1dhsqc2d.jkr	1	2560	^{1}H: 0.1462272	^{1}H: 2048 9 points	^{1}H: 14.0019	^{1}H: 4.705	500	
^{1}H-^{15}N HSQC	hsqcetfpgpsi2	1	64	^{1}H: 0.1462272 ^{15}N: 0.0507348	^{1}H: 2048 ^{15}N: 144	^{1}H: 14.0019 ^{15}N: 28.0000	^{1}H: 4.705 ^{15}N: -261.500	500	
Apelin-55 in LPPG at 37 °C									**^{15}N-labeled/ Diffusion**
^{1}H-DOSY	ledbpgppr2s	1	32	^{1}H: 0.8579424	^{1}H: 12016 16 points	^{1}H: 14.0019	^{1}H: 4.705	500	
^{15}N-DOSY	led1dhsqc2d.jkr	1	2560	^{1}H: 0.1462272	^{1}H: 2048 9 points	^{1}H: 14.0019	^{1}H: 4.705	500	

^{1}H-^{15}N HSQC	hsqcetfpgpsi2	1	64	^{1}H: 0.1462272 ^{15}N: 0.0507348	^{1}H: 2048 ^{15}N: 144	^{1}H: 14.0019 ^{15}N: 28.0000	^{1}H: 4.705 ^{15}N: -261.500	500	
Apelin-55 in SDS at 37 °C									**^{15}N-labeled/ Diffusion**
^{1}H-DOSY	ledbpgppr2s	1	32	^{1}H: 0.8579424	^{1}H: 12016 16 points	^{1}H: 14.0019	^{1}H: 4.705	500	
^{15}N-DOSY	led1dhsqc2d.jkr	1	2560	^{1}H: 0.1462272	^{1}H: 2048 9 points	^{1}H: 14.0019	^{1}H: 4.705	500	
^{1}H-^{15}N HSQC	hsqcetfpgpsi2	1	64	^{1}H: 0.1462272 ^{15}N: 0.0507348	^{1}H: 2048 ^{15}N: 144	^{1}H: 14.0019 ^{15}N: 28.0000	^{1}H: 4.705 ^{15}N: -261.500	500	
Apelin-36 in buffer at 37 °C									**^{15}N-labeled/ Diffusion**
^{15}N-DOSY	led1dhsqc2d.jkr	1	2560	^{1}H: 0.1703936	^{1}H: 2048 13 points	^{1}H: 12.0160	^{1}H: 4.706	500	
^{1}H-^{15}N HSQC	hsqcetfpgpsi2	1	64	^{1}H: 0.1703936 ^{15}N: 0.0526138	^{1}H: 2048 ^{15}N: 160	^{1}H: 12.0160 ^{15}N: 30.0000	^{1}H: 4.706 ^{15}N: -261.500	500	
Apelin-36 in DPC at 37 °C									**^{15}N-labeled/ Diffusion**
^{15}N-DOSY	led1dhsqc2d.jkr	1	2560	^{1}H: 0.1703936	^{1}H: 2048 13 points	^{1}H: 12.0160	^{1}H: 4.706	500	
^{1}H-^{15}N HSQC	hsqcetfpgpsi2	1	64	^{1}H: 0.1703936 ^{15}N: 0.0526138	^{1}H: 2048 ^{15}N: 160	^{1}H: 12.0160 ^{15}N: 30.0000	^{1}H: 4.706 ^{15}N: -261.500	500	
Apelin-36 in LPPG at 37 °C									**^{15}N-labeled/ Diffusion**
^{15}N-DOSY	led1dhsqc2d.jkr	1	2560	^{1}H: 0.1703936	^{1}H: 2048 13 points	^{1}H: 12.0160	^{1}H: 4.707	500	
^{1}H-^{15}N HSQC	hsqcetfpgpsi2	1	64	^{1}H: 0.1703936 ^{15}N: 0.0526138	^{1}H: 2048 ^{15}N: 160	^{1}H: 12.0160 ^{15}N: 30.0000	^{1}H: 4.707 ^{15}N: -261.500	500	
Apelin-36 in SDS at 37 °C									**^{15}N-labeled/ Diffusion**
^{15}N-DOSY	led1dhsqc2d.jkr	1	2560	^{1}H: 0.1703936	^{1}H: 2048 13 points	^{1}H: 12.0160	^{1}H: 4.708	500	

^{1}H-^{15}N HSQC	hsqcetfpgpsi2	1	64	^{1}H: 0.1703936 ^{15}N: 0.0526138	^{1}H: 2048 ^{15}N: 160	^{1}H: 12.0160 ^{15}N: 30.0000	^{1}H: 4.708 ^{15}N: -261.500	500	
Buffer at 37 °C									**^{15}N-labeled/ Diffusion**
^{1}H-DOSY (water)	ledbpgp2s	1	8	^{1}H: 0.9997312	^{1}H: 12016 16 points	^{1}H: 12.0160	^{1}H: 4.706	500	
Brij-35 at 37 °C									**^{15}N-labeled/ Diffusion**
^{1}H-DOSY	ledbpgppr2s	1	32	^{1}H: 0.8579424	^{1}H: 12016 16 points	^{1}H: 14.0019	^{1}H: 4.706	500	
^{1}H-DOSY (water)	ledbpgp2s	1	8	^{1}H: 0.9997428	^{1}H: 14002 16 points	^{1}H: 14.0019	^{1}H: 4.706	500	
DPC at 37 °C									**^{15}N-labeled/ Diffusion**
^{31}P DOSY	ledbpgp2s	1	16	^{31}P: 1.0223616	^{31}P: 16384 16 points	^{31}P: 39.5780	^{31}P: 0.00	500	
LPPG at 37 °C									**^{15}N-labeled/ Diffusion**
^{31}P DOSY	ledbpgp2s	1	16	^{31}P: 1.0223616	^{31}P: 16384 16 points	^{31}P: 39.5780	^{31}P: 0.00	500	
SDS at 37 °C									**^{15}N-labeled/ Diffusion**
^{1}H DOSY	ledbpgppr2s	1	32	^{1}H: 0.8579424	^{1}H: 12016 16 points	^{1}H: 14.0019	^{1}H: 4.705	500	

Table 7.2: Viscosity-corrected diffusion coefficients (D_{ob}) of the free micelles, free peptide and peptide in the presence of each micelle conditions for apelin-55 and apela-36 as determined by DOSY.

Experimental set	Component	Nucleus detected[#]	# of gradient steps	Gradient amplitude[#]	Δ (ms)	δ (ms)	η (mPa·s)	D_{ob} (10^{-10} m^2 s^{-1})	f_b
Apelin-55	Free apelin-55	$^{15}N/^{1}H$	9/16	^{15}N: 2-98% ^{1}H: 2-95%	100	1.25/2	0.715 ± 0.003	1.850 ± 0.006	NA
	Apelin-55 with DPC micelle	$^{15}N/^{1}H$	9/16	^{15}N: 2-98% ^{1}H: 2-95%	100	1.75/3	0.738 ± 0.002	1.570 ± 0.009	0.266 ± 0.11
	Apelin-55 with SDS micelle	$^{15}N/^{1}H$	9/16	^{15}N: 2-98% ^{1}H: 2-95%	100	1.75/3	0.738 ± 0.001	1.070 ± 0.004	0.731 ± 0.08
	Apelin-55 with LPPG micelle	$^{15}N/^{1}H$	9/16	^{15}N: 2-98% ^{1}H: 2-95%	100	1.75/3	0.780 ± 0.002	0.796 ± 0.006	0.835 ± 0.10
	Apelin-55 with Brij-35 micelle	^{15}N	13	2-98%	100	2	NA	1.623 ± 0.001*	0.167 ± 0.05
Apelin-36	Free apelin-36	^{15}N	13	2-98%	100	1.25	0.711 ± 0.006	2.780 ± 0.006	NA
	Apelin-36 with DPC micelle	^{15}N	13	2-98%	100	1.25	0.756 ± 0.001	2.640 ± 0.003	0.076 ± 0.03
	Apelin-36 with SDS micelle	^{15}N	13	2-98%	100	1.75	0.739 ± 0.007	1.420 ± 0.000	0.794 ± 0.05
	Apelin-36 with LPPG micelle	^{15}N	13	2-98%	100	2.25	0.896 ± 0.002	1.300 ± 0.001	0.720 ± 0.04
Control	No protein/micelle	NA	NA	NA	NA	NA	0.712 ± 0.002	NA	NA
	Free DPC micelle	^{31}P	16	2-95%	300	4	0.746 ± 0.004	1.306 ± 0.001	NA
	Free SDS micelle	^{1}H	16	2-95%	100	3	0.753 ± 0.001	1.337 ± 0.004	NA
	Free LPPG micelle	^{31}P	16	2-95%	500	4	0.884 ± 0.003	0.817 ± 0.001	NA
	Free Brij-35 micelle	^{1}H	16	2-95%	150	4	NA	0.633 ± 0.002*	NA

Fraction of binding (f_b) values were determined using the model detailed in Appendix B. Viscosity (η) and the optimized gradient length (δ) and diffusion time (Δ) are also listed. (presented as mean ± SEM). [#] ^{15}N represents detection of amide protons through 1D ^{1}H-^{15}N HSQC experiments coupled to DOSY using indicated gradient amplitude range. *Apelin-55 with Brij-35 and Free Brij-35 D_{ob} values were viscosity corrected by an indirect method using the D_{ob} of water molecules of the "No protein/micelle" control (37.6 ± 0.1 x 10^{-10} m^2 s^{-1}) relative to those observed with Brij-35 micelles (No protein control: 37.0 ± 0.05 x 10^{-10} m^2 s^{-1}, with protein: 37.0 ± 0.1 x 10^{-10} m^2 s^{-1}).

Table 7.3: Assignment report for apelin-55 in indicated conditions

Atom type	Buffer[§]	DPC	SDS	LPPG
H_N*	44/47 (94%)	43/47 (91%)	47/47 (100%)	44/47 (94%)
N[‡]	44/47 (94%)	43/47 (91%)	47/47 (100%)	44/47 (94%)
C’	54/56 (96%)	54/56 (96%)	56/56 (100%)	53/56 (95%)
C_α	54/56 (96%)	54/56 (96%)	55/56 (98%)	55/56 (98%)
C_β	44/46 (95%)	40/46 (87%)	42/46 (91%)	34/46 (74%)

[§]Assignment report for apelin-55 in buffer at 37 °C shown again for comparison
*N-terminal H_N was excluded
[‡]Proline residues and N-terminal N were excluded

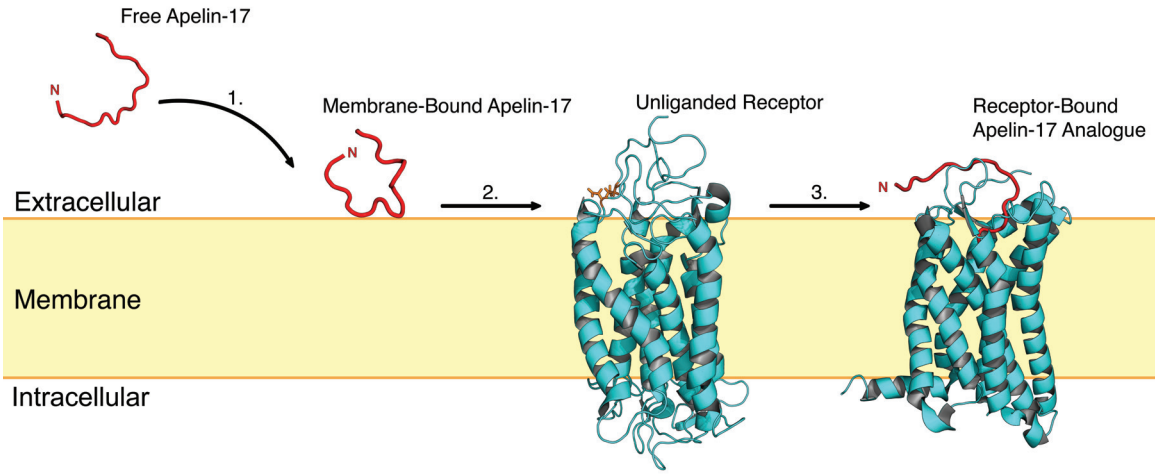

Figure 7.1: Representation of membrane catalysis theory using apelin-17 and AR. Sequentially, (1) apelin is proposed to bind to the membrane, increasing the likelihood of (2) its interaction with and recognition by an unliganded apelin receptor (AR) on a cell surface followed by (3) receptor binding and activation. Structures of apelin-17 in buffer (BMRB entry 20029 [197]) and bound to SDS micelles (BMRB entry 20082 [329]); and, of AR in absence of ligand with anionic patch residues E20 and D23 illustrated [78] and bound to apelin-17 analog AMG3054 (PDB entry: 5VBL [69]) were employed. This figure was made with Dr. Jan K Rainey and Mr. Calem Kenward and is taken from Shin *et al.* (accepted) ***Comprehensive Physiology*** [67]**.**

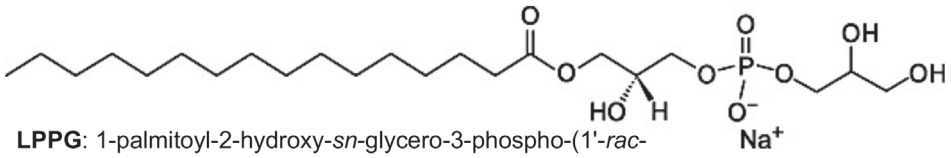

LPPG: 1-palmitoyl-2-hydroxy-*sn*-glycero-3-phospho-(1'-*rac*-glycerol)

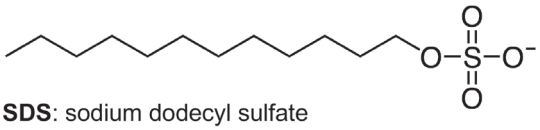

SDS: sodium dodecyl sulfate

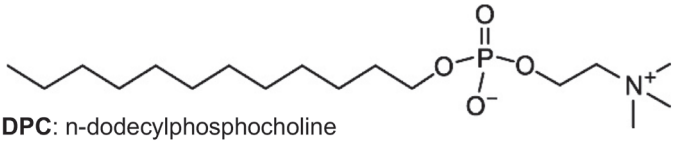

DPC: n-dodecylphosphocholine

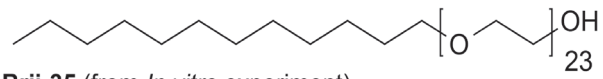

Brij-35 (from *In vitro* experiment)

Figure 7.2: Structures of membrane-mimetic surfactants used to study apelin and apela [222] micelle interactions.

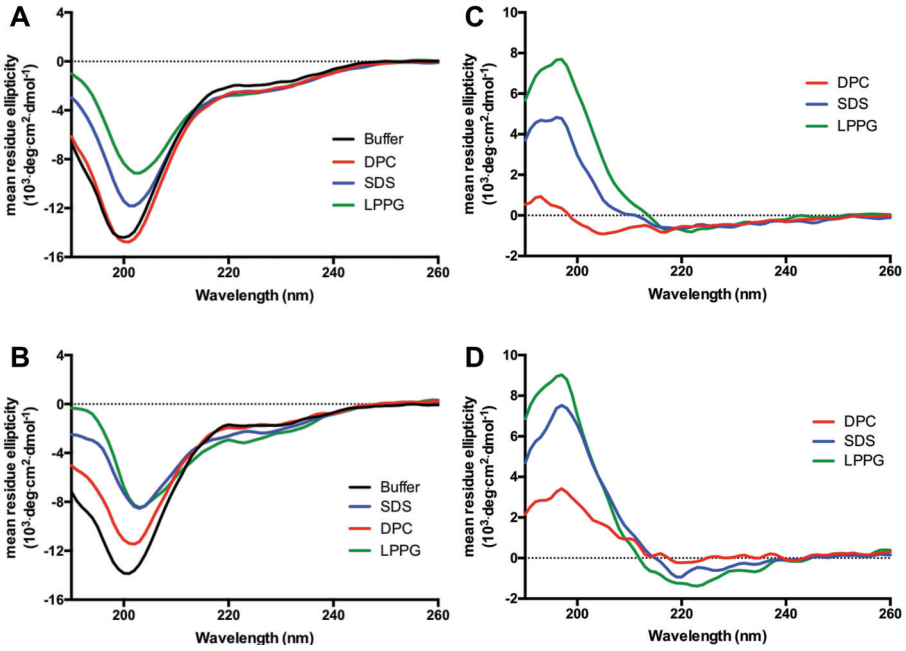

Figure 7.3: Apelin-micelle interactions characterized by CD spectropolarimetry. Far-UV CD spectra of (A) apelin-55 and (B) apelin-36 were acquired at a 1:2 protein-to-micelle ratio. Difference spectra following subtraction of mean residue ellipticity in buffer from that in a given micelle are shown for (C) apelin-55 and (D) apelin-36.

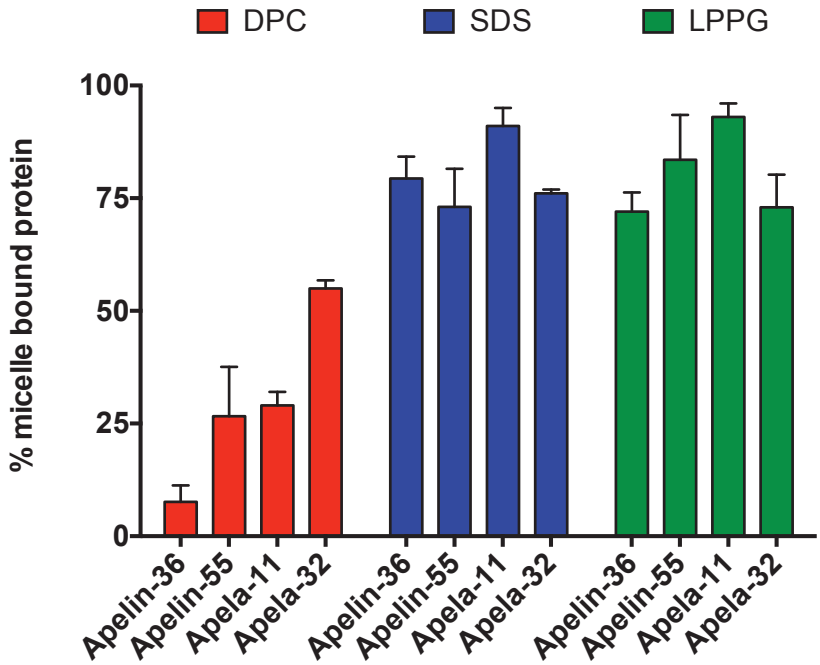

Figure 7.4: Percent micelle-bound peptide population for the given condition. Note: the percentages of micelle-bound apela-32 and -11 were reported in Huang *et al.* [222] and are plotted for direct comparison to apelin-55 and -36.

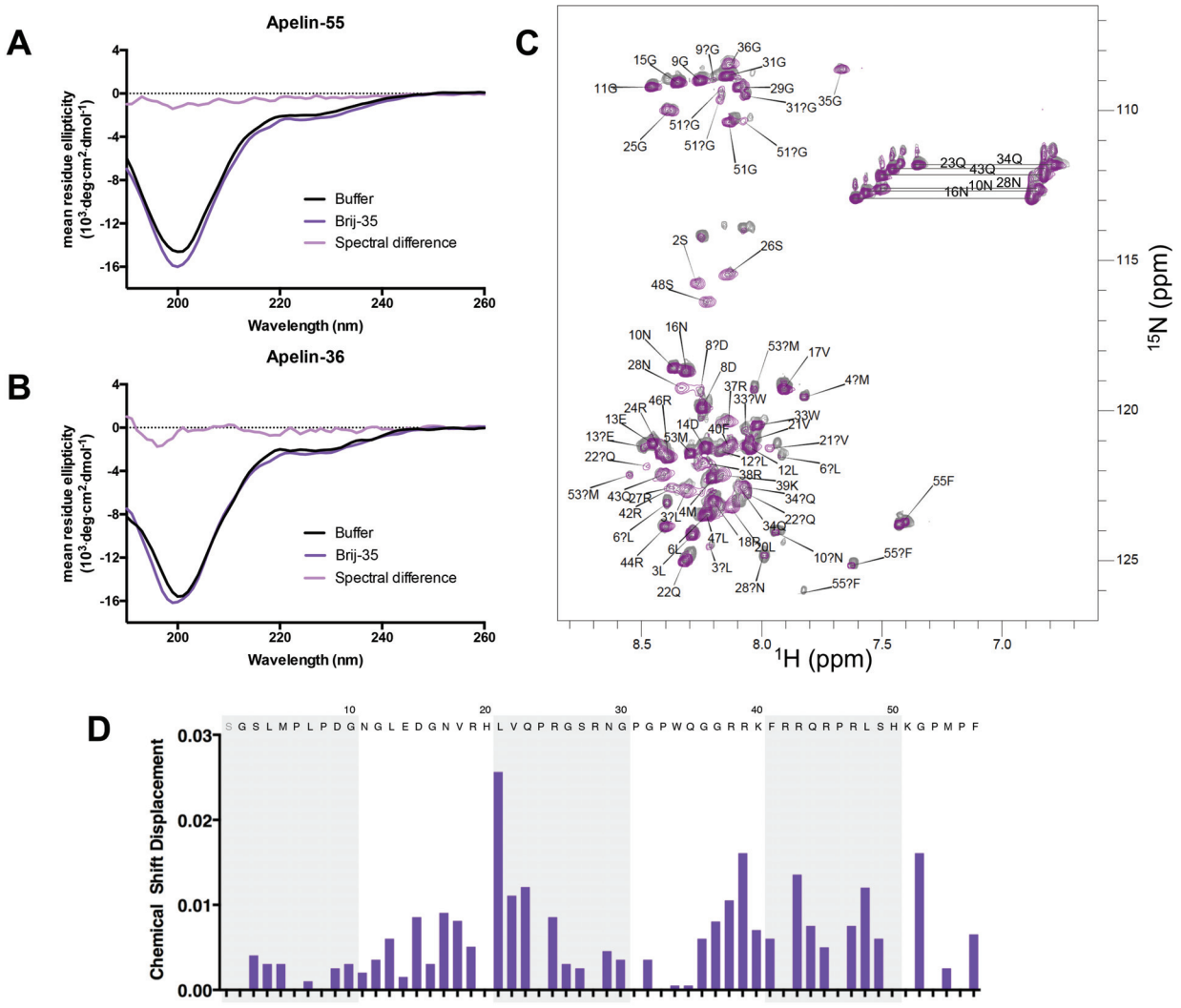

Figure 7.5: Summary of apelin-Brij-35 interaction.
A-B) Far-UV CD spectra of A) apelin-55 and B) apelin-36 in the presence of Brij-35 micelles. C) Annotated ^{1}H-^{15}N HSQC spectrum of apelin-55 with Brij-35 overlaid upon that of apelin-55 in buffer. D) Chemical shift displacement for apelin-55 with Brij-35 relative to buffer.

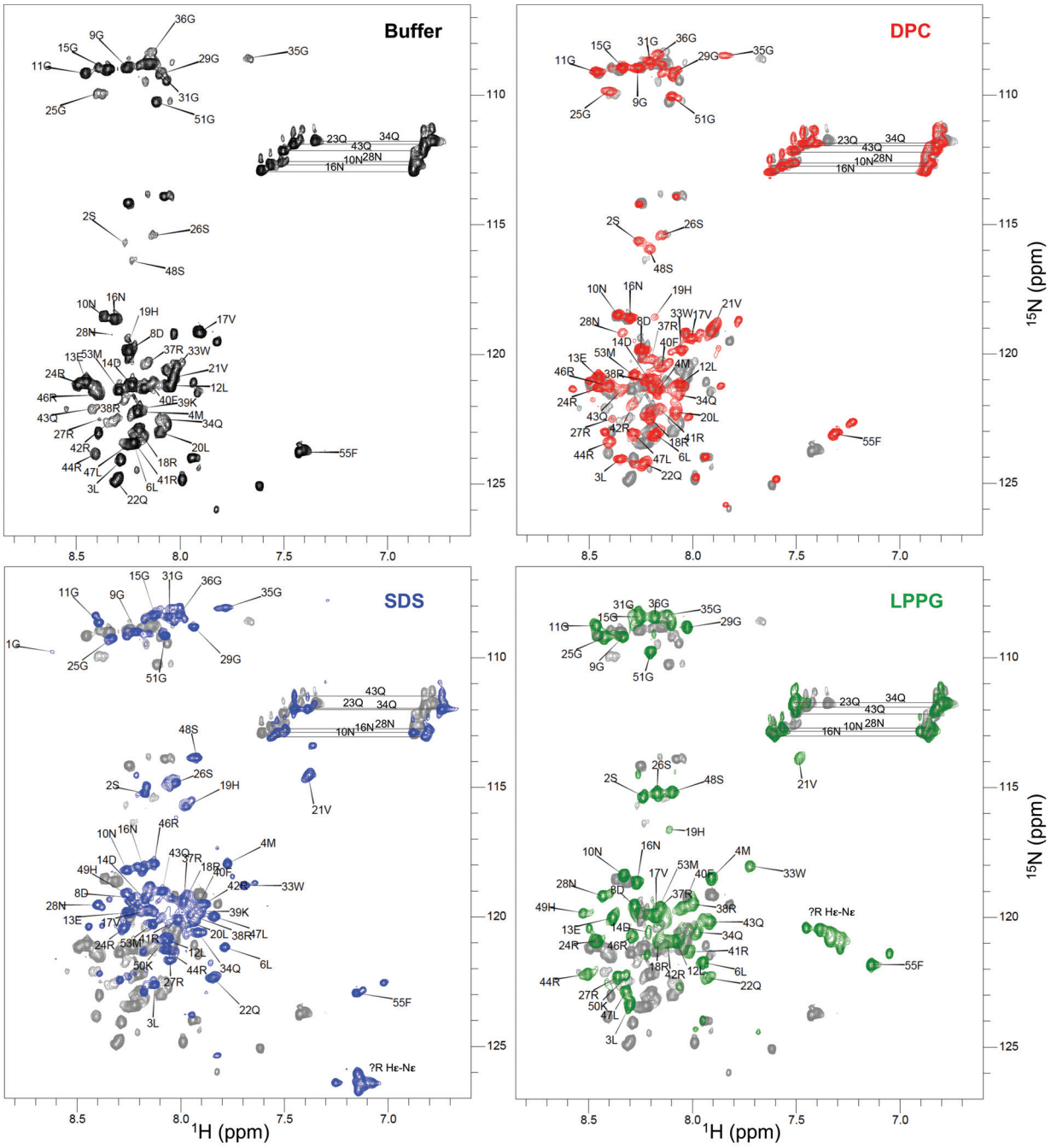

Figure 7.6: ^{1}H-^{15}N HSQC spectra of apelin-55 in indicated conditions. Cross-peaks are annotated by residue number in the sequence and the one-letter amino acid code for the primary sequentially-assigned chain. The spectra of apelin-55 in micellar conditions (coloured) are overlaid upon the spectrum in buffer (grey).

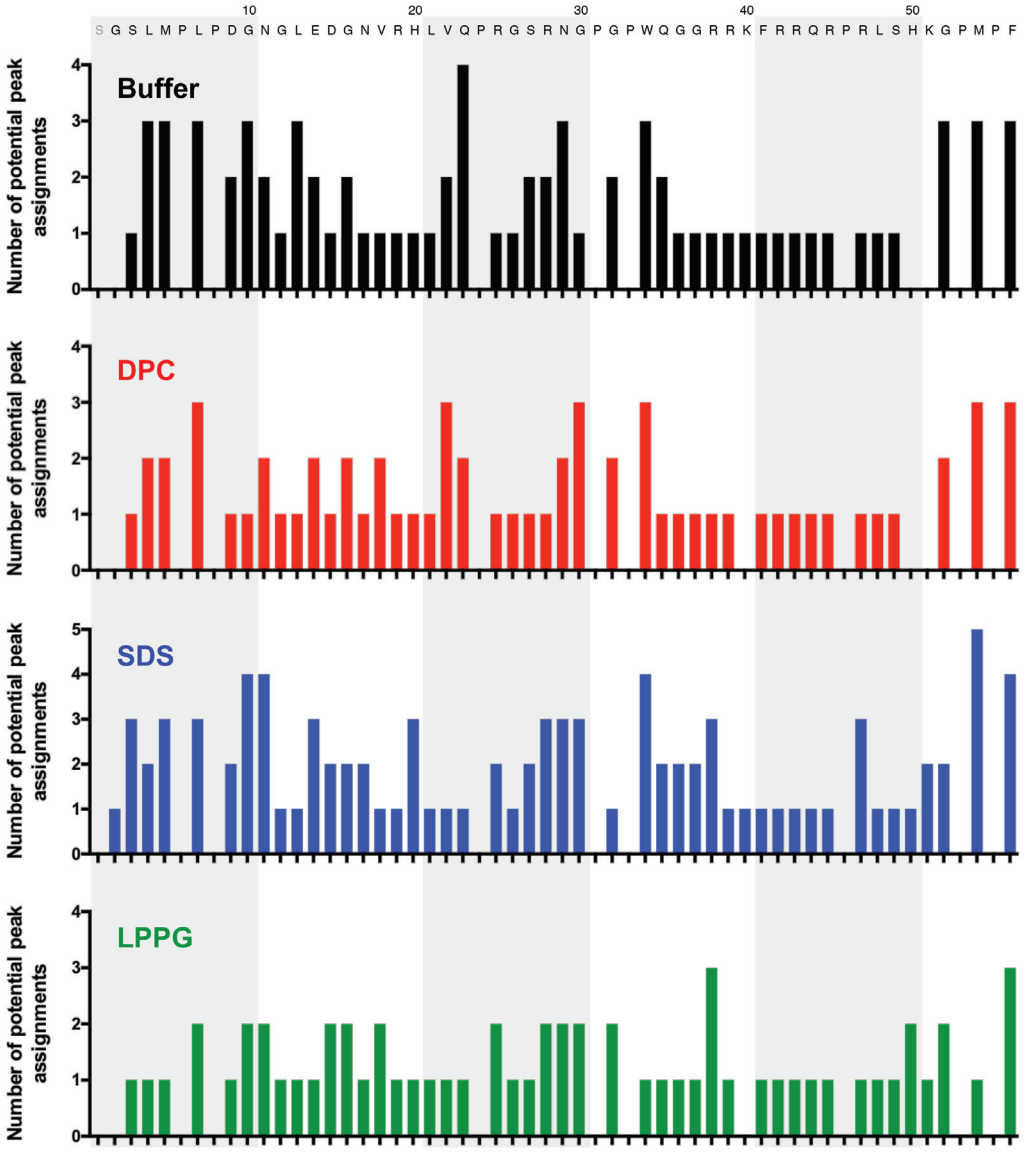

Figure 7.7: Number of potential spin system assignments per residue of apelin-55 in indicated buffer or micellar condition.

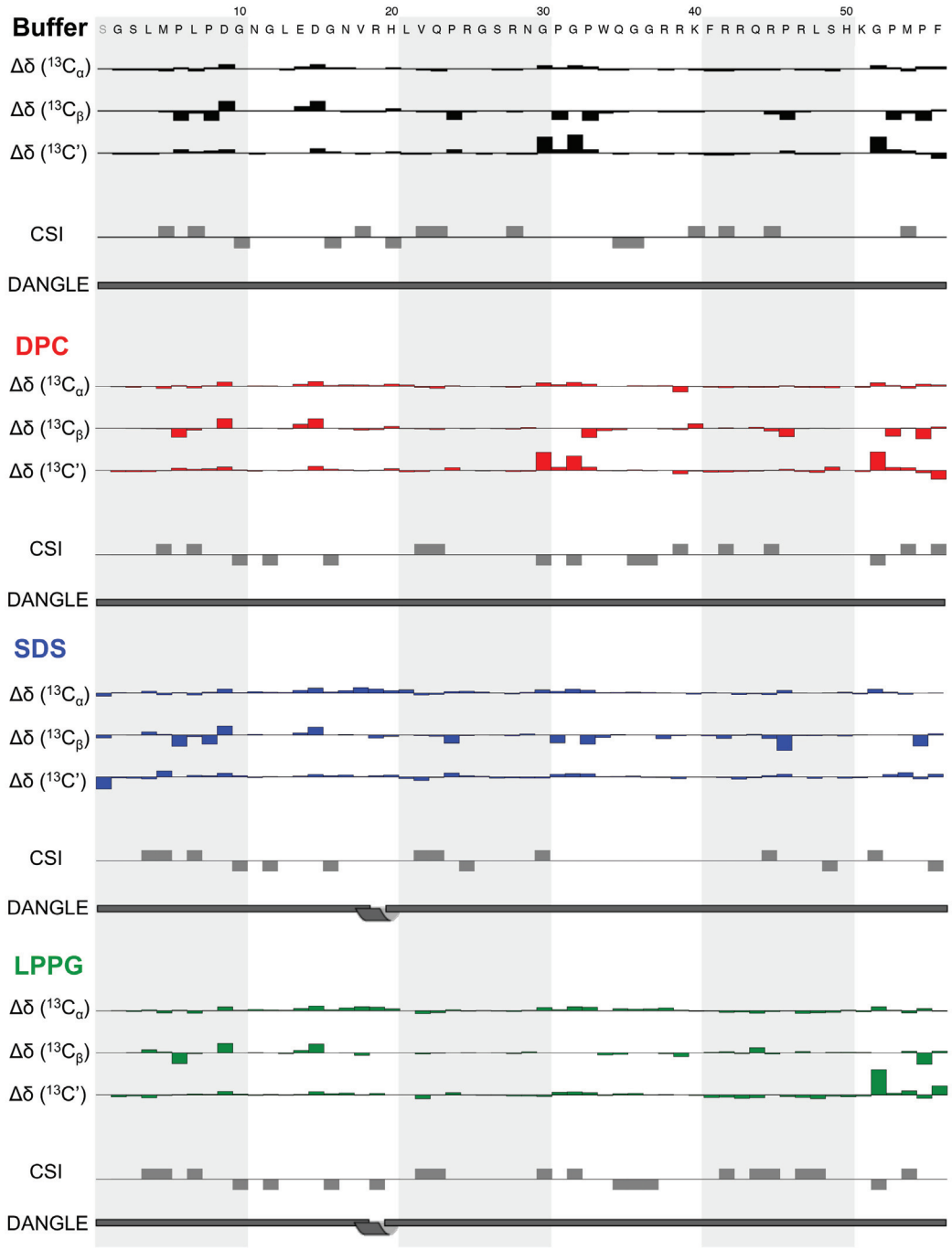

Figure 7.8: Secondary chemical shifts (Δδ) for given nucleus, CSI, and structure predicted by DANGLE for apelin-55 in indicated micelle condition.

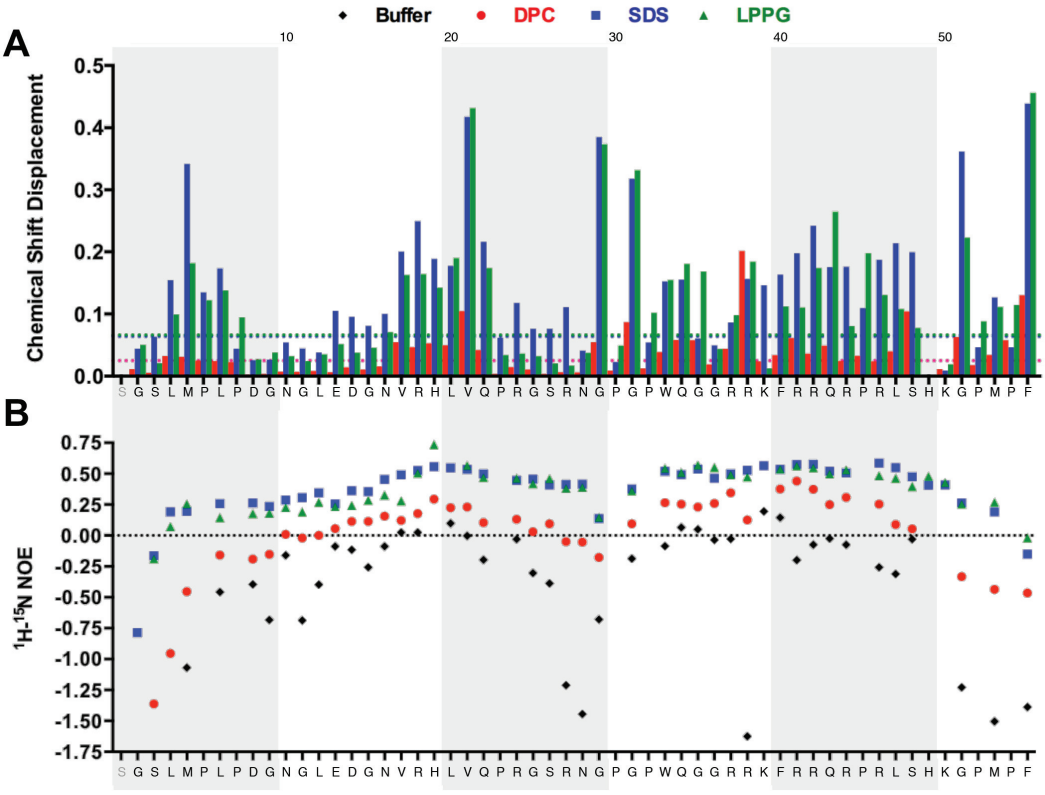

Figure 7.9: Micelle headgroup-dependent conformational and dynamic changes in apelin-55.
A) Euclidian combined chemical shift displacement (CSD) for H_N, N, C_α, C'; B) ^{1}H-^{15}N heteronuclear NOE enhancement factor of apelin-55 in presence of indicated micelle relative to buffer chemical shifts (Chapter 6). Dashed lines represent corrected standard deviation (σ_0) of CSD determined using a modification on the approach detailed by Schumann *et al*. [59]. Specifically, the standard deviation (σ) of the shift changes were calculated and any residues with shift changes greater than 3σ were excluded. The remaining shift changes were then used to re-calculate the σ, giving σ_0.

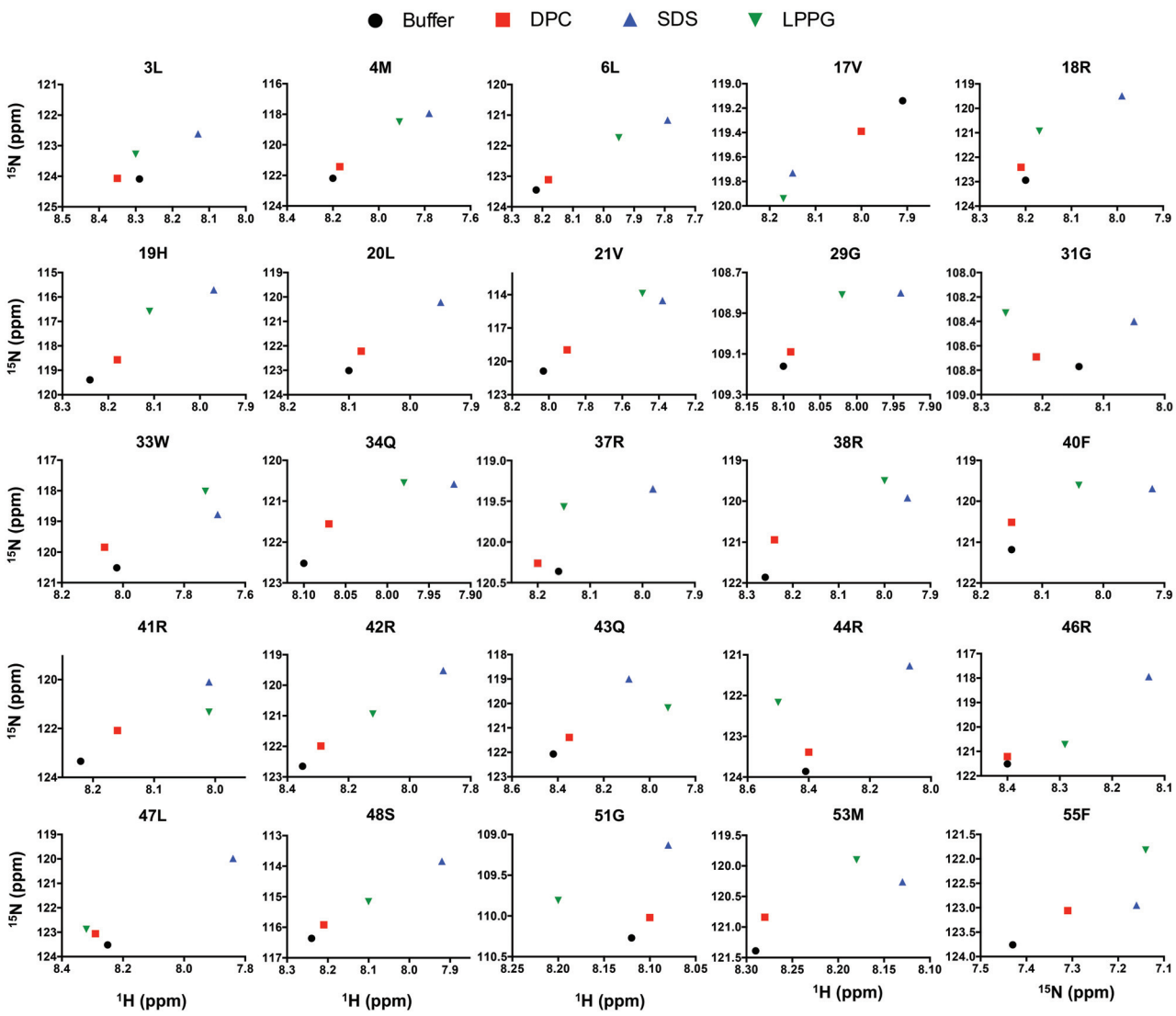

Figure 7.10: Micelle-dependent modulation of assigned H_N and N resonances for indicated residues.

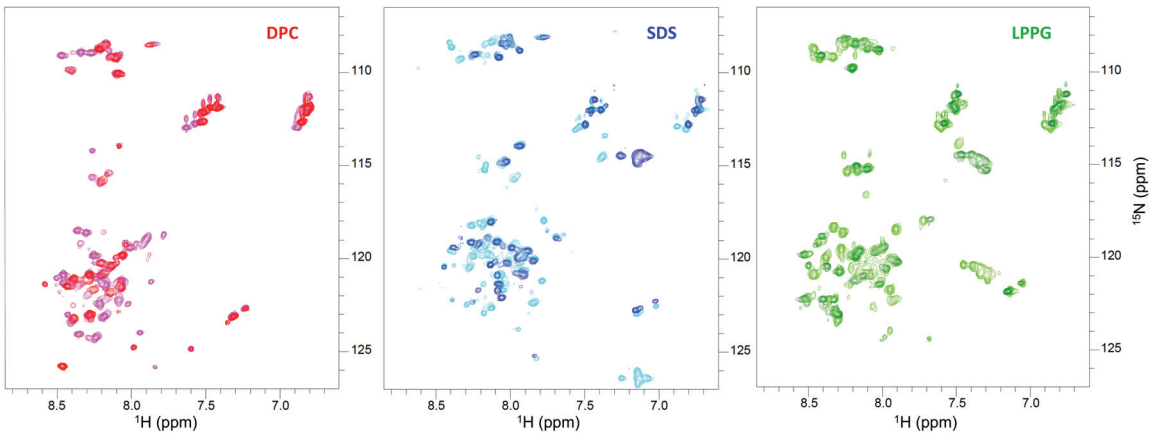

Figure 7.11: Comparison of apelin-36 and apelin-55 conformation in micellar conditions. ^{1}H-^{15}N HSQC spectra of apelin-36 (red, blue, and green) are overlaid on those of apelin-55 (magenta, cyan, and lime) in the indicated micellar condition.

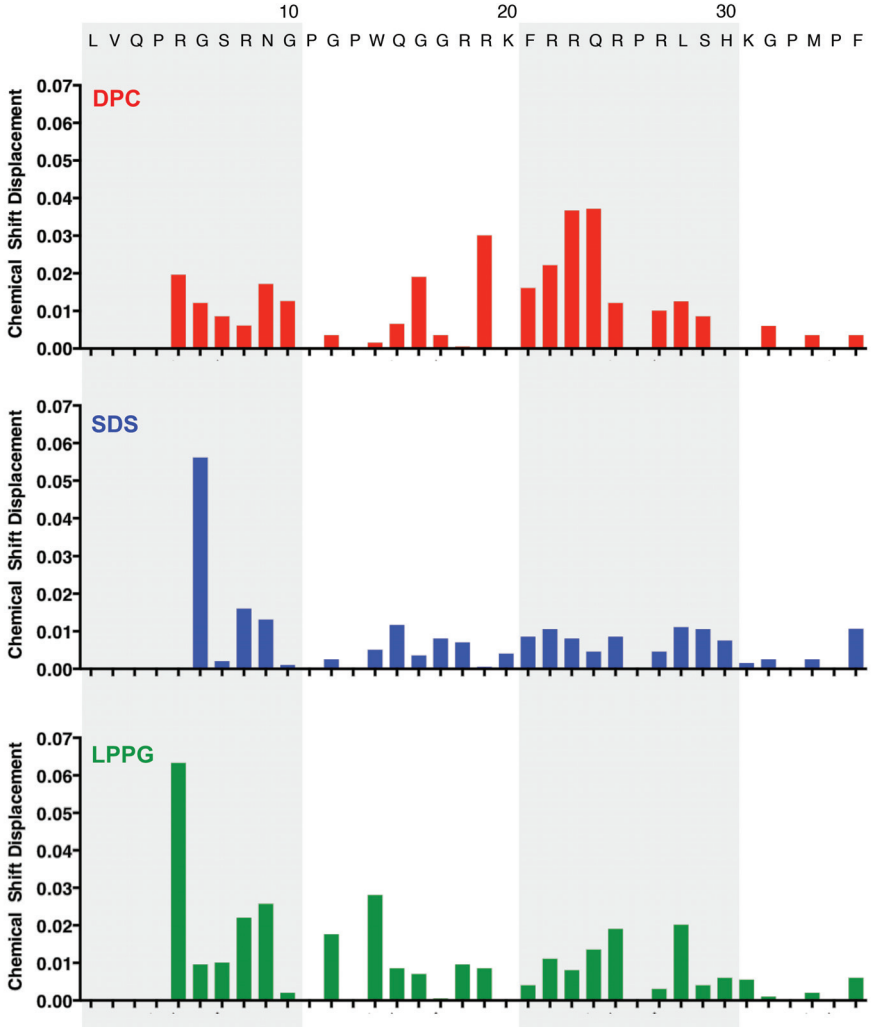

Figure 7.12: Chemical shift displacement of apelin-36 relative to apelin-55. Determined using H and H_N chemical shifts in each indicated micellar condition.

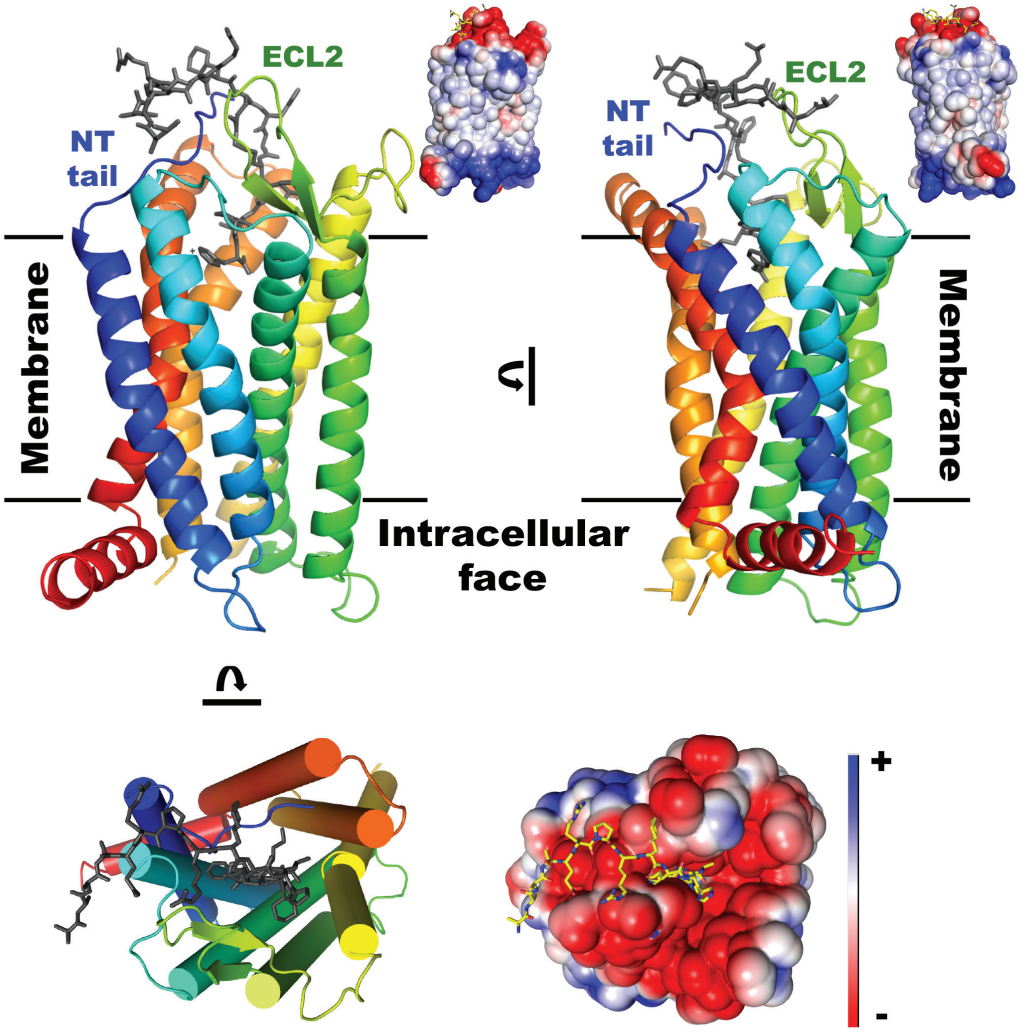

Figure 7.13: Crystal structure of the AR in an inactive-like state in complex with the agonistic apelin-17 analog AMG3054 (PDB entry 5VBL; [69]).
Cartoon and cylinder diagrams are colored from blue (N-terminus) to red (C-terminus), with the ligand shown as grey sticks. Surface representations colored (as indicated on lower right) from a charge of -2 as red to +2 as blue were generated using the PyMol (Schrödinger, Cambridge, MA) adaptive Poisson-Boltzmann Solver plugin. Membrane positioning is as estimated by TMDET [367]. Figure made by Dr. Jan K Rainey is taken from Shin *et al.* (accepted) ***Comprehensive Physiology*** [67].

CHAPTER 8 DISCUSSION

8.1 UPDATED APELIN PROCESSING PATHWAY

Based upon the results presented herein and upon other studies discussed, the previous apelin processing theory can be updated in several ways (visually represented in Figure 8.1). First, the new apelin processing mechanism begins at apelin-55, the longest bioactive isoform. This isoform can be N-terminally truncated directly into shorter isoforms in a protease-dependent manner. All of these retain 12 C-terminal residues of apelin-55, which adopt similar conformations to bind and activate the AR (Chapter 6). To date, only PCSK3 has been identified as cleaving apelin-55 (Chapter 4) – notably, this is specific and preferential for apelin-13 production. Since my work was reported, PCSK3 was also shown to cleave apelin-36 [203]. In contrast, PCSK subtypes 1, 5, 6, and 7 showed no processing properties ((Chapter 4) and [203]) and no other endoproteases have been shown to produce other isoforms. Also, while Figure 8.1 only illustrates the formation of apelin-36, -17, and -13, it should be recalled that apelin isoforms of other lengths have been detected in bovine colostrum and milk [93], and in my *in situ* processing studies (Chapter 5).

The findings discussed in Chapter 5 demonstrating the potential of extracellular apelin-55 processing, and in Chapter 6 showing apelin-55 to be a bioactive isoform, also expand our insight into apelin processing (Fig. 8.2). Specifically, this demonstrates that processing is not limited to intracellular secretory pathway, rationalizing detection of longer isoform in biological fluids [93, 94]. These secreted isoforms can then be processed in response to the enzymes available and accessible. This will be in direct

competition, however, with the potential of apelin-55 to bind to and activate AR (Chapter 6). In summary, apelin may either be released as a desired shorter isoform or as apelin-55 (Fig. 8.2). If the latter occurs, apelin-55 may undergo processing at various extracellular sites or it may act as the 55-residue form. Given the known isoform-dependent potencies, efficacies and regulation of receptor recycling, a control of specific isoform production in proximity to the AR would provide a potentially critical mechanism to regulate downstream effects.

8.2 POTENTIAL RAMIFICATIONS OF MEMBRANE INTERACTION IN THE APELINERGIC SYSTEM

As detailed in Chapter 7, distinct membrane interaction behaviour does not explain the functional differences observed between apelin isoforms. However, the implications of membrane involvement cannot be disregarded as a potential factor in the discrepancies observed between apelin and apela.

Differences in potency were observed between Pyr-apelin-13 and apela-32 in ERK phosphorylation, fluid homeostasis [113], and cardiac contractility and output [112]. This difference likely stems from composition of the outer cell membrane. Given that the outer membrane of most cells is largely composed of zwitterionic headgroup lipids [351], a greater quantity of apela-32 would be localized onto the cell membrane in comparison to apelin isoforms. According to the membrane catalysis hypothesis (Section 7.1.1), this would increase the probability of apela-32-receptor complex formation and provide a correspondingly increased potency than apelin isoforms.

More specifically, one may imagine that a large population of apela-32 peptides will undergo a significant reduction in its conformational space upon reaching the cell membrane. The peptide could first be drawn to zwitterionic regions of the membrane via localized interactions at the N-terminal α-helical region of apela-32, resulting in a decrease in dynamics. Furthermore, the N-terminal α-helical domain in apela-32 likely anchors to the membrane and prevent disassociation from the cell surface, to provide the observed f_b differences observed between apela and apelin. For apelin isoforms, despite multiple domains that are responsible for membrane binding, interaction with zwitterionic regions of membrane would be relatively limited compared to apela-32. But, as stated in Chapter 7, this will allow for a less hindered diffusional search for the receptor with a high local concentration proximal, but not associated, to the membrane. Thus, while apela-32 will be more stably anchored on the zwitterionic cell surface, apelin isoforms will rapidly traverse the extracellular face of the membrane, with an increased propensity for membrane binding only in the presence of an anionic patch of the cell surface. Collectively, these mechanisms will increase the concentration of apela near the AR, which increase potency in accordance to the membrane catalysis hypothesis. Notably, any intrinsic or membrane-induced variation in structure among the two families of AR ligands may also result in the activation of specific signalling pathways (e.g., $G\alpha_i$ vs. B-arrestin pathways) with distinct intracellular and physiological consequences.

Interestingly, a hypothesis that logically follows from ligand-dependent membrane interaction is membrane-mediated signalling mechanisms (e.g., autocrine vs. endocrine). Again, with the mammalian cell membrane outer leaflet being composed of mostly zwitterionic lipids, peptide hormones that favourably interact with zwitterionic lipids

(e.g., apela-32) would likely bind to the host cell or nearby cells upon secretion and, hence, act in an autocrine or paracrine fashion (Fig. 8.3A). Conversely, hormones without such a preference such as apelin, would have the potential to much more readily diffuse away from the cell, favouring endocrine signalling (Fig. 8.3B).

8.3 POTENTIAL FUTURE DIRECTIONS

Although there are many potential directions to go, this section details some of the major experiments that I was personally interested in, but could not address due to time constraints. In relevant sections, I will describe any obstacles that I encountered, or that may hamper the success of the experiments described below.

8.3.1 FURTHER CHARACTERIZATION *IN VITRO* AND *IN SITU* APELIN AND APELA PROCESSING

It is currently unknown which proteases process apela. Following our introduction of recombinant apela-32 expression, the development of *in vitro* processing assay for apela should be rapid. The relatively similar amino acid sequence of the two ligands (Table 3.1) imply that PCSK3 has a strong potential to process apela. If this is not the case, my *in situ* processing experiments (Chapter 5) imply that apelin processing involves additional proteases. In short, testing for processing of apela by PCSK3 and of apelin or apela by other proteases should be very readily possible through extension of my robust *in vitro* assay to study apelin processing (Chapter 4).

One set of experiments that I had hoped to carry out was to test the potential for membrane catalysis to influence processing by the introduction of membrane mimetics into the *in vitro* assay. The major obstacle that I encountered in this class of experiments

was the introduction of surfactants to the RP-HPLC assay, which greatly affected the elution times for apelin isoforms. In the future, this problem could be solved through commercially available lipid extraction kits or through the use of other separation techniques. The observation of an increased processing rate, or difference in isoform specificity, upon addition of a given membrane-mimetic would greatly strengthen my hypothesis of membrane-catalyzed proprotein processing.

As mentioned in Section 4.3.3, an additional complication that arose in my *in vitro* processing assay was my dependence on commercially available PCSK enzymes, which are tested using a non-physiological substrate and produced to meet a certain threshold. As a result, significant variations in specific activity were noted between batches of enzyme. Thus, it seems likely that the *in vitro* assay could be greatly improved through use of PCSK enzymes produced in-house, coupled with consistent testing using physiological substrates to ensure proper enzyme folding and measure specific activity prior to characterization.

In situ, different cell-lines produced varying processing patterns as observed by RP-HPLC. Thus, other cell lines that express apelin (e.g., cardiovascular or brain cells; etc.) may also demonstrate additional processing patterns. Screening these cell-lines would, in turn, provide an alternative means of identifying other proteases involved in both the processing and/or deactivation of apelin or apela. Furthermore, the results reported in Chapter 5 could be strengthened by characterizing apelin processing in cell lines, such as LoVo cells [368], that do not produce PCSK enzymes. In addition, or conversely, siRNA-mediated knockdowns of PCSK expression in HEK293A cells and 3T3-L1 adipocytes could be used to further clarify the role of PCSKs in processing.

Based on the results detailed in Chapter 5, there are also unanswered questions. For example, it is not yet clear whether apelin-55Δ15 production in HEK293A cells is occurring due to cleavage directly N-terminal to apelin-15, or if the N-terminal domain is undergoing cleavage by exoproteases following apelin-13 production. One way to characterize this would be the recombinant production of the His-apelin-55Δ13 domain, and analysis using an identical assay to His-apelin-55. Use of His-apelin-55 with mutations (as applied in Chapter 6 to characterize CD spectral behaviour) could also be applied to test for the importance of motifs within apelin for its processing in both HEK293A and 3T3-L1 cell-lines. Secondly, although apelin-36 production was observed in 3T3-L1 adipocytes, it is unknown which protease was responsible. Use of mutants that prevent processing may prove helpful in this case to predict the endoproteases involved in processing based upon recognition/processing sites. Furthermore, if this mutant interacted with the enzyme, then it could be applicable for affinity-based purification of unknown enzymes for further identification and characterization.

8.3.2 BIOPHYSICAL CHARACTERIZATION OF APELIN AND APELA IN MORE PHYSIOLOGICAL MEMBRANE-MIMETICS/EXTRACELLULAR ENVIRONMENT, OR IN THE PRESENCE OF BINDING PARTNERS

Another aspect of my study that I wanted to expand on was the use of more physiologically-relevant membrane-mimetics to study apelin-membrane interactions. Numerous studies have indicated that membrane-mimetic detergents may hamper protein structure and function [369-371]. This tends to be related to larger polytopic membrane proteins with distinct folds and structuring; thus, it may not be critical for peptides such as apelin and apela. However, I was interested in characterizing direct binding

preferences and motifs of apelin and apela in response to more physiological membrane-mimetics such as bicelles, lipid nanodiscs, and/or liposomes. Furthermore, membrane surfaces are also composed of diverse types of lipids, some with complex post-translational modifications (e.g. glycosylation), and are highly dynamic [372]. Thus, I was also intrigued by the idea of studying apelin-membrane interaction with membrane mimetics composed of modified lipid headgroups. Unfortunately, these experiments were not possible due to time constraints.

In addition to more physiological membrane mimetics, my future experiments would have incorporated potential extracellular molecules that may regulate apelin-membrane interaction. The membrane catalysis theory (Section 7.1.1) does not explicitly consider the roles of interactions with molecules beyond the membrane surface. This is an important omission, as these extracellular molecules may act as binding partners, hypothetically inhibiting interaction between apelin and the membrane surface. Steric interference may also decrease peptide-membrane interaction. Thus, future experiments could also focus on characterizing apelin- and apela-membrane interactions in the presence of species (i.e., other extracellular molecules) that may compete or interfere with the peptide-membrane interaction.

I had also hoped to characterize apelin conformation in the presence of processing enzymes. In Chapter 4, apelin-17 production was not observed in the presence of PCSK3, even though its cleavage site is relatively close to apelin-13 and is proximal to a similar dibasic site. Initially, I had hypothesized that secondary structuring of apelin-55 may obstruct recognition or processing by PCSK3. Although Chapter 6 showed that apelin-55 did not have secondary structures nor showed evidence of stable long-range interactions

in solution, it remains unknown whether apelin-55 adopts a different structure in response to binding to PCSK3, thereby restricting interaction with PCSK3 at the apelin-13 cleavage site.

If physiologically active PCSK3 enzymes had been readily available commercially, I would have carried out solution-state NMR spectroscopy (e.g., ^{1}H-^{15}N HSQC) experiments to quickly identify which residues of apelin-55 are near and/or binding to PCSK3 enzymes. If large chemical shift perturbations for a number of residues were observed, indicative of binding and potentially secondary structuring, the production of an inactive PCSK3 or new non-competitive inhibitors would likely be required since currently available non-competitive inhibitors are known to act through steric exclusion of substrates [373]. The interaction between PCSK3 and apelin (or apela) could then be studied by 3D NMR experiments to determine ^{13}C chemical shifts, and supplement ^{1}H and ^{15}N chemical shifts to help in predicting secondary structuring.

As alluded to in Chapter 6 and 7, apelin isoforms do not present conformational differences relative to each other, whether in solution or in micellar environments. These results indicate that the differences observed in potency and efficacy between apelin isoforms likely originated from apelin isoform-dependent changes in AR conformation and dynamics. On this note, although not discussed here, previous members of the Rainey lab have optimized recombinant expression systems to produce different constructs of AR, including N-terminus with first transmembrane domain [78] and N-terminus with the first three transmembrane domains [12]. Using these constructs, Mr. Calem Kenward and I carried out a number of ^{19}F NMR experiments to gain insight into ligand/isoform-dependent changes in AR conformations and dynamics that may explain the

pharmacological differences observed between ligands and isoforms. Although we did indeed gain some information into their interaction, further work is required to identify the most optimal conditions. Furthermore, expression of the full receptor is likely essential to characterize ligand/isoform-dependent changes in the AR.

8.4 IMPLICATIONS OF MULTIPLE BIOACTIVE ISOFORMS IN THE APELINERGIC SYSTEM

The studies detailed in this thesis and in the context of other studies provide a clear demonstration that apelin and apela isoforms differ in their pharmacological and biophysical properties. Hypothetically, these differences may have greatly varying consequences. Specifically, if one isoform of one ligand is predominantly produced, the level of AR recycling or degradation will be correspondingly controlled by this isoform, resulting in either continuous or transient signalling. Logically, isoform-dependent differences in pharmacology will contribute to either physiological or pathological effects in the apelinergic system. This also translates to the location of signalling (i.e., at the cell membrane or intracellularly) and the signalling pathway (e.g., G-protein vs. β-arrestin), since longer isoforms cause prolonged receptor internalization and more potent β-arrestin signalling relative to shorter isoforms.

If a given tissue requires one class of signalling over another for an appropriate downstream physiological effect, tissue-dependent processing of apelin/apela peptides may, arguably, be the simplest way to achieve the desired effect. Specifically, by regulating which isoform is predominantly produced from the corresponding preprotein, it should be possible to directly regulate the function of apelin and apela at the tissue

level. However, if mixtures of isoforms of apelin, apela, or both peptides are released, the isoform closest to the AR will be likely to bind the receptor first, determining the final physiological effect. If so, factors other than simply preferential isoform processing may be required in order to elevate the local concentration of the required isoform near the receptor. Following from the membrane catalysis hypothesis and the noted potential for differences in isoform-specific membrane interaction, changing the composition of lipid headgroups at the cell surface may provide a means of assisting in altering the level of a required isoform on the cell surface. In other words, differences in the membrane binding preferences of apelin and apela and their isoforms for apela may be exploited to regulate the downstream signalling. Furthermore, since apelin and apela are secreted prior to interaction with their cell-surface receptor, both preferential processing and membrane interaction propensities may simultaneously act to fine-tune regulation in the apelinergic system.

Unfortunately, the exact purpose of the production of multiple apelin and apela isoforms remains speculative, at best, and the precise mechanisms underlying the regulation of relative levels of isoforms remain elusive. Notwithstanding this lack of mechanistic understanding, the currently available data clearly indicate that isoforms have distinct signalling bias (i.e., $G\alpha_i$ vs. β-arrestin signalling pathways), with distinct intracellular and physiological consequences. As a whole, therefore, further elucidation of apelin and apela processing (e.g., the identification of other proteases and their roles, mechanisms regulating production of various isoforms, a more comprehensive characterization of isoform levels as a function of location and pathophysiological state,

etc.) is critical to fully define the regulation and function of this important signalling system.

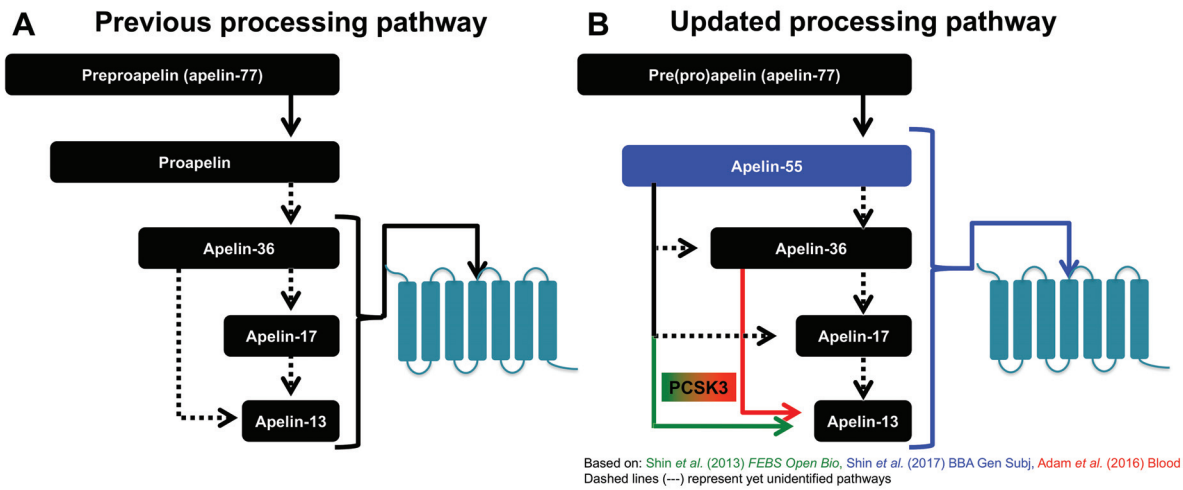

Figure 8.1: Updated mechanism of apelin processing.
A) Previously theorized "apelin-36 precursor" processing pathway. B) Current "myriad" processing pathway theory based on this thesis and work of Adam *et al.* [203]. Proapelin is also now specifically denoted instead as apelin-55, as it has been shown herein to be an additional bioactive GPCR ligand in the apelinergic system.

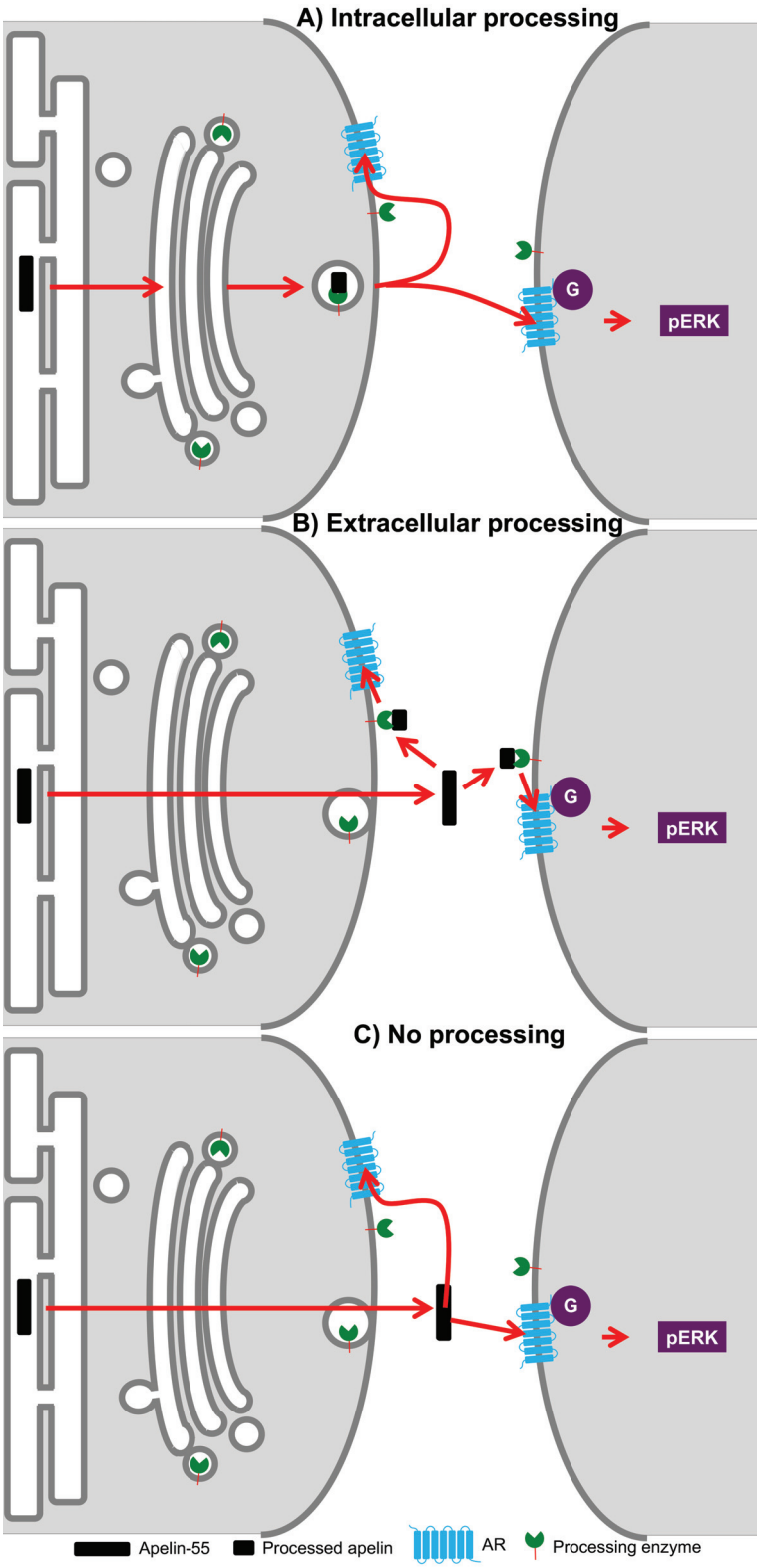

Figure 8.2: Implications of distinct apelin-55 processing events.
Comparison of processing occurring A) intracellularly, B) extracellularly, or C) not at all. Ligand-mediated apelin receptor (AR) activation is represented by G-protein binding and subsequent ERK phosphorylation (pERK)

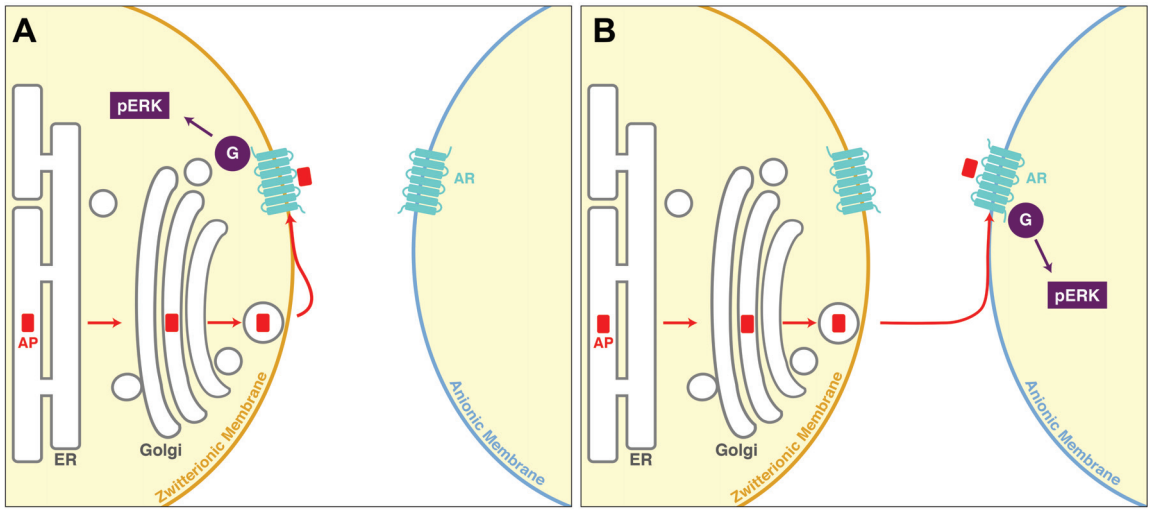

Figure 8.3: Implications of membrane-dependent signalling in the apelinergic system. A) Autocrine and B) paracrine/endocrine signalling of apelin or apela (denoted as "AP") may be regulated by variation in preferential membrane headgroup association and composition of target cell membrane. Ligand-mediated apelin receptor (AR) activation is represented by G-protein binding and subsequent ERK phosphorylation (pERK), although many other signalling pathways are possible. This figure was made in collaboration with Mr. Calem Kenward and is taken from Shin *et al.* (accepted) ***Comprehensive Physiology*** [67].

BIBLIOGRAPHY

1. Pandey A, Shin K, Patterson RE, Liu XQ, and Rainey JK. (2016). Current strategies for protein production and purification enabling membrane protein structural biology. *Biochem Cell Biol* 94: 507-527.

2. Sezonov G, Joseleau-Petit D, and D'Ari R. (2007). *Escherichia coli* physiology in Luria-Bertani broth. *J Bacteriol* 189: 8746-8749.

3. Shiloach J, and Fass R. (2005). Growing *E. coli* to high cell density--a historical perspective on method development. *Biotechnol Adv* 23: 345-357.

4. Marley J, Lu M, and Bracken C. (2001). A method for efficient isotopic labeling of recombinant proteins. *J Biomol NMR* 20: 71-75.

5. Sorensen HP, and Mortensen KK. (2005). Advanced genetic strategies for recombinant protein expression in *Escherichia coli*. *J Biotechnol* 115: 113-128.

6. Studier FW. (1991). Use of bacteriophage T7 lysozyme to improve an inducible T7 expression system. *J Mol Biol* 219: 37-44.

7. Wagner S, Klepsch MM, Schlegel S, Appel A, Draheim R, Tarry M, Hogbom M, van Wijk KJ, Slotboom DJ, Persson JO, and de Gier JW. (2008). Tuning *Escherichia coli* for membrane protein overexpression. *Proc Natl Acad Sci U S A* 105: 14371-14376.

8. Kanz C, Aldebert P, Althorpe N, Baker W, Baldwin A, Bates K, Browne P, van den Broek A, Castro M, Cochrane G, Duggan K, Eberhardt R, Faruque N, Gamble J, Diez FG, Harte N, Kulikova T, Lin Q, Lombard V, Lopez R, Mancuso R, McHale M, Nardone F, Silventoinen V, Sobhany S, Stoehr P, Tuli MA, Tzouvara K, Vaughan R, Wu D, Zhu W, and Apweiler R. (2005). The EMBL nucleotide sequence database. *Nucleic Acids Res* 33: D29-33.

9. Iost I, Guillerez J, and Dreyfus M. (1992). Bacteriophage T7 RNA polymerase travels far ahead of ribosomes *in vivo*. *J Bacteriol* 174: 619-622.

10. Kefala G, Kwiatkowski W, Esquivies L, Maslennikov I, and Choe S. (2007). Application of Mistic to improving the expression and membrane integration of histidine kinase receptors from *Escherichia coli*. *J Struct Funct Genomics* 8: 167-172.

11. Leviatan S, Sawada K, Moriyama Y, and Nelson N. (2010). Combinatorial method for overexpression of membrane proteins in *Escherichia coli*. *J Biol Chem* 285: 23548-23556.

12. Pandey A, Sarker M, Liu XQ, and Rainey JK. (2014). Small expression tags enhance bacterial expression of the first three transmembrane segments of the apelin receptor. *Biochem Cell Biol* 92: 269-278.

13. Hwang PM, Pan JS, and Sykes BD. (2014). Targeted expression, purification, and cleavage of fusion proteins from inclusion bodies in *Escherichia coli*. *FEBS Lett* 588: 247-252.

14. Better M, Bernhard SL, Lei SP, Fishwild DM, Lane JA, Carroll SF, and Horwitz AH. (1993). Potent anti-CD5 ricin A chain immunoconjugates from bacterially produced Fab' and F(ab')2. *Proc Natl Acad Sci U S A* 90: 457-461.

15. de Marco A. (2009). Strategies for successful recombinant expression of disulfide bond-dependent proteins in *Escherichia coli*. *Microb Cell Fact* 8: 26.

16. Butt TR, Edavettal SC, Hall JP, and Mattern MR. (2005). SUMO fusion technology for difficult-to-express proteins. *Protein Expr Purif* 43: 1-9.

17. Marblestone JG, Edavettal SC, Lim Y, Lim P, Zuo X, and Butt TR. (2006). Comparison of SUMO fusion technology with traditional gene fusion systems: enhanced expression and solubility with SUMO. *Protein Sci* 15: 182-189.

18. Hochuli E, Bannwarth W, Dobeli H, Gentz R, and Stuber D. (1988). Genetic approach to facilitate purification of recombinant proteins with a novel metal chelate adsorbent. *Nat Biotech* 6: 1321-1325.

19. Costa SJ, Almeida A, Castro A, Domingues L, and Besir H. (2013). The novel Fh8 and H fusion partners for soluble protein expression in *Escherichia coli*: a comparison with the traditional gene fusion technology. *Appl Microbiol Biotechnol* 97: 6779-6791.

20. Pryor KD, and Leiting B. (1997). High-level expression of soluble protein in Escherichia coli using a His6-tag and maltose-binding-protein double-affinity fusion system. *Protein Expr Purif* 10: 309-319.

21. Kohno T, Kusunoki H, Sato K, and Wakamatsu K. (1998). A new general method for the biosynthesis of stable isotope-enriched peptides using a decahistidine-tagged ubiquitin fusion system: an application to the production of mastoparan-X uniformly enriched with ^{15}N and $^{15}N/^{13}C$. *J Biomol NMR* 12: 109-121.

22. Majtan T, and Kraus JP. (2012). Folding and activity of mutant cystathionine β-synthase depends on the position and nature of the purification tag: characterization of the R266K CBS mutant. *Protein Expr Purif* 82: 317-324.

23. Sabaty M, Grosse S, Adryanczyk G, Boiry S, Biaso F, Arnoux P, and Pignol D. (2013). Detrimental effect of the 6 His C-terminal tag on YedY enzymatic activity and influence of the TAT signal sequence on YedY synthesis. *BMC Biochem* 14: 28.

24. Singh P, Sharma L, Kulothungan SR, Adkar BV, Prajapati RS, Ali PS, Krishnan B, and Varadarajan R. (2013). Effect of signal peptide on stability and folding of *Escherichia coli* thioredoxin. *PLoS One* 8: e63442.

25. Parks TD, Leuther KK, Howard ED, Johnston SA, and Dougherty WG. (1994). Release of proteins and peptides from fusion proteins using a recombinant plant virus proteinase. *Anal Biochem* 216: 413-417.

26. Malakhov MP, Mattern MR, Malakhova OA, Drinker M, Weeks SD, and Butt TR. (2004). SUMO fusions and SUMO-specific protease for efficient expression and purification of proteins. *J Struct Funct Genomics* 5: 75-86.

27. Chong S, Mersha FB, Comb DG, Scott ME, Landry D, Vence LM, Perler FB, Benner J, Kucera RB, Hirvonen CA, Pelletier JJ, Paulus H, and Xu MQ. (1997). Single-column purification of free recombinant proteins using a self-cleavable affinity tag derived from a protein splicing element. *Gene* 192: 271-281.

28. Crimmins DL, Mische SM, and Denslow ND. (2005). Chemical cleavage of proteins in solution. *Curr Protoc Protein Sci* 11.

29. Bird IM. (1989). High performance liquid chromatography: principles and clinical applications. *BMJ* 299: 783-787.

30. Bornhorst JA, and Falke JJ. (2000). Purification of proteins using polyhistidine affinity tags. *Methods Enzymol* 326: 245-254.

31. Mann M, Hendrickson RC, and Pandey A. (2001). Analysis of proteins and proteomes by mass spectrometry. *Annu Rev Biochem* 70: 437-473.

32. Shah B, Kozlowski RL, Han J, and Borchers CH. (2011). Emerging mass spectrometry-based technologies for analyses of chromatin changes: analysis of histones and histone modifications. *Methods Mol Biol* 773: 259-303.

33. Karas M, and Hillenkamp F. (1988). Laser desorption ionization of proteins with molecular masses exceeding 10,000 daltons. *Anal Chem* 60: 2299-2301.

34. Fenn JB, Mann M, Meng CK, Wong SF, and Whitehouse CM. (1989). Electrospray ionization for mass spectrometry of large biomolecules. *Science* 246: 64-71.

35. Kelly SM, Jess TJ, and Price NC. (2005). How to study proteins by circular dichroism. *Biochim Biophys Acta* 1751: 119-139.

36. Ranjbar B, and Gill P. (2009). Circular dichroism techniques: biomolecular and nanostructural analyses- a review. *Chem Biol Drug Des* 74: 101-120.

37. Woody RW. (1974). Studies of theoretical circular dichroism of polypeptides: contributions of β turns. In: *Peptides, Polypeptides and Proteins* John Wiley and Sons Inc., p. 338-348.

38. Greenfield NJ. (2004). Analysis of circular dichroism data. *Methods Enzymol* 383: 282-317.

39. Greenfield NJ. (2006). Using circular dichroism spectra to estimate protein secondary structure. *Nat Protoc* 1: 2876-2890.

40. Whitmore L, and Wallace BA. (2008). Protein secondary structure analyses from circular dichroism spectroscopy: methods and reference databases. *Biopolymers* 89: 392-400.

41. Levitt MH. (2008). *Spin Dynamics: basics of nuclear magnetic resonance*. Chichester, England; Hoboken, NJ: John Wiley & Sons.

42. Keeler J. (2010). *Understanding NMR spectroscopy*. John Wiley & Sons, Ltd.

43. Wishart DS, Bigam CG, Yao J, Abildgaard F, Dyson HJ, Oldfield E, Markley JL, and Sykes BD. (1995). ^{1}H, ^{13}C and ^{15}N chemical shift referencing in biomolecular NMR. *J Biomol NMR* 6: 135-140.

44. Cavanagh J, Fairbrother WJ, Palmer III AG, Rance M, and Skelton NJ. (2006). *Protein NMR spectroscopy, principles and practice*. Academic Press.

45. James TL. (1975). Appendix 2 - Table of nuclear propoerties. In: *Nuclear Magnetic Resonance in Biochemistry*Academic Press, p. 392-399.

46. Williamson MP. (2013). Using chemical shift perturbation to characterise ligand binding. *Prog Nucl Magn Reson Spectrosc* 73: 1-16.

47. Dixon HBF. (1984). IUPAC-IUB Joint Commission on Biochemical Nomenclature (JCBN). Nomenclature and symbolism for amino acids and peptides. Recommendations 1983. *Biochem J* 219: 345-373.

48. Tremblay ML, Banks AW, and Rainey JK. (2010). The predictive accuracy of secondary chemical shifts is more affected by protein secondary structure than solvent environment. *J Biomol NMR* 46: 257-270.

49. Kay LE, Ikura M, Tschudin R, and Bax A. (1990). Three-dimensional triple-resonance NMR spectroscopy of isotopically enriched proteins. *J Magn Reson* 89: 496-514.

50. Bax A, and Ikura M. (1991). An efficient 3D NMR technique for correlating the proton and ^{15}N backbone amide resonances with the α-carbon of the preceding residue in uniformly $^{15}N/^{13}C$ enriched proteins. *J Biomol NMR* 1: 99-104.

51. Clubb RT, Thanabal V, and Wagner G. (1992). A constant-time three-dimensional triple-resonance pulse scheme to correlate intraresidue $^{1}H_{N}$, ^{15}N, and $^{13}C'$ chemical shifts in ^{15}N-^{13}C-labelled proteins. *J Magn Reson* 97: 213-217.

52. Grzesiek S, and Bax A. (1992). Correlating backbone amide and side chain resonances in larger proteins by multiple relayed triple resonance NMR. *J Am Chem Soc* 114: 6291-6293.

53. Griesinger C, Otting G, Wuethrich K, and Ernst RR. (1988). Clean TOCSY for proton spin system identification in macromolecules. *J Am Chem Soc* 110: 7870-7872.

54. Bax A, Clore GM, and Gronenborn AM. (1990). ^{1}H-^{1}H correlation via isotropic mixing of ^{13}C magnetization, a new three-dimensional approach for assigning ^{1}H and ^{13}C spectra of ^{13}C-enriched proteins. *J Magn Reson* 88: 425-431.

55. Wishart DS, and Sykes BD. (1994). The ^{13}C chemical-shift index: a simple method for the identification of protein secondary structure using ^{13}C chemical-shift data. *J Biomol NMR* 4: 171-180.

56. Wishart DS, Sykes BD, and Richards FM. (1992). The chemical shift index: a fast and simple method for the assignment of protein secondary structure through NMR spectroscopy. *Biochemistry* 31: 1647-1651.

57. Cheung MS, Maguire ML, Stevens TJ, and Broadhurst RW. (2010). DANGLE: a Bayesian inferential method for predicting protein backbone dihedral angles and secondary structure. *J Magn Reson* 202: 223-233.

58. Shen Y, Delaglio F, Cornilescu G, and Bax A. (2009). TALOS+: a hybrid method for predicting protein backbone torsion angles from NMR chemical shifts. *J Biomol NMR* 44: 213-223.

59. Schumann FH, Riepl H, Maurer T, Gronwald W, Neidig KP, and Kalbitzer HR. (2007). Combined chemical shift changes and amino acid specific chemical shift mapping of protein-protein interactions. *J Biomol NMR* 39: 275-289.

60. Teilum K, Olsen JG, and Kragelund BB. (2011). Protein stability, flexibility and function. *Biochim Biophys Acta* 1814: 969-976.

61. Reddy T, and Rainey JK. (2010). Interpretation of biomolecular NMR spin relaxation parameters. *Biochem Cell Biol* 88: 131-142.

62. Kay LE, Torchia DA, and Bax A. (1989). Backbone dynamics of proteins as studied by ^{15}N inverse detected heteronuclear NMR spectroscopy: application to staphylococcal nuclease. *Biochemistry* 28: 8972-8979.

63. Rule GS, and Hitchens TK. (2006). *Fundamentals of protein NMR spectroscopy*. Springer Netherlands.

64. Morris KF, and Johnson CS. (1993). Resolution of discrete and continuous molecular size distributions by means of diffusion-ordered 2D NMR spectroscopy. *J Am Chem Soc* 115: 4291-4299.

65. Wu DH, Chen AD, and Johnson CS. (1995). An improved diffusion-ordered spectroscopy experiment incorporating bipolar-gradient pulses. *J Magn Reson A* 115: 260-264.

66. Stejskal EO, and Tanner JE. (1965). Spin diffusion measurements: spin echoes in the presence of a time-dependent field gradient. *J Chem Phys* 42: 288-292.

67. Shin K, Kenward C, and Rainey JK. (2017). Apelinergic system structure and function. *Compr Physiol* Accepted.

68. O'Dowd BF, Heiber M, Chan A, Heng HH, Tsui LC, Kennedy JL, Shi X, Petronis A, George SR, and Nguyen T. (1993). A human gene that shows identity with the gene encoding the angiotensin receptor is located on chromosome 11. *Gene* 136: 355-360.

69. Ma Y, Yue Y, Ma Y, Zhang Q, Zhou Q, Song Y, Shen Y, Li X, Ma X, Li C, Hanson MA, Han GW, Sickmier EA, Swaminath G, Zhao S, Stevens RC, Hu LA, Zhong W, Zhang M, and Xu F. (2017). Structural basis for apelin control of the human apelin receptor. *Structure* 25: 858-866 e854.

70. Vermeire K, Schols D, and Bell TW. (2006). Inhibitors of HIV infection via the cellular CD4 receptor. *Curr Med Chem* 13: 731-743.

71. Edinger AL, Hoffman TL, Sharron M, Lee B, Yi Y, Choe W, Kolson DL, Mitrovic B, Zhou Y, Faulds D, Collman RG, Hesselgesser J, Horuk R, and Doms RW. (1998). An orphan seven-transmembrane domain receptor expressed widely in the brain functions as a coreceptor for human immunodeficiency virus type 1 and simian immunodeficiency virus. *J Virol* 72: 7934-7940.

72. Chen X, Bai B, Tian Y, Du H, and Chen J. (2014). Identification of serine 348 on the apelin receptor as a novel regulatory phosphorylation site in apelin-13-induced G protein-independent biased signaling. *J Biol Chem* 289: 31173-31187.

73. Chapman NA, Dupre DJ, and Rainey JK. (2014). The apelin receptor: physiology, pathology, cell signalling, and ligand modulation of a peptide-activated class A GPCR. *Biochem Cell Biol* 92: 431-440.

74. Tatemoto K, Hosoya M, Habata Y, Fujii R, Kakegawa T, Zou MX, Kawamata Y, Fukusumi S, Hinuma S, Kitada C, Kurokawa T, Onda H, and Fujino M. (1998). Isolation

and characterization of a novel endogenous peptide ligand for the human APJ receptor. *Biochem Biophys Res Commun* 251: 471-476.

75. Chng SC, Ho L, Tian J, and Reversade B. (2013). ELABELA: a hormone essential for heart development signals via the apelin receptor. *Dev Cell* 27: 672-680.

76. Pauli A, Norris ML, Valen E, Chew GL, Gagnon JA, Zimmerman S, Mitchell A, Ma J, Dubrulle J, Reyon D, Tsai SQ, Joung JK, Saghatelian A, and Schier AF. (2014). Toddler: an embryonic signal that promotes cell movement via Apelin receptors. *Science* 343: 1248636.

77. Zhou N, Zhang X, Fan X, Argyris E, Fang J, Acheampong E, DuBois GC, and Pomerantz RJ. (2003). The N-terminal domain of APJ, a CNS-based coreceptor for HIV-1, is essential for its receptor function and coreceptor activity. *Virology* 317: 84-94.

78. Langelaan DN, Reddy T, Banks AW, Dellaire G, Dupre DJ, and Rainey JK. (2013). Structural features of the apelin receptor N-terminal tail and first transmembrane segment implicated in ligand binding and receptor trafficking. *Biochim Biophys Acta* 1828: 1471-1483.

79. Ye L, Van Eps N, Zimmer M, Ernst OP, and Prosser RS. (2016). Activation of the A_{2A} adenosine G-protein-coupled receptor by conformational selection. *Nature* 533: 265-268.

80. Volkoff H. (2015). Cloning and tissue distribution of appetite-regulating peptides in pirapitinga (*Piaractus brachypomus*). *J Anim Physiol Anim Nutr (Berl)* 99: 987-1001.

81. Lee DK, Cheng R, Nguyen T, Fan T, Kariyawasam AP, Liu Y, Osmond DH, George SR, and O'Dowd BF. (2000). Characterization of apelin, the ligand for the APJ receptor. *J Neurochem* 74: 34-41.

82. Sentinelli F, Capoccia D, Bertoccini L, Barchetta I, Incani M, Coccia F, Manconi E, Lenzi A, Cossu E, Leonetti F, Cavallo MG, and Baroni MG. (2016). Search for genetic variant in the apelin gene by resequencing and association study in European subjects. *Genet Test Mol Biomarkers* 20: 98-102.

83. Li WW, Niu WQ, Zhang Y, Wu S, Gao PJ, and Zhu DL. (2009). Family-based analysis of apelin and *AGTRL1* gene polymorphisms with hypertension in Han Chinese. *J Hypertens* 27: 1194-1201.

84. Zhang R, Lu J, Hu C, Wang C, Yu W, Jiang F, Tang S, Bao Y, Xiang K, and Jia W. (2012). Associations of common variants at *APLN* and hypertension in Chinese subjects with and without diabetes. *Exp Diabetes Res* 2012: 917496.

85. Zhang R, Hu C, Wang CR, Ma XJ, Bao YQ, Xu J, Lu JY, Qin W, Xiang KS, and Jia WP. (2009). Association of apelin genetic variants with type 2 diabetes and related clinical features in Chinese Hans. *Chin Med J (Engl)* 122: 1273-1276.

86. Liao YC, Chou WW, Li YN, Chuang SC, Lin WY, Lakkakula BV, Yu ML, and Juo SH. (2011). Apelin gene polymorphism influences apelin expression and obesity phenotypes in Chinese women. *Am J Clin Nutr* 94: 921-928.

87. Jin W, Su X, Xu M, Liu Y, Shi J, Lu L, and Niu W. (2012). Interactive association of five candidate polymorphisms in apelin/APJ pathway with coronary artery disease among Chinese hypertensive patients. *PLoS One* 7: e51123.

88. Habata Y, Fujii R, Hosoya M, Fukusumi S, Kawamata Y, Hinuma S, Kitada C, Nishizawa N, Murosaki S, Kurokawa T, Onda H, Tatemoto K, and Fujino M. (1999). Apelin, the natural ligand of the orphan receptor APJ, is abundantly secreted in the colostrum. *Biochim Biophys Acta* 1452: 25-35.

89. Lee DK, Saldivia VR, Nguyen T, Cheng R, George SR, and O'Dowd BF. (2005). Modification of the terminal residue of apelin-13 antagonizes its hypotensive action. *Endocrinology* 146: 231-236.

90. Mitra J, Tang X, Almo SC, and Shields D. (1998). Temperature-induced conformational changes in prosomatostatin-II: implications for processing. *Biochem J* 334: 275-282.

91. Seidah NG, and Prat A. (2012). The biology and therapeutic targeting of the proprotein convertases. *Nat Rev Drug Discov* 11: 367-383.

92. Kleinz MJ, and Davenport AP. (2005). Emerging roles of apelin in biology and medicine. *Pharmacol Ther* 107: 198-211.

93. Mesmin C, Fenaille F, Becher F, Tabet JC, and Ezan E. (2011). Identification and characterization of apelin peptides in bovine colostrum and milk by liquid chromatography-mass spectrometry. *J Proteome Res* 10: 5222-5231.

94. Foldes G, Horkay F, Szokodi I, Vuolteenaho O, Ilves M, Lindstedt KA, Mayranpaa M, Sarman B, Seres L, Skoumal R, Lako-Futo Z, deChatel R, Ruskoaho H, and Toth M. (2003). Circulating and cardiac levels of apelin, the novel ligand of the orphan receptor APJ, in patients with heart failure. *Biochem Biophys Res Commun* 308: 480-485.

95. Valle A, Hoggard N, Adams AC, Roca P, and Speakman JR. (2008). Chronic central administration of apelin-13 over 10 days increases food intake, body weight, locomotor activity and body temperature in C57BL/6 mice. *J Neuroendocrinol* 20: 79-84.

96. Shin K, Pandey A, Liu XQ, Anini Y, and Rainey JK. (2013). Preferential apelin-13 production by the proprotein convertase PCSK3 is implicated in obesity. *FEBS Open Bio* 3: 328-333.

97. Zhen EY, Higgs RE, and Gutierrez JA. (2013). Pyroglutamyl apelin-13 identified as the major apelin isoform in human plasma. *Anal Biochem* 442: 1-9.

98. Van Coillie E, Proost P, Van Aelst I, Struyf S, Polfliet M, De Meester I, Harvey DJ, Van Damme J, and Opdenakker G. (1998). Functional comparison of two human monocyte chemotactic protein-2 isoforms, role of the amino-terminal pyroglutamic acid and processing by CD26/dipeptidyl peptidase IV. *Biochemistry* 37: 12672-12680.

99. Vickers C, Hales P, Kaushik V, Dick L, Gavin J, Tang J, Godbout K, Parsons T, Baronas E, Hsieh F, Acton S, Patane M, Nichols A, and Tummino P. (2002). Hydrolysis of biological peptides by human angiotensin-converting enzyme-related carboxypeptidase. *J Biol Chem* 277: 14838-14843.

100. Wang W, McKinnie SM, Farhan M, Paul M, McDonald T, McLean B, Llorens-Cortes C, Hazra S, Murray AG, Vederas JC, and Oudit GY. (2016). Angiotensin-converting enzyme 2 metabolizes and partially inactivates pyr-apelin-13 and apelin-17: Physiological effects in the cardiovascular system. *Hypertension* 68: 365-377.

101. Yang P, Kuc RE, Brame AL, Dyson A, Singer M, Glen RC, Cheriyan J, Wilkinson IB, Davenport AP, and Maguire JJ. (2017). [Pyr1] Apelin-13(1-12) is a biologically active ACE2 metabolite of the endogenous cardiovascular peptide [Pyr1] apelin-13. *Front Neurosci* 11: 92.

102. Ceraudo E, Galanth C, Carpentier E, Banegas-Font I, Schonegge AM, Alvear-Perez R, Iturrioz X, Bouvier M, and Llorens-Cortes C. (2014). Biased signaling favoring

G_i over β-arrestin promoted by an apelin fragment lacking the C-terminal phenylalanine. *J Biol Chem* 289: 24599-24610.

103. McKinnie SM, Fischer C, Tran KM, Wang W, Mosquera F, Oudit GY, and Vederas JC. (2016). The Metalloprotease neprilysin degrades and inactivates apelin peptides. *Chembiochem* 17: 1495-1498.

104. Tatemoto K, Takayama K, Zou MX, Kumaki I, Zhang W, Kumano K, and Fujimiya M. (2001). The novel peptide apelin lowers blood pressure via a nitric oxide-dependent mechanism. *Regul Pept* 99: 87-92.

105. Zhang Y, Maitra R, Harris DL, Dhungana S, Snyder R, and Runyon SP. (2014). Identifying structural determinants of potency for analogs of apelin-13: integration of C-terminal truncation with structure-activity. *Bioorg Med Chem* 22: 2992-2997.

106. Murza A, Belleville K, Longpre JM, Sarret P, and Marsault E. (2014). Stability and degradation patterns of chemically modified analogs of apelin-13 in plasma and cerebrospinal fluid. *Biopolymers* 102: 297-303.

107. Hosoya M, Kawamata Y, Fukusumi S, Fujii R, Habata Y, Hinuma S, Kitada C, Honda S, Kurokawa T, Onda H, Nishimura O, and Fujino M. (2000). Molecular and functional characteristics of APJ. Tissue distribution of mRNA and interaction with the endogenous ligand apelin. *J Biol Chem* 275: 21061-21067.

108. Kawamata Y, Habata Y, Fukusumi S, Hosoya M, Fujii R, Hinuma S, Nishizawa N, Kitada C, Onda H, Nishimura O, and Fujino M. (2001). Molecular properties of apelin: tissue distribution and receptor binding. *Biochim Biophys Acta* 1538: 162-171.

109. Medhurst AD, Jennings CA, Robbins MJ, Davis RP, Ellis C, Winborn KY, Lawrie KW, Hervieu G, Riley G, Bolaky JE, Herrity NC, Murdock P, and Darker JG.

(2003). Pharmacological and immunohistochemical characterization of the APJ receptor and its endogenous ligand apelin. *J Neurochem* 84: 1162-1172.

110. O'Carroll AM, Lolait SJ, Harris LE, and Pope GR. (2013). The apelin receptor APJ: journey from an orphan to a multifaceted regulator of homeostasis. *J Endocrinol* 219: R13-35.

111. Perjes A, Kilpio T, Ulvila J, Magga J, Alakoski T, Szabo Z, Vainio L, Halmetoja E, Vuolteenaho O, Petaja-Repo U, Szokodi I, and Kerkela R. (2016). Characterization of apela, a novel endogenous ligand of apelin receptor, in the adult heart. *Basic Res Cardiol* 111: 2.

112. Yang P, Read C, Kuc RE, Buonincontri G, Southwood M, Torella R, Upton PD, Crosby A, Sawiak SJ, Carpenter TA, Glen RC, Morrell NW, Maguire JJ, and Davenport AP. (2017). Elabela/Toddler is an endogenous agonist of the apelin APJ receptor in the adult cardiovascular system, and exogenous administration of the peptide compensates for the downregulation of its expression in pulmonary arterial hypertension. *Circulation* 135: 1160-1173.

113. Deng C, Chen H, Yang N, Feng Y, and Hsueh AJ. (2015). Apela regulates fluid homeostasis by binding to the APJ receptor to activate G_i signaling. *J Biol Chem* 290: 18261-18268.

114. Wang Z, Yu D, Wang M, Wang Q, Kouznetsova J, Yang R, Qian K, Wu W, Shuldiner A, Sztalryd C, Zou M, Zheng W, and Gong DW. (2015). Elabela-apelin receptor signaling pathway is functional in mammalian systems. *Sci Rep* 5: 8170.

115. Maguire JJ, Kleinz MJ, Pitkin SL, and Davenport AP. (2009). [Pyr1]apelin-13 identified as the predominant apelin isoform in the human heart: vasoactive mechanisms and inotropic action in disease. *Hypertension* 54: 598-604.

116. De Mota N, Reaux-Le Goazigo A, El Messari S, Chartrel N, Roesch D, Dujardin C, Kordon C, Vaudry H, Moos F, and Llorens-Cortes C. (2004). Apelin, a potent diuretic neuropeptide counteracting vasopressin actions through inhibition of vasopressin neuron activity and vasopressin release. *Proc Natl Acad Sci U S A* 101: 10464-10469.

117. Azizi M, Iturrioz X, Blanchard A, Peyrard S, De Mota N, Chartrel N, Vaudry H, Corvol P, and Llorens-Cortes C. (2008). Reciprocal regulation of plasma apelin and vasopressin by osmotic stimuli. *J Am Soc Nephrol* 19: 1015-1024.

118. Miettinen KH, Magga J, Vuolteenaho O, Vanninen EJ, Punnonen KR, Ylitalo K, Tuomainen P, and Peuhkurinen KJ. (2007). Utility of plasma apelin and other indices of cardiac dysfunction in the clinical assessment of patients with dilated cardiomyopathy. *Regul Pept* 140: 178-184.

119. Charles C. (2008). The apelin peptides as putative targets in cardiovascular drug discovery and development. *Expert Opin Drug Discov* 3: 51-64.

120. Mesmin C, Dubois M, Becher F, Fenaille F, and Ezan E. (2010). Liquid chromatography/tandem mass spectrometry assay for the absolute quantification of the expected circulating apelin peptides in human plasma. *Rapid Commun Mass Spectrom* 24: 2875-2884.

121. Ohno S, Yakabi K, Ro S, Ochiai M, Onouchi T, Sakurada T, Takabayashi H, Ishida S, and Takayama K. (2012). Apelin-12 stimulates acid secretion through an increase of histamine release in rat stomachs. *Regul Pept* 174: 71-78.

122. Antuschevich H, Kapica M, Krawczynska A, Herman A, Kato I, Kuwahara A, and Zabielski R. (2016). The role of apelin in the modulation of gastric and pancreatic enzymes activity in adult rats. *J Physiol Pharmacol* 67: 403-409.

123. Wang G, Anini Y, Wei W, Qi X, AM OC, Mochizuki T, Wang HQ, Hellmich MR, Englander EW, and Greeley GH, Jr. (2004). Apelin, a new enteric peptide: localization in the gastrointestinal tract, ontogeny, and stimulation of gastric cell proliferation and of cholecystokinin secretion. *Endocrinology* 145: 1342-1348.

124. Fournel A, Drougard A, Duparc T, Marlin A, Brierley SM, Castro J, Le-Gonidec S, Masri B, Colom A, Lucas A, Rousset P, Cenac N, Vergnolle N, Valet P, Cani PD, and Knauf C. (2017). Apelin targets gut contraction to control glucose metabolism via the brain. *Gut* 66: 258-269.

125. Taheri S, Murphy K, Cohen M, Sujkovic E, Kennedy A, Dhillo W, Dakin C, Sajedi A, Ghatei M, and Bloom S. (2002). The effects of centrally administered apelin-13 on food intake, water intake and pituitary hormone release in rats. *Biochem Biophys Res Commun* 291: 1208-1212.

126. Reaux A, De Mota N, Skultetyova I, Lenkei Z, El Messari S, Gallatz K, Corvol P, Palkovits M, and Llorens-Cortes C. (2001). Physiological role of a novel neuropeptide, apelin, and its receptor in the rat brain. *J Neurochem* 77: 1085-1096.

127. Clarke KJ, Whitaker KW, and Reyes TM. (2009). Diminished metabolic responses to centrally-administered apelin-13 in diet-induced obese rats fed a high-fat diet. *J Neuroendocrinol* 21: 83-89.

128. O'Shea M, Hansen MJ, Tatemoto K, and Morris MJ. (2003). Inhibitory effect of apelin-12 on nocturnal food intake in the rat. *Nutr Neurosci* 6: 163-167.

129. Sunter D, Hewson AK, and Dickson SL. (2003). Intracerebroventricular injection of apelin-13 reduces food intake in the rat. *Neurosci Lett* 353: 1-4.

130. Lv SY, Yang YJ, Qin YJ, Mo JR, Wang NB, Wang YJ, and Chen Q. (2012). Central apelin-13 inhibits food intake via the CRF receptor in mice. *Peptides* 33: 132-138.

131. Volkoff H, and Wyatt JL. (2009). Apelin in goldfish (*Carassius auratus*): cloning, distribution and role in appetite regulation. *Peptides* 30: 1434-1440.

132. Lin F, Wu H, Chen H, Xin Z, Yuan D, Wang T, Liu J, Gao Y, Zhang X, Zhou C, Wei R, Chen D, Yang S, Wang Y, Pu Y, and Li Z. (2014). Molecular and physiological evidences for the role in appetite regulation of apelin and its receptor APJ in Ya-fish (*Schizothorax prenanti*). *Mol Cell Endocrinol* 396: 46-57.

133. Penney CC, and Volkoff H. (2014). Peripheral injections of cholecystokinin, apelin, ghrelin and orexin in cavefish (*Astyanax fasciatus mexicanus*): effects on feeding and on the brain expression levels of tyrosine hydroxylase, mechanistic target of rapamycin and appetite-related hormones. *Gen Comp Endocrinol* 196: 34-40.

134. Ferrante C, Orlando G, Recinella L, Leone S, Chiavaroli A, Di Nisio C, Shohreh R, Manippa F, Ricciuti A, Vacca M, and Brunetti L. (2016). Central apelin-13 administration modulates hypothalamic control of feeding. *J Biol Regul Homeost Agents* 30: 883-888.

135. Tekin S, Erden Y, Sandal S, Etem Onalan E, Ozyalin F, Ozen H, and Yilmaz B. (2017). Effects of apelin on reproductive functions: relationship with feeding behavior and energy metabolism. *Arch Physiol Biochem* 123: 9-15.

136. Khaksari M, Aboutaleb N, Nasirinezhad F, Vakili A, and Madjd Z. (2012). Apelin-13 protects the brain against ischemic reperfusion injury and cerebral edema in a transient model of focal cerebral ischemia. *J Mol Neurosci* 48: 201-208.

137. Gu Q, Zhai L, Feng X, Chen J, Miao Z, Ren L, Qian X, Yu J, Li Y, Xu X, and Liu CF. (2013). Apelin-36, a potent peptide, protects against ischemic brain injury by activating the PI3K/Akt pathway. *Neurochem Int* 63: 535-540.

138. Yang Y, Zhang X, Cui H, Zhang C, Zhu C, and Li L. (2014). Apelin-13 protects the brain against ischemia/reperfusion injury through activating PI3K/Akt and ERK1/2 signaling pathways. *Neurosci Lett* 568: 44-49.

139. Bao HJ, Zhang L, Han WC, and Dai DK. (2015). Apelin-13 attenuates traumatic brain injury-induced damage by suppressing autophagy. *Neurochem Res* 40: 89-97.

140. Than A, He HL, Chua SH, Xu D, Sun L, Leow MK, and Chen P. (2015). Apelin enhances brown adipogenesis and browning of white adipocytes. *J Biol Chem* 290: 14679-14691.

141. Xin Q, Cheng B, Pan Y, Liu H, Yang C, Chen J, and Bai B. (2015). Neuroprotective effects of apelin-13 on experimental ischemic stroke through suppression of inflammation. *Peptides* 63: 55-62.

142. Yan XG, Cheng BH, Wang X, Ding LC, Liu HQ, Chen J, and Bai B. (2015). Lateral intracerebroventricular injection of apelin-13 inhibits apoptosis after cerebral ischemia/reperfusion injury. *Neural Regen Res* 10: 766-771.

143. Hajimashhadi Z, Aboutaleb N, and Nasirinezhad F. (2017). Chronic administration of [Pyr1] apelin-13 attenuates neuropathic pain after compression spinal cord injury in rats. *Neuropeptides* 61: 15-22.

144. Xu N, Wang H, Fan L, and Chen Q. (2009). Supraspinal administration of apelin-13 induces antinociception via the opioid receptor in mice. *Peptides* 30: 1153-1157.

145. Turtay MG, Karabas M, Parlakpinar H, Colak C, and Sagir M. (2015). The analgesic effect of apelin-13 and its mechanism of action within the nitric oxide and serotonin pathways. *Hippokratia* 19: 319-323.

146. Canpolat S, Ozcan M, Saral S, Kalkan OF, and Ayar A. (2016). Effects of apelin-13 in mice model of experimental pain and peripheral nociceptive signaling in rat sensory neurons. *J Recept Signal Transduct Res* 36: 243-247.

147. Yang P, Maguire JJ, and Davenport AP. (2015). Apelin, Elabela/Toddler, and biased agonists as novel therapeutic agents in the cardiovascular system. *Trends Pharmacol Sci* 36: 560-567.

148. Szokodi I, Tavi P, Foldes G, Voutilainen-Myllyla S, Ilves M, Tokola H, Pikkarainen S, Piuhola J, Rysa J, Toth M, and Ruskoaho H. (2002). Apelin, the novel endogenous ligand of the orphan receptor APJ, regulates cardiac contractility. *Circ Res* 91: 434-440.

149. Ishida J, Hashimoto T, Hashimoto Y, Nishiwaki S, Iguchi T, Harada S, Sugaya T, Matsuzaki H, Yamamoto R, Shiota N, Okunishi H, Kihara M, Umemura S, Sugiyama F, Yagami K, Kasuya Y, Mochizuki N, and Fukamizu A. (2004). Regulatory roles for APJ, a seven-transmembrane receptor related to angiotensin-type 1 receptor in blood pressure *in vivo*. *J Biol Chem* 279: 26274-26279.

150. Jia YX, Lu ZF, Zhang J, Pan CS, Yang JH, Zhao J, Yu F, Duan XH, Tang CS, and Qi YF. (2007). Apelin activates L-arginine/nitric oxide synthase/nitric oxide pathway in rat aortas. *Peptides* 28: 2023-2029.

151. Chun HJ, Ali ZA, Kojima Y, Kundu RK, Sheikh AY, Agrawal R, Zheng L, Leeper NJ, Pearl NE, Patterson AJ, Anderson JP, Tsao PS, Lenardo MJ, Ashley EA, and Quertermous T. (2008). Apelin signaling antagonizes Ang II effects in mouse models of atherosclerosis. *J Clin Invest* 118: 3343-3354.

152. Dray C, Knauf C, Daviaud D, Waget A, Boucher J, Buleon M, Cani PD, Attane C, Guigne C, Carpene C, Burcelin R, Castan-Laurell I, and Valet P. (2008). Apelin stimulates glucose utilization in normal and obese insulin-resistant mice. *Cell Metab* 8: 437-445.

153. Hus-Citharel A, Bouby N, Frugiere A, Bodineau L, Gasc JM, and Llorens-Cortes C. (2008). Effect of apelin on glomerular hemodynamic function in the rat kidney. *Kidney Int* 74: 486-494.

154. Jia YX, Pan CS, Zhang J, Geng B, Zhao J, Gerns H, Yang J, Chang JK, Tang CS, and Qi YF. (2006). Apelin protects myocardial injury induced by isoproterenol in rats. *Regul Pept* 133: 147-154.

155. Atluri P, Morine KJ, Liao GP, Panlilio CM, Berry MF, Hsu VM, Hiesinger W, Cohen JE, and Joseph Woo Y. (2007). Ischemic heart failure enhances endogenous myocardial apelin and APJ receptor expression. *Cell Mol Biol Lett* 12: 127-138.

156. Zeng XJ, Zhang LK, Wang HX, Lu LQ, Ma LQ, and Tang CS. (2009). Apelin protects heart against ischemia/reperfusion injury in rat. *Peptides* 30: 1144-1152.

157. Soltani Hekmat A, Najafipour H, Nekooian AA, Esmaeli-Mahani S, and Javanmardi K. (2011). Cardiovascular responses to apelin in two-kidney-one-clip hypertensive rats and its receptor expression in ischemic and non-ischemic kidneys. *Regul Pept* 172: 62-68.

158. Najafipour H, Soltani Hekmat A, Nekooian AA, and Esmaeili-Mahani S. (2012). Apelin receptor expression in ischemic and non- ischemic kidneys and cardiovascular responses to apelin in chronic two-kidney-one-clip hypertension in rats. *Regul Pept* 178: 43-50.

159. Rastaldo R, Cappello S, Folino A, Berta GN, Sprio AE, Losano G, Samaja M, and Pagliaro P. (2011). Apelin-13 limits infarct size and improves cardiac postischemic mechanical recovery only if given after ischemia. *Am J Physiol Heart Circ Physiol* 300: H2308-2315.

160. Wang M, Gupta RC, Rastogi S, Kohli S, Sabbah MS, Zhang K, Mohyi P, Hogie M, Fischer Y, and Sabbah HN. (2013). Effects of acute intravenous infusion of apelin on left ventricular function in dogs with advanced heart failure. *J Card Fail* 19: 509-516.

161. Pang H, Han B, Yu T, and Zong Z. (2014). Effect of apelin on the cardiac hemodynamics in hypertensive rats with heart failure. *Int J Mol Med* 34: 756-764.

162. Zhang BH, Guo CX, Wang HX, Lu LQ, Wang YJ, Zhang LK, Du FH, and Zeng XJ. (2014). Cardioprotective effects of adipokine apelin on myocardial infarction. *Heart Vessels* 29: 679-689.

163. Azizi Y, Faghihi M, Imani A, Roghani M, Zekri A, Mobasheri MB, Rastgar T, and Moghimian M. (2015). Post-infarct treatment with [Pyr(1)]apelin-13 improves myocardial function by increasing neovascularization and overexpression of angiogenic growth factors in rats. *Eur J Pharmacol* 761: 101-108.

164. Chung WJ, Cho A, Byun K, Moon J, Ge X, Seo HS, Moon E, Dash R, and Yang PC. (2016). Apelin-13 infusion salvages the peri-infarct region to preserve cardiac function after severe myocardial injury. *Int J Cardiol* 222: 361-367.

165. Li L, Zeng H, and Chen JX. (2012). Apelin-13 increases myocardial progenitor cells and improves repair postmyocardial infarction. *Am J Physiol Heart Circ Physiol* 303: H605-618.

166. Boal F, Roumegoux J, Alfarano C, Timotin A, Calise D, Anesia R, Drougard A, Knauf C, Lagente C, Roncalli J, Desmoulin F, Tronchere H, Valet P, Parini A, and Kunduzova O. (2015). Apelin regulates FoxO3 translocation to mediate cardioprotective responses to myocardial injury and obesity. *Sci Rep* 5: 16104.

167. Pisarenko O, Shulzhenko V, Studneva I, Pelogeykina Y, Timoshin A, Anesia R, Valet P, Parini A, and Kunduzova O. (2015). Structural apelin analogues: mitochondrial ROS inhibition and cardiometabolic protection in myocardial ischaemia reperfusion injury. *Br J Pharmacol* 172: 2933-2945.

168. Boal F, Timotin A, Roumegoux J, Alfarano C, Calise D, Anesia R, Parini A, Valet P, Tronchere H, and Kunduzova O. (2016). Apelin-13 administration protects against ischaemia/reperfusion-mediated apoptosis through the FoxO1 pathway in high-fat diet-induced obesity. *Br J Pharmacol* 173: 1850-1863.

169. Azizi Y, Imani A, Fanaei H, Khamse S, Parvizi MR, and Faghihi M. (2017). Post-infarct treatment with [Pyr1]apelin-13 exerts anti-remodelling and anti-apoptotic effects in rats' hearts. *Kardiol Pol* 75: 605-613.

170. Chaves-Almagro C, Castan-Laurell I, Dray C, Knauf C, Valet P, and Masri B. (2015). Apelin receptors: From signaling to antidiabetic strategy. *Eur J Pharmacol* 763: 149-159.

171. Hu H, He L, Li L, and Chen L. (2016). Apelin/APJ system as a therapeutic target in diabetes and its complications. *Mol Genet Metab* 119: 20-27.

172. Sorhede Winzell M, Magnusson C, and Ahren B. (2005). The apj receptor is expressed in pancreatic islets and its ligand, apelin, inhibits insulin secretion in mice. *Regul Pept* 131: 12-17.

173. Guo L, Li Q, Wang W, Yu P, Pan H, Li P, Sun Y, and Zhang J. (2009). Apelin inhibits insulin secretion in pancreatic β-cells by activation of PI3-kinase-phosphodiesterase 3B. *Endocr Res* 34: 142-154.

174. Ringstrom C, Nitert MD, Bennet H, Fex M, Valet P, Rehfeld JF, Friis-Hansen L, and Wierup N. (2010). Apelin is a novel islet peptide. *Regul Pept* 162: 44-51.

175. Frier BC, Williams DB, and Wright DC. (2009). The effects of apelin treatment on skeletal muscle mitochondrial content. *Am J Physiol Regul Integr Comp Physiol* 297: R1761-1768.

176. Zheng XT, Than A, Ananthanaraya A, Kim DH, and Chen P. (2013). Graphene quantum dots as universal fluorophores and their use in revealing regulated trafficking of insulin receptors in adipocytes. *ACS Nano* 7: 6278-6286.

177. Yue P, Jin H, Xu S, Aillaud M, Deng AC, Azuma J, Kundu RK, Reaven GM, Quertermous T, and Tsao PS. (2011). Apelin decreases lipolysis via G_q, G_i, and AMPK-dependent mechanisms. *Endocrinology* 152: 59-68.

178. Than A, Cheng Y, Foh LC, Leow MK, Lim SC, Chuah YJ, Kang Y, and Chen P. (2012). Apelin inhibits adipogenesis and lipolysis through distinct molecular pathways. *Mol Cell Endocrinol* 362: 227-241.

179. Masaki T, Yasuda T, and Yoshimatsu H. (2012). Apelin-13 microinjection into the paraventricular nucleus increased sympathetic nerve activity innervating brown adipose tissue in rats. *Brain Res Bull* 87: 540-543.

180. Higuchi K, Masaki T, Gotoh K, Chiba S, Katsuragi I, Tanaka K, Kakuma T, and Yoshimatsu H. (2007). Apelin, an APJ receptor ligand, regulates body adiposity and favors the messenger ribonucleic acid expression of uncoupling proteins in mice. *Endocrinology* 148: 2690-2697.

181. Attane C, Foussal C, Le Gonidec S, Benani A, Daviaud D, Wanecq E, Guzman-Ruiz R, Dray C, Bezaire V, Rancoule C, Kuba K, Ruiz-Gayo M, Levade T, Penninger J, Burcelin R, Penicaud L, Valet P, and Castan-Laurell I. (2012). Apelin treatment increases complete fatty acid oxidation, mitochondrial oxidative capacity, and biogenesis in muscle of insulin-resistant mice. *Diabetes* 61: 310-320.

182. Ceylan-Isik AF, Kandadi MR, Xu X, Hua Y, Chicco AJ, Ren J, and Nair S. (2013). Apelin administration ameliorates high fat diet-induced cardiac hypertrophy and contractile dysfunction. *J Mol Cell Cardiol* 63: 4-13.

183. Akcilar R, Turgut S, Caner V, Akcilar A, Ayada C, Elmas L, and Ozcan TO. (2015). The effects of apelin treatment on a rat model of type 2 diabetes. *Adv Med Sci* 60: 94-100.

184. Galon-Tilleman H, Yang H, Bednarek MA, Spurlock SM, Paavola KJ, Ko B, To C, Luo J, Tian H, Jermutus L, Grimsby J, Rondinone CM, Konkar A, and Kaplan DD. (2017). Apelin-36 modulates blood glucose and body weight independently of canonical APJ receptor signaling. *J Biol Chem* 292: 1925-1933.

185. Chen H, Zheng C, Zhang X, Li J, Li J, Zheng L, and Huang K. (2011). Apelin alleviates diabetes-associated endoplasmic reticulum stress in the pancreas of Akita mice. *Peptides* 32: 1634-1639.

186. Zhu S, Sun F, Li W, Cao Y, Wang C, Wang Y, Liang D, Zhang R, Zhang S, Wang H, and Cao F. (2011). Apelin stimulates glucose uptake through the PI3K/Akt pathway and improves insulin resistance in 3T3-L1 adipocytes. *Mol Cell Biochem* 353: 305-313.

187. Cheng X, Cheng XS, and Pang CC. (2003). Venous dilator effect of apelin, an endogenous peptide ligand for the orphan APJ receptor, in conscious rats. *Eur J Pharmacol* 470: 171-175.

188. Dai L, Smith PM, Kuksis M, and Ferguson AV. (2013). Apelin acts in the subfornical organ to influence neuronal excitability and cardiovascular function. *J Physiol* 591: 3421-3432.

189. Kagiyama S, Fukuhara M, Matsumura K, Lin Y, Fujii K, and Iida M. (2005). Central and peripheral cardiovascular actions of apelin in conscious rats. *Regul Pept* 125: 55-59.

190. Duparc T, Colom A, Cani PD, Massaly N, Rastrelli S, Drougard A, Le Gonidec S, Mouledous L, Frances B, Leclercq I, Llorens-Cortes C, Pospisilik JA, Delzenne NM, Valet P, Castan-Laurell I, and Knauf C. (2011). Central apelin controls glucose homeostasis via a nitric oxide-dependent pathway in mice. *Antioxid Redox Signal* 15: 1477-1496.

191. Drougard A, Duparc T, Brenachot X, Carneiro L, Gouaze A, Fournel A, Geurts L, Cadoudal T, Prats AC, Penicaud L, Vieau D, Lesage J, Leloup C, Benani A, Cani PD, Valet P, and Knauf C. (2014). Hypothalamic apelin/reactive oxygen species signaling controls hepatic glucose metabolism in the onset of diabetes. *Antioxid Redox Signal* 20: 557-573.

192. Drougard A, Fournel A, Marlin A, Meunier E, Abot A, Bautzova T, Duparc T, Louche K, Batut A, Lucas A, Le-Gonidec S, Lesage J, Fioramonti X, Moro C, Valet P, Cani PD, and Knauf C. (2016). Central chronic apelin infusion decreases energy expenditure and thermogenesis in mice. *Sci Rep* 6: 31849.

193. Day RT, Cavaglieri RC, and Feliers D. (2013). Apelin retards the progression of diabetic nephropathy. *Am J Physiol Renal Physiol* 304: F788-800.

194. Chen H, Li J, Jiao L, Petersen RB, Li J, Peng A, Zheng L, and Huang K. (2014). Apelin inhibits the development of diabetic nephropathy by regulating histone acetylation in Akita mouse. *J Physiol* 592: 505-521.

195. Guo C, Liu Y, Zhao W, Wei S, Zhang X, Wang W, and Zeng X. (2015). Apelin promotes diabetic nephropathy by inducing podocyte dysfunction via inhibiting proteasome activities. *J Cell Mol Med* 19: 2273-2285.

196. Zhang BH, Wang W, Wang H, Yin J, and Zeng XJ. (2013). Promoting effects of the adipokine, apelin, on diabetic nephropathy. *PLoS One* 8: e60457.

197. Langelaan DN, Bebbington EM, Reddy T, and Rainey JK. (2009). Structural insight into G-protein coupled receptor binding by apelin. *Biochemistry* 48: 537-548.

198. Kasai A, Shintani N, Oda M, Kakuda M, Hashimoto H, Matsuda T, Hinuma S, and Baba A. (2004). Apelin is a novel angiogenic factor in retinal endothelial cells. *Biochem Biophys Res Commun* 325: 395-400.

199. De Mota N, Lenkei Z, and Llorens-Cortes C. (2000). Cloning, pharmacological characterization and brain distribution of the rat apelin receptor. *Neuroendocrinology* 72: 400-407.

200. Sawane M, Kidoya H, Muramatsu F, Takakura N, and Kajiya K. (2011). Apelin attenuates UVB-induced edema and inflammation by promoting vessel function. *Am J Pathol* 179: 2691-2697.

201. Gerbier R, Alvear-Perez R, Margathe JF, Flahault A, Couvineau P, Gao J, De Mota N, Dabire H, Li B, Ceraudo E, Hus-Citharel A, Esteoulle L, Bisoo C, Hibert M, Berdeaux A, Iturrioz X, Bonnet D, and Llorens-Cortes C. (2017). Development of original metabolically stable apelin-17 analogs with diuretic and cardiovascular effects. *FASEB J* 31: 687-700.

202. Simpkin JC, Yellon DM, Davidson SM, Lim SY, Wynne AM, and Smith CC. (2007). Apelin-13 and apelin-36 exhibit direct cardioprotective activity against ischemia-reperfusion injury. *Basic Res Cardiol* 102: 518-528.

203. Adam F, Khatib AM, Lopez JJ, Vatier C, Turpin S, Muscat A, Soulet F, Aries A, Jardin I, Bobe R, Stepanian A, de Prost D, Dray C, Rosado JA, Valet P, Feve B, and Siegfried G. (2016). Apelin: an antithrombotic factor that inhibits platelet function. *Blood* 127: 908-920.

204. Cirillo P, Ziviello F, Pellegrino G, Conte S, Cimmino G, Giaquinto A, Pacifico F, Leonardi A, Golino P, and Trimarco B. (2015). The adipokine apelin-13 induces expression of prothrombotic tissue factor. *Thromb Haemost* 113: 363-372.

205. Picault FX, Chaves-Almagro C, Projetti F, Prats H, Masri B, and Audigier Y. (2014). Tumour co-expression of apelin and its receptor is the basis of an autocrine loop involved in the growth of colon adenocarcinomas. *Eur J Cancer* 50: 663-674.

206. Sakamoto K, Murakami Y, Sawada S, Ushikubo H, Mori A, Nakahara T, and Ishii K. (2016). Apelin-36 is protective against N-methyl-D-aspartic-acid-induced retinal ganglion cell death in the mice. *Eur J Pharmacol* 791: 213-220.

207. Iturrioz X, Alvear-Perez R, De Mota N, Franchet C, Guillier F, Leroux V, Dabire H, Le Jouan M, Chabane H, Gerbier R, Bonnet D, Berdeaux A, Maigret B, Galzi JL, Hibert M, and Llorens-Cortes C. (2010). Identification and pharmacological properties of E339-3D6, the first nonpeptidic apelin receptor agonist. *FASEB J* 24: 1506-1517.

208. Lee DK, Ferguson SS, George SR, and O'Dowd BF. (2010). The fate of the internalized apelin receptor is determined by different isoforms of apelin mediating differential interaction with β-arrestin. *Biochem Biophys Res Commun* 395: 185-189.

209. Evans NA, Groarke DA, Warrack J, Greenwood CJ, Dodgson K, Milligan G, and Wilson S. (2001). Visualizing differences in ligand-induced β-arrestin-GFP interactions and trafficking between three recently characterized G protein-coupled receptors. *J Neurochem* 77: 476-485.

210. Pope GR, Tilve S, McArdle CA, Lolait SJ, and O'Carroll AM. (2016). Agonist-induced internalization and desensitization of the apelin receptor. *Mol Cell Endocrinol* 437: 108-119.

211. Zhou N, Fan X, Mukhtar M, Fang J, Patel CA, DuBois GC, and Pomerantz RJ. (2003). Cell-cell fusion and internalization of the CNS-based, HIV-1 co-receptor, APJ. *Virology* 307: 22-36.

212. Masri B, Morin N, Pedebernade L, Knibiehler B, and Audigier Y. (2006). The apelin receptor is coupled to G_{i1} or G_{i2} protein and is differentially desensitized by apelin fragments. *J Biol Chem* 281: 18317-18326.

213. Choe W, Albright A, Sulcove J, Jaffer S, Hesselgesser J, Lavi E, Crino P, and Kolson DL. (2000). Functional expression of the seven-transmembrane HIV-1 co-receptor APJ in neural cells. *J Neurovirol* 6 Suppl 1: S61-69.

214. El Messari S, Iturrioz X, Fassot C, De Mota N, Roesch D, and Llorens-Cortes C. (2004). Functional dissociation of apelin receptor signaling and endocytosis: implications for the effects of apelin on arterial blood pressure. *J Neurochem* 90: 1290-1301.

215. Iturrioz X, Gerbier R, Leroux V, Alvear-Perez R, Maigret B, and Llorens-Cortes C. (2010). By interacting with the C-terminal Phe of apelin, Phe255 and Trp259 in helix VI of the apelin receptor are critical for internalization. *J Biol Chem* 285: 32627-32637.

216. Gerbier R, Leroux V, Couvineau P, Alvear-Perez R, Maigret B, Llorens-Cortes C, and Iturrioz X. (2015). New structural insights into the apelin receptor: identification of key residues for apelin binding. *FASEB J* 29: 314-322.

217. Scott IC, Masri B, D'Amico LA, Jin SW, Jungblut B, Wehman AM, Baier H, Audigier Y, and Stainier DY. (2007). The G protein-coupled receptor *agtrl1b* regulates early development of myocardial progenitors. *Dev Cell* 12: 403-413.

218. Zeng XX, Wilm TP, Sepich DS, and Solnica-Krezel L. (2007). Apelin and its receptor control heart field formation during zebrafish gastrulation. *Dev Cell* 12: 391-402.

219. Charo DN, Ho M, Fajardo G, Kawana M, Kundu RK, Sheikh AY, Finsterbach TP, Leeper NJ, Ernst KV, Chen MM, Ho YD, Chun HJ, Bernstein D, Ashley EA, and Quertermous T. (2009). Endogenous regulation of cardiovascular function by apelin-APJ. *Am J Physiol Heart Circ Physiol* 297: H1904-1913.

220. Paskaradevan S, and Scott IC. (2012). The Aplnr GPCR regulates myocardial progenitor development via a novel cell-non-autonomous, $G_{\alpha i/o}$ protein-independent pathway. *Biol Open* 1: 275-285.

221. Apweiler R, Bairoch A, Wu CH, Barker WC, Boeckmann B, Ferro S, Gasteiger E, Huang H, Lopez R, Magrane M, Martin MJ, Natale DA, O'Donovan C, Redaschi N, and Yeh LS. (2004). UniProt: the universal protein knowledgebase. *Nucleic Acids Res* 32: D115-119.

222. Huang SK, Shin K, Sarker M, and Rainey JK. (2017). Apela exhibits isoform- and headgroup-dependent modulation of micelle binding, peptide conformation and dynamics. *Biochim Biophys Acta* 1859: 767-778.

223. Murza A, Sainsily X, Coquerel D, Cote J, Marx P, Besserer-Offroy E, Longpre JM, Laine J, Reversade B, Salvail D, Leduc R, Dumaine R, Lesur O, Auger-Messier M, Sarret P, and Marsault E. (2016). Discovery and structure-activity relationship of a bioactive fragment of ELABELA that modulates vascular and cardiac functions. *J Med Chem* 59: 2962-2972.

224. Santoso P, Maejima Y, Kumamoto K, Takenoshita S, and Shimomura K. (2015). Central action of ELABELA reduces food intake and activates arginine vasopressin and corticotropin-releasing hormone neurons in the hypothalamic paraventricular nucleus. *Neuroreport* 26: 820-826.

225. Lide DR. (2008). Biochemistry. In: *CRC Handbook of Chemistry and Physics*, edited by Lide DRCRC Press, Boca Raton, FL.

226. Fan X, Zhou N, Zhang X, Mukhtar M, Lu Z, Fang J, DuBois GC, and Pomerantz RJ. (2003). Structural and functional study of the apelin-13 peptide, an endogenous ligand of the HIV-1 coreceptor, APJ. *Biochemistry* 42: 10163-10168.

227. Murza A, Parent A, Besserer-Offroy E, Tremblay H, Karadereye F, Beaudet N, Leduc R, Sarret P, and Marsault E. (2012). Elucidation of the structure-activity relationships of apelin: influence of unnatural amino acids on binding, signaling, and plasma stability. *ChemMedChem* 7: 318-325.

228. Murza A, Besserer-Offroy E, Cote J, Berube P, Longpre JM, Dumaine R, Lesur O, Auger-Messier M, Leduc R, Sarret P, and Marsault E. (2015). C-Terminal modifications of apelin-13 significantly change ligand binding, receptor signaling, and hypotensive action. *J Med Chem* 58: 2431-2440.

229. Murza A, Sainsily X, Cote J, Bruneau-Cossette L, Besserer-Offroy E, Longpre JM, Leduc R, Dumaine R, Lesur O, Auger-Messier M, Sarret P, and Marsault E. (2017). Structure-activity relationship of novel macrocyclic biased apelin receptor agonists. *Org Biomol Chem* 15: 449-458.

230. Bai B, Jiang Y, Cai X, and Chen J. (2014). Dynamics of apelin receptor/G protein coupling in living cells. *Exp Cell Res* 328: 401-409.

231. Yao F, Lv YC, Zhang M, Xie W, Tan YL, Gong D, Cheng HP, Liu D, Li L, Liu XY, Zheng XL, and Tang CK. (2015). Apelin-13 impedes foam cell formation by activating Class III PI3K/Beclin-1-mediated autophagic pathway. *Biochem Biophys Res Commun* 466: 637-643.

232. Moon MJ, Oh DY, Moon JS, Kim DK, Hwang JI, Lee JY, Kim JI, Cho S, Kwon HB, and Seong JY. (2007). Cloning and activation of the bullfrog apelin receptor: $G_{i/o}$ coupling and high affinity for [Pro1]apelin-13. *Mol Cell Endocrinol* 277: 51-60.

233. Bai B, Tang J, Liu H, Chen J, Li Y, and Song W. (2008). Apelin-13 induces ERK1/2 but not p38 MAPK activation through coupling of the human apelin receptor to the G_{i2} pathway. *Acta Biochim Biophys Sin (Shanghai)* 40: 311-318.

234. Read C, Fitzpatrick CM, Yang P, Kuc RE, Maguire JJ, Glen RC, Foster RE, and Davenport AP. (2016). Cardiac action of the first G protein biased small molecule apelin agonist. *Biochem Pharmacol* 116: 63-72.

235. Masri B, Morin N, Cornu M, Knibiehler B, and Audigier Y. (2004). Apelin (65-77) activates p70 S6 kinase and is mitogenic for umbilical endothelial cells. *FASEB J* 18: 1909-1911.

236. Xie H, Tang SY, Cui RR, Huang J, Ren XH, Yuan LQ, Lu Y, Yang M, Zhou HD, Wu XP, Luo XH, and Liao EY. (2006). Apelin and its receptor are expressed in human osteoblasts. *Regul Pept* 134: 118-125.

237. O'Donnell LA, Agrawal A, Sabnekar P, Dichter MA, Lynch DR, and Kolson DL. (2007). Apelin, an endogenous neuronal peptide, protects hippocampal neurons against excitotoxic injury. *J Neurochem* 102: 1905-1917.

238. Smith CC, Mocanu MM, Bowen J, Wynne AM, Simpkin JC, Dixon RA, Cooper MB, and Yellon DM. (2007). Temporal changes in myocardial salvage kinases during reperfusion following ischemia: studies involving the cardioprotective adipocytokine apelin. *Cardiovasc Drugs Ther* 21: 409-414.

239. Tang SY, Xie H, Yuan LQ, Luo XH, Huang J, Cui RR, Zhou HD, Wu XP, and Liao EY. (2007). Apelin stimulates proliferation and suppresses apoptosis of mouse osteoblastic cell line MC3T3-E1 via JNK and PI3-K/Akt signaling pathways. *Peptides* 28: 708-718.

240. Xie H, Yuan LQ, Luo XH, Huang J, Cui RR, Guo LJ, Zhou HD, Wu XP, and Liao EY. (2007). Apelin suppresses apoptosis of human osteoblasts. *Apoptosis* 12: 247-254.

241. Zhang Z, Yu B, and Tao GZ. (2009). Apelin protects against cardiomyocyte apoptosis induced by glucose deprivation. *Chin Med J (Engl)* 122: 2360-2365.

242. Cui RR, Mao DA, Yi L, Wang C, Zhang XX, Xie H, Wu XP, Liao XB, Zhou H, Meng JC, Yuan LQ, and Liao EY. (2010). Apelin suppresses apoptosis of human vascular smooth muscle cells via APJ/PI3-K/Akt signaling pathways. *Amino Acids* 39: 1193-1200.

243. Liu C, Su T, Li F, Li L, Qin X, Pan W, Feng F, Chen F, Liao D, and Chen L. (2010). PI3K/Akt signaling transduction pathway is involved in rat vascular smooth muscle cell proliferation induced by apelin-13. *Acta Biochim Biophys Sin (Shanghai)* 42: 396-402.

244. Yue P, Jin H, Aillaud M, Deng AC, Azuma J, Asagami T, Kundu RK, Reaven GM, Quertermous T, and Tsao PS. (2010). Apelin is necessary for the maintenance of insulin sensitivity. *Am J Physiol Endocrinol Metab* 298: E59-67.

245. Shan PF, Lu Y, Cui RR, Jiang Y, Yuan LQ, and Liao EY. (2011). Apelin attenuates the osteoblastic differentiation of vascular smooth muscle cells. *PLoS One* 6: e17938.

246. Sun X, Iida S, Yoshikawa A, Senbonmatsu R, Imanaka K, Maruyama K, Nishimura S, Inagami T, and Senbonmatsu T. (2011). Non-activated APJ suppresses the angiotensin II type 1 receptor, whereas apelin-activated APJ acts conversely. *Hypertens Res* 34: 701-706.

247. Tao J, Zhu W, Li Y, Xin P, Li J, Liu M, Li J, Redington AN, and Wei M. (2011). Apelin-13 protects the heart against ischemia-reperfusion injury through inhibition of ER-dependent apoptotic pathways in a time-dependent fashion. *Am J Physiol Heart Circ Physiol* 301: H1471-1486.

248. Koguchi W, Kobayashi N, Takeshima H, Ishikawa M, Sugiyama F, and Ishimitsu T. (2012). Cardioprotective effect of apelin-13 on cardiac performance and remodeling in end-stage heart failure. *Circ J* 76: 137-144.

249. Zeng X, Yu SP, Taylor T, Ogle M, and Wei L. (2012). Protective effect of apelin on cultured rat bone marrow mesenchymal stem cells against apoptosis. *Stem Cell Res* 8: 357-367.

250. Modgil A, Guo L, O'Rourke ST, and Sun C. (2013). Apelin-13 inhibits large-conductance Ca^{2+}-activated K^{+} channels in cerebral artery smooth muscle cells via a PI3-kinase dependent mechanism. *PLoS One* 8: e83051.

251. Wang C, Liu N, Luan R, Li Y, Wang D, Zou W, Xing Y, Tao L, Cao F, and Wang H. (2013). Apelin protects sarcoplasmic reticulum function and cardiac performance in ischaemia-reperfusion by attenuating oxidation of sarcoplasmic reticulum Ca^{2+}-ATPase and ryanodine receptor. *Cardiovasc Res* 100: 114-124.

252. Berta J, Hoda MA, Laszlo V, Rozsas A, Garay T, Torok S, Grusch M, Berger W, Paku S, Renyi-Vamos F, Masri B, Tovari J, Groger M, Klepetko W, Hegedus B, and

Dome B. (2014). Apelin promotes lymphangiogenesis and lymph node metastasis. *Oncotarget* 5: 4426-4437.

253. Guo M, Chen F, Lin T, Peng Y, Li W, Zhu X, Lin L, and Chen Y. (2014). Apelin-13 decreases lipid storage in hypertrophic adipocytes *in vitro* through the upregulation of AQP7 expression by the PI3K signaling pathway. *Med Sci Monit* 20: 1345-1352.

254. Than A, Zhang X, Leow MK, Poh CL, Chong SK, and Chen P. (2014). Apelin attenuates oxidative stress in human adipocytes. *J Biol Chem* 289: 3763-3774.

255. Yang X, Zhu W, Zhang P, Chen K, Zhao L, Li J, Wei M, and Liu M. (2014). Apelin-13 stimulates angiogenesis by promoting crosstalk between AMP-activated protein kinase and Akt signaling in myocardial microvascular endothelial cells. *Mol Med Rep* 9: 1590-1596.

256. Busch R, Strohbach A, Pennewitz M, Lorenz F, Bahls M, Busch MC, and Felix SB. (2015). Regulation of the endothelial apelin/APJ system by hemodynamic fluid flow. *Cell Signal* 27: 1286-1296.

257. Liu QF, Yu HW, Sun LL, You L, Tao GZ, and Qu BZ. (2015). Apelin-13 upregulates Egr-1 expression in rat vascular smooth muscle cells through the PI3K/Akt and PKC signaling pathways. *Biochem Biophys Res Commun* 468: 617-621.

258. Luo K, Long H, Xu B, and Luo Y. (2015). Apelin attenuates postburn sepsis via a phosphatidylinositol 3-kinase/protein kinase B dependent mechanism: A randomized animal study. *Int J Surg* 21: 22-27.

259. Wang C, Wen J, Zhou Y, Li L, Cui X, Wang J, Pan L, Ye Z, Liu P, and Wu L. (2015). Apelin induces vascular smooth muscle cells migration via a PI3K/Akt/FoxO3a/MMP-2 pathway. *Int J Biochem Cell Biol* 69: 173-182.

260. Xie F, Liu W, Feng F, Li X, He L, Lv D, Qin X, Li L, Li L, and Chen L. (2015). Apelin-13 promotes cardiomyocyte hypertrophy via PI3K-Akt-ERK1/2-p70S6K and PI3K-induced autophagy. *Acta Biochim Biophys Sin (Shanghai)* 47: 969-980.

261. Yang S, Li H, Tang L, Ge G, Ma J, Qiao Z, Liu H, and Fang W. (2015). Apelin-13 protects the heart against ischemia-reperfusion injury through the RISK-GSK-β-mPTP pathway. *Arch Med Sci* 11: 1065-1073.

262. Li E, Deng H, Wang B, Fu W, You Y, and Tian S. (2016). Apelin-13 exerts antidepressant-like and recognition memory improving activities in stressed rats. *Eur Neuropsychopharmacol* 26: 420-430.

263. Zou Y, Wang B, Fu W, Zhou S, Nie Y, and Tian S. (2016). Apelin-13 protects PC12 cells from corticosterone-induced apoptosis through PI3K and ERKs activation. *Neurochem Res* 41: 1635-1644.

264. Ishimaru Y, Sumino A, Kajioka D, Shibagaki F, Yamamuro A, Yoshioka Y, and Maeda S. (2017). Apelin protects against NMDA-induced retinal neuronal death via an APJ receptor by activating Akt and ERK1/2, and suppressing TNF-α expression in mice. *J Pharmacol Sci* 133: 34-41.

265. Attane C, Daviaud D, Dray C, Dusaulcy R, Masseboeuf M, Prevot D, Carpene C, Castan-Laurell I, and Valet P. (2011). Apelin stimulates glucose uptake but not lipolysis in human adipose tissue *ex vivo*. *J Mol Endocrinol* 46: 21-28.

266. Pchejetski D, Foussal C, Alfarano C, Lairez O, Calise D, Guilbeau-Frugier C, Schaak S, Seguelas MH, Wanecq E, Valet P, Parini A, and Kunduzova O. (2012). Apelin prevents cardiac fibroblast activation and collagen production through inhibition of sphingosine kinase 1. *Eur Heart J* 33: 2360-2369.

267. Xu S, Han P, Huang M, Wu JC, Chang C, Tsao PS, and Yue P. (2012). *In vivo*, *ex vivo*, and *in vitro* studies on apelin's effect on myocardial glucose uptake. *Peptides* 37: 320-326.

268. Dray C, Sakar Y, Vinel C, Daviaud D, Masri B, Garrigues L, Wanecq E, Galvani S, Negre-Salvayre A, Barak LS, Monsarrat B, Burlet-Schiltz O, Valet P, Castan-Laurell I, and Ducroc R. (2013). The intestinal glucose-apelin cycle controls carbohydrate absorption in mice. *Gastroenterology* 144: 771-780.

269. Yang Y, Zhang XJ, Li LT, Cui HY, Zhang C, Zhu CH, and Miao JY. (2016). Apelin-13 protects against apoptosis by activating AMP-activated protein kinase pathway in ischemia stroke. *Peptides* 75: 96-100.

270. Masri B, Lahlou H, Mazarguil H, Knibiehler B, and Audigier Y. (2002). Apelin (65-77) activates extracellular signal-regulated kinases via a PTX-sensitive G protein. *Biochem Biophys Res Commun* 290: 539-545.

271. Li F, Li L, Qin X, Pan W, Feng F, Chen F, Zhu B, Liao D, Tanowitz H, Albanese C, and Chen L. (2008). Apelin-induced vascular smooth muscle cell proliferation: the regulation of cyclin D1. *Front Biosci* 13: 3786-3792.

272. Cook DR, Gleichman AJ, Cross SA, Doshi S, Ho W, Jordan-Sciutto KL, Lynch DR, and Kolson DL. (2011). NMDA receptor modulation by the neuropeptide apelin: implications for excitotoxic injury. *J Neurochem* 118: 1113-1123.

273. Li L, Li L, Xie F, Zhang Z, Guo Y, Tang G, Lv D, Lu Q, Chen L, and Li J. (2013). Jagged-1/Notch3 signaling transduction pathway is involved in apelin-13-induced vascular smooth muscle cells proliferation. *Acta Biochim Biophys Sin (Shanghai)* 45: 875-881.

274. Bai B, Cai X, Jiang Y, Karteris E, and Chen J. (2014). Heterodimerization of apelin receptor and neurotensin receptor 1 induces phosphorylation of ERK(1/2) and cell proliferation via $G_{\alpha q}$-mediated mechanism. *J Cell Mol Med* 18: 2071-2081.

275. Perjes A, Skoumal R, Tenhunen O, Konyi A, Simon M, Horvath IG, Kerkela R, Ruskoaho H, and Szokodi I. (2014). Apelin increases cardiac contractility via protein kinase Cε- and extracellular signal-regulated kinase-dependent mechanisms. *PLoS One* 9: e93473.

276. Yang L, Su T, Lv D, Xie F, Liu W, Cao J, Sheikh IA, Qin X, Li L, and Chen L. (2014). ERK1/2 mediates lung adenocarcinoma cell proliferation and autophagy induced by apelin-13. *Acta Biochim Biophys Sin (Shanghai)* 46: 100-111.

277. Peng X, Li F, Wang P, Jia S, Sun L, and Huo H. (2015). Apelin-13 induces MCF-7 cell proliferation and invasion via phosphorylation of ERK1/2. *Int J Mol Med* 36: 733-738.

278. Huang Q, Liu X, Cao C, Lei J, Han D, Chen G, Yu J, Chen L, Lv D, and Li Z. (2016). Apelin-13 induces autophagy in hepatoma HepG2 cells through ERK1/2 signaling pathway-dependent upregulation of Beclin1. *Oncol Lett* 11: 1051-1056.

279. Shin K, Chapman NA, Sarker M, Kenward C, Huang SK, Weatherbee-Martin N, Pandey A, Dupre DJ, and Rainey JK. (2017). Bioactivity of the putative apelin proprotein expands the repertoire of apelin receptor ligands. *Biochim Biophys Acta* 1861: 1901-1912.

280. Hashimoto T, Kihara M, Ishida J, Imai N, Yoshida S, Toya Y, Fukamizu A, Kitamura H, and Umemura S. (2006). Apelin stimulates myosin light chain

phosphorylation in vascular smooth muscle cells. *Arterioscler Thromb Vasc Biol* 26: 1267-1272.

281. Wang C, Du JF, Wu F, and Wang HC. (2008). Apelin decreases the SR Ca^{2+} content but enhances the amplitude of $[Ca^{2+}]_i$ transient and contractions during twitches in isolated rat cardiac myocytes. *Am J Physiol Heart Circ Physiol* 294: H2540-2546.

282. Chamberland C, Barajas-Martinez H, Haufe V, Fecteau MH, Delabre JF, Burashnikov A, Antzelevitch C, Lesur O, Chraibi A, Sarret P, and Dumaine R. (2010). Modulation of canine cardiac sodium current by apelin. *J Mol Cell Cardiol* 48: 694-701.

283. Liu XY, Lu Q, Ouyang XP, Tang SL, Zhao GJ, Lv YC, He PP, Kuang HJ, Tang YY, Fu Y, Zhang DW, and Tang CK. (2013). Apelin-13 increases expression of ATP-binding cassette transporter A1 via activating protein kinase C α signaling in THP-1 macrophage-derived foam cells. *Atherosclerosis* 226: 398-407.

284. Zou MX, Liu HY, Haraguchi Y, Soda Y, Tatemoto K, and Hoshino H. (2000). Apelin peptides block the entry of human immunodeficiency virus (HIV). *FEBS Lett* 473: 15-18.

285. Cox CM, D'Agostino SL, Miller MK, Heimark RL, and Krieg PA. (2006). Apelin, the ligand for the endothelial G-protein-coupled receptor, APJ, is a potent angiogenic factor required for normal vascular development of the frog embryo. *Dev Biol* 296: 177-189.

286. Zeng XJ, Yu SP, Zhang L, and Wei L. (2010). Neuroprotective effect of the endogenous neural peptide apelin in cultured mouse cortical neurons. *Exp Cell Res* 316: 1773-1783.

287. Alastalo TP, Li M, Perez Vde J, Pham D, Sawada H, Wang JK, Koskenvuo M, Wang L, Freeman BA, Chang HY, and Rabinovitch M. (2011). Disruption of PPARγ/β-catenin-mediated regulation of apelin impairs BMP-induced mouse and human pulmonary arterial EC survival. *J Clin Invest* 121: 3735-3746.

288. Wang XL, Tao Y, Lu Q, and Jiang YR. (2012). Apelin supports primary rat retinal Muller cells under chemical hypoxia and glucose deprivation. *Peptides* 33: 298-306.

289. Lu Q, Jiang YR, Qian J, and Tao Y. (2013). Apelin-13 regulates proliferation, migration and survival of retinal Muller cells under hypoxia. *Diabetes Res Clin Pract* 99: 158-167.

290. Wattanachanya L, Lu WD, Kundu RK, Wang L, Abbott MJ, O'Carroll D, Quertermous T, and Nissenson RA. (2013). Increased bone mass in mice lacking the adipokine apelin. *Endocrinology* 154: 2069-2080.

291. Chen L, Tao Y, Feng J, and Jiang YR. (2015). Apelin protects primary rat retinal pericytes from chemical hypoxia-induced apoptosis. *J Ophthalmol* 2015: 186946.

292. Hamada J, Baasanjav A, Ono N, Murata K, Kako K, Ishida J, and Fukamizu A. (2015). Possible involvement of downregulation of the apelin-APJ system in doxorubicin-induced cardiotoxicity. *Am J Physiol Heart Circ Physiol* 308: H931-941.

293. Yang F, Bai Y, and Jiang Y. (2015). Effects of apelin on RAW264.7 cells under both normal and hypoxic conditions. *Peptides* 69: 133-143.

294. Zhou Y, Deng L, Zhao D, Chen L, Yao Z, Guo X, Liu X, Lv L, Leng B, Xu W, Qiao G, and Shan H. (2016). MicroRNA-503 promotes angiotensin II-induced cardiac fibrosis by targeting Apelin-13. *J Cell Mol Med* 20: 495-505.

295. Hou J, Zhong T, Guo T, Miao C, Zhou C, Long H, Wu H, Zheng S, Wang L, and Wang T. (2017). Apelin promotes mesenchymal stem cells survival and vascularization under hypoxic-ischemic condition *in vitro* involving the upregulation of vascular endothelial growth factor. *Exp Mol Pathol* 102: 203-209.

296. Jeong K, Oh Y, Kim SJ, Kim H, Park KC, Kim SS, Ha J, Kang I, and Choe W. (2014). Apelin is transcriptionally regulated by ER stress-induced ATF4 expression via a p38 MAPK-dependent pathway. *Apoptosis* 19: 1399-1410.

297. Han S, Wang G, Qiu S, de la Motte C, Wang HQ, Gomez G, Englander EW, and Greeley GH, Jr. (2007). Increased colonic apelin production in rodents with experimental colitis and in humans with IBD. *Regul Pept* 142: 131-137.

298. Hashimoto T, Kihara M, Imai N, Yoshida S, Shimoyamada H, Yasuzaki H, Ishida J, Toya Y, Kiuchi Y, Hirawa N, Tamura K, Yazawa T, Kitamura H, Fukamizu A, and Umemura S. (2007). Requirement of apelin-apelin receptor system for oxidative stress-linked atherosclerosis. *Am J Pathol* 171: 1705-1712.

299. Kunduzova O, Alet N, Delesque-Touchard N, Millet L, Castan-Laurell I, Muller C, Dray C, Schaeffer P, Herault JP, Savi P, Bono F, and Valet P. (2008). Apelin/APJ signaling system: a potential link between adipose tissue and endothelial angiogenic processes. *FASEB J* 22: 4146-4153.

300. Berta J, Kenessey I, Dobos J, Tovari J, Klepetko W, Jan Ankersmit H, Hegedus B, Renyi-Vamos F, Varga J, Lorincz Z, Paku S, Ostoros G, Rozsas A, Timar J, and Dome B. (2010). Apelin expression in human non-small cell lung cancer: role in angiogenesis and prognosis. *J Thorac Oncol* 5: 1120-1129.

301. Yu QC, Hirst CE, Costa M, Ng ES, Schiesser JV, Gertow K, Stanley EG, and Elefanty AG. (2012). Apelin promotes hematopoiesis from human embryonic stem cells. *Blood* 119: 6243-6254.

302. Qin D, Zheng XX, and Jiang YR. (2013). Apelin-13 induces proliferation, migration, and collagen I mRNA expression in human RPE cells via PI3K/Akt and MEK/Erk signaling pathways. *Mol Vis* 19: 2227-2236.

303. Samura M, Morikage N, Suehiro K, Tanaka Y, Nakamura T, Nishimoto A, Ueno K, Hosoyama T, and Hamano K. (2016). Combinatorial treatment with apelin-13 enhances the therapeutic efficacy of a preconditioned cell-based therapy for peripheral ischemia. *Sci Rep* 6: 19379.

304. Hoffmann M, Fiedor E, and Ptak A. (2017). Bisphenol A and its derivatives tetrabromobisphenol A and tetrachlorobisphenol A induce apelin expression and secretion in ovarian cancer cells through a peroxisome proliferator-activated receptor gamma-dependent mechanism. *Toxicol Lett* 269: 15-22.

305. Kalin RE, Kretz MP, Meyer AM, Kispert A, Heppner FL, and Brandli AW. (2007). Paracrine and autocrine mechanisms of apelin signaling govern embryonic and tumor angiogenesis. *Dev Biol* 305: 599-614.

306. Kojima Y, Kundu RK, Cox CM, Leeper NJ, Anderson JA, Chun HJ, Ali ZA, Ashley EA, Krieg PA, and Quertermous T. (2010). Upregulation of the apelin-APJ pathway promotes neointima formation in the carotid ligation model in mouse. *Cardiovasc Res* 87: 156-165.

307. Liu QF, Yu HW, You L, Liu MX, Li KY, and Tao GZ. (2013). Apelin-13-induced proliferation and migration induced of rat vascular smooth muscle cells is mediated by the upregulation of Egr-1. *Biochem Biophys Res Commun* 439: 235-240.

308. Lv D, Li L, Lu Q, Li Y, Xie F, Li H, Cao J, Liu M, Wu D, He L, and Chen L. (2016). PAK1-cofilin phosphorylation mediates human lung adenocarcinoma cells migration induced by apelin-13. *Clin Exp Pharmacol Physiol* 43: 569-579.

309. Izgut-Uysal VN, Gemici B, Birsen I, Acar N, and Ustunel I. (2017). The effect of apelin on the functions of peritoneal macrophages. *Physiol Res* 66: 489-496.

310. Ho L, Tan SY, Wee S, Wu Y, Tan SJ, Ramakrishna NB, Chng SC, Nama S, Szczerbinska I, Chan YS, Avery S, Tsuneyoshi N, Ng HH, Gunaratne J, Dunn NR, and Reversade B. (2015). ELABELA is an endogenous growth factor that sustains hESC self-renewal via the PI3K/AKT pathway. *Cell Stem Cell* 17: 435-447.

311. Trzaskowski B, Latek D, Yuan S, Ghoshdastider U, Debinski A, and Filipek S. (2012). Action of molecular switches in GPCRs--theoretical and experimental studies. *Curr Med Chem* 19: 1090-1109.

312. Hulme EC. (2013). GPCR activation: a mutagenic spotlight on crystal structures. *Trends Pharmacol Sci* 34: 67-84.

313. Pitkin SL, Maguire JJ, Bonner TI, and Davenport AP. (2010). International Union of Basic and Clinical Pharmacology. LXXIV. Apelin receptor nomenclature, distribution, pharmacology, and function. *Pharmacol Rev* 62: 331-342.

314. Nakayama K. (1997). Furin: a mammalian subtilisin/Kex2p-like endoprotease involved in processing of a wide variety of precursor proteins. *Biochem J* 327: 625-635.

315. Seidah NG. (2011). The proprotein convertases, 20 years later. *Methods Mol Biol* 768: 23-57.

316. Thomas G. (2002). Furin at the cutting edge: from protein traffic to embryogenesis and disease. *Nat Rev Mol Cell Biol* 3: 753-766.

317. Shinde U, and Thomas G. (2011). Insights from bacterial subtilases into the mechanisms of intramolecular chaperone-mediated activation of furin. *Methods Mol Biol* 768: 59-106.

318. Brakch N, Rholam M, Boussetta H, and Cohen P. (1993). Role of β-turn in proteolytic processing of peptide hormone precursors at dibasic sites. *Biochemistry* 32: 4925-4930.

319. Beaubien G, Schafer MK, Weihe E, Dong W, Chretien M, Seidah NG, and Day R. (1995). The distinct gene expression of the pro-hormone convertases in the rat heart suggests potential substrates. *Cell Tissue Res* 279: 539-549.

320. Enomoto T, Shibata R, Ohashi K, Kambara T, Kataoka Y, Uemura Y, Yuasa D, Murohara T, and Ouchi N. (2012). Regulation of adipolin/CTRP12 cleavage by obesity. *Biochem Biophys Res Commun* 428: 155-159.

321. Paroutis P, Touret N, and Grinstein S. (2004). The pH of the secretory pathway: measurement, determinants, and regulation. *Physiology (Bethesda)* 19: 207-215.

322. Molloy SS, Bresnahan PA, Leppla SH, Klimpel KR, and Thomas G. (1992). Human furin is a calcium-dependent serine endoprotease that recognizes the sequence Arg-X-X-Arg and efficiently cleaves anthrax toxin protective antigen. *J Biol Chem* 267: 16396-16402.

323. Rholam M, and Fahy C. (2009). Processing of peptide and hormone precursors at the dibasic cleavage sites. *Cell Mol Life Sci* 66: 2075-2091.

324. Scamuffa N, Basak A, Lalou C, Wargnier A, Marcinkiewicz J, Siegfried G, Chretien M, Calvo F, Seidah NG, and Khatib AM. (2008). Regulation of prohepcidin processing and activity by the subtilisin-like proprotein convertases Furin, PC5, PACE4 and PC7. *Gut* 57: 1573-1582.

325. Jean F, Basak A, Rondeau N, Benjannet S, Hendy GN, Seidah NG, Chretien M, and Lazure C. (1993). Enzymic characterization of murine and human prohormone convertase-1 (mPC1 and hPC1) expressed in mammalian GH4C1 cells. *Biochem J* 292: 891-900.

326. Remacle AG, Shiryaev SA, Oh ES, Cieplak P, Srinivasan A, Wei G, Liddington RC, Ratnikov BI, Parent A, Desjardins R, Day R, Smith JW, Lebl M, and Strongin AY. (2008). Substrate cleavage analysis of furin and related proprotein convertases. A comparative study. *J Biol Chem* 283: 20897-20906.

327. Siegfried G, Basak A, Cromlish JA, Benjannet S, Marcinkiewicz J, Chretien M, Seidah NG, and Khatib AM. (2003). The secretory proprotein convertases furin, PC5, and PC7 activate VEGF-C to induce tumorigenesis. *J Clin Invest* 111: 1723-1732.

328. Artenstein AW, and Opal SM. (2011). Proprotein convertases in health and disease. *N Engl J Med* 365: 2507-2518.

329. Langelaan DN, and Rainey JK. (2009). Headgroup-dependent membrane catalysis of apelin-receptor interactions is likely. *J Phys Chem B* 113: 10465-10471.

330. Sargent DF, and Schwyzer R. (1986). Membrane lipid phase as catalyst for peptide-receptor interactions. *Proc Natl Acad Sci U S A* 83: 5774-5778.

331. Gill SC, and von Hippel PH. (1989). Calculation of protein extinction coefficients from amino acid sequence data. *Anal Biochem* 182: 319-326.

332. Remacle AG, Gawlik K, Golubkov VS, Cadwell GW, Liddington RC, Cieplak P, Millis SZ, Desjardins R, Routhier S, Yuan XW, Neugebauer WA, Day R, and Strongin AY. (2010). Selective and potent furin inhibitors protect cells from anthrax without significant toxicity. *Int J Biochem Cell Biol* 42: 987-995.

333. Skidgel RA, Davis RM, and Tan F. (1989). Human carboxypeptidase M. Purification and characterization of a membrane-bound carboxypeptidase that cleaves peptide hormones. *J Biol Chem* 264: 2236-2241.

334. Tipnis SR, Hooper NM, Hyde R, Karran E, Christie G, and Turner AJ. (2000). A human homolog of angiotensin-converting enzyme. Cloning and functional expression as a captopril-insensitive carboxypeptidase. *J Biol Chem* 275: 33238-33243.

335. Japp AG, Cruden NL, Amer DA, Li VK, Goudie EB, Johnston NR, Sharma S, Neilson I, Webb DJ, Megson IL, Flapan AD, and Newby DE. (2008). Vascular effects of apelin *in vivo* in man. *J Am Coll Cardiol* 52: 908-913.

336. Kuipers BJ, and Gruppen H. (2007). Prediction of molar extinction coefficients of proteins and peptides using UV absorption of the constituent amino acids at 214 nm to enable quantitative reverse phase high-performance liquid chromatography-mass spectrometry analysis. *J Agric Food Chem* 55: 5445-5451.

337. Delaglio F, Grzesiek S, Vuister GW, Zhu G, Pfeifer J, and Bax A. (1995). NMRPipe: a multidimensional spectral processing system based on UNIX pipes. *J Biomol NMR* 6: 277-293.

338. Vranken WF, Boucher W, Stevens TJ, Fogh RH, Pajon A, Llinas M, Ulrich EL, Markley JL, Ionides J, and Laue ED. (2005). The CCPN data model for NMR spectroscopy: development of a software pipeline. *Proteins* 59: 687-696.

339. Castan-Laurell I, Dray C, Attane C, Duparc T, Knauf C, and Valet P. (2011). Apelin, diabetes, and obesity. *Endocrine* 40: 1-9.

340. Brahms S, Brahms J, Spach G, and Brack A. (1977). Identification of β,β-turns and unordered conformations in polypeptide chains by vacuum ultraviolet circular dichroism. *Proc Natl Acad Sci U S A* 74: 3208-3212.

341. Ulrich EL, Akutsu H, Doreleijers JF, Harano Y, Ioannidis YE, Lin J, Livny M, Mading S, Maziuk D, Miller Z, Nakatani E, Schulte CF, Tolmie DE, Kent Wenger R, Yao H, and Markley JL. (2008). BioMagResBank. *Nucleic Acids Res* 36: D402-408.

342. Bai Y, Milne JS, Mayne L, and Englander SW. (1993). Primary structure effects on peptide group hydrogen exchange. *Proteins* 17: 75-86.

343. Langelaan DN, Ngweniform P, and Rainey JK. (2011). Biophysical characterization of G-protein coupled receptor-peptide ligand binding. *Biochem Cell Biol* 89: 98-105.

344. Zimmerman SS, and Scheraga HA. (1976). Stability of *cis*, *trans*, and nonplanar peptide groups. *Macromolecules* 9: 408-416.

345. Schwarzinger S, Kroon GJ, Foss TR, Wright PE, and Dyson HJ. (2000). Random coil chemical shifts in acidic 8 M urea: implementation of random coil shift data in NMRView. *J Biomol NMR* 18: 43-48.

346. Lide DR. (2008). Fluid Properties. In: *CRC Handbook of Chemistry and Physics*, edited by Lide DRCRC Press, Boca Raton, FL, p. 6-4.

347. Dyson HJ, and Wright PE. (2005). Intrinsically unstructured proteins and their functions. *Nat Rev Mol Cell Biol* 6: 197-208.

348. Manglik A, Kim TH, Masureel M, Altenbach C, Yang Z, Hilger D, Lerch MT, Kobilka TS, Thian FS, Hubbell WL, Prosser RS, and Kobilka BK. (2015). Structural insights into the dynamic process of β2-adrenergic receptor signaling. *Cell* 161: 1101-1111.

349. Staus DP, Strachan RT, Manglik A, Pani B, Kahsai AW, Kim TH, Wingler LM, Ahn S, Chatterjee A, Masoudi A, Kruse AC, Pardon E, Steyaert J, Weis WI, Prosser RS, Kobilka BK, Costa T, and Lefkowitz RJ. (2016). Allosteric nanobodies reveal the dynamic range and diverse mechanisms of G-protein-coupled receptor activation. *Nature* 535: 448-452.

350. Langelaan DN, and Rainey JK. (2010). Membrane catalysis of peptide-receptor binding. *Biochem Cell Biol* 88: 203-210.

351. van Meer G, Voelker DR, and Feigenson GW. (2008). Membrane lipids: where they are and how they behave. *Nat Rev Mol Cell Biol* 9: 112-124.

352. Thomas S, Preda-Pais A, Casares S, and Brumeanu TD. (2004). Analysis of lipid rafts in T cells. *Mol Immunol* 41: 399-409.

353. Korade Z, and Kenworthy AK. (2008). Lipid rafts, cholesterol, and the brain. *Neuropharmacology* 55: 1265-1273.

354. Honke K. (2013). Biosynthesis and biological function of sulfoglycolipids. *Proc Jpn Acad Ser B Phys Biol Sci* 89: 129-138.

355. Patterson RE, Weatherbee-Martin N, and Rainey JK. (2017). Pyrene-apelin conjugation modulates fluorophore- and peptide-micelle interactions. *J Phys Chem B* 121: 4768-4777.

356. Lipfert J, Columbus L, Chu VB, Lesley SA, and Doniach S. (2007). Size and shape of detergent micelles determined by small-angle X-ray scattering. *J Phys Chem B* 111: 12427-12438.

357. Anachkov SE, Danov KD, Basheva ES, Kralchevsky PA, and Ananthapadmanabhan KP. (2012). Determination of the aggregation number and charge of ionic surfactant micelles from the stepwise thinning of foam films. *Adv Colloid Interface Sci* 183-184: 55-67.

358. Becher P. (1961). Nonionic surface-active compounds IV. Micelle formation by polyoxyethylene alkanols and alkyl phenols in aqueous solution. *J Colloid Sci* 16: 49-56.

359. Palmer AG, Cavanagh J, Wright PE, and Rance M. (1991). Sensitivity improvement in proton-detected two-dimensional heteronuclear correlation NMR spectroscopy. *J Magn Reson* 93: 151-170.

360. Kay LE, Keifer P, and Saarinen T. (1992). Pure absorption gradient enhanced heteronuclear single quantum correlation spectroscopy with improved sensitivity. *J Am Chem Soc* 114: 10663-10665.

361. Schleucher J, Schwendinger M, Sattler M, Schmidt P, Schedletzky O, Glaser SJ, Sorensen OW, and Griesinger C. (1994). A general enhancement scheme in heteronuclear multidimensional NMR employing pulsed field gradients. *J Biomol NMR* 4: 301-306.

362. Grzesiek S, and Bax A. (1993). The importance of not saturating H_2O in protein NMR - application to sensitivity enhancement and NOE measurements. *J Am Chem Soc* 115: 12593-12594.

363. Stilbs P. (1982). Fourier transform NMR pulsed-gradient spin—echo (FT-PGSE) self-diffusion measurements of solubilization equilibria in SDS solutions. *J Colloid Interface Sci* 87: 385-394.

364. Toth G, and Madarasz A. (2006). Structure of BRIJ-35 nonionic surfactant in water: a reverse Monte Carlo study. *Langmuir* 22: 590-597.

365. Jönsson B, Wennerström H, Nilsson PG, and Linse P. (1986). Self-diffusion of small molecules in colloidal systems. *Colloid Polym Sci* 264: 77-88.

366. Kleckner IR, and Foster MP. (2011). An introduction to NMR-based approaches for measuring protein dynamics. *Biochim Biophys Acta* 1814: 942-968.

367. Tusnady GE, Dosztanyi Z, and Simon I. (2005). TMDET: web server for detecting transmembrane regions of proteins by using their 3D coordinates. *Bioinformatics* 21: 1276-1277.

368. Takahashi S, Kasai K, Hatsuzawa K, Kitamura N, Misumi Y, Ikehara Y, Murakami K, and Nakayama K. (1993). A mutation of furin causes the lack of precursor-processing activity in human colon carcinoma LoVo cells. *Biochem Biophys Res Commun* 195: 1019-1026.

369. Hagn F, Etzkorn M, Raschle T, and Wagner G. (2013). Optimized phospholipid bilayer nanodiscs facilitate high-resolution structure determination of membrane proteins. *J Am Chem Soc* 135: 1919-1925.

370. Susac L, Horst R, and Wuthrich K. (2014). Solution-NMR characterization of outer-membrane protein A from *E. coli* in lipid bilayer nanodiscs and detergent micelles. *Chembiochem* 15: 995-1000.

371. Ding Y, Fujimoto LM, Yao Y, Plano GV, and Marassi FM. (2015). Influence of the lipid membrane environment on structure and activity of the outer membrane protein Ail from *Yersinia pestis*. *Biochim Biophys Acta* 1848: 712-720.

372. Nicolson GL. (2014). The fluid-mosaic model of membrane structure: still relevant to understanding the structure, function and dynamics of biological membranes after more than 40 years. *Biochim Biophys Acta* 1838: 1451-1466.

373. Dahms SO, Creemers JW, Schaub Y, Bourenkov GP, Zogg T, Brandstetter H, and Than ME. (2016). The structure of a furin-antibody complex explains non-competitive inhibition by steric exclusion of substrate conformers. *Sci Rep* 6: 34303.

374. Johnson CS. (1999). Diffusion ordered nuclear magnetic resonance spectroscopy: principles and applications. *Prog Nucl Mag Res Sp* 34: 203-256.

APPENDIX A H_N, H_α, H_β, H_δ, H_γ, N, C', C_α, C_β chemical shifts (ppm) of apelin isoforms at indicated conditions

Table A.1: H_N, H_α, H_β, H_δ, H_γ, N, C', C_α, C_β chemical shifts (ppm) of apelin-55 for all potential conformers at 37 °C

Residue	H_N	N	C'	C_α	C_β	H_α	H_β	H_δ	H_γ	Comments
0Ser	**-**	**-**	**-**	**-**	**-**	**-**	**-**	**-**	**-**	No assignable peaks
1Gly	**-**	**-**	**173.87**	**45.33**	**-**	**-**	**-**	**-**	**-**	Coming from **2Ser**
2Ser	**8.27**	**115.69**	**174.35**	**58.28**	**64.03**	**4.49**	**3.86**	**-**	**-**	-
3?Leu #1	8.31	122.55	173.93	53.07	41.22	4.82	1.62	-	-	-
3?Leu #2	8.21	124.46	175.69	55.35	42.60	4.36	1.61	-	-	-
3Leu	**8.29**	**124.09**	**176.94**	**55.28**	**42.40**	**4.39**	**1.63**	**0.92**	**-**	-
4?Met #1	7.82	119.52	174.62	52.93	34.09	4.57	1.93	-	2.49	-
4?Met #2	8.24	122.30	173.93	53.09	33.00	4.81	1.96	-	2.58	-
4Met	**8.20**	**122.19**	**173.92**	**53.15**	**32.54**	**4.80**	**1.95, 2.06**	**-**	**2.58**	-
5?Pro #1	-	-	175.66	63.18	-	-	-	-	-	Coming from 6?Leu #1 No assignable C_β peak
5?Pro #2	-	-	175.77	62.64	34.50	-	-	-	-	Coming from 6?Leu #2
5Pro	**-**	**-**	**176.48**	**63.00**	**32.04**	**-**	**-**	**-**	**-**	Coming from **6Leu**
6?Leu #1	7.92	121.42	175.87	52.88	43.12	4.33	1.60	-	-	-
6?Leu #2	8.39	123.05	175.78	53.43	41.68	4.58	1.63	-	-	-
6Leu	**8.22**	**123.45**	**175.66**	**52.97**	**41.94**	**4.63**	**1.60**	**0.96**	**-**	-
7?Pro #1	-	-	175.82	63.47	31.97	-	-	-	-	Coming from 8?Asp #1
7Pro	**-**	**-**	**176.66**	**63.42**	**32.01**	**-**	**-**	**-**	**-**	Coming from **8Asp**
8?Asp #1	8.25	119.34	176.86	54.33	44.06	-	-	-	-	No assignable TOCSY peaks
8Asp	**8.25**	**119.86**	**176.85**	**54.34**	**41.42**	**4.60**	**2.69**	**-**	**-**	-

9?Gly #1	8.20	108.86	174.01	45.64	-	3.98	-	-	-	-
9?Gly #2	8.15	108.81	173.10	45.52	-	3.94	-	-	-	-
9Gly	**8.26**	**108.94**	**174.29**	**45.71**	**-**	**3.98**	**-**	**-**	**-**	-
10?Asn #1	7.94	124.01	174.17	54.93	41.03	4.54	2.73, 2.83	-	-	-
10Asn	**8.37**	**118.55**	**175.78**	**53.51**	**39.19**	**4.73**	**2.83**	**-**	**-**	-
11Gly	**8.46**	**109.15**	**174.20**	**45.69**	**-**	**3.97**	**-**	**-**	**-**	-
12?Leu #1	8.18	121.31	177.62	55.41	42.58	-	1.62	-	-	-
12?Leu #2	8.25	120.17	176.85	54.50	41.57	-	-	-	-	No assignable TOCSY peaks
12Leu	**8.04**	**121.20**	**177.56**	**55.32**	**42.50**	**4.38**	**1.64**	**-**	**-**	-
13?Glu #1	8.49	121.18	176.27	56.78	30.17	4.30	1.95, 2.07	-	2.25	Connect to 12?Leu #1
13Glu	**8.45**	**121.08**	**176.27**	**56.77**	**30.15**	**4.31**	**1.95, 2.07**	**-**	**2.26**	-
14Asp	**8.23**	**121.18**	**176.93**	**54.52**	**41.41**	**4.59**	**2.70**	**-**	**-**	-
15?Gly #1	8.40	108.95	174.34	45.73	-	3.95	-	-	-	-
15Gly	**8.35**	**109.01**	**174.42**	**45.88**	**-**	**3.95**	**-**	**-**	**-**	-
16Asn	**8.32**	**118.63**	**175.54**	**53.62**	**38.92**	**4.71**	**2.82**	**-**	**-**	-
17Val	**7.91**	**119.14**	**176.16**	**62.80**	**32.43**	**4.07**	**2.11**	**-**	**0.90**	-
18Arg	**8.20**	**122.94**	**176.05**	**56.40**	**30.65**	**4.28**	**1.74**	**3.17**	**1.58**	-
19His	**8.24**	**119.39**	**174.63**	**55.80**	**29.90**	**4.47**	**-**	**-**	**-**	-
20Leu	**8.10**	**123.01**	**176.96**	**55.40**	**42.47**	**4.36**	**1.61**	**-**	**-**	-
21?Val #1	7.94	121.09	174.99	62.35	32.78	4.10	2.04	-	0.92	-
21Val	**8.03**	**120.87**	**175.72**	**62.26**	**32.70**	**4.11**	**2.05**	**-**	**0.92**	-
22?Gln #1	8.06	122.73	174.31	53.29	30.04	4.46	1.86	-	2.33	Connected to 21?Val #1
22?Gln #2	8.30	124.77	173.85	53.61	29.12	4.62	2.07	-	2.33	-
22?Gln #3	8.48	121.84	176.21	57.49	29.87	-	-	-	-	No assignable TOCSY peaks
22Gln	**8.31**	**124.89**	**173.87**	**53.60**	**29.12**	**4.62**	**1.92**	**-**	**2.36**	-
23Pro	**-**	**-**	**176.97**	**63.26**	**32.15**	**-**	**-**	**-**	**-**	Coming from **24Arg**

24Arg	**8.41**	**121.33**	**176.94**	**56.50**	**30.77**	**4.32**	**1.90**	**3.20**	**1.66**	-
25Gly	**8.39**	**109.94**	**174.09**	**45.35**	**-**	**3.99**	**-**	**-**	**-**	-
26?Ser #1	8.13	115.36	174.34	58.44	64.16	-	-	-	-	No distinct TOCSY peaks compared to 26Ser
26Ser	**8.14**	**115.42**	**174.74**	**58.44**	**64.07**	**4.46**	**3.87**	**-**	**-**	-
27?Arg #1	8.32	122.49	175.07	56.11	30.96	4.40	1.74	-	-	Connected to 26?Ser #1
27Arg	**8.38**	**122.57**	**175.95**	**56.28**	**30.68**	**4.55**	**1.72**	**-**	**-**	-
28?Asn #1	7.99	124.83	174.12	54.90	40.74	4.50	2.71, 2.84	-	-	Connected to 27?Arg #1
28?Asn #2	7.91	124.39	174.17	54.78	40.81	-	-	-	-	No assignable TOCSY peaks
28Asn	**8.33**	**119.15**	**175.18**	**53.26**	**39.33**	**4.77**	**2.70**	**-**	**-**	-
29Gly	**8.10**	**109.16**	**176.89**	**44.74**	**-**	**4.13**	**-**	**-**	**-**	-
30?Pro #1	-	-	177.10	63.47	32.39	-	-	-	-	Coming from 31?Gly #1
30Pro	**-**	**-**	**177.28**	**63.36**	**32.37**	**-**	**-**	**-**	**-**	Coming from **31Gly**
31?Gly #1	8.07	109.44	177.18	43.27	-	3.30, 2.83	-	-	-	-
31Gly	**8.14**	**108.77**	**177.31**	**44.63**	**-**	**3.88, 4.03**	**-**	**-**	**-**	-
32?Pro #1	-	-	176.88	63.49	31.83	-	-	-	-	Coming from 33?Trp #1
32?Pro #2	-	-	176.88	63.49	-	-	-	-	-	Coming from 33?Trp #2
32Pro	**-**	**-**	**176.88**	**63.48**	**31.84**	**-**	**-**	**-**	**-**	No assignable C_β peak Coming from **33Trp**
33?Trp #1	8.07	120.63	176.56	57.50	29.15	4.69	3.29	-	-	-
33?Trp #2	7.98	120.14	176.57	57.48	29.07	4.67	3.29	-	-	-
33Trp	**8.02**	**120.51**	**176.55**	**57.46**	**29.09**	**4.68**	**3.29**	**-**	**-**	-
34?Gln #1	8.07	122.51	176.15	56.09	29.21	4.25	2.18	-	-	-
34Gln	**8.10**	**122.52**	**176.16**	**56.07**	**29.28**	**4.25**	**2.02, 2.18**	**-**	**-**	-
35Gly	**7.68**	**108.61**	**174.55**	**45.55**	**-**	**3.81**	**-**	**-**	**-**	-
36Gly	**8.14**	**108.42**	**174.24**	**45.38**	**-**	**3.95**	**-**	**-**	**-**	-
37Arg	**8.16**	**120.36**	**176.41**	**56.33**	**30.77**	**4.31**	**1.78**	**-**	**-**	-

38Arg	**8.26**	**121.86**	**176.04**	**56.31**	**30.81**	**4.78**	**1.96, 2.11**	**2.60**	**1.70**	-
39Lys	**8.17**	**122.11**	**176.01**	**56.35**	**33.08**	**4.76**	**1.65**	**-**	**-**	-
40Phe	**8.15**	**121.18**	**175.35**	**57.55**	**39.87**	**-**	**2.99, 3.11**	**-**	**-**	-
41Arg	**8.22**	**123.34**	**175.67**	**55.94**	**31.15**	**-**	**1.73**	**-**	**-**	-
42Arg	**8.35**	**122.65**	**176.06**	**56.20**	**30.94**	**-**	**1.72, 1.97**	**-**	**-**	-
43Gln	**8.42**	**122.07**	**175.57**	**55.76**	**29.77**	**4.35**	**1.98**	**-**	**-**	-
44Arg	**8.41**	**123.86**	**174.14**	**54.16**	**30.10**	**-**	**1.69, 1.86**	**3.23**	**-**	-
45Pro	**-**	**-**	**176.59**	**63.20**	**32.19**	**-**	**-**	**-**	**-**	Coming from **46Arg**
46Arg	**8.40**	**121.51**	**176.22**	**56.26**	**30.77**	**4.32**	**1.65**	**-**	**-**	-
47Leu	**8.25**	**123.52**	**177.11**	**55.10**	**42.56**	**4.41**	**1.61**	**-**	**-**	-
48Ser	**8.24**	**116.36**	**174.24**	**58.15**	**64.01**	**-**	**3.82**	**-**	**-**	-
49His	**-**	**-**	**-**	**-**	**-**	**-**	**-**	**-**	**-**	-
50?Lys #1	-	-	176.35	56.30	33.26	-	-	-	-	Coming from 51?Gly #1
50?Lys #2	-	-	176.23	56.26	33.25	-	-	-	-	Coming from 51?Gly #2
50Lys	**-**	**-**	**176.33**	**56.26**	**33.22**	**-**	**-**	**-**	**-**	Coming from **51Gly**
51?Gly #1	8.05	110.22	176.45	44.50	-	4.10	-	-	-	-
51?Gly #2	8.17	109.52	177.17	44.26	-	4.06	-	-	-	-
51Gly	**8.12**	**110.27**	**176.77**	**44.50**	**-**	**4.11**	**-**	**-**	**-**	-
52?Pro #1	-	-	176.05	63.15	32.21	-	-	-	-	Coming from 53?Met #1
52?Pro #2	-	-	176.59	62.81	34.61	-	-	-	-	Coming from 53?Met #2
52Pro	**-**	**-**	**176.96**	**63.23**	**32.13**	**-**	**-**	**-**	**-**	Coming from **53Met**
53?Met #1	8.03	119.21	174.76	53.48	33.65	4.43	1.88	-	2.36, 2.51	-
53?Met #2	8.55	122.12	174.58	53.57	32.13	-	-	-	-	No assignable TOCSY peaks
53Met	**8.29**	**121.39**	**174.59**	**53.15**	**32.43**	**4.75**	**1.94**	**-**	**2.55, 2.65**	-
54?Pro #1	-	-	174.95	63.25	34.22	-	-	-	-	Coming from 55?Phe #1
54?Pro #2	-	-	174.92	63.27	-	-	-	-	-	Coming from 55?Phe #2 No assignable C_β peak

54Pro	**-**	**-**	**175.41**	**63.51**	**31.73**	**-**	**-**	**-**	**-**	Coming from **55Phe**
55?Phe #1	7.62	125.10	174.78	58.85	39.74	4.41	3.07, 3.16	-	-	-
55?Phe #2	7.83	126.00	174.88	59.15	39.84	4.44	3.03	-	-	-
55Phe	**7.43**	**123.76**	**174.82**	**58.80**	**40.20**	**4.41**	**3.03, 3.14**	**-**	**-**	-

Table A.2: H_N, H_α, H_β, H_δ, H_γ, N, C', C_α, C_β chemical shifts (ppm) of apelin-55 for all potential conformers at 5 °C

Residue	H_N	N	C'	C_α	C_β	H_α	H_β	H_δ	H_γ	Comments
0Ser	-	-	**178.58**	**57.51**	**63.12**	-	-	-	-	Coming from **1Gly**
1Gly	**8.83**	**109.69**	**173.85**	**45.07**	-	**4.03**	-	-	-	-
2Ser	**8.46**	**116.07**	**174.42**	**58.23**	**63.91**	**4.43**	**3.81**	-	-	-
3?Leu #1	8.56	124.45	177.15	55.15	42.25	-	-	-	-	Connect to 4?Met #1 No assignable TOCSY peaks
3?Leu #2	8.42	124.99	175.86	55.27	42.35	4.30	1.56	-	-	Connect to 4?Met #2
3Leu	**8.50**	**124.41**	**177.16**	**55.07**	**42.24**	**4.34**	**1.57**	-	-	-
4?Met #1	8.45	123.11	173.98	52.94	-	-	-	-	-	No assignable C_β peak and discernable TOCSY peaks from **4Met**
4?Met #2	7.99	119.77	174.69	52.55	33.84	4.56	1.87	-	-	-
4Met	**8.41**	**123.01**	**173.96**	**52.96**	**32.14**	**4.79**	**1.9**	-	**2.56**	-
5?Pro #1	-	-	175.79	62.45	-	-	-	-	-	Coming from 6?Leu #1 No assignable C_β peak
5Pro	-	-	**176.48**	**63.00**	**32.04**	-	-	-	-	Coming from **6Leu**
6?Leu #1	8.16	121.71	-	52.75	42.42	-	-	-	-	No assignable C' peak and no TOCSY peaks
6Leu	**8.59**	**123.23**	**176.06**	**53.41**	**41.26**	**4.52**	**1.57**	-	-	-
7?Pro #1	-	-	176.59	62.78	32.02	-	-	-	-	Coming from 8?Asp #1
7Pro	-	-	**176.67**	**63.22**	**31.99**	**4.37**	**1.91, 2.24**	-	-	Coming from **8Asp**
8?Asp #1	8.51	124.10	175.59	52.99	41.43	4.56	-	-	-	-
8Asp	**8.47**	**120.56**	**176.89**	**54.26**	**41.22**	**4.55**	**2.66**	-	-	-
9?Gly #1	8.37	109.43	174.06	45.41	-	3.93	-	-	-	Connect to 10?Asn #1
9?Gly #2	8.30	109.31	173.16	45.31	-	3.90	-	-	-	Connect to 10?Asn #2
9Gly	**8.43**	**109.52**	**174.31**	**45.51**	-	**3.93**	-	-	-	-
10?Asn #1	8.38	120.32	176.91	54.45	41.28	4.57	2.66	-	-	Connect to 11?Gly #1
10?Asn #2	8.10	124.05	179.56	54.79	40.73	4.50	2.72	-	-	-

10Asn	**8.50**	**118.64**	**175.89**	**53.35**	**38.92**	**4.71**	**2.77**	**7.00, 7.69**	**-**	-
11?Gly #1	8.54	109.35	174.36	45.59	-	3.89	-	-	-	Connect to 12?Leu #1
11Gly	**8.60**	**109.48**	**174.26**	**45.52**	**-**	**3.91**	**-**	**-**	**-**	-
12?Leu #1	8.36	121.44	177.79	55.24	42.41	4.32	1.56	-	-	Connect to 13?Glu #1
12Leu	**8.19**	**121.32**	**177.73**	**55.15**	**42.29**	**4.33**	**1.52,1.60**	**-**	**-**	-
13?Glu #1	8.64	121.48	176.30	56.53	29.97	4.25	1.87	-	2.21	-
13?Glu #2	8.49	122.89	175.18	56.00	30.72	4.34	1.52, 1.66			Connect to 14?Asp #2
13Glu	**8.61**	**121.4**	**176.32**	**56.55**	**29.83**	**4.26**	**1.90,2.00**	**-**	**2.21**	-
14?Asp #1	8.18	124.58	-	54.86	40.26	4.48	-	-	-	No assignable C' peak
14?Asp #2	8.13	124.86	179.49	54.73	40.42	4.44	2.67	-	-	-
14Asp	**8.40**	**121.65**	**176.97**	**54.43**	**41.12**	**4.53**	**2.68**	**-**	**-**	-
15Gly	**8.5**	**109.51**	**174.35**	**45.7**	**-**	**-**	**-**	**-**	**-**	-
16Asn	**8.38**	**118.76**	**175.56**	**53.4**	**38.81**	**4.68**	**2.77**	**7.00,7.74**	**-**	-
17Val	**8.04**	**120.05**	**176.19**	**62.8**	**32.37**	**4**	**2.04**	**-**	**0.84**	-
18Arg	**8.39**	**123.61**	**176.04**	**56.13**	**30.5**	**4.23**	**1.69**	**-**	**-**	-
19His	**8.47**	**119.58**	**174.34**	**55.26**	**29.2**	**4.63**	**3.15**	**-**	**-**	-
20Leu	**8.35**	**123.64**	**177.11**	**55.2**	**42.3**	**4.31**	**1.54**	**-**	**-**	-
21?Val #1	8.17	122.23	175.05	64.41	32.57	4.02	-	-	-	-
21?Val #2	8.30	122.05	175.85	62.23	32.62	-	-	-	-	No discernable TOCSY peaks from **21Val**
21Val	**8.31**	**122.27**	**175.88**	**62.24**	**32.58**	**4.04**	**1.97**	**-**	**0.87**	-
22?Gln #1	8.28	123.38	174.33	53.05	29.87	4.39	1.73, 1.99	-	-	Connect to 21?Val #1
22?Gln #2	8.57	125.85	173.80	53.43	-	-	-	-	-	No discernable TOCSY and C_β peaks from **22Gln**
22Gln	**8.58**	**126.08**	**173.81**	**53.45**	**28.88**	**4.56**	**1.84, 2.01**	**-**	**2.31**	-
23Pro	**-**	**-**	**176.95**	**63.04**	**32.15**	**4.38**	**2.24**	**-**	**-**	Coming from **24Arg**
24Arg	**8.66**	**122.15**	**177.09**	**56.62**	**30.59**	**4.22**	**1.64,1.79**	**-**	**-**	-
25Gly	**8.61**	**110.57**	**174.11**	**45.13**	**-**	**3.94**	**-**	**-**	**-**	-

26?Ser #1	8.33	115.93	-	58.63	63.84	-	-	-	-	No assignable TOCSY and C' peaks
26Ser	**8.28**	**115.71**	**174.84**	**58.42**	**63.98**	**4.4**	**3.83**	-	-	-
27Arg	**8.57**	**123.04**	**176.05**	**56.26**	**30.38**	**4.25**	**1.67**	-	**1.49**	-
28Asn	**8.49**	**119.43**	**175.25**	**53.19**	**39.2**	**4.76**	**2.66, 2.80**	**6.97, 7.66**	-	-
29?Gly #1	8.21	109.39	179.02	44.44	-	3.84	-	-	-	-
29Gly	**8.25**	**109.46**	**178.62**	**44.62**	**-**	**4.09**	-	-	-	-
30?Pro #1	-	-	177.38	63.26	32.32	-	-	-	-	Coming from 31?Gly #1
30?Pro #2	-	-	177.09	63.44	-	-	-	-	-	Coming from 31?Gly #2
30?Pro #3	-	-	177.19	63.43	32.25					Coming from 31?Gly #3
30Pro	-	-	**177.34**	**63.25**	**32.33**	**4.45**	-	-	-	Coming from **31Gly**
31?Gly #1	8.38	109.34	178.87	44.45	-	3.95	-	-	-	-
31?Gly #2	8.23	110.75	178.89	42.71	-	-	-	-	-	No assignable TOCSY peaks
31?Gly #3	8.25	110.50	178.91	42.75	-	-	-	-	-	No assignable TOCSY peaks
31Gly	**8.35**	**109.32**	**178.86**	**44.47**	**-**	**3.87, 3.98**	-	-	-	-
32?Pro #1	-	-	176.94	63.21	31.84	-	-	-	-	Coming from 33?Trp #1
32?Pro #2	-	-	175.87	62.20	34.87	-	-	-	-	Coming from 33?Trp #2
32?Pro #3	-	-	176.90	63.25	31.79	-	-	-	-	Coming from 33?Trp #3
32Pro	-	-	**176.91**	**63.25**	**31.83**	**4.37**	-	-	-	Coming from **33Trp**
33?Trp #1	8.74	121.95	176.20	57.55	29.87	4.86	3.08	-	-	-
33?Trp #2	8.39	121.66	176.77	57.61	29.18	4.63	3.22	-	-	-
33?Trp #3	8.26	121.21	176.76	57.55	28.94	-	-	-	-	No assignable TOCSY peaks
33Trp	**8.30**	**121.37**	**176.71**	**57.54**	**28.98**	**4.63**	**3.25**	-	-	-
34?Gln #1	8.73	122.88	176.43	55.94	29.49	4.33	-	-	-	Connect to the 33?Trp #1
34?Gln #2	8.70	122.72	176.36	55.84	29.46	4.33	-	-	-	-
34?Gln #3	8.29	123.51	176.03	55.74	29.19	4.17	-	-	-	-
34Gln	**8.24**	**123.49**	**176.05**	**55.77**	**29.2**	**4.17**	**1.74, 2.10**	-	-	-

35?Gly #1	8.34	110.48	174.63	45.40	-	3.85	-	-	-	Connect to 34?Gln #1
35?Gly #2	7.39	108.46	174.41	45.37	-	-	-	-	-	No assignable TOCSY peaks
35Gly	**7.52**	**108.6**	**174.48**	**45.38**	**-**	**3.69**	**-**	**-**	**-**	-
36?Gly #1	8.41	108.82	174.11	45.18	-	3.95	-	-	-	Connect to 35?Gly #1
36Gly	**8.26**	**108.63**	**174.17**	**45.14**	**-**	**3.91**	**-**	**-**	**-**	-
37?Arg #1	8.36	120.76	176.48	56.14	30.82	4.26	-	-	-	Connect to 36?Gly #1
37Arg	**8.29**	**120.67**	**176.51**	**56.25**	**30.71**	**4.26**	**1.58, 1.73**	**-**	**-**	-
38Arg	**8.46**	**122.54**	**176.16**	**56.23**	**30.71**	**4.17**	**1.64**	**-**	**1.45**	-
39Lys	**8.37**	**122.74**	**176.09**	**56.28**	**33.07**	**4.18**	**1.6**	**-**	**-**	-
40Phe	**8.35**	**121.78**	**175.32**	**57.59**	**39.79**	**4.56**	**3.01**	**-**	**-**	-
41Arg	**8.34**	**123.98**	**175.62**	**55.72**	**31.06**	**4.23**	**1.65**	**-**	**-**	-
42Arg	**8.55**	**123.47**	**176.21**	**56.15**	**30.83**	**4.2**	**1.62, 1.73**	**-**	**-**	-
43Gln	**8.64**	**122.75**	**175.67**	**55.56**	**29.71**	**4.28**	**1.92**	**-**	**2.31**	-
44Arg	**8.63**	**124.57**	**174.14**	**54.12**	**29.87**	**4.54**	**1.68**	**-**	**-**	-
45Pro	**-**	**-**	**176.59**	**63.04**	**32.19**	**4.36**	**2.25**	**-**	**-**	Coming from **46Arg**
46Arg	**8.62**	**122.34**	**176.32**	**56.11**	**30.75**	**4.27**	**1.61, 1.74**	**-**	**-**	-
47Leu	**8.50**	**124.14**	**177.2**	**54.91**	**42.31**	**4.36**	**1.56**	**-**	**-**	-
48Ser	**8.41**	**116.89**	**174.21**	**58.08**	**63.86**	**4.39**	**3.79**	**-**	**-**	-
49?His #1	8.56	121.27	174.32	55.71	29.59	-	-	-	-	No assignable TOCSY peaks
49His	**8.6**	**121.32**	**174.42**	**55.8**	**29.69**	**4.62**	**3.14**	**-**	**-**	-
50?Lys #1	8.45	123.16	176.53	56.36	33.26	-	-	-	-	No assignable TOCSY peaks
50Lys	**8.47**	**123.46**	**176.45**	**56.17**	**33.18**	**4.32**	**1.66**	**-**	**1.34**	-
51?Gly #1	8.38	110.02	178.92	44.12	-	3.78, 4.05	-	-	-	Connect to the 50?Lys #1
51?Gly #2	8.28	110.81	178.12	44.38	-	4.06	-	-	-	-
51Gly	**8.36**	**110.9**	**178.45**	**44.38**	**-**	**4.07**	**-**	**-**	**-**	-
52?Pro #1	-	-	176.20	62.94	32.31	4.45	-	-	-	Coming from 53?Met #1
52?Pro #2	-	-	176.67	62.59	34.52	-	-	-	-	Coming from 53?Met #2

52Pro	**-**	**-**	**177.1**	**63.03**	**-**	**4.4**	**-**	**-**	**-**	No discernable C_β peak from **53Met** C_β Coming from **53Met**
53?Met #1	8.25	119.42	174.80	53.34	33.31	4.31	1.79	-	2.24	-
53?Met #2	8.77	122.80	174.58	53.49	31.31	4.79	1.97	-	2.64	No assignable TOCSY peaks
53Met	**8.54**	**122.09**	**174.58**	**53.03**	**32.14**	**4.74**	**1.89**	**-**	**2.53**	-
54?Pro #1	-	-	175.00	62.92	34.19	-	-	-	-	Coming from 55?Phe #1
54?Pro #2	-	-	174.96	63.05	-	-	-	-	-	Coming from 55?Phe #2
54Pro	**-**	**-**	**175.53**	**63.35**	**31.82**	**-**	**-**	**-**	**-**	No assignable C_β peak Coming from **55Phe**
55?Phe #1	7.74	125.51	173.20	58.72	39.46	4.40	3.03	-	-	-
55?Phe #2	8.00	126.82	173.27	59.20	39.52	-	-	-	-	No TOCSY peaks
55Phe	**7.66**	**124.37**	**173.15**	**58.95**	**40.01**	**4.36**	**3.02**	**-**	**-**	-

Table A.3: H_N, H_δ, H_ε, N, C', C_α, C_β chemical shifts (ppm) of apelin-55 with DPC micelles

Residue	H_N	N	C'	C_α	C_β	H_δ	H_ε	Comments
0Ser	**-**	**-**	**-**	**-**	**-**	**-**	**-**	
1Gly	**-**	**-**	**173.8**	**45.31**	**-**	**-**	**-**	
2Ser	**8.26**	**115.63**	**174.36**	**58.27**	**64.05**	**-**	**-**	**-**
3?Leu #1	8.29	124.27	175.54	55.46	-	-	-	No visible Cβ peak
3Leu	**8.35**	**124.07**	**176.8**	**55.41**	**42.39**	**-**	**-**	**-**
4?Met #1	7.78	118.72	174.65	52.89	34.11	-	-	-
4Met	**8.17**	**121.43**	**173.89**	**53.11**	**32.79**	**-**	**-**	**-**
5?Pro #1	-	-	175.58	63.27	-	-	-	Coming from 6?Leu #1
5?Pro #2	-	-	175.75	62.56	34.40	-	-	Coming from 6?Leu #2
5Pro	**-**	**-**	**176.3**	**62.98**	**31.98**	**-**	**-**	**Coming from 6Leu**
6?Leu #1	7.86	121.25	175.70	52.78	43.13	-	-	-
6?Leu #2	8.42	123.05	175.69	53.47	41.64	-	-	-
6Leu	**8.18**	**123.11**	**175.62**	**52.92**	**41.96**	**-**	**-**	**-**
7Pro	**-**	**-**	**176.55**	**63.35**	**-**	**-**	**-**	**Coming from 8Asp**
8Asp	**8.25**	**119.84**	**176.82**	**54.34**	**41.44**	**-**	**-**	**-**
9Gly	**8.27**	**108.92**	**174.29**	**45.7**	**-**	**-**	**-**	**-**
10?Asn #1	7.94	124.00	173.37	54.90	41.06	-	-	-
10Asn	**8.36**	**118.47**	**175.75**	**53.50**	**39.14**	**6.86, 7.57**	**-**	**-**
11Gly	**8.47**	**109.08**	**174.23**	**45.68**	**-**	**-**	**-**	**-**
12Leu	**8.06**	**121.17**	**177.54**	**55.34**	**42.32**	**-**	**-**	**-**
13?Glu #1	8.50	121.03	176.26	56.77	30.12	-	-	-
13Glu	**8.45**	**120.88**	**176.26**	**56.78**	**30.19**	**-**	**-**	**-**
14Asp	**8.21**	**120.97**	**176.9**	**54.55**	**41.41**	**-**	**-**	**-**
15?Gly #1	8.39	108.91	175.37	45.72	-	-	-	-
15Gly	**8.34**	**108.89**	**174.36**	**45.90**	**-**	**-**	**-**	**-**
16Asn	**8.30**	**118.58**	**175.65**	**53.58**	**38.92**	**6.88, 7.63**	**-**	**-**
17?Val #1	7.96	119.22	176.22	63.03	32.32	**-**	**-**	-
17Val	**8.00**	**119.39**	**176.22**	**63.15**	**32.33**	**-**	**-**	**-**
18Arg	**8.21**	**122.41**	**176.24**	**56.70**	**30.56**	**-**	**-**	**-**
19His	**8.18**	**118.57**	**174.77**	**55.93**	**29.80**	**-**	**-**	**-**
20Leu	**8.08**	**122.22**	**176.88**	**55.71**	**42.41**	**-**	**-**	**-**
21?Val #1	7.88	119.88	174.91	62.27	-	-	-	No visible Cβ peak
21?Val #2	7.91	119.19	175.57	62.27	32.69	-	-	-
21Val	**7.90**	**118.96**	**175.52**	**62.08**	**32.66**	**-**	**-**	**-**
22?Gln #1	8.02	122.44	174.02	53.31	30.23	-	-	-
22Gln	**8.24**	**124.24**	**173.77**	**53.57**	**29.16**	**-**	**6.82, 7.47**	**-**
23Pro	**-**	**-**	**176.96**	**63.24**	**-**	**-**	**-**	**Coming from 24Arg**
24Arg	**8.45**	**121.28**	**176.94**	**56.45**	**30.8**	**-**	**-**	**-**
25Gly	**8.41**	**109.84**	**174.1**	**45.31**	**-**	**-**	**-**	**-**
26Ser	**8.15**	**115.44**	**174.74**	**58.43**	**64.00**	**-**	**-**	**-**
27Arg	**8.39**	**122.52**	**175.96**	**56.31**	**30.66**	**-**	**-**	**-**

28?Asn #1	7.98	124.77	173.30	54.85	40.73	-	-	-
28Asn					**39.38**	**6.85,7.53**	**-**	**-**
	8.34	**119.14**	**175.14**	**53.25**				
29?Gly #1	8.15	109.17	177.87	44.77	-	-	-	-
29?Gly #2	8.07	109.03	177.93	44.46	-	-	-	-
29Gly	**8.09**	**109.09**	**177.65**	**44.70**	**-**	**-**	**-**	**-**
30?Pro #1	-	-	177.04	63.37	-	-	-	Coming from 31?Gly #1 No visible Cβ peak
30Pro	**-**	**-**	**177.27**	**63.30**	**31.89**	**-**	**-**	**Coming from 31Gly**
31?Gly #1	8.10	109.23	177.98	43.35	-	-	-	-
31Gly	**8.21**	**108.69**	**176.25**	**44.62**	**-**	**-**	**-**	**-**
32?Pro #1	-	-	176.84	63.43	-	-	-	Coming from 33?Trp #1 No visible Cβ peak
32?Pro #2	-	-	176.91	63.52	-	-	-	Coming from 33?Trp #2 No visible Cβ peak
32Pro	**-**	**-**	**176.86**	**63.56**	**31.89**	**-**	**-**	**Coming from 33Trp**
33?Trp #1	8.11	120.27	176.39	57.61	29.21	-	-	-
33?Trp #2	8.11	119.98	176.39	57.56	29.06	-	-	-
33Trp	**8.06**	**119.84**	**176.46**	**57.56**	**29.05**	**-**	**10.35**	**-**
34Gln	**8.07**	**121.56**	**176.37**	**56.28**	**29.14**	**-**	**6.80, 7.41**	**-**
35Gly	**7.84**	**108.45**	**174.69**	**45.63**	**-**	**-**	**-**	**-**
36Gly	**8.17**	**108.42**	**174.25**	**45.55**	**-**	**-**	**-**	**-**
37Arg	**8.20**	**120.26**	**176.55**	**56.69**	**30.73**	**-**	**-**	**-**
38Arg	**8.24**	**120.94**	**175.08**	**54.52**	**30.55**	**-**	**-**	**-**
39Lys	**-**	**-**	**176.14**	**56.41**	**34.66**	**-**	**-**	**Coming from 40Phe**
40Phe	**8.15**	**120.52**	**175.3**	**57.77**	**39.76**	**-**	**-**	**-**
41Arg	**8.16**	**122.08**	**175.79**	**56.05**	**31.11**	**-**	**-**	**-**
42Arg	**8.29**	**121.99**	**175.99**	**56.2**	**30.94**	**-**	**-**	**-**
43Gln	**8.35**	**121.39**	**175.46**	**55.64**	**29.92**	**-**	**6.82, 7.51**	**-**
44Arg	**8.40**	**123.39**	**174.09**	**54.27**	**30.07**	**-**	**-**	**-**
45Pro	**-**	**-**	**176.34**	**63.19**	**32.18**	**-**	**-**	**Coming from 46Arg**
46Arg	**8.40**	**121.21**	**176.11**	**56.11**	**30.86**	**-**	**-**	**-**
47Leu	**8.29**	**123.06**	**176.9**	**55.02**	**42.5**	**-**	**-**	**-**
48Ser	**8.21**	**115.92**	**175.6**	**58.15**	**64.02**	**-**	**-**	**-**
49His	**-**	**-**	**-**	**-**	**-**	**-**	**-**	-
50?Lys #1	-	-	176.24	56.19	-	-	-	Coming from 51?Gly #1 No assignable Cβ peak
50Lys	**-**	**-**	**176.29**	**56.21**	**-**	**-**	**-**	**Coming from 51Gly** **No assignable Cβ peak**
51?Gly #1	8.07	110.16	177.28	44.47	-	-	-	-
51Gly	**8.10**	**110.02**	**177.58**	**44.49**	**-**	**-**	**-**	**-**
52?Pro #1	-	-	175.96	63.16	-	-	-	Coming from 53?Met #1 No visible Cβ peak
52?Pro #2	-	-	176.42	62.74	34.31	-	-	Coming from 53?Met #2
52Pro	**-**	**-**	**176.82**	**63.23**	**32.34**	**-**	**-**	**Coming from 53Met**
53?Met #1	8.04	119.20	174.65	53.40	33.91	-	-	-
53?Met #2	8.58	121.34	174.94	53.41	32.19	-	-	-
53Met	**8.28**	**120.84**	**174.79**	**53.07**	**33.02**	**-**	**-**	**-**

54?Pro #1	-	-	174.73	63.33	34.19	-	-	Coming from 55?Phe #1
54?Pro #2	-	-	174.74	63.47	31.32	-	-	Coming from 55?Phe #2
54Pro	**-**	**-**	**175.02**	**63.44**	**31.51**	**-**	**-**	**Coming from 55Phe**
55?Phe #1	7.60	124.83	173.79	58.79	39.70	**-**	**-**	-
55?Phe #2	7.23	122.65	173.59	58.40	40.23	**-**	**-**	-
55Phe	**7.31**	**123.06**	**173.75**	**58.56**	**40.24**	**-**	**-**	**-**

Table A.4: H_N, H_δ, H_ε, N, C', C_α, C_β chemical shifts (ppm) of apelin-55 with SDS micelles

Residue	H_N	N	C'	C_α	C_β	H_δ	H_ε	Comments
0Ser	-	-	**171.46**	**57.72**	**63.11**	-	-	
1Gly	**8.62**	**109.76**	**173.92**	**45.63**	-	-	-	
2?Ser #1	8.21	115.30	-	58.72	-	-	-	No assignable C' and C_β peak
2?Ser #2	8.16	114.98	174.30	58.60	64.12	-	-	-
2Ser	**8.17**	**115.20**	**174.36**	**58.68**	**64.04**	-	-	-
3?Leu #1	8.18	122.85	175.20	56.57	43.50	-	-	-
3Leu	**8.13**	**122.61**	**176.52**	**56.08**	**43.48**	-	-	-
4?Met #1	7.82	117.36	174.96	53.09	33.29	-	-	-
4?Met #2	7.36	113.38	177.20	52.47	33.97	-	-	-
4Met	**7.78**	**117.94**	**175.87**	**53.25**	**33.14**	-	-	-
5?Pro #1	-	-	175.70	62.98	-	-	-	Coming from 6?Leu #1 No assignable C_β peak
5?Pro #2	-	-	175.60	62.83	-	-	-	Coming from 6?Leu #2 No assignable C_β peak
5Pro	-	-	**175.58**	**62.83**	**31.18**	-	-	**Coming from 6Leu**
6?Leu #1	7.86	121.80	-	52.88	-	-	-	No assignable C' and C_β peaks
6?Leu #2	7.84	121.27	-	52.96	-	-	-	No assignable C' and C_β peaks
6Leu	**7.79**	**121.16**	**175.66**	**52.85**	**41.99**	-	-	-
7?Pro #1	-	-	176.21	63.07	-	-	-	Coming from 8?Asp #1 No assignable C_β peaks
7Pro	-	-	**176.38**	**63.35**	**31.91**	-	-	**Coming from 8Asp**
8?Asp #1	8.54	120.68	-	54.46	-	-	-	No assignable C' and C_β peaks
8Asp	**8.24**	**119.24**	**176.91**	**54.28**	**41.16**	-	-	-
9?Gly #1	8.26	109.11	174.47	45.77	-	-	-	-
9?Gly #2	8.41	108.37	174.43	45.80	-	-	-	-
9?Gly #3	8.15	109.06	173.34	45.52	-	-	-	-
9Gly	**8.22**	**108.97**	**174.45**	**45.8**	-	-	-	-
10?Asn #1	7.98	123.76	-	54.85	-	-	-	No assignable C' and C_β peak
10?Asn #2	7.95	123.76	-	54.82	40.81	-	-	No assignable C' peak
10?Asn #3	8.33	118.18	-	53.73	38.84	-	-	No assignable C' peak
10Asn	**8.26**	**118.2**	**175.74**	**53.75**	**39.28**	**6.83, 7.56**	-	-
11Gly	**8.4**	**108.61**	**174.38**	**45.76**	-	-	-	-
12Leu	**8.06**	**120.94**	**177.7**	**55.6**	-	-	-	**No assignable C_β peak**
13?Glu #1	8.21	119.49	176.41	57.04	29.54	-	-	-
13?Glu #2	8.38	120.39	176.21	56.82	29.54	-	-	-
13Glu	**8.25**	**119.83**	**176.38**	**57.03**	**29.60**	-	-	-
14?Asp #1	8.20	119.74	176.47	54.40	-	-	-	No assignable C_β peak

14Asp	**8.18**	**119.32**	**176.45**	**54.61**	**40.88**	-	-	-
15?Gly #1	8.18	108.52	174.23	45.77	-	-	-	-
15Gly	**8.13**	**108.34**	**174.29**	**45.89**	-	-	-	-
16?Asn #1	8.21	118.06	175.71	53.99	39.42	-	-	-
16Asn	**8.18**	**118.12**	**176.07**	**53.92**	**39.24**	**6.88, 7.54**	-	-
17Val	**8.15**	**119.73**	**176.48**	**64.47**	-	-	-	**No assignable C_β peak**
18Arg	**7.99**	**119.49**	**176.5**	**57.69**	**29.93**	-	-	-
19?His #1	8.02	116.10	-	55.96	-	-	-	No assignable C' and C_β peak
19?His #2	7.95	115.44	174.84	56.12	-	-	-	No assignable C_β peak
19His	**7.97**	**115.71**	**174.80**	**56.07**	**28.71**	-	-	-
20Leu	**7.95**	**120.22**	**176.81**	**56.35**	-	-	-	-
21Val	**7.38**	**114.53**	**174.74**	**61.74**	**32.65**	-	-	-
22Gln	**7.84**	**122.34**	**173.57**	**53.84**	**29.16**	-	**6.74, 7.39**	-
23?Pro #1	-	-	176.13	62.31	34.64	-	-	Coming from 24?Arg #1
23Pro	-	-	**177.28**	**63.44**	**32.21**	-	-	**Coming from 24Arg**
24?Arg #1	8.30	122.42	176.14	54.00	32.29	-	-	-
24Arg	**8.28**	**120.43**	**177.3**	**57.13**	**30.75**	-	-	-
25Gly	**8.33**	**109.24**	**174.46**	**45.67**	-	-	-	-
26?Ser #1	8.06	114.82	174.36	58.62	64.03	-	-	-
26Ser	**8.03**	**114.82**	**174.41**	**58.64**	**64.04**	-	-	-
27?Arg #1	8.02	121.32	175.84	56.16	-	-	-	No assignable C_β peak
27?Arg #2	8.17	122.06	176.02	56.18	30.81	-	-	-
27Arg	**8.05**	**121.65**	**175.99**	**56.32**	**30.66**	-	-	-
28?Asn #1	8.35	119.34	175.82	53.25	39.45	-	-	-
28?Asn #2	8.44	119.88	-	53.29	-	-	-	No assignable C' and C_β peak
28Asn	**8.40**	**119.53**	**175.04**	**53.34**	**39.47**	**6.80, 7.50**	-	-
29?Gly #1	7.98	108.50	171.84	44.70	-	-	-	-
29?Gly #2	7.98	108.50	171.84	44.44	-	-	-	-
29Gly	**7.94**	**108.80**	**171.59**	**44.70**	-	-	-	-
30Pro	-	-	**177.11**	**63.35**	**32.32**	-	-	**Coming from 31Gly**
31Gly	**8.05**	**108.4**	**172.78**	**44.65**	-	-	-	-
32?Pro #1	-	-	176.18	62.32	-	-	-	Coming from 33?Trp #1 No assignable C_β peak
32?Pro #2	-	-	176.76	63.92	-	-	-	Coming from 33?Trp #2 No assignable C_β peak
32?Pro #3	-	-	176.84	63.83	-	-	-	Coming from 33?Trp #3 No assignable C_β peak
32Pro	-	-	**176.81**	**63.84**	**31.9**	-	-	**Coming from 33Trp**
33?Trp #1	8.39	122.16	176.38	57.70	29.63	-	-	-
33?Trp #2	7.64	118.73	176.63	57.87	29.05	-	-	-
33?Trp #3	7.73	118.89	176.64	57.83	-	-	-	**No assignable C_β peak**

33Trp	**7.69**	**118.78**	**176.67**	**57.75**	**28.97**	-	**10.02**	-
34?Gln #1	8.25	122.34	176.30	55.93	29.51	-	-	-
34Gln	**7.92**	**120.58**	**176.68**	**56.52**	**29.63**	-	**6.74, 7.45**	-
35?Gly #1	7.82	108.05	174.79	45.62	-	-	-	-
35Gly	**7.78**	**108.05**	**174.79**	**45.65**	-	-	-	-
36?Gly #1	8.04	108.11	174.42	45.56	-	-	-	-
36Gly	**8.01**	**108.33**	**174.19**	**45.56**	-	-	-	-
37?Arg #1	8.04	119.28	176.43	56.63	29.79	-	-	-
37?Arg #2	8.18	121.35	174.49	55.59	-	-	-	No assignable C_β peak
37Arg	**7.98**	**119.35**	**176.36**	**56.53**	**29.79**	-	-	-
38Arg	**7.95**	**119.92**	**175.57**	**56.31**	**30.68**	-	-	-
39Lys	**7.91**	**119.81**	**176.21**	**56.19**	**33.2**	-	-	-
40Phe	**7.92**	**119.69**	**175.76**	**58.22**	**39.48**	-	-	-
41Arg	**8.01**	**120.1**	**176.09**	**56.52**	**29.83**	-	-	-
42Arg	**7.89**	**119.52**	**175.52**	**55.98**	**30.79**	-	-	-
43Gln	**8.09**	**119.00**	**175.34**	**55.77**	**29.76**	-	**6.74, 7.45**	-
44Arg	**8.07**	**121.27**	**174.41**	**54.03**	**29.81**	-	-	-
45?Pro #1	-	-	176.17	62.21	-	-	-	Coming from 46?Arg #1 No assignable C_β peak
45?Pro #2	-	-	176.46	62.44	-	-	-	Coming from 46?Arg #2 No assignable C_β peak
45Pro	**-**	**-**	**176.79**	**63.87**	**29.87**	**-**	**-**	**Coming from 46Arg**
46?Arg #1	8.60	121.59	-	56.73	-	-	-	No assignable C' or C_β peak
46?Arg #2	8.46	121.53	-	56.72	-	-	-	No assignable C' or C_β peak
46Arg	**8.13**	**117.94**	**176.46**	**56.48**	**30.7**	-	-	-
47Leu	**7.84**	**119.98**	**177.04**	**55.37**	**42.22**	-	-	-
48Ser	**7.92**	**113.84**	**174.54**	**58.73**	**63.99**	-	-	-
49His	**8.27**	**119.06**	**174.04**	**55.73**	**28.77**	-	-	-
50?Lys #1	8.06	120.26	176.07	56.12	-	-	-	No assignable C_β peak
50Lys	**8.08**	**120.86**	**176.37**	**56.29**	**33.26**	-	-	-
51?Gly #1	8.00	108.09	171.80	44.07	-	-	-	-
51Gly	**8.08**	**109.13**	**171.80**	**44.66**	-	-	-	-
52?Pro #1	-	-	175.78	63.36	-	-	-	Coming from 53?Met #1 No assignable C_β peak
52?Pro #2	-	-	176.22	63.45	29.30	-	-	Coming from 53?Met #2 No assignable C_β peak
52?Pro #3	-	-	176.30	62.38	34.80	-	-	Coming from 53?Met #3
52?Pro #4	-	-	176.57	62.23	-	-	-	Coming from 53?Met #4
52Pro	**-**	**-**	**176.62**	**63.20**	**-**	**-**	**-**	**Coming from 53Met** **No assignable C_β peak**
53?Met #1	7.75	118.46	174.51	54.08	-	-	-	-

53?Met #2	8.15	118.84	174.04	54.25	31.83	-	-	-
53?Met #3	8.44	120.38	175.54	53.53	32.94	-	-	-
53?Met #4	8.11	120.09	177.14	53.36	33.01	-	-	-
53Met	**8.13**	**120.26**	**175.31**	**53.35**	**32.99**	-	-	-
54?Pro #1	-	-	174.82	63.50	28.20	-	-	Coming from 55?Phe #2
54?Pro #2	-	-	175.23	62.68	34.18	-	-	Coming from 55?Phe #2
54Pro	-	-	**175.07**	**63.48**	**31.29**	-	-	**Coming from 55Phe**
55?Phe #1	7.02	122.55	179.58	58.02	40.27	-	-	-
55?Phe #2	7.82	125.34	180.44	59.09	39.75	-	-	-
55Phe	**7.16**	**122.95**	**179.76**	**58.16**	**40.18**	-	-	-

Table A.5: H_N, H_δ, H_ε, N, C', C_α, C_β chemical shifts (ppm) of apelin-55 with LPPG micelles

Residue	H_N	N	C'	C_α	C_β	H_δ	H_ε	Comments
0Ser	**-**	**-**	**-**	**-**	**-**	**-**	**-**	-
1Gly	**-**	**-**	**173.62**	**45.48**	**-**	**-**	**-**	**-**
2Ser	**8.24**	**115.34**	**174.39**	**58.31**	**64.16**	**-**	**-**	**-**
3Leu	**8.30**	**123.28**	**176.22**	**55.77**	**43.45**	**-**	**-**	**-**
4Met	**7.91**	**118.5**	**173.75**	**53.07**	**33.28**	**-**	**-**	**-**
5?Pro #1	-	-	176.01	62.91	-	-	-	Coming from 6?Leu #1
5Pro	**-**	**-**	**175.66**	**62.85**	**31.42**	**-**	**-**	**Coming from 6Leu**
6?Leu #1	8.06	122.69	-	52.74	-	-	-	No assignable C' and C_β peaks
6Leu	**7.95**	**121.74**	**175.51**	**52.69**	**42.20**	**-**	**-**	**-**
7Pro	**-**	**-**	**176.19**	**63.14**	**-**	**-**	**-**	**Coming from 8Asp No assignable C_β peak**
8Asp	**8.28**	**119.53**	**176.87**	**54.18**	**41.29**	**-**	**-**	**-**
9?Gly #1	8.19	109.10	173.22	45.52	-	-	-	-
9Gly	**8.33**	**109.17**	**174.40**	**45.83**	**-**	**-**	**-**	**-**
10?Asn #1	7.95	123.95	-	54.89	40.82	-	-	No assignable C' peak
10Asn	**8.33**	**118.37**	**175.75**	**53.76**	**39.19**	**6.90, 7.61**	**-**	**-**
11Gly	**8.46**	**108.79**	**174.37**	**45.76**	**-**	**-**	**-**	**-**
12Leu	**8.08**	**120.93**	**177.49**	**55.54**	**42.21**	**-**	**-**	**-**
13Glu	**8.38**	**120.02**	**176.24**	**56.85**	**29.68**	**-**	**-**	**-**
14?Asp #1	8.16	119.86	176.66	54.50	41.06	-	-	-
14Asp	**8.21**	**120.61**	**176.66**	**54.50**	**41.08**	**-**	**-**	**-**
15?Gly #1	8.29	108.66	174.26	45.79	-	-	-	-
15Gly	**8.26**	**108.40**	**174.31**	**45.89**	**-**	**-**	**-**	**-**
16Asn	**8.27**	**118.65**	**176.08**	**54**	**39.05**	**6.86, 7.60**	**-**	**-**
17?Val #1	8.12	120.12	175.97	63.35	-	-	-	No assignable C_β peak
17Val	**8.17**	**119.94**	**176.21**	**63.98**	**32.06**	**-**	**-**	**-**
18Arg	**8.17**	**120.93**	**176.64**	**57.49**	**-**	**-**	**-**	**-**
19His	**8.11**	**116.59**	**-**	**55.85**	**-**	**-**	**-**	**No assignable C' and C_β peak**
20Leu	**-**	**-**	**176.59**	**56.54**	**-**	**-**	**-**	**Coming from 21Val**
21Val	**7.49**	**113.88**	**174.65**	**61.43**	**32.48**	**-**	**-**	**-**
22Gln	**7.93**	**122.35**	**173.64**	**53.6**	**29.4**	**-**	**6.80, 7.50***	**-**
23Pro	**-**	**-**	**176.77**	**63.33**	**-**	**-**	**-**	**Coming from 24Arg**
24?Arg #1	8.50	120.40	175.34	53.27	33.08	-	-	-
24Arg	**8.46**	**120.92**	**176.84**	**56.39**	**30.99**	**-**	**-**	**-**
25Gly	**8.42**	**109.19**	**174.09**	**45.44**	**-**	**-**	**-**	**-**

26Ser	**8.17**	**115.19**	**174.65**	**58.46**	**64.08**	**-**	**-**	**-**
27?Arg #1	8.39	122.56	175.90	56.10	30.77	-	-	-
27Arg	**8.36**	**122.30**	**175.92**	**56.33**	**30.69**	**-**	**-**	**-**
28?Asn #1	8.39	119.09	175.08	53.27	39.46	-	-	-
28Asn	**8.43**	**119.17**	**175.01**	**53.24**	**39.44**	**6.85, 7.57**	**-**	**-**
29?Gly #1	8.10	108.69	171.75	44.46	-	-	-	-
29Gly	**8.02**	**108.81**	**171.45**	**44.70**	**-**	**-**	**-**	**-**
30?Pro #1	-	-	177.16	63.20	-	-	-	Coming from 31?Gly #1 No assignable C_β peak
30Pro	**-**	**-**	**177.1**	**63.15**	**-**	**-**	**-**	**Coming from 31Gly** **No assignable C_β peak**
31?Gly #1	8.10	108.27	-	44.60	-	-	-	No assignable C' peak
31Gly	**8.26**	**108.33**	**172.7**	**44.62**	**-**	**-**	**-**	**-**
32Pro	**-**	**-**	**176.55**	**63.96**	**-**	**-**	**-**	**Coming from 33Trp** **No assignable C_β peak**
33Trp	**7.73**	**118.02**	**176.33**	**57.54**	**29.06**	**-**	**10.36**	**-**
34Gln	**7.98**	**120.55**	**176.9**	**56.93**	**29.06**	**-**	**6.81, 7.50***	**-**
35Gly	**8.12**	**108.35**	**175.03**	**45.89**	**-**	**-**	**-**	**-**
36Gly	**8.18**	**108.44**	**174.24**	**45.91**	**-**	**-**	**-**	**-**
37?Arg #1	8.22	121.47	-	55.45	-	-	-	No assignable C' or C_β peak
37?Arg #2	8.22	119.36	-	56.81	-	-	-	No assignable C' or C_β peak
37Arg	**8.15**	**119.57**	**176.65**	**57.29**	**30.66**	**-**	**-**	**-**
38Arg	**8.00**	**119.5**	**-**	**56.52**	**29.73**	**-**	**-**	**-**
39Lys	**-**	**-**	**176.1**	**56.34**	**-**	**-**	**-**	**Coming from 40Phe** **No assignable C_β peak**
40Phe	**8.04**	**119.61**	**175**	**57.91**	**39.98**	**-**	**-**	**-**
41Arg	**8.01**	**121.33**	**175.57**	**55.93**	**31.3**	**-**	**-**	**-**
42Arg	**8.12**	**120.94**	**175.12**	**55.98**	**30.7**	**-**	**-**	**-**
43Gln	**7.92**	**120.18**	**174.71**	**55.16**	**31.15**	**-**	**6.83, 7.50***	**-**
44Arg	**8.50**	**122.17**	**174.00**	**54.26**	**30.57**	**-**	**-**	**-**
45Pro	**-**	**-**	**175.38**	**62.84**	**-**	**-**	**-**	**Coming from 46Arg** **No assignable C_β peak**
46Arg	**8.29**	**120.72**	**175.58**	**55.58**	**31.36**	**-**	**-**	**-**
47Leu	**8.32**	**122.88**	**176.3**	**54.73**	**-**	**-**	**-**	**No assignable C_β peak**
48Ser	**8.10**	**115.16**	**174.11**	**58.09**	**64.28**	**-**	**-**	**-**
49?Lys #1	8.49	119.85	173.86	55.61	29.36	-	-	-
49His	**8.52**	**119.84**	**173.88**	**55.65**	**29.35**	**-**	**-**	-
50Lys	**8.32**	**122.29**	**176.25**	**56.19**	**33.38**	**-**	**-**	**-**
51?Gly #1	8.11	108.69	-	44.31	-	-	-	No assignable C' peak
51Gly	**8.20**	**109.81**	**179.72**	**44.59**	**-**	**-**	**-**	**-**
52Pro	**-**	**-**	**176.4**	**63.09**	**-**	**-**	**-**	**Coming from 53Met** **No assignable C_β peak**

53Met	**8.18**	**119.9**	**175.21**	**53.04**	**33.43**	**-**	**-**	**-**
54?Pro #1	-	-	174.57	63.31	-	-	-	Coming from 55?Phe #1 No assignable C_β peak
54?Pro #2	-	-	174.38	63.51	-	-	-	Coming from 55?Phe #2 No assignable C_β peak
54Pro	**-**	**-**	**174.59**	**63.42**	**31.19**	**-**	**-**	**Coming from 55Phe**
55?Phe #1	7.68	124.41	180.02	58.65	-	-	-	No assignable C_β peak
55?Phe #2	7.05	121.39	179.24	57.89	40.30	-	-	-
55Phe	**7.14**	**121.82**	**179.34**	**58.00**	**40.29**	**-**	**-**	**-**

*based on peak inference from assigned ^{1}H-^{15}N HSQC spectrum of apelin-55 in buffer at 37 °C

Table A.6: H_N and N chemical shifts (ppm) of apelin-55 with Brij-35 micelles based on peak inference from apelin-55 in buffer

Residue	H_N	N	C'	C_α	C_β	H_δ	H_ε	Comments
0Ser	-	-	-	-	-	-	-	-
1Gly	-	-	-	-	-	-	-	-
2Ser	**8.27**	**115.77**	-	-	-	-	-	-
3?Leu #1	8.22	124.54	-	-	-	-	-	-
3?Leu #2	8.31	122.67	-	-	-	-	-	-
3Leu	**8.29**	**124.15**	-	-	-	-	-	-
4?Met #1	7.82	119.54	-	-	-	-	-	-
4Met	**8.20**	**122.25**	-	-	-	-	-	-
5Pro	-	-	-	-	-	-	-	-
6?Leu #1	7.93	121.54	-	-	-	-	-	-
6?Leu #2	8.39	123.09	-	-	-	-	-	-
6Leu	**8.22**	**123.43**	-	-	-	-	-	-
7Pro	-	-	-	-	-	-	-	-
8?Asp #1	8.25	119.31	-	-	-	-	-	-
8Asp	**8.25**	**119.91**	-	-	-	-	-	-
9?Gly #1	8.20	108.98	-	-	-	-	-	-
9Gly	**8.26**	**109.00**	-	-	-	-	-	-
10?Asn #1	7.94	124.06	-	-	-	-	-	-
10Asn	**8.37**	**118.59**	-	-	-	**6.88, 7.57**	-	-
11Gly	**8.46**	**109.22**	-	-	-	-	-	-
12?Leu #1	8.17	121.36	-	-	-	-	-	-
12Leu	**8.05**	**121.22**	-	-	-	-	-	-
13?Glu #1	8.49	121.22	-	-	-	-	-	-
13Glu	**8.45**	**121.11**	-	-	-	-	-	-
14Asp	**8.24**	**121.25**	-	-	-	-	-	-
15Gly	**8.35**	**109.07**	-	-	-	-	-	-
16Asn	**8.31**	**118.71**	-	-	-	**6.88, 7.61**	-	-
17Val	**7.91**	**119.3**	-	-	-	-	-	-
18Arg	**8.2**	**123.04**	-	-	-	-	-	-
19His	-	-	-	-	-	-	-	-
20Leu	**8.13**	**123.22**	-	-	-	-	-	-
21?Val #1	7.96	121.26	-	-	-	-	-	-
21Val	**8.04**	**120.99**	-	-	-	-	-	-
22?Gln #1	8.47	121.85	-	-	-	-	-	-
22?Gln #2	8.06	122.78	-	-	-	-	-	-
22Gln	**8.32**	**125.03**	-	-	-	-	**6.82, 7.46**	-
23Pro	-	-	-	-	-	-	-	-
24Arg	**8.42**	**121.4**	-	-	-	-	-	-
25Gly	**8.39**	**110**	-	-	-	-	-	-
26Ser	**8.14**	**115.47**	-	-	-	-	-	-

27Arg	**8.38**	**122.57**	-	-	-	-	-	-
28?Asn #1	8.34	119.24	-	-	-	-	-	-
28Asn	**8.33**	**119.24**	-	-	-	**6.85, 7.51**	-	-
29Gly	**8.1**	**109.23**	-	-	-	-	-	-
30Pro	-	-	-	-	-	-	-	-
31?Gly #1	8.07	109.51	-	-	-	-	-	-
31Gly	**8.14**	**108.84**	-	-	-	-	-	-
32Pro	-	-	-	-	-	-	-	-
33?Trp #1	8.07	120.66	-	-	-	-	-	-
33Trp	**8.02**	**120.50**	-	-	-	-	**10.18**	-
34?Gln #1	8.07	122.54	-	-	-	-	-	-
34Gln	**8.1**	**122.51**	-	-	-	-	**6.78, 7.35**	-
35Gly	**7.67**	**108.63**	-	-	-	-	-	-
36Gly	**8.13**	**108.48**	-	-	-	-	-	-
37Arg	**8.14**	**120.37**	-	-	-	-	-	-
38Arg	**8.24**	**121.74**	-	-	-	-	-	-
39Lys	**8.16**	**122.15**	-	-	-	-	-	-
40Phe	**8.14**	**121.2**	-	-	-	-	-	-
41Arg	-	-	-	-	-	-	-	-
42Arg	**8.37**	**122.58**	-	-	-	-	-	-
43Gln	**8.41**	**122.12**	-	-	-	-	**6.83, 7.50**	-
44Arg	**8.4**	**123.86**	-	-	-	-	-	-
45Pro	-	-	-	-	-	-	-	-
46Arg	**8.39**	**121.56**	-	-	-	-	-	-
47Leu	**8.23**	**123.48**	-	-	-	-	-	-
48Ser	**8.23**	**116.38**	-	-	-	-	-	-
49His	-	-	-	-	-	-	-	-
50Lys	-	-	-	-	-	-	-	-
51?Gly #1	8.08	110.36	-	-	-	-	-	-
51?Gly #2	8.17	109.29	-	-	-	-	-	-
51?Gly #3	8.18	109.64	-	-	-	-	-	-
51Gly	**8.14**	**110.39**	-	-	-	-	-	-
52Pro	-	-	-	-	-	-	-	-
53?Met #1	8.55	122.15	-	-	-	-	-	-
53?Met #2	8.03	119.30	-	-	-	-	-	-
53Met	**8.29**	**121.44**	-	-	-	-	-	-
54Pro	-	-	-	-	-	-	-	-
55?Phe #1	7.62	125.16	-	-	-	-	-	-
55?Phe #2	7.85	126.11	-	-	-	-	-	-
55Phe	**7.42**	**123.79**	-	-	-	-	-	-

Table A.7: H_N and N chemical shifts (ppm) of apelin-36 in buffer, DPC, SDS, and LPPG micelles based on peak inference from apelin-55.

	Buffer		DPC		SDS		LPPG		
Residue	H_N	N	H_N	N	H_N	N	H_N	N	Comments
1Leu	8.12	123.18	-	-	-	-	-	-	No visible peak
2Val	-	-	-	-	-	-	-	-	No visible peak
3Gln	-	-	-	-	-	-	-	-	No visible peak
4Pro	-	-	-	-	-	-	-	-	No visible peak
5Arg	8.41	121.28	8.43	121.47	8.36	109.36	8.38	120.46	-
6Gly	8.39	110.03	8.4	109.98	8.24	109.02	8.41	109.1	-
7Ser	8.14	115.44	8.16	115.51	8.03	114.78	8.18	115.09	-
8Arg	8.4	122.62	8.39	122.64	8.08	121.67	8.4	122.26	-
9Asn	8.32	119.27	8.35	119.38	8.39	119.37	8.41	118.86	-
10Gly	8.11	109.26	8.21	108.76	7.94	108.82	8.02	108.77	-
11Pro	-	-	-	-	-	-	-	-	-
12Gly	8.15	108.82	8.21	108.76	8.05	108.45	8.24	108.18	-
13Pro			-	-	-	-	-	-	-
14Trp	8.03	120.59	8.06	119.81	7.69	118.88	7.68	117.96	-
15Gln	8.1	122.63	8.06	121.53	7.92	120.81	7.97	120.62	-
16Gly	7.64	108.58	7.87	108.53	7.78	108.12	8.13	108.39	-
17Gly	8.15	108.48	8.17	108.49	8.02	108.39	8.18	108.45	-
18Arg	8.16	120.39	8.2	120.25	7.99	119.39	8.16	119.66	-
19Arg	8.27	121.87	8.19	120.84	7.95	119.91	7.99	119.43	-
20Lys	8.17	122.17	-	-	7.91	119.89	-	-	No inferable peak in apelin-55
21Phe	8.15	121.22	8.13	120.4	7.93	119.76	8.04	119.69	-
22Arg	8.22	123.31	8.14	121.84	8.02	120.21	8.02	121.45	-
23Arg	8.35	122.69	8.25	121.66	7.88	119.58	8.13	121	-
24Gln	8.42	122.08	8.3	121.15	8.09	119.09	7.90	120.25	-
25Arg	8.4	123.88	8.39	123.25	8.08	121.34	8.53	122.25	-
26Pro	-	-	-	-	-	-	-	-	-
27Arg	8.4	121.55	8.39	121.11	8.13	118.03	8.29	120.78	-
28Leu	8.25	123.5	8.27	123.01	7.85	120.1	8.30	123.08	-
29Ser	8.23	116.32	8.2	115.85	7.93	113.95	8.10	115.24	-
30His	-	-	-	-	8.26	119.11	8.53	119.86	No inferable peak in apelin-55
31Lys	-	-	-	-	8.08	120.89	8.33	122.30	No inferable peak in apelin-55
32Gly	8.12	110.27	8.09	110.04	8.08	109.18	8.20	109.79	-
33Pro	-	-	-	-	-	-	-	-	-
34Met	8.3	121.42	8.03	119.26	8.13	120.31	8.18	119.94	-
35Pro	-	-	-	-	-	-	-	-	-
36Phe	7.43	123.79	7.31	123.13	7.16	122.74	7.15	121.84	-

APPENDIX B Fast two-state exchange model and representative DOSY fits for apelin-55 and -36 in indicated micelle conditions

(Note: The derivation and assumptions made for f_b calculation was developed by Ms. Shuya Kate Huang working with Dr. Jan Rainey, and was detailed in our jointly first-authored paper in ***BBA Biomembranes*** 1859(5): 767-778. Given the importance of this model in Chapter 7 and 8, it is discussed in detail below)

Using NMR spectroscopy to study protein-micelle interactions

As introduced in Section 2.5, NMR spectroscopy offers a number of means to study intermolecular interactions or supramolecular assembly processes. Of these, DOSY is particularly pertinent, as it provides the capability to quantify translational diffusion coefficients (D) for a protein-micelle complex and for each of the free species (i.e, the micelle vs. the peptide). These can, in turn, be used to quantify peptide-micelle binding. In my thesis, I applied a fast two-state exchange model for quantification, which is given by the expression [363]:

$$D_{ob} = f_b D_b + (1 - f_b) D_p \tag{B.1}$$

where D_{ob} is the ensemble-averaged diffusion coefficient observed for the peptide population, f_b is the fraction of the micelle-bound peptides, and D_p is the diffusion coefficient of free peptide (i.e., non-micelle bound peptides). Herein, binding between a peptide and a micelle are considered as a simple equilibrium between the free and the bound state. To apply this model, several assumptions were made. First, micelles were presumed spherical to allow the relationship between particle size and the translational

diffusion coefficient in laminar flow to be determined by the Stokes-Einstein equation [374]:

$$D = \frac{kT}{6\pi\eta r_s} \tag{B.2}$$

where k is the Boltzmann constant, T the absolute temperature, η is the viscosity, and r_s the hydrodynamic radius of the particle. Secondly, the hydrodynamic radius of a bound peptide-micelle complex (r_b) was assumed to be the sum of its individual components (i.e., peptide (r_p) and micelle (r_m)):

$$r_p + r_m = r_b \tag{B.3}$$

Based upon the Stokes-Einstein equation, this equation could then be modified to represent the relationship in terms of D_b, D_p and D_m:

$$\frac{1}{D_p} + \frac{1}{D_m} = \frac{1}{D_b} \tag{B.4}$$

Thus, by determining D_p and D_m through measuring samples of apelin in the absence of micelles and micelles in the absence of apelin, respectively, D_b could be estimated. The calculated D_b, in turn, could then be used to determine the f_b from equation B.1.

Brij-35 blank

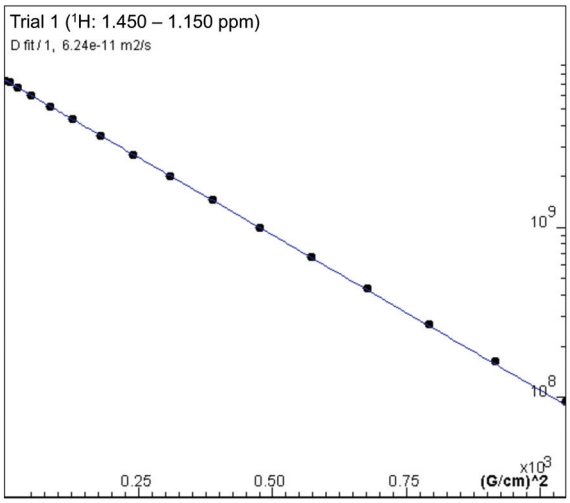

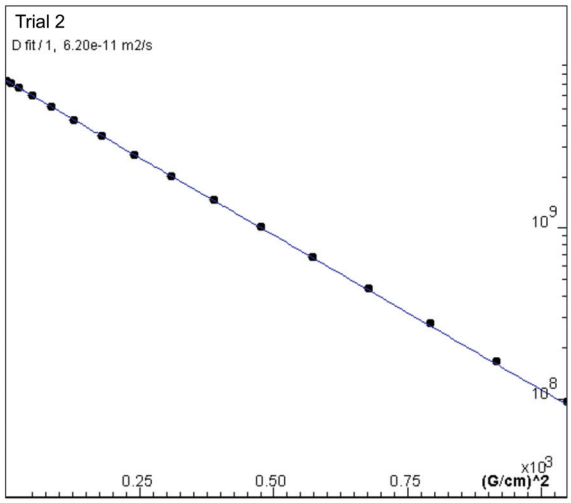

DPC blank

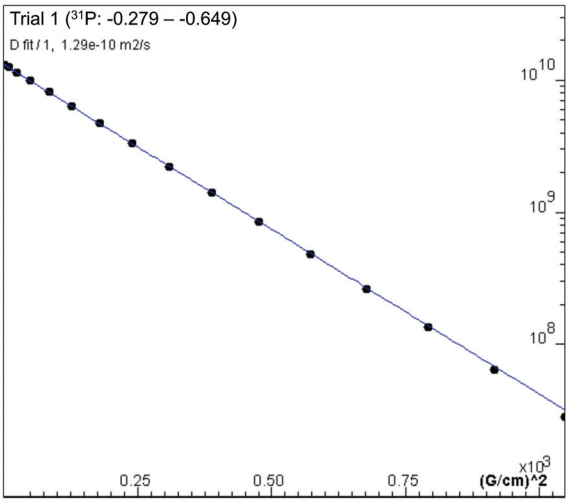

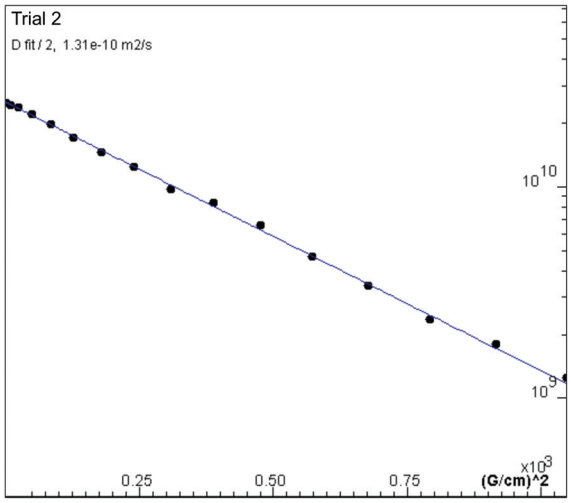

LPPG blank

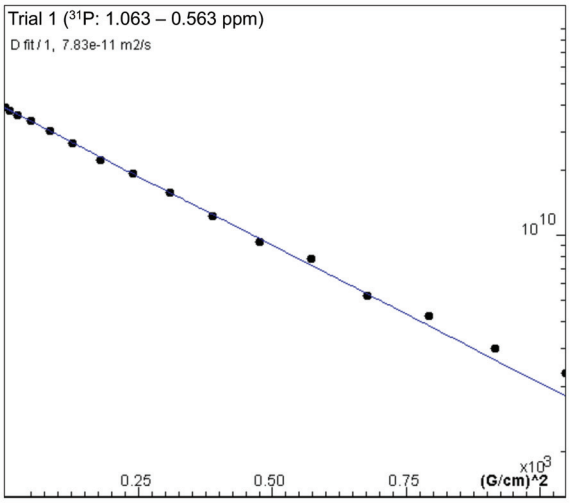

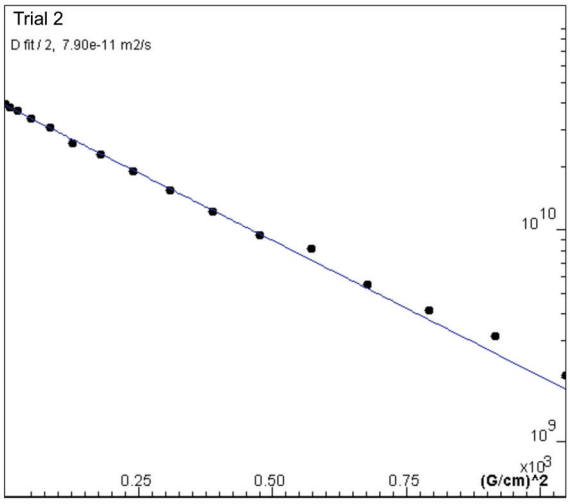

SDS blank

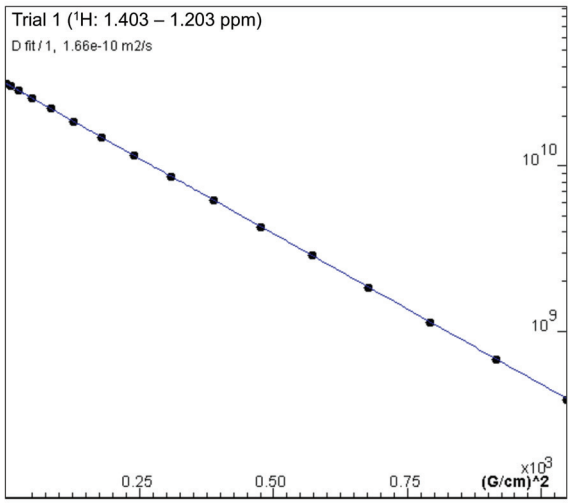

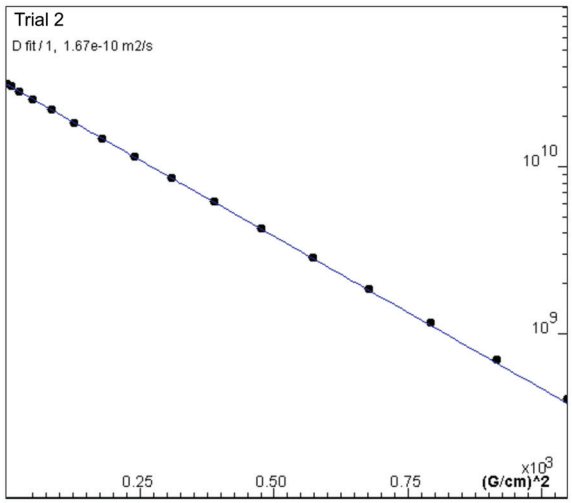

Apelin-36 in Buffer

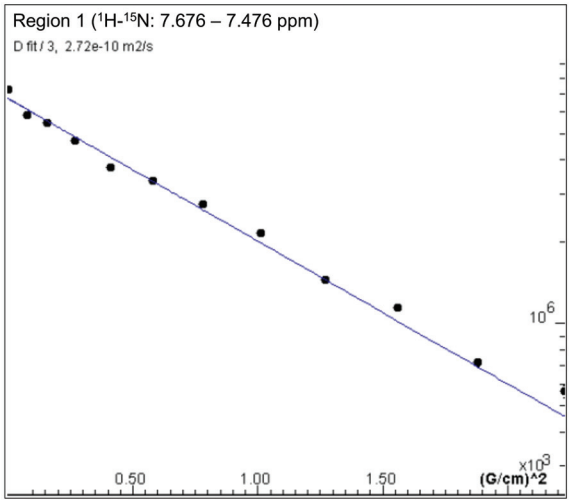

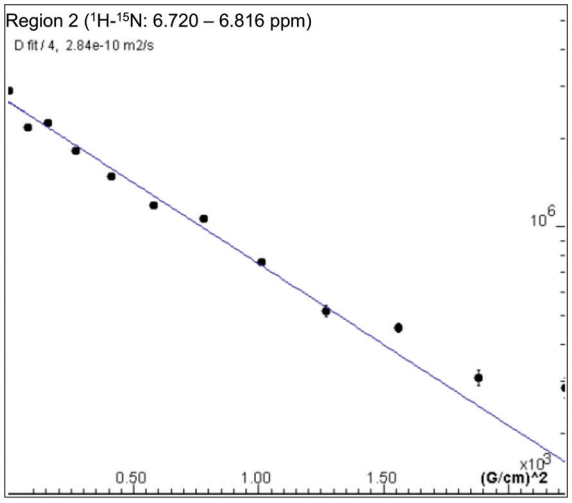

Apelin-36 in DPC

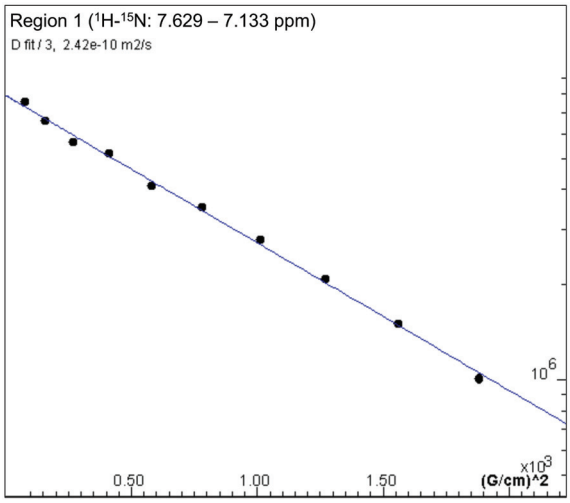

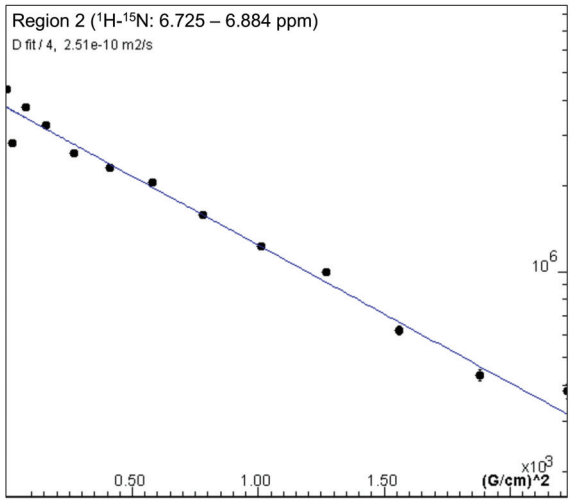

Apelin-36 in LPPG

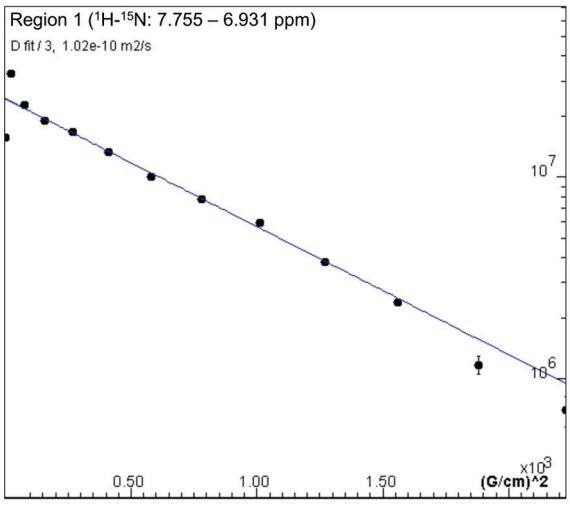

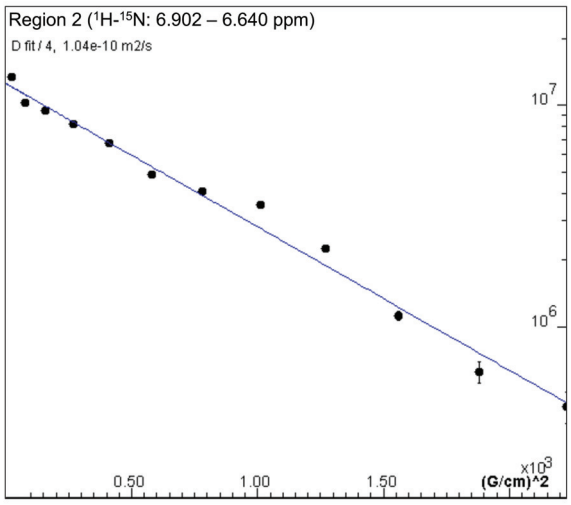

Apelin-36 in SDS

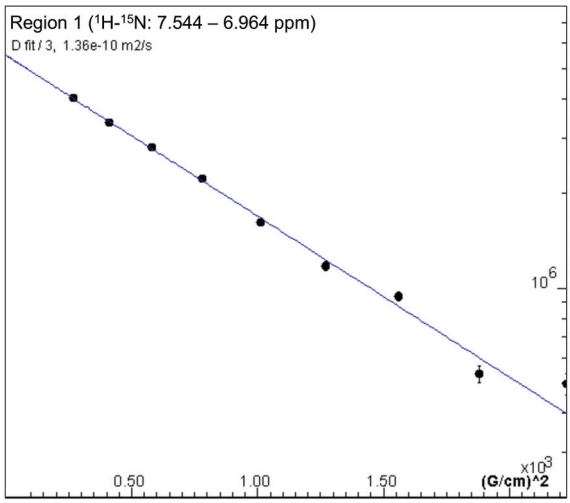

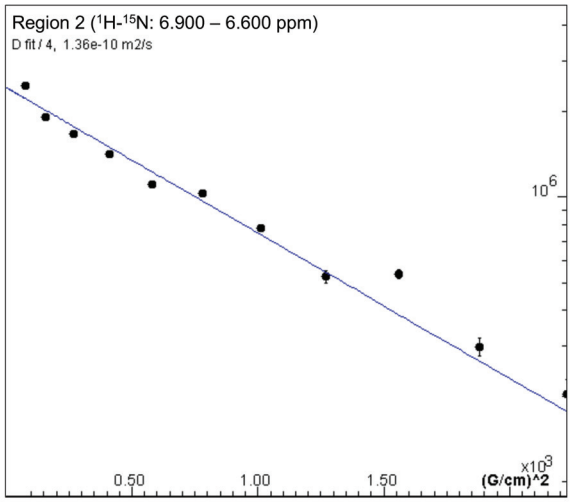

Apelin-55 in Brij-35

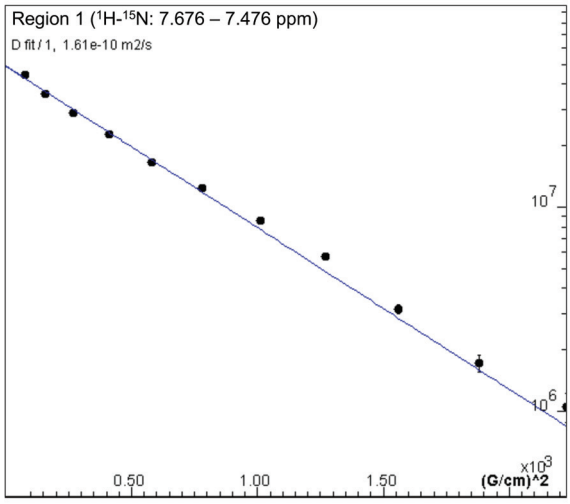

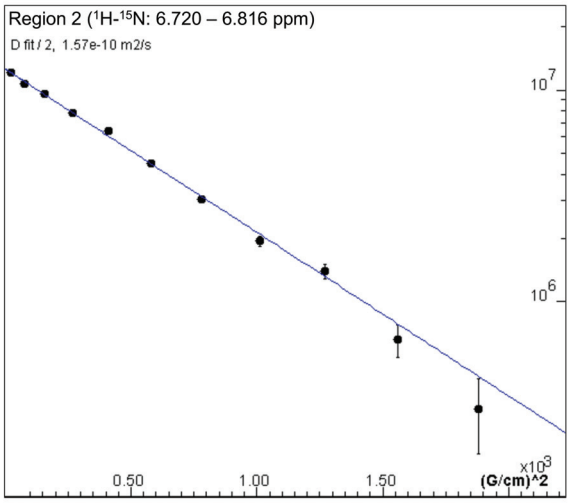

Apelin-55 in Buffer

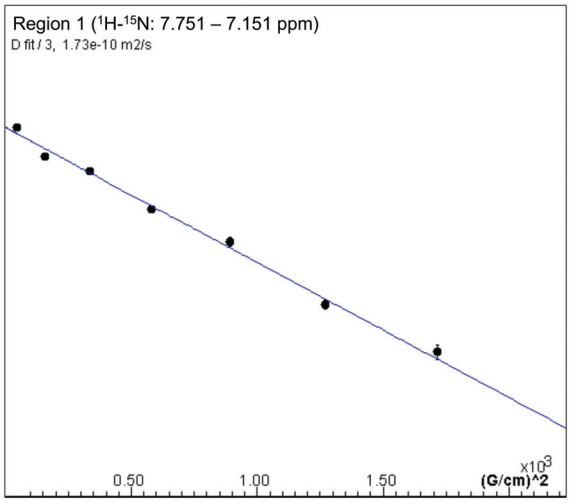

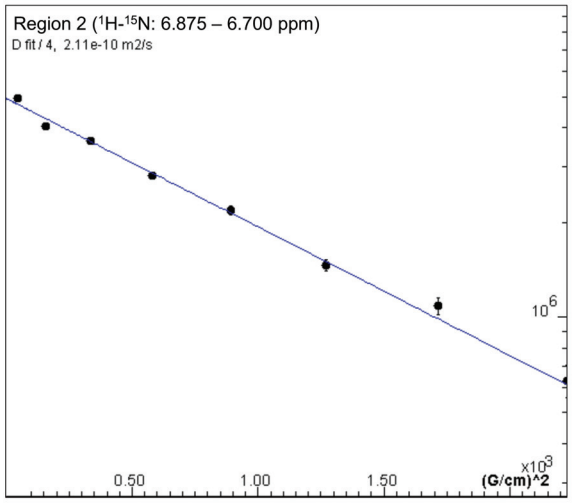

Apelin-55 in Buffer

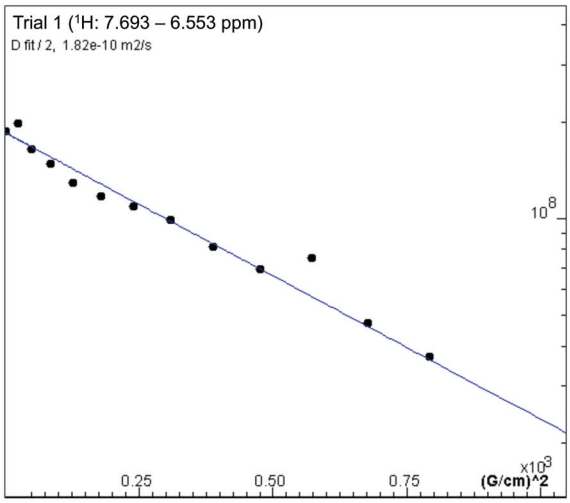

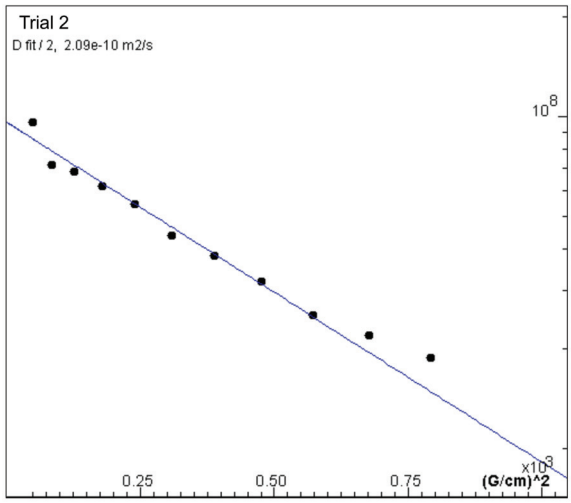

Apelin-55 in DPC

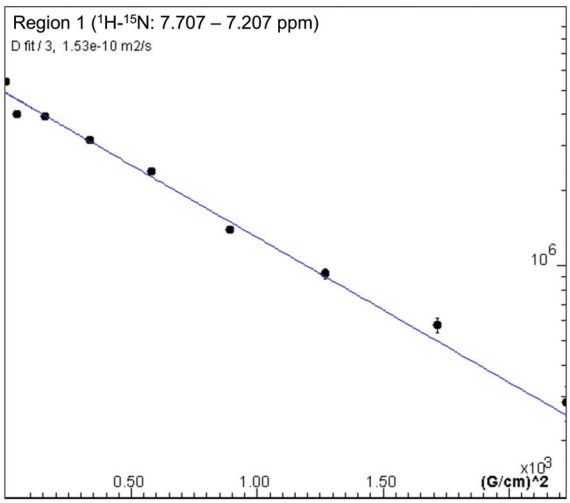

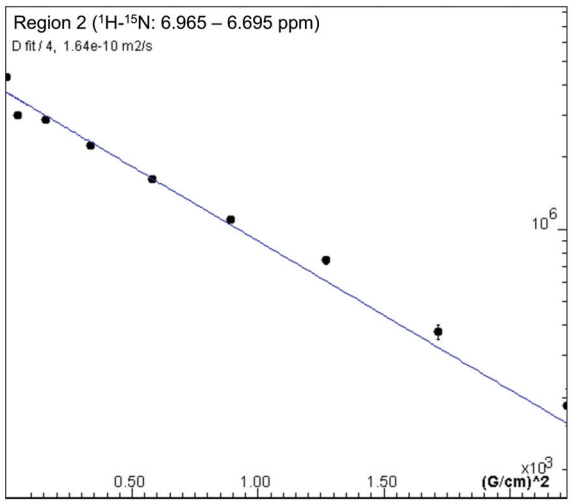

Apelin-55 in DPC

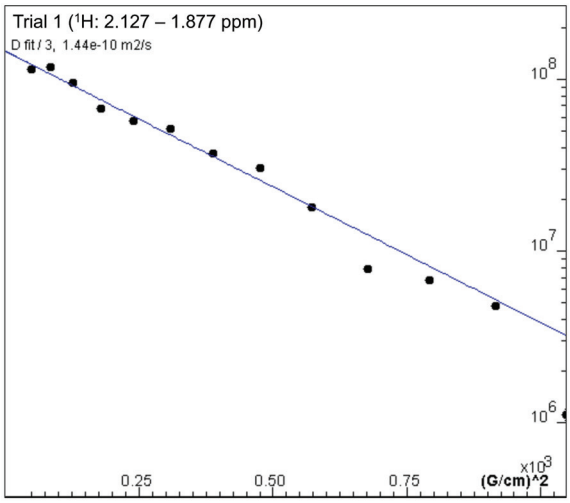

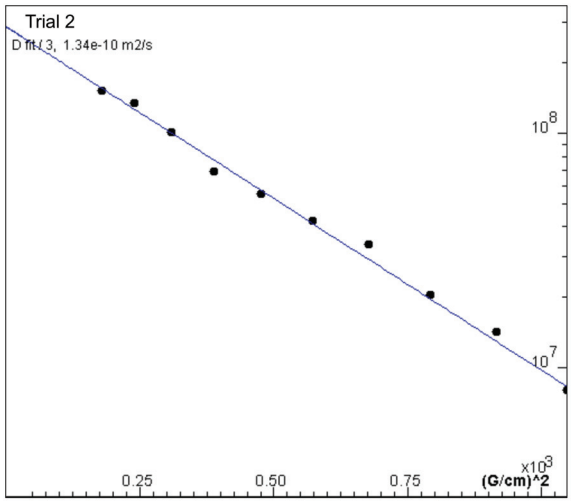

Apelin-55 in LPPG

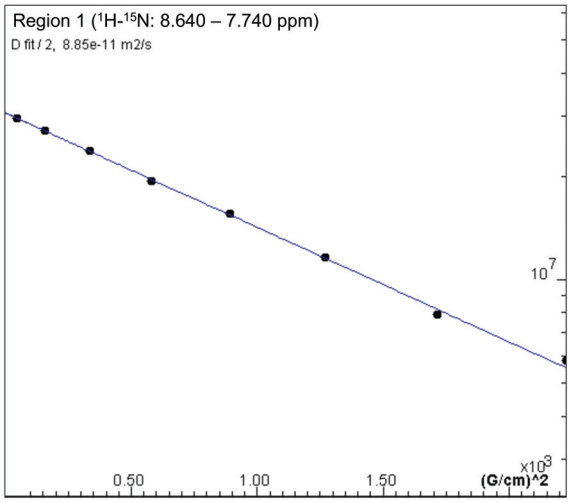

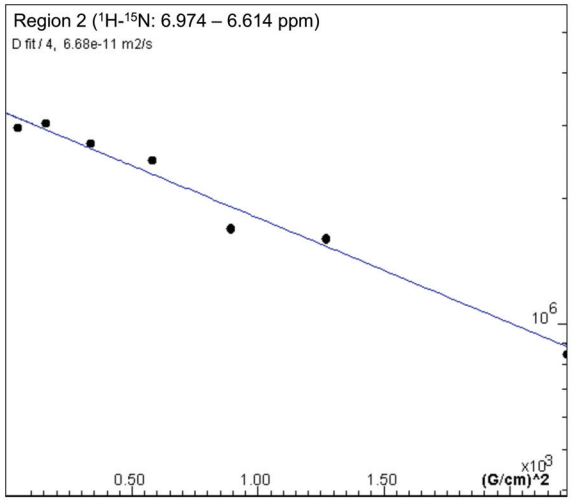

Apelin-55 in LPPG

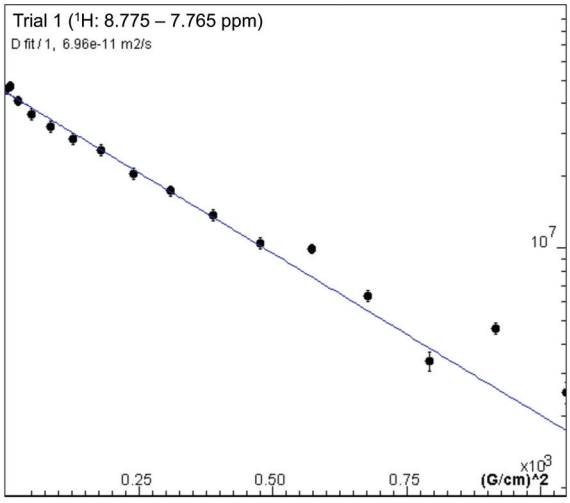

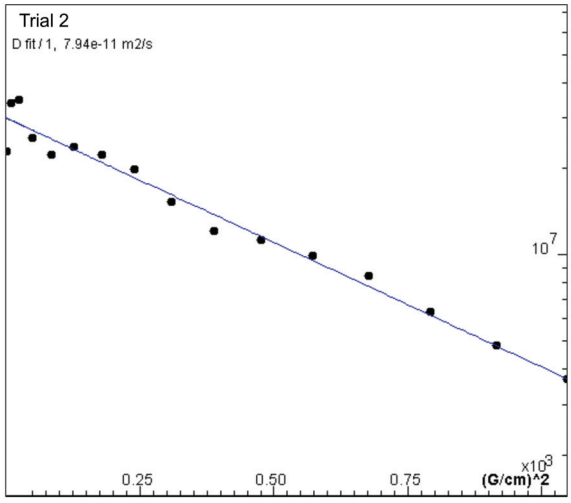

Apelin-55 in SDS

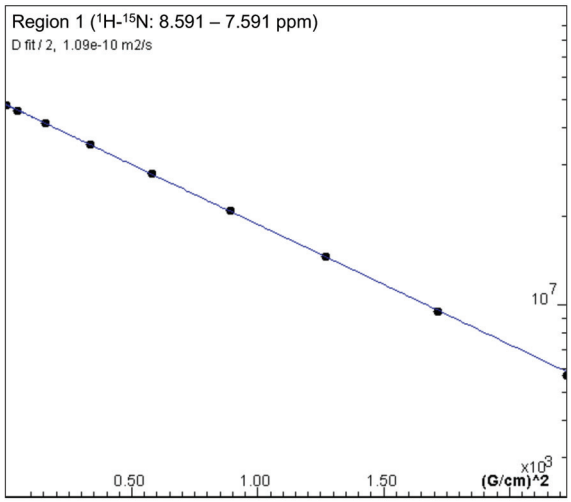

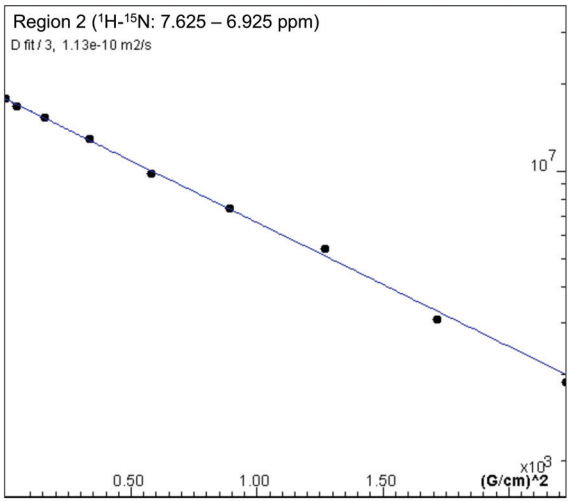

Apelin-55 in SDS

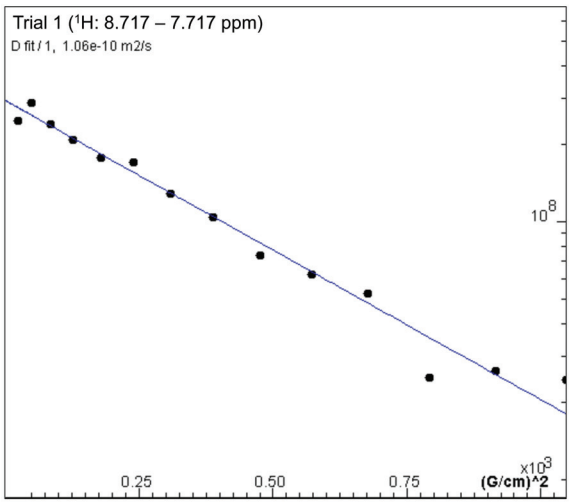

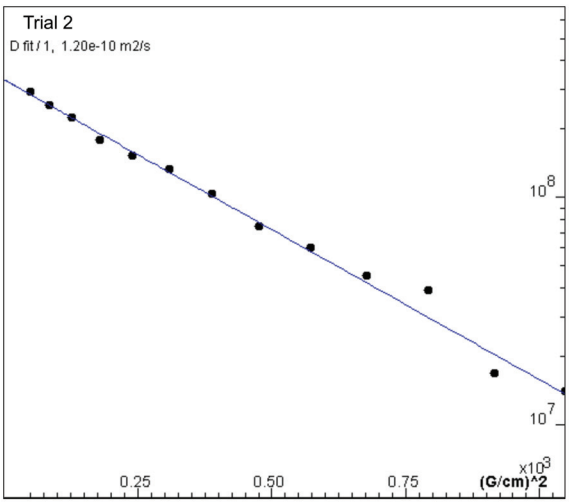

APPENDIX C Copyright permission letter

From: **Permissions Helpdesk** permissionshelpdesk@elsevier.com
Subject: RE: Permission to include publication for academic thesis
Date: June 19, 2017 at 2:39 PM
To: Kyung Shin K.Shin@Dal.Ca

PH

Dear Mr. Shin:

As we discussed, Elsevier journal authors retain the right to Include the article in a thesis or dissertation (provided that this is not to be published commercially) whether in full or in part, subject to proper acknowledgment (in this case "Modified from __" or "Based on ___"); see https://www.elsevier.com/about/our-business/policies/copyright/personal-use for more information. As this is a retained right, no written permission from Elsevier is necessary.

As outlined in our permissions licenses, this extends to the inclusion of your thesis in the Library and Archives of Canada's thesis on-demand services:

19. Thesis/Dissertation: If your license is for use in a thesis/dissertation your thesis may be submitted to your institution in either print or electronic form. Should your thesis be published commercially, please reapply for permission. These requirements include permission for the Library and Archives of Canada to supply single copies, on demand, of the complete thesis and include permission for Proquest/UMI to supply single copies, on demand, of the complete thesis. Should your thesis be published commercially, please reapply for permission. Theses and dissertations which contain embedded PJAs as part of the formal submission can be posted publicly by the awarding institution with DOI links back to the formal publications on ScienceDirect

Best of luck with your thesis and best regards,
Hop

Hop Wechsler
Permissions Helpdesk Manager
ELSEVIER | Global E-Operations Books
+1 215-239-3520 office
h.wechsler@elsevier.com

Contact the Permissions Helpdesk
+1 800-523-4069 x3808 | permissionshelpdesk@elsevier.com